Mechanics of Composites

Edited by
I. F. OBRAZTSOV and V. V. VASIL'EV

Advances in Science and Technology in the USSR

Mathematics and Mechanics Series

MIR Publishers
Moscow

Mir Publishers Moscow

Advances
in
Science
and
Technology
in
the USSR

Mathematics and
Mechanics Series

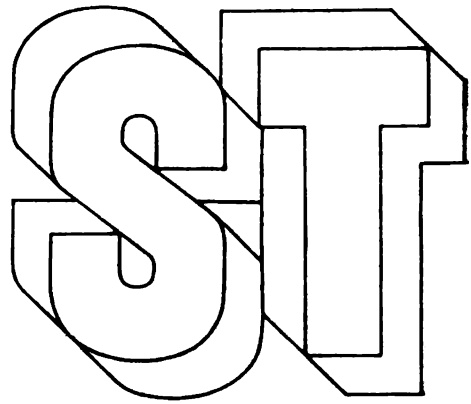

Mechanics of Composites

Edited by
I.F. OBRAZTSOV,
Mem. USSR Acad. Sc.,
and V.V. VASIL'EV,
D.Sc. (Eng.)

Translated from the Russian
by V.I. ILYUSHCHENKO
Cand. Sc. (Phys.-Math.)

MIR Publishers
Moscow

Механика композитных сред
Под ред. академика И.Ф. Образцова
и д-ра техн. наук В.В. Васильева
Издательство «Мир» Москва

Translation edited by V.V. VASIL'EV, D.Sc. (Eng.)
First published 1982

На английском языке

© Издательство «Мир», 1982
© English translation, Mir Publishers, 1982

Printed in the Union of Soviet Socialist Republics

CONTENTS

Preface		7
1	**Some Problems of Composite Mechanics,** *I. F. Obraztsov*	9
1.1	Introduction	9
1.2	Micromechanics of Composites	9
1.3	Macromechanics of Composites	12
1.4	Design of Structural Elements	15
2	**Fracture of Composites,** *V. V. Bolotin*	20
2.1	Introduction	20
2.2	General Relations	25
2.3	Granular Composite	29
2.4	Unidirectional Fibrous Composite with Elastic Matrix	34
2.5	Unidirectional Fibrous Composite with Plastic Matrix	40
2.6	Some Generalizations	42
3	**Theory of Microheterogeneous Fibrous Media,** *G. A. Vanin*	50
3.1	Introduction	50
3.2	Fundamental Propositions	53
3.3	Local Fractures	60
3.4	Local Fracture of Heterogeneous Phase Media	67
4	**Strength and Creep Micromechanics of Composites,** *A. M. Skudra and F. Ya. Bulavs*	77
4.1	Introduction	77
4.2	Strength Micromechanics	78
4.3	Creep Micromechanics	89
5	**Polymeric Composites with Reinforced Matrix,** *G. M. Gunyaev and B.V. Perov*	110
5.1	Production Methods and Structure of Matrix-Reinforced Composites	110
5.2	Characteristics of Whisker-Reinforced Matrix	116
5.3	Mechanical Characteristics of Reinforced-Matrix Composites	121
6	**Mechanics of Metal-Matrix Fibrous Composites,** *S. T. Mileiko*	129
6.1	Introduction	129
6.2	Effective Elastic Characteristics	131

6.3	Inelastic Behaviour	137
6.4	Composite Failure under Short-Time Static Loading	141
6.5	Creep Strength	157
6.6	Fatigue	158
7	**Deformation and Failure of Fibrous Composites with Brittle Polymeric Matrix under Plane Stress,** *N.A. Alfutov and P.A. Zinov'ev*	166
7.1	Introduction. Main Approaches to Description of the Behaviour of Multilayer Composites	166
7.2	Failure Model of Multilayer Composites	169
7.3	Results of Experimental Studies	171
7.4	Discussion and Conclusions	180
8	**Technological Problems in Composite Winding Mechanics,** *Yu.M. Tarnopol'skii, G.G. Portnov, and A.I. Beil'*	186
8.1	Introduction	186
8.2	Winding Stage	188
8.3	Mechanics of Postwinding Technological Stages	204
8.4	Methods to Govern Initial Stresses	211
8.5	Conclusion	219
9	**Theory of Composite Shells,** *V.V. Vasil'ev*	223
9.1	Introduction	223
9.2	Derivation of Governing Equations	224
9.3	A Cylindrical Shell	229
9.4	Axially Symmetric Generalized Plane Strain of an Orthotropic Laminated Cylinder	235
9.5	Static Buckling of Orthotropic Laminated Cylindrical Shells	238
9.6	Local Loading of Orthotropic Cylindrical Shells	244
10	**Optimum Design of Membrane Composite Shells of Revolution,** *V.A. Bunakov, V.D. Protasov, and S.B. Cherevatskii*	252
10.1	Introduction	252
10.2	Governing Equations in the Theory of Membrane Composite Shells of Revolution	253
10.3	Design of a Meridian Shape with Prescribed Orientation Pattern	258
10.4	General Relations for Uniformly Stressed Filament Wound Shells of Revolution	264
10.5	General Problem Formulation of Optimum Reinforcement of Shells of Revolution	274

PREFACE

Technological progress results in the continuous expansion of structural material types and in an improvement of their properties. Generally, new materials emerge because of a natural desire to improve the efficiency of proposed structures. These materials in turn afford new opportunities to produce totally updated designs and fabrication methods, while the subsequent development of structures and technology presents materials science with new tasks.

One of the clearest manifestations of such an interrelated process in the development of materials, structures and technology is closely associated with the development and application of reinforced composites. The emergence of glass-reinforced plastics, which have found extensive application because of their high strength and low density compared to conventional structural materials, has allowed the development of promising design concepts and efficient fabrication methods, being followed in turn by new advanced materials based on carbon, organic, or boron fibers dispersed in polymeric or metal matrices.

Modern composite materials not only have a wide range of properties with advantages over conventional materials, but these properties can be changed according to the designation of the structure. The idea of combining two or more components to produce a material with properties very different from those of the individual components has been used by man from time immemorial. In modern composites such components are high-strength fibers providing mechanical properties of materials and a matrix realizing these properties in a design. The resulting material has precisely oriented features which can be controlled by changing the structural parameters of the composites. There is no need to prove that such a special material, with all the properties required for the specific design, will always be more effective compared to conventional all-purpose isotropic metals and alloys. The principle of specialized properties can be accurately traced, e.g. in all natural materials which have emerged as a result of a prolonged evolution after having been subjected to gravitational, wind and other static and dynamic loads.

It is quite natural that the directed character of composite properties assumes that high performance in some directions will be balanced by low performance in others. The effective realization of merits of these materials in specific designs calls for the solution of a series of problems including: selecting the matching initial components—fibers and matrices; determining the reasonable structure of materials adequate to the external load field and other influences; taking account of the specific properties of the material and processing limitations in the design. It is only too simple to realize the worst possible design using the

best available composite than to make it from metal. During the short period of their intense development composites underwent the most various treatment on the part of designers—beginning with zealous attempts for the total replacement of metals by composites up to the absolute disregard of the latter as a structural material. Both sank into oblivion.

It is now quite possible to state that in spite of the imperfections of the first samples of composites, the very idea of making such materials (maybe realizable in a more complete and effective way in composites to come) did form the basis of a promising trend in engineering and other fields. The composites, without supplanting conventional structural materials, will take their due place among them.

A substantial contribution to the realization of this idea and to the solution of the problem of successful composite application in critical load-bearing structures is being made by the extensive research being carried out in the field of composite mechanics. The present collection of papers contains some results obtained in recent years by Soviet scientists in this advanced field of research. The papers are presented by experts in the mechanics of solids, structures and materials and contain both the discussion of general problems and the analysis of specific theoretical and applied problems of micro- and macromechanics, the formulation of fracture theory, the phenomenological and structural criteria of material integrity and strength, models of its nonlinear deformation, studies of possible ways of reinforcing the materials, the processing problems of composite mechanics, and questions of calculation and design of composite shells.

It is only natural that the papers which follow do not in any way exhaust even the basic results obtained in the USSR in the mechanics of composites.

The editors wish to thank MIR Publishers for their initiative in publishing the present collection and for their support of the new and promising research. The editors hope that the publication of this collection will encourage the further development of research into the mechanics of composites.

I.F. Obraztsov
V.V. Vasil'ev

1 Some Problems of Composite Mechanics

I. F. Obraztsov, *Mem. USSR Acad. Sc.*

1.1 INTRODUCTION

Composite materials are finding ever new applications in different engineering fields. This is primarily owing to the excellent mechanical properties of these materials at relatively low densities and their other merits offering advantages over conventional structural materials. The specific structural features and properties of composite materials, together with their great practical importance, have resulted in a new area of scientific research—the mechanics of composites, which has now a number of effective analytical methods and some significant results.

The present paper covers some topical problems of composite mechanics and, since the notion of "composite material" is now very diffuse and as yet has not been established in a finished form, the problems discussed below will generally involve the most popular composites, which are based on continuous fibers and polimeric matrix, and Soviet researchers' results will mainly be used.

It is a well-known fact that a composite is essentially a heterogeneous medium formed from two basic phases—reinforcing elements (fibers, threads, fabrics, etc.) providing the high strength and rigidity of the material and an isotropic matrix (polimeric or metal) providing the integrity of the material and the efficient action of reinforcing elements. In real structures composites, as a rule, possess two levels of heterogeneity—a microheterogeneity owing to the presence of at least two phases, and a macroheterogeneity owing to the laminated structure of the material, which is formed by a set of layers with different orientations or character of the reinforcing elements.

1.2 MICROMECHANICS OF COMPOSITES

The first level of heterogeneity is analysed by composite micromechanics. It aims at determining the properties of the material from the properties of its components and their relative volume fraction.

A large number of microstructural models of composites and descriptional approaches have now been proposed including: (1) the simplest models which allow for the volume fraction of fibers only and disregard the effects of stress concentration; (2) models

which allow for the form and relative packing of fibers assuming uniaxial stress for the matrix when elementary loads are applied along and across fibers; (3) models with a cylindrical fiber imbedded in a matrix or medium with composite-like properties; (4) energy methods which, proceeding from variational principles of possible change in stressed or strained states yield the lower and upper bounds of elastic constants; (5) exact or approximate solutions of problems in the theory of elasticity for an isotropic matrix having some regular inclusions—fibers or periodically spaced groups of fibers; (6) statistical methods based on averaging stress and strain fields for a medium with inclusions scattered at random; (7) numerical methods of stress analysis in the neighbourhood of a fiber; (8) photoelastic methods.

Microstructural models and calculational methods have been constructed describing the elastic properties, linear expansion coefficients, thermophysical and rheological properties of materials containing cylindrical fibers of equal or different diameters, fibers with a noncircular cross-section and hollow fibers, as well as the multicomponent materials with fibers of different types, and materials with three-dimensional reinforcement. Problems of the micromechanics of composites are discussed in [1-10].

A comparative analysis of the existing microstructural theories and their comparison against experiments show that, as far as the elastic properties along fibers are concerned, when the law of mechanical mixtures holds, all theories are in good agreement both with one another and with experiments. As to the transverse and shear elastic properties the deviation of theoretical values from experimental ones reaches 20% on average. This is conditioned by such factors lying outside the framework of the theoretical model as the nonuniform distribution of fibers in a macrovolume of material depending on the fabrication method, or the presence of voids, etc. From the practical point of view the results of micromechanics are intended not so much for the determination of material properties to be used in calculations (they can be found in a more exact and simpler way by experiment), as for the comparative analysis and study of the influence of structural parameters on material properties at the development stage.

One of the major fields of application of micromechanical results is closely associated with the formulation of the integrity conditions of fibrous composite materials determining a sound compromise between the properties of fibers and matrices [1].

The condition of integrity provides for the joint deformation of composite components up to the point of failure; the violation of this condition results in partial use of fiber properties and decreases the material efficiency. Three aspects of the problem of fibrous material integrity can be considered:

(a) Conditions of integrity under longitudinal tension of fibers assume the presence of matrix rigidity, deformability and adhesive strength sufficient to guarantee a uniform distribution of load between fibers up to the point of failure. Modern combinations of fibers and matrices in general satisfy all these conditions.

(b) The integrity conditions under longitudinal compression both afford the composites with compression strength, comparable to that under longitudinal tension, and exclude a premature fracture of the matrix and the elastic buckling of fibers. The systems now in use generally do not satisfy these conditions in total but have quite adequate properties.

(c) The loss of composite integrity under transverse tension is conditioned mainly by the low deformability of material in this direction compared to the longitudinal one. Since in a laminated system under arbitrary loading the layers are subjected not only to longitudinal but also to transverse normal and shearing stresses, the loss of integrity appearing as cracks parallel to fibers takes place substantially earlier than fiber fracture. For a properly designed structure this phenomenon is practically not accompanied by a drop in static strength, yet it results in a number of undesirable effects (the total loss of tightness, the penetration of moisture into material, the nonreproducibility of loading-unloading cycles, the accumulation of permanent deformations, etc.) whose consequences are difficult to predict.

The solution of the last problem is associated with an increase in the deformability of unidirectional material under transverse loading and is exceptionally complicated. The realization of the most natural way—an increase in matrix deformability—depends on overcoming fundamental difficulties because: (1) here as a rule the matrix elastic modulus is decreased, conditions (a) are violated. and the main parameter of the material—ultimate strength under longitudinal loading—is substantially reduced, and (2) the plastic properties of matrix under uniaxial loading are practically not manifested in the material because in microvolumes limited by fibers the matrix is found to be in three-dimensional stressed state.

The obtaining of a monolithic material, in the sense of provision (c), is an integrated problem of materials science and micromechanics. Futher progress in micromechanics must be concerned with the construction of models allowing for the real structure of materials in a more effective way and based not on the hypothetical distribution of fibers but on the geometrical analysis of microsections corresponding to a certain specific fabrication method.

It should be noted here that if in determining averaged elastic constants the microstructure influences the final result comparatively slightly, then in analyzing local effects which influence the strength and fracture mode of matrix the calculational model should

allow for the most realistic form of fiber distribution. This point seems to be essential when solving such pressing problems, linked intimately with the above mentioned task of micromechanics as the analysis of composites having an elastic-plastic matrix, because the development of plastic zones is influenced by local interfiber spacings rather than by the mean volume fraction of components.

1.3 MACROMECHANICS OF COMPOSITES

A key problem of macromechanics is the determination of the elastic properties of laminated materials composed of a number of arbitrarily oriented layers made, in the general case, from different materials. The properties of layers and the structure of material are assumed to be specified. The features of macrostructural analysis are conditioned by the given calculational model of the composite. The simplest approach to the description of rigidity-based properties of laminated material proposes substitution of the laminated medium by some conventional homogeneous and anisotropic one with the subsequent determination of its elastic constants by experimental means. Featuring a high accuracy, this approach presupposes a vast amount of experimental work since the results obtained are only valid for some very specific physical structure. The most popular model is a discrete-continual one which describes material as a system of elementary layers. The properties of this system are determined by elastic constants, dimensions and angles of layer reinforcement from calculations assuming a rigid interlaminar bond. The properties of a unidirectional layer can be found by different methods. Generally, they are determined from experimental data using samples of unidirectional material. The resultant macromechanical relations give, on the one hand, sufficiently high accuracy and, on the other, universality sufficient for the description of materials with greatly varying structures. In principle, the properties of an elementary layer can be found even by means of micromechanical relations for composites, but their above-cited inaccuracy in the determination of layer transverse and shear parameters may become unacceptable for practical calculations. A simplified discrete-continual model is widely applied in design problems and preliminary estimates of material properties. This model assumes the existence of an elementary unidirectional layer with rigidity only along fibers (net analysis). The longitudinal elastic modulus of the layer is determined experimentally or by the simple and exact formulas of micro-mechanics.

Nowadays the relations of macromechanics of composites have been obtained making it possible to describe all elastic constants, thermophysical and rheological parameters of composites and to allow for the specific features of their internal structure and defor-

mation under loading. The problems of macromechanics of composites are treated in [3, 5, 8, 12, 13].

Let us consider problems of strength and fracture of laminated composites. In accordance with the above models—homogeneous as well as structurally oriented heterogeneous—two main lines in strength analysis of composite systems can be specified. From a standard phenomenological point of view the material in a structure can be taken as homogeneous and anisotropic, described with one of the many strength criteria developed to date, and the limiting stresses included in these criteria under different loading conditions are determined experimentally for cut or model specimens. A review of the phenomenological strength criteria is presented in [14]. The structural approach, being more versatile, envisages the use of a strength criterion for an individual layer and the subsequent evaluation of material strength through calculations. These two methods, both having some advantages and disadvantages, are being developed thoroughly enough for a practical estimate of the strength of composite structures.

Let us clarify some details of the most widespread structural approach to the estimate of strength of laminated layers. According to the above model of a composite seen as a laminated system of homogeneous orthotropic layers the calculation is realized in the following way: (1) determination of elastic moduli and ultimate stresses of an elementary layer in tension and compression both along and across fibers, and in shear; (2) determination of membrane, bending and coupling generalized rigidities of laminated material; (3) determination of average deformations of a composite in a coordinate system unified for all layers; (4) determination of stresses in every layer using coordinates agreed with orthotropy axes of the layer; (5) estimation of layer strength according to a standard fracture criterion. The last of the above steps is of greatest interest for discussion. To analyze the limiting state of a layer phenomenological models have been developed proceeding from the criteria of static, long-term and cyclic strength of an orthotropic body, and microstructural methods based on statistical models of material and analysis of stress concentration in the matrix in the neighbourhood of fibers. To estimate the static strength one usually takes the simplest criteria of the type of the first or second theory of strength (of maximum stresses and strains) or the quadratic criteria of Mises-Hill type. The analysis of data thus obtained shows that the fracture of fibrous composites has a complicated and multistep character, the matrix failing first, i.e. here takes place the loss of integrity [see 1.2(*c*)]. As noted earlier, after all this the layer generally continues to bear loading. It has been found recently that the cause of this phenomenon is the absence of a substantial stress concentration in fibers and the breaking of interlaminar bonds as

allow for the most realistic form of fiber distribution. This point seems to be essential when solving such pressing problems, linked intimately with the above mentioned task of micromechanics as the analysis of composites having an elastic-plastic matrix, because the development of plastic zones is influenced by local interfiber spacings rather than by the mean volume fraction of components.

1.3 MACROMECHANICS OF COMPOSITES

A key problem of macromechanics is the determination of the elastic properties of laminated materials composed of a number of arbitrarily oriented layers made, in the general case, from different materials. The properties of layers and the structure of material are assumed to be specified. The features of macrostructural analysis are conditioned by the given calculational model of the composite. The simplest approach to the description of rigidity-based properties of laminated material proposes substitution of the laminated medium by some conventional homogeneous and anisotropic one with the subsequent determination of its elastic constants by experimental means. Featuring a high accuracy, this approach presupposes a vast amount of experimental work since the results obtained are only valid for some very specific physical structure. The most popular model is a discrete-continual one which describes material as a system of elementary layers. The properties of this system are determined by elastic constants, dimensions and angles of layer reinforcement from calculations assuming a rigid interlaminar bond. The properties of a unidirectional layer can be found by different methods. Generally, they are determined from experimental data using samples of unidirectional material. The resultant macromechanical relations give, on the one hand, sufficiently high accuracy and, on the other, universality sufficient for the description of materials with greatly varying structures. In principle, the properties of an elementary layer can be found even by means of micromechanical relations for composites, but their above-cited inaccuracy in the determination of layer transverse and shear parameters may become unacceptable for practical calculations. A simplified discrete-continual model is widely applied in design problems and preliminary estimates of material properties. This model assumes the existence of an elementary unidirectional layer with rigidity only along fibers (net analysis). The longitudinal elastic modulus of the layer is determined experimentally or by the simple and exact formulas of micro-mechanics.

Nowadays the relations of macromechanics of composites have been obtained making it possible to describe all elastic constants, thermophysical and rheological parameters of composites and to allow for the specific features of their internal structure and defor-

mation under loading. The problems of macromechanics of composites are treated in [3, 5, 8, 12, 13].

Let us consider problems of strength and fracture of laminated composites. In accordance with the above models—homogeneous as well as structurally oriented heterogeneous—two main lines in strength analysis of composite systems can be specified. From a standard phenomenological point of view the material in a structure can be taken as homogeneous and anisotropic, described with one of the many strength criteria developed to date, and the limiting stresses included in these criteria under different loading conditions are determined experimentally for cut or model specimens. A review of the phenomenological strength criteria is presented in [14]. The structural approach, being more versatile, envisages the use of a strength criterion for an individual layer and the subsequent evaluation of material strength through calculations. These two methods, both having some advantages and disadvantages, are being developed thoroughly enough for a practical estimate of the strength of composite structures.

Let us clarify some details of the most widespread structural approach to the estimate of strength of laminated layers. According to the above model of a composite seen as a laminated system of homogeneous orthotropic layers the calculation is realized in the following way: (1) determination of elastic moduli and ultimate stresses of an elementary layer in tension and compression both along and across fibers, and in shear; (2) determination of membrane, bending and coupling generalized rigidities of laminated material; (3) determination of average deformations of a composite in a coordinate system unified for all layers; (4) determination of stresses in every layer using coordinates agreed with orthotropy axes of the layer; (5) estimation of layer strength according to a standard fracture criterion. The last of the above steps is of greatest interest for discussion. To analyze the limiting state of a layer phenomenological models have been developed proceeding from the criteria of static, long-term and cyclic strength of an orthotropic body, and microstructural methods based on statistical models of material and analysis of stress concentration in the matrix in the neighbourhood of fibers. To estimate the static strength one usually takes the simplest criteria of the type of the first or second theory of strength (of maximum stresses and strains) or the quadratic criteria of Mises-Hill type. The analysis of data thus obtained shows that the fracture of fibrous composites has a complicated and multistep character, the matrix failing first, i.e. here takes place the loss of integrity [see 1.2(*c*)]. As noted earlier, after all this the layer generally continues to bear loading. It has been found recently that the cause of this phenomenon is the absence of a substantial stress concentration in fibers and the breaking of interlaminar bonds as

a consequence of cracking in the matrix. Therefore to continue the analysis of composite behaviour it is necessary to clarify the role of a layer with the failed matrix in the bearing of external load, i.e. to construct its calculational model.

A number of such models have been elaborated to date which assume the following after the failure of the matrix:

— the properties of a layer do not change in the longitudinal direction, and under transverse tension and shear a layer has zero rigidity and strength;

— if the law of elasticity conservation in the longitudinal direction holds, then relative to transverse tension and shear the layer is modelled as an ideally plastic body and the level of transverse normal and tangential stresses at the moment of matrix failure will further be maintained owing to the bonds with the adjacent layers;

— the relation between transverse normal and tangential stresses and their connection with the rate of corresponding deformations are governed by the associated flow rules of the theory of the ideal plastic body.

Incorporating such a model of a layer with cracks into step (1) of the above calculational scheme and repeating steps (2) to (5) it is possible to describe the matrix failure in all layers in succession and find the value of loading which corresponds to fracture of fibers, leading as a rule to the exhaustion of the bearing strength of the material. It should be noted that such a scheme of step-by-step description of all the stages of material fracture does not correspond to the traditional approach based on the correlation of stresses found with a chosen strength criterion. After the occurrence of a new form of fracture the material rigidity changes and the calculation has to be repeated. Here the calculational models appear to be nonlinear and the analysis can cause substantial difficulties. These are especially pronounced for the nonuniform stressed state when the boundaries of zones where the matrix fails are unknown a priori and layers in these zones have different properties under transverse tension and compression. Thus, the standard phenomenological approach, notwithstanding all its disadvantages, in a number of cases can become the only real one.

As to the above structural approach based on the analysis of successive failure of matrix in layers, it seems now to be too forced because design according to a loading level not causing the crazing of polimeric matrix results in a too conservative safety factor. In principle, the violation of the integrity of material is undoubtedly harmful and if only part of the effort on the description of this effect had been devoted to its elimination, it is highly possible that there would now be no necessity to discuss these matters at all.

Structural macroheterogeneity of laminated composites and sharp

anisotropy of their elastic and strength properties are responsible for some additional peculiarities of their behaviour and fracture. Among other things, between the pairs of layers with different angles of orientation relative to the direction of loading there takes place a specific interaction, with moments whose vector is orthogonal to the plane of layers. In the vicinity of a free edge in these systems, as a result of the breaking of fiber continuity, an edge effect occurs which in turn involves the delamination of material. This effect has been investigated in a number of works.

An analysis of crack propagation in composites and an estimate of fracture toughness, excluding some results obtained using microstructural models which are basically only of theoretical significance, are both based on the phenomenological approach envisaging the extension of the technique of fracture mechanics to orthotropic media. Of significant interest are the recent studies of crack extension in laminated media proceeding from the equations given in [15].

1.4 DESIGN OF STRUCTURAL ELEMENTS

As is well-known, the effective application of composites in structures requires (1) rational design of material, (2) allowance for the specific character of material under design, (3) integrated design-fabrication approach to designing, (4) allowance for material features during the checking calculations.

Composites have a sharply pronounced anisotropy of mechanical properties, and therefore, the main problem which decisively influences the efficiency of the material consists in the determination of structural parameters (reinforcement pattern, thickness of layers, etc.) best corresponding to the working conditions and functions of the structure. Let us remark here that the possibility of the creation of a material with directed anisotropy is considered in some cases an advantage of composites over traditional structural materials. Actually, this advantage resides in a high specific strength and rigidity, and the fact that they are realizable only in a single direction—along fibers—is the main disadvantage of fibrous composites (partially eliminated by the optimization of their structure). For example, for the same strength of materials the thickness of a cylindrical pressure vessel made of composite would be 1.5 times greater than that of a metal vessel, and of a spherical vessel, 2 times. The optimum internal structure is as a rule necessary and in some cases is even the only form of the material's existence in which it can successfully compete with metals. The theory of optimum reinforcement affording the rational design of material, however far from perfect, has a number of results which are successfully used nowadays. These include the selection methods for material structure to provide maximum strength and rigidity of structural ele-

ments in a plane stress state and, additionally, for shells under static and dynamic loading. For simple structures like pressure vessels, reservoirs, smooth-walled shells and panels the problem of deciding the rational fiber orientation has been in general solved. As the criteria of optimum selection there are generally used the conditions of minimum mass, uniform strength, maximum critical force, and minimum mean deviation of the natural frequency spectrum from a given one. Such problems of optimum reinforcement are dealt with in [3, 12, 16, 17]. Further development is required for integrated methods of designing sophisticated structures with simultaneous determination of the material structure for all elements, optimal for a sum of forces and other actions.

It might be well to point out that the application of numerical methods for the solution of problems of sophisticated design optimization runs into some difficulties connected with uncertainty of the number of layers, whose thickness and angles of orientation are determined at the design stage, and with nonuniqueness of the optimum structure. By and large one can surmount these difficulties by the use of generalized rigidity-based parameters of composite elements determined at the first stage of design work, and further as a second step one finds the composite structure ensuring the required rigidity. A sufficiently effective method now popular is the narrowing of the class of varied parameters through specifying the material type and the number of layers from the design-fabrication point of view, selecting the angles of orientation from a preliminary set of values.

As an additional topical problem one should point out here the formulation of the theory of optimum spatial reinforcement of composites. Modern methods can control the rigidity and the strength of material only in the layer plane, thus not allowing an increase in interlaminar shear rigidity and delamination resistance of material. The development of theoretical and processing methods ensuring the realization of optimum spatial reinforcement in the vicinity of boundary zones, points of application of local loads, etc. will be of great help in extending the sphere of application of composites.

A number of negative properties of composites, such as low shearing and crushing strength occurring as a result of fibers' shearing-off requires an exact allowance for the specific character of a material even at the initial design stage. Attempts to substitute metal by composite without substantial modifications in design as a rule will not enable one to use the potentialities of the material in full. The specific features of composite should be taken into account in the formation of cuts, stiffeners, regions of local loading, and in the selection of methods of joining the structural elements. It should be emphasized that composite materials generally do not exist separately from the structure and its specific fabrication methods.

The opportunities of existing techniques for the fabrication of working members (winding, pressing, moulding, etc.) are very wide though not infinite, and technological limitations play a much more essential role in the design of composite structures than in the design of metal structures. In such a way the successful designing of composite systems requires a comprehensive approach to the selection of material, determination of its physical structure and design configuration of members taking into consideration the possible ways of their technical realization.

The specific features of composites must be taken into account in the analysis of the strength and rigidity of structures too. Despite a number of peculiar properties of composites as compared to metals it has been universally accepted that the stressed-strained state of a composite structure can be evaluated by the conventional methods of mechanics of continua ignoring the structural microheterogeneity of the material. The specific features to be allowed for in the calculation include the anisotropy of mechanical properties, heterogeneity (lamination) of the material throughout the thickness, rheological properties of the matrix and the above-mentioned nonlinear character of deformation produced by successive fracture of material elements in the course of loading.

One of the essential composite parameters in the calculations of thin-walled laminated structures is their low rigidity under interlaminar shearing. Owing to this, the introduction of classical kinematic hypotheses from the theories of bending of beams, plates and shells in the composite system calculation appears to be less grounded than in the calculation of thin-walled structures made of standard materials. It is to be noted that with a small relative thickness of about 0.02 classical theory of anisotropic plates and shells (see [18-20]) gives fairly acceptable results. With the increase of relative thickness or a rise in temperature, which substantially lowers rigidity under interlaminar shearing, the classical theory needs to be modified. At present several versions of the improved applied theories of orthotropic laminated plates and shells have been formulated —which are based on the following:

(1) the exact allowance for transverse shearing strain and the neglect of normal strain [3, 15, 21];

(2) the approximation of shearing stress distributions or transverse shearing strain throughout the thickness [18, 22-25];

(3) the expansion of displacements into series throughout the thickness [26];

(4) the introduction of kinematic hypothesis for every layer [15].

The main outstanding problem is as before not so much the formulation of a new improved version of the theory based on some particular hypothesis, as their comparative analysis and the elucidation of rational manifold of corrections to the classical theory

in order to describe composite systems with a reasonable accuracy and the minimum of expense.

In general, the development of methods to determine the average stressed-strained state of composite structures is in full accord with the state-of-the-art as regards traditional material structures. As mentioned above, from the specified average stresses of a composite seen as a quasi-homogeneous material it is possible to find the macro- and microstructural stresses in individual layers and even in the fibers and the matrix using one of the microstructural models.

Several problems of composite system mechanics have been considered above which are of interest in the author's opinion but which, naturally, do not reflect the whole complex of problems involved. The papers of this collection contain both specific results and surveys dedicated to a number of the questions considered.

References

1. Van Fo Fi, G.A., *Theory of Reinforced Materials*, Naukova dumka, Kiev, 1971 (in Russian).
2. Van Fo Fi, G.A., *Reinforced Plastic Structures*, Tekhnika, Kiev, 1971 (in Russian).
3. Elpat'evskii, A.N., and Vasil'ev, V.V., *Strength of Cylindrical Shells from Reinforced Materials*, Mashinostroyenie, Moscow, 1972 (in Russian).
4. Zhigun, I.G., and Polyakov, V.A., *Properties of Spatially Reinforced Plastics*, Zinatne, Riga, 1978 (in Russian).
5. Malmeister, A.K., Tamuzs, V.P., and Teters, G.A., *Resistance of Rigid Polimer Materials*, Zinatne, Riga, 1972 (in Russian).
6. Rabotnov, Yu.N., *Mechanics of Deformable Solids*, Nauka, Moscow, 1979 (in Russian).
7. Skudra, A.M., Bulavs, F.Ya., and Rotsens, K.A., *Creep and Static Fatigue of Reinforced Plastics*, Zinatne, Riga, 1971 (in Russian).
8. Skudra, A.M., and Bulavs, F.Ya, *Structural Theory of Reinforced Plastics*, Zinatne, Riga, 1978 (in Russian).
9. Tamuzs, V.P., and Kuksenko, V.S., *Micromechanics of Polymer Material Fracture*, Zinatne, Riga, 1978 (in Russian).
10. Shermergor, T.D., *Elasticity Theory of Heterogeneous Media*, Nauka, Moscow, 1977 (in Russian).
11. Roginskii, S.L., Kanovich, M.Z., and Koltunov, M.A., *High-Strength Fiber-Glass Plastics*, Khimia, Moscow, 1979 (in Russian).
12. Obraztsov, I.F., Vasil'ev, V. V., and Bunakov, V.A., *Optimum Design of Composite Shells of Revolution*, Mashinostroyenie, Moscow, 1977 (in Russian).
13. Tarnopol'skii, Yu.M., and Skudra, A.M., *Structural Strength and Deformability of Fiber-Glass Plastics*, Zinatne, Riga, 1966 (in Russian).
14. Goldenblat, I.I., and Kopnov, V.A., *Strength and Plasticity Criteria of Structural Materials*, Mashinostroyenie, Moscow, 1968 (in Russian).
15. Bolotin, V.V., and Novichkov, Yu.N., *Mechanics of Multilayered Structures*, Mashinostroyenie, Moscow, 1980 (in Russian).
16. Rikards, R.B., and Teters, G.A., *Stability of Composite Shells*, Zinatne, Riga, 1974 (in Russian).
17. Teters, G.A., Rikards, R.B., and Narusberg, V.L., *Optimization of Laminated Composite Shells*, Zinatne, Riga, 1978 (in Russian).

18. Ambartsumyan, S.A., *General Theory of Anisotropic Shells*, Nauka, Moscow, 1974 (in Russian).
19. Grigorenko, Ya.M., *Isotropic and Anisotropic Laminated Shells of Revolution with Variable Rigidity*, Naukova dumka, Kiev, 1973 (in Russian).
20. Lekhnitskii, S.G., *Anisotropic Plates* (translated from the 2nd Russian edition), Gordon and Breach, 1968.
21. Tarnopolskii, Yu.M., and Roze, A.B., *Design Peculiarities of Reinforced Plastic Elements*, Zinatne, Riga, 1969 (in Russian).
22. Ambartsumyan, S.A., *Theory of Anisotropic Plates* (translated from Russian), Technomic, Stanford, Conn., 1970.
23. Korolyov, V.I., *Laminated Anisotropic Plates and Shells from Reinforced Plastics*, Mashinostroyenie, Moscow, 1965 (in Russian).
24. Pelekh, B.L., *Theory of Shells with Finite Shear Rigidity*, Naukova dumka, Kiev, 1973 (in Russian).
25. Pikul', V.V., *General Applied Theory of Thin Elastic Plates and Shallow Shells*, Nauka, Moscow, 1977 (in Russian).
26. Pelekh, B.L., and Sukhorol'skii, M.A., *Contact Problems in the Theory of Elastic Anisotropic Shells*, Naukova dumka, Kiev, 1980 (in Russian).

2 Fracture of Composites

V. V. Bolotin, *Corr. Mem. USSR Acad. Sc.*

2.1 INTRODUCTION

The rapid progress in the field of fracture mechanics that we are now witnessing is a phenomenon worth analysing.

Within decades the well-known results of the mechanics of cracks became classic yet isolated items. Nowadays, almost every third expert in the mechanics of deformable solids is engaged in fracture mechanics or its applications.

Papers on fracture mechanics form a considerable fraction of all publications on the mechanics of materials and structures.

There are at least two reasons giving rise to the rapid progress in fracture mechanics. Firstly, the disappointment with the many years' efforts of an army of researchers to systematize and arrange the results of material and structure testing under different loads, thermal and other actions. Everyone felt the necessity for a sounder theoretical basis to describe mechanisms of fracture than was the case with the phenomenological criteria of yield and fracture. Secondly, the improvement in the engineering level of observations of structures in operation and those in emergencies. It turned out that many structures functioned properly even though their elements and parts had fatigue cracks and other crack-like defects. It was understood that cracks could be stable and their growth can be controlled and predicted. To be able to judge the operational capacities of practical structures and to predict their lifetime and residual strength it was necessary to develop the mechanics of fracture.

At the same time fracture mechanics has its own growing pains. At present this science is developing basically as the mechanics of cracked solids. Although the cracks are generally represented as mathematical cuts in a body of intact material, yet in reality the process of fracture consists of two stages. The first corresponds to the accumulation of dispersed damage and can take a significant proportion of the structure's lifetime preceding the stage of macroscopic cracking. If there were no inherent macrocracks in a structural element, the nucleation of the first macrocrack is the result of dispersed damage accumulation. The process of damage accumulation continues after the beginning of crack growth so that both processes interact. Although there are many reliable and fundamental results in the mechanics of cracked solids, the mechanics of dispersed dam-

age is still in general a phenomenological and semiempirical science. Moreover there is no satisfactory relation between the description of the damage accumulation and that of the growth of macrocracks. It is difficult to speak of the application of fracture mechanics to predict the lifetime of structures at the design stage until this relation is understood. Owing to the shortcomings of nondestructive testing means and the risk of crack omission this caveat will also apply to the prediction of the lifetime of structures in operation according to their current state.

Fracture mechanics is of much greater importance for composite materials than for conventional structural materials. The properties of composites have been little studied, and every year hundreds of new composites are developed. The composite as a material very often appears together with a structure. Small specimen tests are rather uniformative since the methods of carrying their results over to the full-sized structures are generally too vague owing to the scale effect being well pronounced yet difficult to predict. As applied to long-lived structures there emerge some additional problems because of the need of a time extrapolation of the short-term testing results. It is difficult to discuss sound techniques of forced and accelerated testing procedures because of lack of knowledge of composite properties. The list of problems could be extended and completed by mentioning that at the design stage the composite specimens are very expensive and are usually available in a totally insufficient quantity for reliable statistical conclusions to be drawn. Therefore those engaged in the study of composite fracture have to rely upon theoretical models to a greater extent than is the case with conventional materials [1, 2].

As is known, real material fracture is random owing to the random nature of constituent elements of these materials. From the standpoint of the mechanics of continua there can be taken as elements of the material structure such units of volume which while following the equations of mechanics of continua have simultaneously to be considered as the elements responsible for the material damage, the nucleation and propagation of macrocracks. This consideration is equally applicable both to conventional structural materials and to composites. Stochastic models of material fracture are of additional interest because they afford opportunities to predict the reliability and the durability of constructural elements.

Only rather primitive models are of practical interest on account of the complexity of the fracture phenomenon of stochastic solids. The more refined models require information which cannot be obtained from macroscopic experiments. These models provide results which are difficult to interpret and use in engineering design. One criterion of the merit of proposed models consists in the comparison of the results of calculations with the known experimental

facts as well as with the main results of fracture mechanics. The majority of the latter are of a deterministic character so that to make comparison with them requires a semideterministic interpretation of the results based on stochastic models. Such interpretation has inevitably an approximate character. Thus, the values of random variables with the probability approaching unity should be correlated, e.g. with that of $1 - e^{-1} = 0.632...$, the values of distribution medians, etc.

In this paper we consider mainly unidirectional fibrous composites in tension along the fibers. At the same time the conditions of material fracture in compression and other more general stress states are discussed. The choice of unidirectional fibrous composites as a basic subject of the investigation is dictated by the fact that these materials are the most commonly used to produce highly efficient structural elements. Generally, highly efficient thin-walled structures have a laminated fibrous composition and every layer of the latter may be considered as formed by the unidirectional fibrous composite. If the conditions of unidirectional composite fracture are known, considerable scope will be offered for the evaluation of the strength of structures composed of the laminated fibrous composite concerned [3-5].

This paper also covers the fracture criterion for granular composites in tension. There is a similarity in the behaviour of such composites compared to the conventional polycrystalline materials for which classical mechanics of fracture has been developed. Therefore, the conclusions, which follow from the application of the theory being considered in this paper for the case of granular materials, can be compared to the results of the classical mechanics of fracture. These are as follows: the Griffith-Irwin criterion for stability of a macrocrack as well as the Paris-Erdogan equation for the rate of crack propagation. Taken in isolation these results can be treated as the simple corollaries of similitude considerations. These relations contain a number of empirical constants. Using the unified stochastic models of damage and fracture we can evaluate these constants and establish the relationships between constants which enter into equations concerning the different stages of the fracture process.

In order to simplify the presentation we shall assume at the very beginning that the field of nominal stresses $s(t)$ is deterministic and homogeneous in the whole of the specimen volume V. The crack sizes l will be taken so small compared to the characteristic dimensions of the specimen that their influence on nominal stresses may be considered negligible.

An approach to the construction of unified models is represented schematically in Fig. 2.1. The specimen is treated as a statistical ensemble of structural elements with random properties. The number

of structural elements N in the specimen volume V is assumed to be very large. On the other hand it is assumed that every element can be additionally treated in the framework of the mechanics of continua.

The grains of a polycrystalline material or grains of inclusions in composites with a spheroidal filler can be taken as examples of structural elements satisfying these conditions. Their characteristic

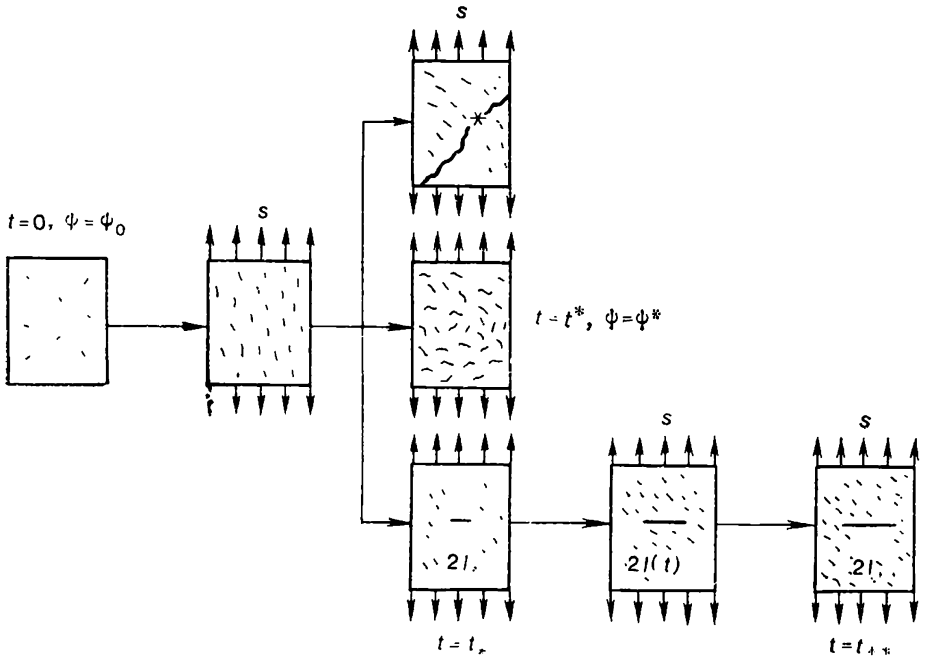

Fig. 2.1 Unified model of composite fracture

sizes ρ are very small compared to the specimen size as well as to the typical range of nominal stress changes. Another example is the segments of fibers of unidirectional fibrous composites. The length of the structural elements is $2\lambda_e$ where λ_e is the elastic transfer length, i.e.

$$\lambda_e \sim \rho\,(E_f/2G_m)^{1/2} \tag{1}$$

Here and below the following notations are used: ρ is the fiber radius, E_f, the fiber Young's modulus, G_m, the matrix shear modulus. The term structural element includes the adjacent parts of matrix. Relation (1) uses the equality sign by the order of magnitude. The more exact formulas contain a factor which has the order of unity when common values of volume fraction of fibers v_f are considered satisfying the conditions $v_f \sim (v_f^{-1/2} - 1)^{1/2} \sim 1$. Below we shall

often use similar approximate estimates to obtain results with an evident physical meaning.

At the damage accumulation stage it is assumed that primary elements are deformed and fractured independently. A typical kinetic equation for the damage rate $\varphi(t)$ of a randomly taken structural element is of the form:

$$d\varphi/dt = f(\varphi, \psi, s, r) \tag{2}$$

the right-hand side containing a nonnegative function of the damage rate of a given element φ, the nominal stress s and the strength r of a structural element. It also contains the composite damage rate ψ. If one considers the process of cyclic loading with slowly varying stress amplitudes then t will be treated as the "slow" time and s, the stress range within a single cycle.

The strength of structural elements r is considered a random quantity with a given function of probability distribution $F_r(r)$. The function $f(\varphi, \psi, s, r)$ on the right-hand side of equation (2) can always be chosen so that the parameter r will have the meaning of the structural element strength for times of the order of the duration of standard short-term tests. Later on it will be assumed that the condition is satisfied.

At the first stage the accumulation of dispersed damage takes place in the weakest individual structural elements. The distribution function of lifetime τ of every element $F_\tau(\tau)$ is to be found as a solution of an inverse boundary-value problem for equation (2) under the boundary conditions $\varphi(0) = \varphi_0$, $\varphi(\tau) = 1$. The composite damage rate is characterized by relation $\psi = N_*/N$, where N_* is the number of the broken structural elements. Strictly speaking, $\psi(t)$ is the step function

$$\psi(t) = (1/N) \sum_{k=1}^{N} \eta(\tau_k - t) \tag{3}$$

where $\eta(t)$ is the Heavyside function and τ_1, τ_2 the lifetimes of individual elements. As will be seen later, to describe the process of the damage accumulation in a composite one needs to introduce additional damage rates, i.e. those characterizing a degree of matrix damage.

The first stage terminates at a moment t_*. The damage rate is as a rule still extremely small compared to unity while the total number of the broken structural elements is $\psi N \gg 1$. There are three possibilities of subsequent developments (Fig. 2.1). First, brittle fracture of specimen can occur due to the rapid propagation of one of the damage centres. Secondly, a system of multiple macrocracks can be formed which develop rapidly and almost simultaneously over the whole of the specimen volume. We shall name this

type of fracture a loss of integrity. The cited fracture types are qualitatively different while in appearance may prove to be similar. A source of brittle fracture is always the local one while loss of integrity develops almost uniformly over the whole of the volume of a homogeneously stressed specimen. If at $t \approx t_*$ there takes place neither brittle fracture nor loss of integrity, the next stage will consist in a steady growth of the macrocrack until at the moment t_{**} its size reaches the critical value l_{**}.

2.2 GENERAL RELATIONS

Let us start with a consideration of dispersed damage accumulation. The function (3) to describe this process is the step-like one. However, since $\psi N \gg 1$ it is possible to use a smoothed approximation of the process $\psi(t)$. By neglecting the interaction between the broken structural elements and applying the Moivre-Laplace theorem one obtains an asymptotic estimate of a distribution function of the process probability $\psi(t)$ [6]:

$$F_\psi(\psi; t) \sim \Phi\left\{\frac{[\psi - F_\tau(t)]\, N^{1/2}}{[1 - F_\tau(t)]^{1/2}\,[F_\tau(t)]^{1/2}}\right\} \tag{4}$$

Here $F_\tau(\tau)$ is the lifetime distribution function of a randomly chosen element. The further approximation is of the form:

$$\psi(t) \sim F_\tau(t) \tag{5}$$

Hence we consider the process of dispersed damage accumulation as a deterministic one (remember that from the very beginning we agreed to consider deterministic loadings only).

The above damage accumulation process ends either in loss of integrity or in crack initiation. In both cases the character of the process is determined by the damage rate value ψ. The critical values ψ^* and ψ_* depend, generally speaking, on the stress level s at the moments t^* and t_*, respectively. The problem of estimation of these critical values is the most significant difficulty in the theory developed.

The condition to determine the moment of loss of integrity t^* is taken as:

$$\psi(t^*) = \psi^* \tag{6}$$

The critical level of damage ψ^* is on the right-hand side. To calculate it in an analytical form it is necessary to solve the stability problem for an ensemble of microcracks formed as a result of the damage accumulation. The value of ψ^* can also be found from experiments.

of ψ^* is defined as a root of the equation:

$$\psi = F_s[s(\psi)]$$

in principle, should be the case.

$\psi N(t_s) \gg n_s$ is defined approximately as

$$F_s(t_s) \sim 1 - \exp[-N\psi^{n_s}(t_s)] \qquad (9)$$

semideterministic estimate:

$$\psi_s \sim N^{-1/n_s} \qquad (10)$$

moments of individual structural elements, the difference in the stress concentration factors, etc. To calculate these one needs to know not only the distribution function $F_\tau(\tau)$ for single fractures of structural elements, but also the conditional probability distribution functions such as $F_\tau^{(2)}(t \mid \tau)$, $F_\tau^{(3)}(t \mid \tau_1, \tau_2)$ up to a second, third fracture, etc. For example, the probability distribution of the occurrence times of a second fracture is expressed in terms of an integral:

$$\int_0^t F_\tau^{(2)}(t \mid \tau)\, dF_\tau(\tau)$$

A number of calculations as applied to unidirectional fibrous composites can be found in [7].

The fracture mode (macrocrack initiation or loss of integrity), depends both on the relationship between the critical levels ψ_*, ψ^* and on the number of structural elements in the volume V (note that with fracture through loss of integrity a distinct scale effect is not detected). Comparing equations (6) and (10) we find that at

$$N \gg (\psi^*)^{n_*} \tag{11}$$

macrocrack initiation is more probable. If the number N is substantially less than the value of the right-hand side of equation (11) then loss of integrity will be more probable.

To obtain an equation describing the growth of a stable crack one needs to analyze damage and fracture of the structural elements located on the crack tip. Since the crack propagation takes place within the damaged material and the damage accumulation process continues at this fracture stage too, both processes should be treated in combination. The formulation of a stochastic problem is greatly complicated because of the necessity to allow for the stress concentration and plastic zone which incorporates the great number of structural elements located close to the crack tip.

The simplest stochastic model can be obtained by disregarding the influence of stress concentration on all structural elements except for those located at the given moment on the crack tip. Let the right-hand side of equation (2) be independent of φ. From this equation the lifetime of an element on the crack tip is given by

$$\Delta\tau \approx \frac{1}{f[\psi, \varkappa(l)\, s, r]}\left[1 - \int_0^t f(\psi, s, r)\, d\tau\right] \tag{12}$$

where $\varkappa(l)$ is the stress concentration factor for an element located on the crack tip. This factor depends on the crack size l. The integral on the right-hand side allows for fracture of an element till this

turns out to be on the crack tip. If the term in brackets proves to be negative one has to put $\Delta\tau \equiv 0$.

For the average crack growth rate a semideterministic equation follows

$$dl/dt \sim 2\rho/\mathbf{E}\,[\Delta\tau] \tag{13}$$

Here $\mathbf{E}\,[\cdot]$ is the mathematical expectation of a random value. This equation is based on an assumption that the number of structural elements on the crack tip is large and forms a representative sample sufficient to treat the crack propagation as a kind of natural averaging.

Classical mechanics of fracture does not allow for dispersed damage when considering the crack growth process. To obtain results in good agreement with fracture mechanics one has to drop the integral on the right-hand side of relation (12) as well as omit the ψ-dependence. Equation (13) will then take the form:

$$dl/dt \sim 2\rho \left\{ \int_0^\infty \frac{p_r(r)\,dr}{f[\varkappa(l)\,s,\ r]} \right\}^{-1} \tag{14}$$

where $p_r(r)$ is the probability density of the parameter r.

The crack grows up to the time t_{**} when the crack size l attains the critical value l_{**}. The calculation of l_{**} is within the scope of the proposed approach. The simplest method consists in discovering l_{**} from the condition of almost every structural element located on the crack tip being almost immediately ruptured with a probability of the order of unity. Since the short-term strength distribution is given under a condition by function $F_r(r)$, the following equation for the evaluation of l_{**} holds:

$$F_r[\varkappa(l)\,s] \sim 1 \tag{15}$$

When increasing the crack size l by one step 2ρ condition (15) will be again satisfied resulting in subsequent crack growth. Thus condition (15) can be interpreted as a critical relation to separate the stable cracks from the unstable ones.

The other method is based on the use of equation (13). If t_c is the characteristic time of rapid fracture, the value of l_{**} can be found from the condition:

$$\mathbf{E}\,[\Delta\tau] \sim t_c \tag{16}$$

A more minute analysis has to allow for the strength scatter between the individual elements. The lower bound on the probability distribution function of critical length l_{**} at the given stress s can be obtained from the condition that with a loss of crack stability all structural elements located on its tip will be broken almost imme-

diately. The total number of these elements is $\sim \pi l_{**}/\rho$. This suggests:

$$F(l_{**}; s) \approx \{F_r[\varkappa(l_{**})\, s]\}^{\pi l_{**}/\rho} \tag{17}$$

Up to now the impact of dispersed damage on macrocrack stability has not been taken into account. The dispersed damage rate ψ is approximately equal to the probability of a random structural element arriving at the crack tip already broken. Hence, instead of (15) one obtains an equation for the determination of l_{**}:

$$F_r[\varkappa(l)\, s] + \psi \sim 1 \tag{18}$$

In order to include the dispersed damage with approximately the same accuracy level it is sufficient to substitute the exponent in equation (17) by $\pi l\,(1 - \psi)/\rho$.

2.3 GRANULAR COMPOSITE

Let us consider a material reinforced with spheroidal grains with a characteristic size of the order of ρ (Fig. 2.2). All grains belong to the same statistical ensemble so that the scattering

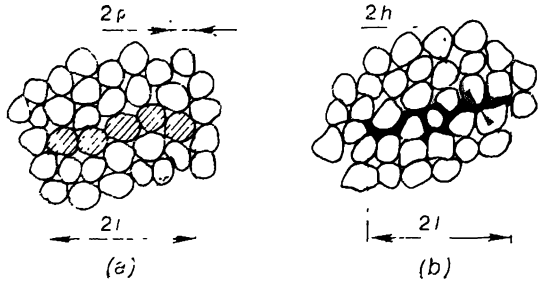

Fig. 2.2 Model of crack in granular composite:
(a) crack passes through grains; *(b)* crack passes through interface

in the grain properties is brought about by the different grain orientations relative to nominal stress and by random grain defects. An analogous assumption is suggested concerning the matrix properties. Given the grain-matrix interface of sufficiently high strength it is only natural to adopt a grain as the structural element. If this interface is weak it is natural to adopt a matrix interlayer as the structural element. In the first case (Fig. 2.2*a*) the fracture of a structural element is the exhaustion of the grain capability of the plastic deformation or the initiation of cracks in this element, with cracks crossing the whole of the grain. By the macrocrack a bonded set of broken grains will be meant, the crack clearance being taken equal to 2ρ and the curvature radius ρ_1 at the crack tip is ρ. In the second case (Fig. 2.2*b*) $\rho_1 \sim h$, where $2h$ is the characteristic thickness of

a matrix layer. Generally both mechanisms take place with $h \leqslant \leqslant \rho_1 \leqslant \rho$. This scheme is also applicable to conventional polycrystalline metals and alloys. The role of grains is played by individual crystallites, and that of the matrix by the interface. The characteristic thickness of $2h$ can be by several orders of magnitude smaller than that of the crystallite.

Equation (2) will be taken in the following form:

$$d\varphi/dt = \begin{cases} 0 & (s < r_0) \\ (1/t_c)\,[(s-r_0)/(r-r_0)]^m & (s \geqslant r_0) \end{cases} \tag{19}$$

Here t_c is the characteristic time of a short-term test and the exponent $m > 0$ characterizes grain properties relative to the delayed fracture, creep, or fatigue. A threshold value of strength $r_0 \gg 0$ is placed in equation (19).

A single random parameter in equation (19) is assumed to be the characteristic grain strength r. Let us take for r the following distribution consistent with the right-hand side of equation (19):

$$F_r(r) = \begin{cases} 0 & (r < r_0) \\ [(r-r_0)/(r_c-r_0)]^\alpha & (r_0 \leqslant r \leqslant r_c) \\ 1 & (r > r_c) \end{cases} \tag{20}$$

At first glance distribution (20) seems to be an artificial one. Yet in fact it reflects the nature of both the granular composites and of the polycrystalline materials. The lower bound of strength r_c corresponds to grains or crystallites oriented in the least favourable way relative to the field of nominal stresses. The upper bound r_c corresponds to the grains or crystallites with the most favourable orientation. The exponent in (20) is $\alpha > 0$. As an example let us take the case of $s = \text{const}$. An approximate expression for the dispersed damage rate follows from relations (5), (19) and (20):

$$\psi(t) \approx \begin{cases} 0 & (s < r_0) \\ [(s-r_0)/(r_c-r_0)]^\alpha\,(t/t_c)^\beta & (r_0 \leqslant s \leqslant r_c) \\ (t/t_c)^\beta & (s > r_c) \end{cases} \tag{21}$$

The exponents α and β are related by $\beta = \alpha/m$.

To find the probability distribution function of the times to macrocrack initiation expression (21) must be substituted into (9). This will result in the three-parameter Weibull distribution. It is of interest to evaluate the magnitude of scale effect in the model considered here. Let us consider, for example, the ratio of the mathematical expectations of the times t_1 and t_2 until the macrocrack appears at the given level of stress. If $r_0 \ll r_c$, then:

$$\mathbf{E}[t_1]/\mathbf{E}(t_2) \approx (N_2/N_1)^{1/\beta n_*} \tag{22}$$

where N_1 and N_2 are the numbers of structural elements in the volumes V_1 and V_2, respectively. If a macrocrack initiates with the same probability at any point of the volume, then $N_1/N_2 = V_1/V_2$. If the crack initiation is conditioned only by the grains located at the specimen surface (this as a rule holds for industrial materials and alloys) then $N_1/N_2 = (V_2/V_1)^{2/3}$ for geometrically similar specimens.

It is essential that the exponent βn_*, characterizing the scale effect at crack initiation, can be obtained from the corresponding exponent for a grain through the multiplication by the number of grains n_* forming the nucleus of a macrocrack. The larger the number n_*, the smaller will be the scatter of the times to the crack initiation and the smaller will be the scale effect.

To obtain equations similar in form to those of fracture mechanics an equation for the rate of macrocrack growth is used in a simplified form (14).

Apart from the function $f(s, r)$ given by the right-hand side of equation (2) and the probability density $p_r(r)$ given by the distribution function $F_r(r)$ this equation also contains the stress concentration factor $\varkappa(l)$ at the crack tip. Let us take as an example a penny-shape crack (while similar results can be produced by a crack under plane strain conditions, an edge crack, etc.) and let us imagine this crack as an oblate ellipsoid with semiaxes l, l and ρ_1. The material is assumed to be linearly elastic up to the moment of fracture. The stress distribution near the ellipsoid cavity can be obtained from the solution of Sack's problem. As an approximate estimate one can take:

$$\varkappa \sim (l/\rho_1)^{1/2} \tag{23}$$

Substituting the above expressions into equation (14) one obtains

$$dl/dt \sim \frac{2\rho}{t_c}\frac{m+\alpha}{\alpha}\left[\frac{(l/\rho_1)^{1/2}s - r_0}{r_c - r_0}\right]^m \tag{24}$$

If as usual one introduces a stress intensity factor

$$K = s(\pi l)^{1/2} \tag{25}$$

equation (24) can then be written as:

$$dl/dt \sim c\,[(K - K_0)/(K_c - K_0)]^m \tag{26}$$

where the following notations

$$r_c \cdot (\pi\rho_1)^{-1/2} = K_c, \quad r_0(\pi\rho_1)^{-1/2} = K_0, \quad c = (2\rho/t_c)\,[(m + \alpha)/\alpha] \tag{27}$$

are introduced.

The parameter K_c holds for the characteristic value of the intensity factor. It will be shown below that the latter approximates the critical value in the Griffith-Irwin stability criterion. The parameter K_0 holds for the threshold value of the intensity factor.

Equation (26) is analogous to that of Paris-Erdogan, transforming into the latter under an assumption of $K_0 \ll K_c$, $K \ll K_c$. The exponent in this equation proves to be the same as that of the quantile stress-time curves for structural elements. A constant c which is stated empirically in the Paris-Erdogan equation, achieves a certain meaning according to the last formula from (27). It is expressed through the exponents entering into the distribution of strength and times to fracture of structural elements, through the characteristic grain size and characteristic time of short-term testing.

Conditions (15)-(17) are used to find the critical size of crack l_{**}. Let us take, e.g., condition (15). It results in the relation $l_{**}/\rho_1 \sim (r_c/s)^2$, which corresponds to the Griffith-Irwin criterion

$$K = K_c \tag{28}$$

Here the critical value of the intensity factor K_c is defined according to the first formula of (27). Similarly relation (10) gives:

$$K \approx K_c + [\alpha/(m+\alpha)]^{1/m} (K_c - K_0) \tag{29}$$

Since generally $m \sim \alpha \gg 1$ relation (29) is almost the same as (28). An approximate expression for the distribution function of the critical crack size is given by formula (17). Substituting expressions (20) and (23) and using notations (27) one obtains:

$$F_K(K;\ l/\rho_1) \approx \begin{cases} 0 & (K < K_0) \\ [(K - K_0)/(K_c - K_0)]^{\pi l\alpha/\rho_1} & (K_0 \leqslant K \leqslant K_c) \\ 1 & (K > K_c) \end{cases} \tag{30}$$

According to formula (30) the critical intensity factor is a random quantity with a distribution within an interval $[K_0,\ K_c]$ depending on the exponent $\pi l\alpha/\rho_1$. Since $\pi l\alpha/\rho_1 \gg 1$, the mathematical expectation is defined as:

$$\mathbf{E}[K] \approx K_c - (\rho_1/\pi l\alpha)(K_c - K_0) \tag{31}$$

It is obvious that relations (29)-(31) are almost equivalent.

To take into account the influence of dispersed damage one uses the approximate relation (18). In terms of stress intensity factors it takes the following form for the model considered here:

$$K \approx K_0 + (K_c - K_0)(1 - \psi)^{1/\alpha} \tag{32}$$

Assume that s = const. The fracture rate is then given by formula (21). In short-term testing $t \sim t_c$. If one introduces an additional assumption $K_0 \ll K_c$ formula (32) will be written as:

$$K \approx K_c [1 - (s/r_c)^\alpha]^{1/\alpha} \tag{33}$$

Similar results will be obtained when one introduces correction for dispersed damage into relations (29) and (30).

We have studied all the main stages of damage and fracture of the granular composite as well as of the polycrystalline materials in the framework of the unified model. It has been possible to obtain the main equations of fracture mechanics and all the parameters entering into these equations appear to be closely correlated. Some conclusions can be verified directly with macroexperiments. For example, it follows from the theory that the exponent of the quantile stress-time curves till the initiation of the macrocrack should approximate the exponent in equations of the Paris-Erdogan type. Generally this is not observed in experiments while the conventional value of $m = 4$ is quite reasonable for some materials. Maybe it could be possible to obtain a better agreement if the finite plastic zone on the crack tip and stress concentration in structural elements located at some distance from the tip are introduced into the analysis.

According to the theory developed the critical value of the intensity factor K_* is close to the value K_c given by the first formula of (27). This formula contains the quantities r_c and ρ_1 which generally can vary within a very broad range. It is known [9] that in the case of crystalline bodies the magnitude of K_* can be calculated using the theoretical strength and the spacing of the crystal lattice as r_c and $2\rho_1$, respectively. For granular composites and polycrystals at fracture along matrix or interface it is practical to take as r_c the ultimate stress along this boundary and as $2\rho_1$ the characteristic thickness of an interface layer. Once fracture proceeds through grains one takes as r_c the maximum grain strength and as $2\rho_1$ the grain characteristic size. With the appropriate choice of these parameters it is always possible to obtain a reasonable (in the sense of order of magnitude) value of the critical intensity factor.

In a rigorous sense the critical value K_* is a random quantity. Its mathematical expectation in the framework of the proposed model is given by formula (31). However, the deviation of this random variable is very small and for the variance coefficient w_K one has an estimate:

$$w_K \sim [\rho_1/\pi l\alpha]\,(1 - K_0/K_c) \tag{34}$$

The variance coefficient of developed cracks appears to be very small compared to unity. This concerns the statistical scatter in the critical intensity factor for materials with macroscopically homogeneous properties. The intensity factor scatter can be influenced by changes of these properties dependent on the batch of material, the specific supplier, etc. Examination of this scatter is beyond the scope of the present analysis.

Additional information on the model parameters can be gained by analysing the crack growth rate. An equation of the type (26)

for the case of cyclic loading is usually written as:

$$dK/dn = c_1 (\Delta K)^m \tag{35}$$

Here n is the number of cycles being taken as a continuous variable under conditions of slow growth of cracks, ΔK, the stress intensity factor range, and c, an empirical constant. Comparing equations (35) and (26) at $K_0 \ll K_c$ and taking into account formulas (27) one can evaluate the constant in equation (35) as:

$$c_1 \sim (2\rho/K_c^m)\,[(m + \alpha)/\alpha] \tag{36}$$

Formula (36) complements a set of the known proposals for the relation of the empirical constant in equation (35) with the material properties. This is, incidentally, the only formula containing the grain size as one of the essential parameters. If one substitutes the values $K_c \sim 10^4$ N mm$^{-3/2}$, $\rho \sim 10^{-2}$ mm into formula (36), then at $\alpha \sim m = 4$ one obtains an estimate of c_1 from 10^{-14} up to 10^{-13} (with N and mm as units). The value of constant c_1 is strongly dependent on the exponent m. If, all other values being equal, one puts $m = 5$, then c_1 will be estimated as 10^{-16} up to 10^{-18}.

2.4 UNIDIRECTIONAL FIBROUS COMPOSITE WITH ELASTIC MATRIX

Let us consider a specimen of unidirectional fibrous composite in tension along the fibers. We will assume fibers being linearly elastic till fracture. The matrix will also be taken as linearly elastic and sufficiently ductile to be barred from fracturing. The definition of a structural element for this case is given by formula (1) for the transfer length in elastic deformation of the matrix. The total number of structural elements in the volume V can be evaluated as $N \sim V/(2\pi\rho^2\lambda_e)$.

Assume that the matrix is sufficiently complient compared to fibers, and fiber strength possesses a prominent scale effect. Under these conditions the transverse crack growth will be accompanied by fiber delamination.

More precisely, the matrix does not fracture yet transfer length increases followed by a drop in the concentration factor at the crack tip and by an increase in acting length of fibers encompassed by the tip. Both mechanisms are followed by stress concentration at the crack tip being not essential for unidirectional composites as opposed to granular composites. In the given model one considers such a case when the stress concentration at the crack tip is negligibly small, and the main factor is fiber delamination. Consider an internal transverse crack in a unidirectional composite and assume that the crack cross-section is circular of radius l. According to the model proposed in [8] the crack will be seen as a three-dimen-

ional domain oblong in the fiber direction. Ruptures of individual ibers will be randomly distributed in the volume represented schenatically as a circular cylinder of radius l and length 2λ (Fig. 2.3). n the case of an ideal elastic matrix the dimension λ is defined he same way as the transfer length (1):

$$\iota \sim (l\rho)^{1/2} (E_f/2G_m)^{1/2} \tag{37}$$

At $l \sim \rho$ formulas (1) and (37) coincide. While there is no real iber delamination, the size 2λ, however, can be treated as the acting ength of fibers encompassed by the crack tip.

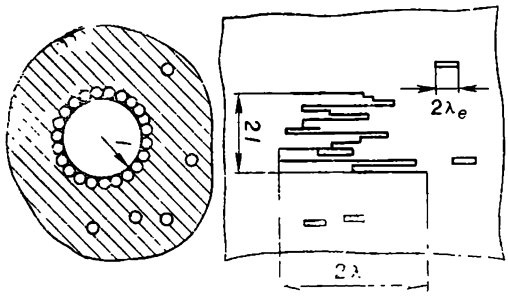

Fig. 2.3 Model of internal transverse crack in unidirectional composite

For structural elements we will take equation (2) allowing for he scale effect of fiber strength. The most natural method is for r o be considered a random variable with the λ-dependent distribuion function. As is often the case in the analysis of fibrous composites we use Weibull's distribution:

$$F_r(r;\ \lambda) = 1 - \exp\{-(\lambda/\rho)\,[(r - r_0)/(r_c - r_0)]^{\alpha}\} \tag{38}$$

The same notations as those in formula (20) are used here, and the scale effect is introduced through the factor λ/ρ. Hence r_c is the characteristic short-term strength of a fiber segment 2ρ long. Since n testing one actually takes significantly longer fibers, the value of r_c is estimated by extrapolation.

Assume that $s = \text{const}$. The fracture rate calculated by means of formulas (8) and (38) is then defined as:

$$\psi(t) = 1 - \exp\{-(\lambda_e/\rho)\,[(s - r_0)/(r_c - r_0)]^{\alpha}\,(t/t_c)^{\beta}\} \tag{39}$$

Plots of $\psi(t)$ are given in Fig. 2.4. The following data were used: $n = 4$, $\lambda_e/\rho = 10^2$, $r_0 = 0$, $s/r_c = 10^{-1}$. The fine lines in Fig. 2.4 show the plots of functions $\psi(t)$ at $\dot{s} = \text{const}$ with $\dot{s}t_c/r_c = 10^{-3}$. The values of the exponent α are indicated near the curves. While he curves are plotted up to the values of $\psi \approx 1$, the model in ques-

tion is unsuitable even at relatively small values of fracture rate This is because interaction between structural elements in thi model at the present stage is not allowed for. Moreover, the critica values ψ^* corresponding to the specimen fracture owing to loss o

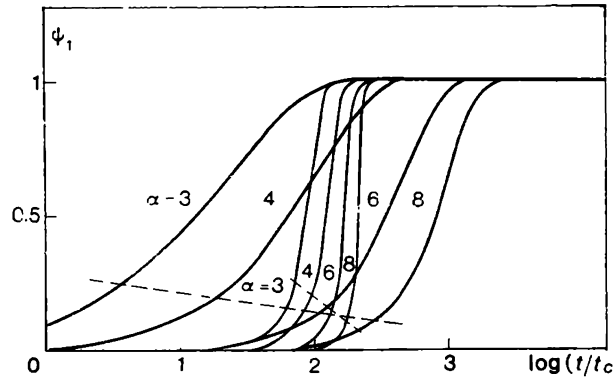

Fig. 2.4 Time variation of damage rate for different loadin modes and different values of exponent α

integrity are rather small, in the order of 10^{-1}. Therefore in th region of model applicability it is possible to use a simpler expres sion for $\psi(t)$:

$$\psi(t) \approx (\lambda_e/\rho)\,[(s - r_0)/(r_c - r_0)]^{\alpha}\,(t/t_c)^{\beta} \qquad (40$$

Plots in Fig. 2.5 show the time dependence of the variable:

$$L = \log(s^2\dot{\psi}/I_0) \qquad (41$$

where I_0 = const. This quantity features the logarithmic level o strain energy released per unit time as a result of fibers rupture To the first approximation, a value from formula (41) may be con sidered proportional to the level of sound emission under nondestruc tive testing. The effects of the matrix fracture as well as the ruptur association are not taken into account by formula (41).

Let us calculate the magnitude of ultimate stress in short-tern testing. For this $t \sim t_c$ is substituted into (40). The use of condi tion (6) gives a formula

$$s^* \sim r_0 + (r_c - r_0)\,(\psi^*)^{1/\alpha}\,(2G_m/E_f)^{1/2\alpha} \qquad (42$$

If $r_0 \ll r_c$, then formula (42) differs from Rosen's estimate [10] b a numerical factor. Since for high-strength fibers $\alpha \gg 1$, the facto $(\psi^*)^{1/\alpha}$ is of the order of unity.

To obtain a theoretical estimate for ψ^* we refer to equation (7) As a first approximation one takes stress in fibers of failed compo sites to be in the order of $s\,(1 - \psi)^{-1}$. Equation (7) with short-tern

strength distribution (38) will then have the form:

$$\psi = 1 - \exp\left\{ -\frac{\lambda_e}{\rho} \left[\frac{s(1-\psi)^{-1} - r_0}{r_c - r_0} \right]^{\alpha} \right\} \tag{43}$$

In Fig. 2.6 plots of the function $s(\psi)$ are shown at $r_0 = 0$, $\lambda_e/\rho = 10^2$ and at different values of the exponent α. The descending branches

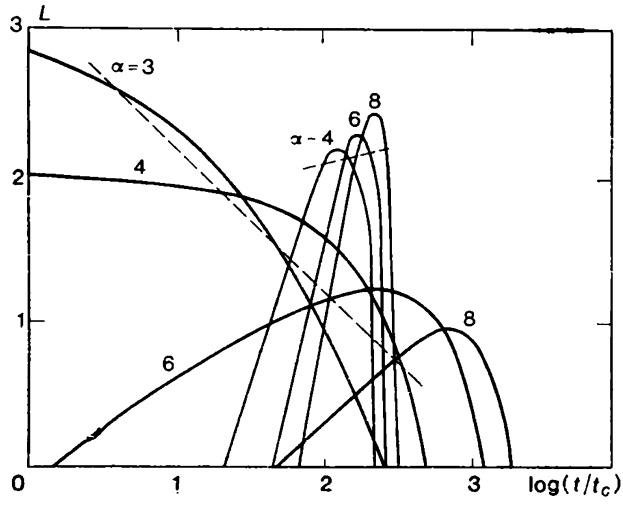

Fig. 2.5 Variation in logarithmic level of released energy for different loading modes and different values of exponent α

of the curves correspond to the critical values ψ^*. The maximum of this function corresponds approximately to the fibers "bundle strength" [2, 10]. At sufficiently large α this maximum is attained in the vicinity of the value:

$$\psi^* \sim 1/(1+\alpha) \tag{44}$$

The dashed lines drawn in Figs. 2.4 and 2.5 correspond to the attainment of the critical value ψ^* by the fracture rate ψ which generally depends on the stress level s. The similar plots at $r_0 = 0.1\, r_c$ are shown in Fig. 2.7. According to these plots the critical values ψ^* are rather strongly dependent on the threshold strength value. Here the maximum of the function $s(\psi)$ is attained near $\psi = 0.1$ for all of the values α considered. At sufficiently large ψ the above plots are unusable since the assumptions under which they were obtained become meaningless.

Let us now consider the initiation and growth of transverse macrocracks. The general formula (9), with allowance made for (39), is of the form (s = const):

$$F_*(t_*) \sim 1 - \exp\left[-N \left(\frac{\lambda_e}{\rho}\right)^{n_*} \left(\frac{s-r}{r_c - r_0}\right)^{\alpha n_*} \left(\frac{t_*}{t_c}\right)^{\beta n_*} \right] \tag{45}$$

and explicitly includes the scale effect. For a hexagonal array o fibers the reasonable estimate of a number of ruptures formin a macrocrack nucleus gives $n_* = 7$.

The approximate equation (14) is used for the crack growth rate Allowing for relations (19), (37), and (38) one obtains:

$$dl/dt \sim \frac{2\rho}{t_c}\left(\frac{l}{\rho}\right)^{1/2\beta}\left(\frac{\varkappa s - r_0}{r_c - r_0}\right)^m \left(\frac{E_f}{2G_m}\right)^{1/2\beta} \tag{46}$$

Here a factor of the order of unity containing an incomplete gamma function is omitted. The effective stress concentration factor $\varkappa$ i

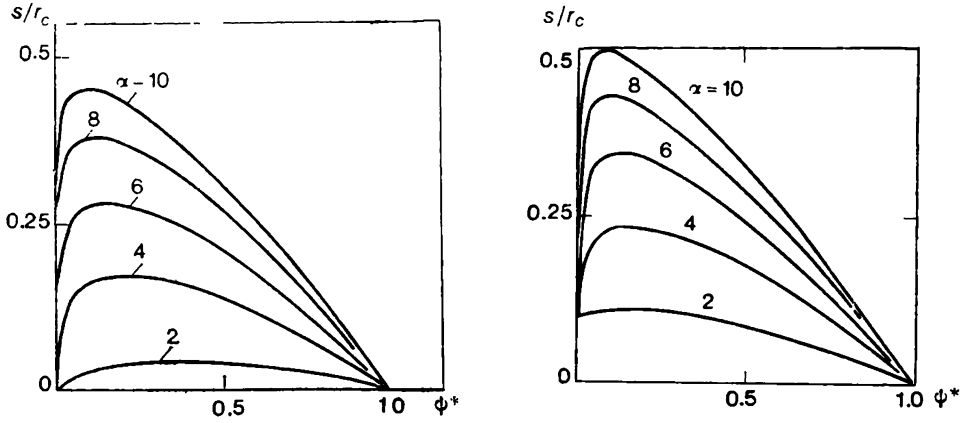

Fig. 2.6 Critical damage level ψ^* versus nominal stress s (descend ing branch of the curve) at $r_0 = 0$

Fig. 2.7 The same as Fig. 2.6, but at $r_0 = 0.1 r_c$

introduced into the right-hand side of equation (46). This facto depends on the transverse crack size l and the longitudinal one λ both being connected in turn through relation (37). Reasons exis to expect that with an increase in the crack size the factor $\varkappa$ doe not increase but even decreases approaching unity.

Let us evaluate the size l_{**} of a transverse crack in unidirectiona composite. It follows from the simplest condition (15) that

$$l_{**} \sim \rho\left(\frac{r_c - r_0}{\varkappa s - r_0}\right)^{2\alpha} \frac{2G_m}{E_f} \tag{47}$$

The critical size l_{**} is a random quantity. Its distribution functio is approximated by a formula similar to (17). Taking into accoun formulas (37) and (38) one then obtains

$$F_l(l_{**}) = \left\{1 - \exp\left[-\frac{\lambda_e}{\rho}\left(\frac{l_{**}}{\rho}\right)^{1/2}\left(\frac{\varkappa s - r_0}{r_c - r_0}\right)^{\alpha}\right]\right\}^{\pi l_{**}/\rho} \tag{48}$$

The diagram of quantiles of a ratio l_{**}/ρ as a function of the stress level s/r_c is shown in Fig. 2.8. The diagram was plotted taking $\varkappa = 1$, $r_0 = 0$, $\alpha = 5$, $\lambda_e/\rho = 10$. It exhibits the weak dependence of critical stress on the crack size, i.e. the high fracture toughness of unidirectional composite. However, it should be noted that this conclusion is related to transverse cracks initiated in a natural

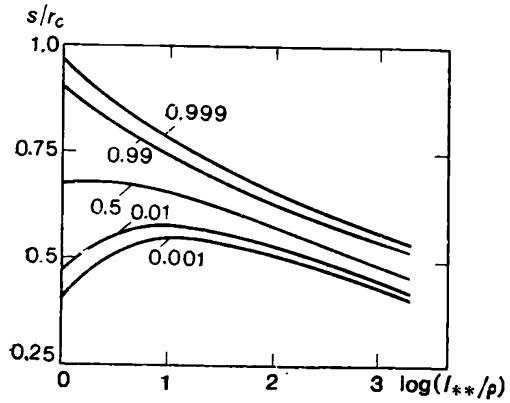

Fig. 2.8 Quantiles of critical crack size l_{**} versus nominal stress level s

way and thus having substantial delamination on the tip. Besides, with the numerical data used in Fig. 2.8 fracture through loss of integrity takes place at much lower stress than that resulting from unstable crack growth.

It is known that the fracture mechanics developed for quasi-homogeneous polycrystalline materials has restricted application to oriented composites. It is especially true in the case of unidirectional fibrous composites. In fact the above estimates coincide with the corresponding results of fracture mechanics only under certain strict conditions. For example, the Paris-Erdogan equation follows from equation (46) only under the condition $\alpha = 1$. This in turn means that Weibull's distribution (38) reduces to the particular case, i.e. to an exponential distribution. It is interesting to note that a similar condition must be placed so that condition (47) coincides with the Griffith-Irwin criterion (the additional condition to have $r_0 \ll r_c$, $\varkappa \sim 1$ is not so onerous).

The above conclusions may seem surprising yet they have a profound meaning. High-strength unidirectional fibrous composites are to a large extent the opposite to conventional materials. Damage and fracture of composites incorporate at least two mechanisms acting simultaneously—rupture and delamination of fibers—and properties of composites are determined at least by two characteristic lengths—by the fiber radius ρ and by the transfer length λ_e.

Therefore one should not expect that fracture mechanics, with its main achievements essentially being the results of similitude relationships, could be applicable to the given case. Yet if $\alpha = 1$ then composite properties closely approach those of conventional materials. However, the above-cited value of α is not encountered in practice. Actually the strength scatter of industrial-use fibers is not so large and the exponent α takes values in the order of $\alpha = 5$ and larger. Therefore the case of $\alpha = 1$ is of academic interest only.

Since the parameters r_c, r_0, α, β can be found from macroscopic experiments, all of the coefficients entering into relations (40)-(48) can be taken as known ones, and these relations applied to obtain approximate estimates of the influence of the component's parameters on the strength and durability of composites.

2.5 UNIDIRECTIONAL FIBROUS COMPOSITE WITH PLASTIC MATRIX

Consider once again a unidirectional fibrous composite in tension along fibers. In contrast to the preceding model let us take the matrix as an ideal plastic one. More exactly, let us assume that when the shear stresses τ_m in the matrix reach the limit $\bar{\tau}_m$ they remain constant and equal to $\bar{\tau}_m$. The quantity $\bar{\tau}_m$ can be interpreted as a yield stress of the matrix material in shear, as a limit stress at the matrix-fiber interface, as a friction stress, or generally as some limit stress including all inelastic phenomena in the matrix occurring close to a crack tip or to a ruptured fiber. Evidently, in the case of a plastic matrix it is impossible to have only a single damage rate ψ. Denote this rate by ψ_1 which is the ratio of the primary broken elements number to their total. As a second damage rate ψ_2 one introduces a ratio of the sum of all damaged fibers' lengths to the total fiber length in the specimen [8]. Considering that the plastic transfer length is estimated as follows:

$$\lambda_p \sim \rho s/(2\bar{\tau}_m) \tag{49}$$

one obtains the following expression for the second damage rate:

$$\psi_2(t) = \int_0^t \Lambda(t, \tau)\, d\psi_1(\tau) \tag{50}$$

The kernel in (50) is of the form:

$$\Lambda(t, \tau) = \begin{cases} 0 & (s(t, \tau) < s_Y) \\ s(t, \tau)/s_Y - 1 & (s(t, \tau) \geqslant s_Y) \end{cases} \tag{51}$$

where $\sigma(t, \tau) = \exp\gamma(\tau_1)$ at $\tau_1 \in [\tau, t]$, and ε_Y is the nominal strain level corresponding to the onset of matrix inelastic deformation. To evaluate the quantity ε_Y it is sufficient to equalize the tensile lengths given by formulas (1) and (40):

$$\varepsilon_Y \sim 2\bar{\tau}_m (E_f/2G_m)^{1/2} \tag{52}$$

If $\sigma(t)$ is a quasistationary increasing function then $\varphi_2 = 0$ at $\varepsilon < \varepsilon_Y$ and $\varphi_1 = 0$ at $\sigma > \sigma_Y$. It is expedient to introduce a third damage rate $\varphi_3 = \varphi_2 - \varphi_1$ equal to the ratio of the sum

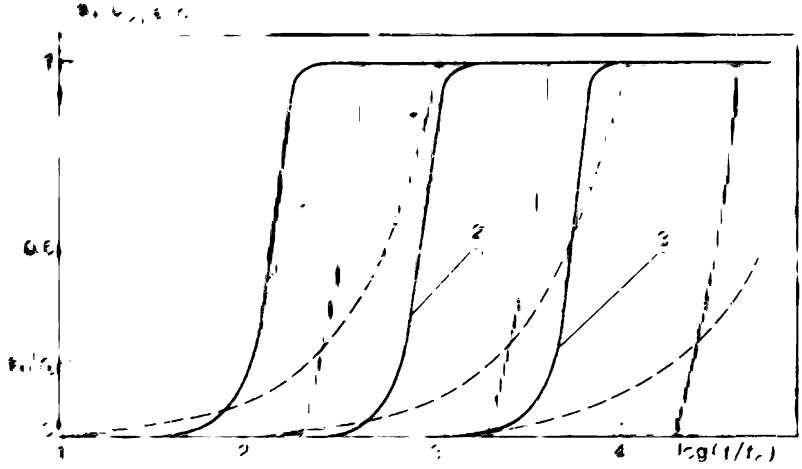

Fig. 2.9. Time damage rates for a composite with plastic matrix

of all tensile lengths to the total length of all fibers. The condition $\varphi_1 = 1$ signifies the fracture of all primary elements and $\varphi_2 = 1$ the total delamination of the specimen. Actually φ_1 and φ_2 are sufficiently small compared to unity because at comparatively low damage densities either composite loss of integrity or macrocrack nucleation takes place.

Results of calculations for $\sigma = \text{const}$ are plotted in Fig. 2.9. Solid lines correspond to φ_1, fine lines correspond to φ_2 and a process $\sigma(t)$ is represented by dashed lines. The numerical data were used as follows: $m = \alpha = 4$, $\lambda_0 = 10^6$, $r_0 = 0$, $\varepsilon_Y r_c = 0.2$. The values of $\sigma_c r$ for the curves 1, 2, and 3 were chosen to be 10^{-6}, 10^{-5}, and 10^{-4}, respectively.

Assume that $\sigma = \varepsilon_Y$. To estimate an order of magnitude of ultimate stress in short-term testing a condition $\varphi_3 = \varphi^*$ is used, on the left-hand side, in contrast to condition (6), the damage rate φ_3 is placed. For monotonously increasing stresses $\varphi_3 = (d\varepsilon_Y)\varphi_1$, where φ_1 is determined by Eq. (44). The ultimate stress σ^* can be

found from the equation:

$$(s/2\bar{\tau}_m)\,[(s-r_0)/(r_c-r_0)]^{\alpha}=\psi^* \tag{53}$$

If $r_0 \approx 0$ the explicit formula follows

$$s^* \sim r_c\,(\psi^*)^{1/(\alpha+1)}\,(2\bar{\tau}_m/r_c)^{1/(\alpha+1)} \tag{54}$$

This formula shows that s^* depends not only on the characteristic fiber strengths and their statistical distribution but also on the degree of matrix plasticity. Formula (54) differs greatly from (42) obtained for the elastically deformed matrix.

As with elastic matrix we will treat the penny-shape transverse crack as a three-dimensional domain in the form of a circular cylinder (Fig. 2.3). Unlike (37) the characteristic crack length along fibers will be:

$$\lambda \sim ls/(2\bar{\tau}_m) \tag{55}$$

Omitting details we give as an estimate of the crack growth rate:

$$dl/dt \sim \frac{2\rho}{t_c}\left(\frac{l}{\rho}\right)^{1/\beta}\left(\frac{\varkappa s-r_0}{r_c-r_0}\right)^{m}\left(\frac{s}{2\bar{\tau}_m}\right)^{1/\beta} \tag{56}$$

Its critical size is

$$l_{**} \sim \rho\,[(r_c-r_0)/(\varkappa s-r_0)]^{\alpha}\,(2\bar{\tau}_m/s) \tag{57}$$

It should be noted that for plastic matrix Paris-Erdogan's equation and Griffith-Irwin's criterion follow from equations (56) and (57) only under the special condition $\alpha = 1$. Besides, one needs to put $r_0 \ll r_c$, $r_0 \ll \varkappa s$. Thus these results of classical mechanics of fracture are applicable to composites with a plastic matrix only for fiber strengths which follow an exponential distribution. It should be noted also that at $\alpha = 1$ the exponent on the right-hand side of equation (56) proves to be $2m$ while for the elastic matrix this index is m.

2.6 SOME GENERALIZATIONS

So far we have only been considered the simplest case of a granular or unidirectional fibrous composite in tension along fibers. This case is also a basic one for subsequent extension to more general cases of reinforcement, loading, and crack initiation. For instance, a specimen of unidirectional composite is assumed to have a cut inclined at an angle θ to the fiber direction (Fig. 2.10*a*). To the first approximation this case can be reduced to the basic one with the characteristic crack size of $l_0 \sin\theta$. After the delamination of the first fibers at the crack tip the situation only slightly differs from that mentioned above (Fig. 2.3). A transition from the inner

circular crack to the edge and through cracks under the condition of nominal plane stress or plane strain requires only very smal modifications of formulas and many estimates of the order of mag nitude remain unchanged. Let us consider the ways of generalizin results for the case when the nominal stress field differs from tensio along fibers. Assume that the stress state is a plane one with th nominal stresses s_x, s_y, and τ where stresses s_x are oriented alon fibers (Fig. 2.10*b*). Here $s_f \sim s_x$. For stresses in the matrix th

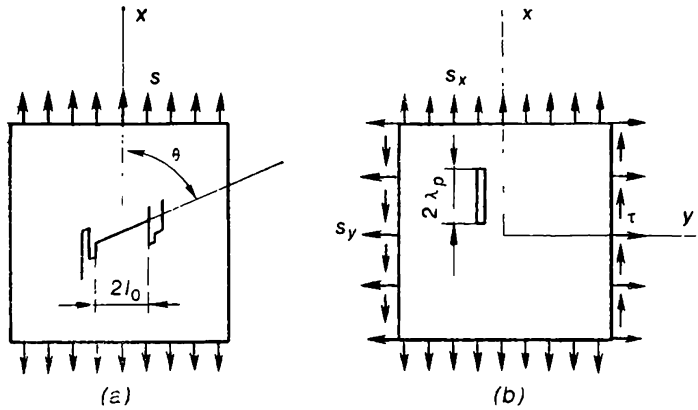

Fig. 2.10 Unidirectional composite with:
(*a*) inclined cut in tension along the fibers; (*b*) transverse crack in nominal plane state o stress

estimates $s_m \sim s_y$, $\tau_m \sim \tau$ are obtained. Let us make a conditio concerning these stresses: in an undamaged composite these do no exceed the limiting values for a matrix. As a condition of the matri strength let us take Mohr's criterion:

$$|\tau| - ks_y < \bar{\tau}_m \tag{58}$$

where $k > 0$ is an empirical constant. Assume that the conditio (58) also includes the matrix flaws and flaws at the matrix-fibe interface of length $\lambda \ll \lambda_e$. As a result the condition of small crac stability in the matrix will be contained in the phenomenologica condition for strength (58).

If the matrix is deformed elastically, the transfer length will b again obtained from formula (1). Therefore, the structural elemen size will be determined as above. The conditions for stress transfe from the broken fibers are substantially changed for inelastic matrix Ineffective segments λ_1 and λ_2 located on different sides of the breal can be found from the condition $2\pi\rho\lambda_{1,2} |\Delta\tau_{1,2}| = \pi\rho^2 s_x$, wher the shear stress increments $\Delta\tau_{1,2}$ are determined from condition (58) $|\tau + \Delta\tau_{1,2}| - ks_y = \bar{\tau}_m$. As a consequence for a half-length o

the damaged zone one obtains $\lambda_p = 1/2\,(\lambda_1 + \lambda_2)$ and instead of formula (1) one obtains:

$$\lambda_p \approx \frac{1}{2}\rho s_x (\bar{\tau}_m + k s_y)\,[(\bar{\tau}_m + k s_y)^2 - \tau^2]^{-1} \tag{59}$$

Composing the equality $\lambda_e = \lambda_p$ one finds the relation between the nominal stresses when the matrix exceeds the bounds of the elasticity range:

$$s_x (\bar{\tau}_m + k s_y) \approx 2\,[(\bar{\tau}_m + k s_y)^2 - \tau^2]\,[E_f/(2G_m)]^{1/2}$$

Formulas (55)-(57) pertaining to cracks with a characteristic transverse size l are changed analogously.

Let us consider the problem of the unidirectional composite fracture in compression along fibers. For a long time it was commonly believed that the fibrous composites fracture in compression along fibers is a local fibers' buckling followed by fiber fracture and matrix cracking. Different methods were used to show [2, 10, 11] that the ultimate stress should have magnitudes in the order of the matrix shear modulus or (which is almost the same in the case of sufficiently compliant matrix) of the order of the composite shear modulus. The simplest estimate of critical stress in composite for the shear (coherent) type of buckling is of the following form:

$$s_* \sim G_m/(1 - v_f) \tag{60}$$

For the incoherent type of buckling one obtains an analogous estimate:

$$s_* \sim [v_f E_f E_m^{tr}/(1 - v_f)]^{1/2} \tag{61}$$

where E_m^{tr} is the matrix transverse Young's modulus calculated taking into account the constraint of the matrix by more rigid fibers. At not so small v_f buckling stress (60) appears to be significantly less than buckling stress (61) and it is precisely the latter which is generally discussed in theoretical and experimental papers.

Formula (60) has been verified experimentally with models of unidirectional fibrous composites as well as with some commercial composites with thick fibers and sufficiently compliant matrix. These experimental results, however, should be approached very carefully. They were produced with very short specimens for the critical stress of overall buckling of the order of the composite shear modulus. Therefore, the corresponding buckling stress should be in any case close to the critical value (60). To obtain the shear mode of buckling experimentally it is necessary to have all fibers parallel and ideally straight.

Commercial fibers possess relatively low strength in compression. This is especially true for organic fibers with a fibrillar structure exhibiting very low strength and stiffness in shear, and, as a conse-

quence, resisting compression very poorly. The fracture of mos commercial composites in compression is accompanied by the fibe breaking and the final fracture pattern is similar to the one observe in testing wood specimens by compression along fibers. The plan of shear can form different angles with the load direction dependin on composite properties. Shear is often observed at angles of about 45° In many cases fracture is accompanied by severe delamination o fibers and even by specimen splitting along vertical planes. Fron all these facts one can infer that even here the basic fracture mecha nism consists in loss of integrity resulting from the fiber breakin and matrix delamination.

The compressed structural elements generally have rather grea flexibility so that the problem of composite strength in compressio is as a rule of minor importance for them. This problem is mor important for bent elements since low resistance in the compresse area can limit the carrying capacity in bending. Hence in the com pressed area even at sufficiently low loading levels loss of integrity cracks and other defects can be produced which are followed by los of sealing, decrease in stiffness in transverse shear and other unde sirable phenomena. The main source of these are inherent techno logical defects, one of which is primarily fiber deviation from a ideal straight form. As the load increases these deviations accumu late accompanied by an increase in matrix shear and compressio ultimate stresses, which after a certain level result in the fractur of matrix material or matrix-fiber interface. To judge the level o composite continuity one requires information concerning the portion of the total fiber length which consists of fiber segment with a failed interface. It must be possible to estimate the maximum possible delamination lengths under the given loading level t compare them to some limiting permissible or critical sizes.

Changing slightly the model of a laminated composite introduced in [11] with small initial irregularities (see also [5]) let us consider a specimen or a certain stressed volume of a fibrous composite in compression along fibers. Let us consider every fiber as having small deviations from the ideal straight form. These deviations represent a sample of a homogeneous random function $w_0(x)$ dependent on the coordinate x taken along the given fiber. Of interest is the character of correlations between the irregularities of adjacent fibers. We shall consider two extreme cases: firstly, when fibers are almost equidistant and, secondly, when no correlation is observed between the irregularities of adjacent fibers. The first case (Fig. 2.11*a*) is typical for composites formed by winding with a relatively large fraction of fiber. In compression of these composites the shear (coherent) mechanism of deformation dominates. The second case is more specific for filament winding and a small fraction of fiber. Here the adjacent fibers are bent almost independently, hence in

compression of the composite along fibers the breaking stress originates in the matrix (Fig. 2.11*b*).

Let us designate the initial irregularities function of the fiber considered as $w_0(x)$ and its spectral density as $S_0(k)$. Here k is the wave number related to the characteristic half-wave length of irregularities by the relation $\lambda_0 = \pi/k$. Assume that both fibers

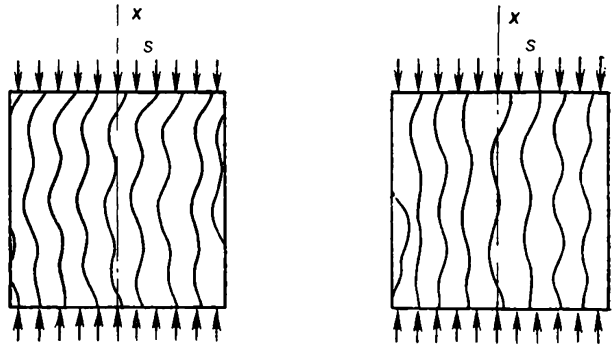

Fig. 2.11 Buckling modes of unidirectional composite in compression:
(*a*) shear (coherent); (*b*) breaking

and matrix remain elastic under the compression load. Then for spectral density $S_w(k)$ of small additional fiber bends $w(x)$ one obtains an approximate formula:

$$S_w(k) = [s/s_*(k) - s]^2 S_0(k) \tag{62}$$

Here $s < s_*(k)$ is the nominal stress in fibers, $s_*(k)$ is the critical magnitude of this stress. The form of the function $s_*(k)$ depends on the deformation mechanism of a fiber embedded in a matrix and interacting with adjacent fibers. With the shear mechanism of deformation one has:

$$s_*(k) = \frac{1}{4} v_f k^2 \rho^2 E_f + G_m/(1 - v_f) \tag{63}$$

With the independent deformation of adjacent fibers when the matrix plays the role of a normally resisting elastic foundation one has:

$$s_*(k) = \frac{1}{4} v_f k^2 \rho^2 E_f + \frac{E_m^{tr}}{k^2 \rho^2 (1 - v_f)} \tag{64}$$

Evidently, the minimization of functions (63) and (64) over the wave-number k leads to estimates (60) and (61), respectively.

Let us consider in more detail the shear mechanism of deformation. For tangential stress in the matrix the estimate is as fol-

lows:

$$\tau_m \sim [G_m/(1 - v_f)]\, \partial w/\partial x$$

which is the source of the formula for the corresponding spectral density:

$$S_\tau(k) = \left[\frac{kG_m}{1-v_f}\,\frac{s}{s_*(k)-s}\right]^2 S_0(k) \tag{65}$$

We may further need the following characteristics too:

$$\sigma_\tau^2 = \int_{-\infty}^{\infty} S_\tau(k)\, dk, \quad \sigma_{\dot\tau}^2 = \int_{-\infty}^{\infty} S_\tau(k)\, k^2\, dk \tag{66}$$

the first of which has the meaning of dispersion of tangential stress τ, and the second one dispersion of the first derivative $d\tau/dx$. If the function of initial irregularities $w_0(x)$ is twice differentiated both integrals of (66) exist.

When at some section of the matrix-fiber interface the tangential stress $\tau_m(x)$ calculated by the given model attains the limiting value $\bar\tau_m$ the above-written relations will, strictly speaking, cease to be applicable. Yet if the sections with a damaged interface occupy a small portion of total fiber length, these relations can be retained since they are related to the composite deformation in total. As a damage rate ψ_4 of the matrix-fiber interface we will use the ratio of the sum of damaged lengths to the total fiber length. This rate can be estimated through the violation probability of the inequality $|\tau_m| < \bar\tau_m$ in any fiber cross-section taken at random. Assume that $w_0(x)$ is a normal random function. Then the function $\tau_m(x)$ will also be a normal one. This suggests that:

$$\psi_4 \sim 2\,[1 - \Phi(\bar\tau_m/\sigma_\tau)] \tag{67}$$

where the relation (66) was used. In the case of large arguments the function $\Phi(u)$ can be replaced by its asymptotic approximation. Omitting the factor of the order of unity one reduces formula (67) to the following form:

$$\psi_4 \sim (\sigma_\tau/\bar\tau_m) \exp(-\bar\tau_m^2/2\sigma_\tau^2) \tag{68}$$

As a numerical example we shall take a case when the initial irregularities spectrum lies in a region of wave numbers with the critical stress $s_*(k)$ adequately determined by formula (60). In conjunction with relations (60), (65) and (66) we find that:

$$\sigma_\tau \sim |s|\,\varphi/(1 - s/s_*) \tag{69}$$

where φ is the mean square value of the deviation angle of fibers in the initial state. In Fig. 2.12 the results of ψ_4 calculations are shown.

Here $\bar{\tau}_m / s_* = 10^{-2}$. The values of angle φ are indicated near the curves. The curve branches at $s < 0$ correspond to composite tension. If $|s| \ll s_*$ the delamination effect will be exhibited in approximately the same way both in compression and in tension.

To evaluate the resistance of composite cracking along fibers one needs to predict the formation of delaminations with a sufficiently large length. Let us illustrate an approach to the solution of this problem. It is known [12] that the distribution of seldom crossings of

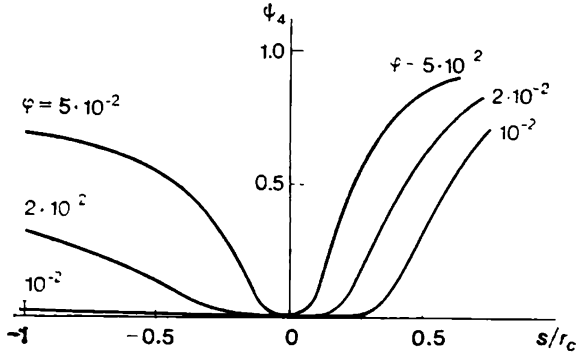

Fig. 2.12 Dependence of delamination rate on nominal stress level in a composite with small fiber waviness

a normal process of the sufficiently high level is described asymptotically by Raleigh's distribution. In application to the given problem for cleavages 2λ long one has a distribution function:

$$F_\lambda(\lambda) \sim 1 - \exp\left\{-\frac{\pi^2}{4}(\lambda^2/\lambda_\tau^2)\,[\bar{\tau}_m^2/(2\sigma_\tau^2)]\right\} \tag{70}$$

where $\lambda_\tau = \sigma_\tau \sigma_*$. On the other hand, the mathematical expectation of the number of crossings off the level $|\tau| < \bar{\tau}_m$ per fiber unit length is defined as:

$$\nu(\bar{\tau}_m) = (1/\lambda_\tau) \exp\left[-\bar{\tau}_m^2/(2\sigma_\tau^2)\right] \tag{71}$$

The portion of crossings with length exceeding 2λ is $1 - F_\lambda(\lambda)$. It is possible to treat such crossings as seldom events and to apply Poisson's model to them. For the probability of an event which consists in the absence of any delaminations with length exceeding 2λ on the segment of the given length L one obtains the formula:

$$P(\lambda) \sim \exp\left\{-\frac{L}{\lambda_\tau}\exp\left[-\frac{\bar{\tau}_m^2}{2\sigma_\tau^2}\left(1+\frac{\pi^2\lambda^2}{4\lambda_\tau^2}\right)\right]\right\} \tag{72}$$

If within the specimen volume all irregularities are coherent the specimen length substitutes for L in formula (72). In the opposite

case one needs to allow for the extent of irregularities correlations in the transverse direction. However, formula (72) remains the basic one in this case too.

The delamination theory of composites is constructed similarly with the completely uncorrelated irregularities of fibers. The critical stress $s_*(k)$ is determined by formula (64) and instead of shear stresses τ_m and $\bar{\tau}_m$ the corresponding normal ultimate stresses s_m and $\bar{s}_m$ are considered. Generally one has to allow for the interaction of these mechanisms and interference of the matrix damage and fiber rupture. If the function $w_0(x)$ is sufficiently narrow-banded, i.e. its samples are sinusoidal functions with slowly changing amplitudes and phases, then the parts where the matrix fracture takes place owing to shear, and the parts where the breaking is most probable will not as a rule coincide. This consideration justifies in part the above-mentioned fracture model with initial fiber imperfections.

References

1. Malmeister, A.K., Tamuzs, V.P., and Teters, G.A., *Strength of Polymer and Composite Materials*, Zinatne, Riga, 1980 (in Russian).
2. Bolotin, V.V. in: *Mechanics of Structures. Present State and Prospects*, Stroiizdat, Moscow, 1972, pp. 65-95 (in Russian).
3. Obraztsov, I.F., and Vasil'ev V.V., in: *Fracture of Composite Materials*, Zinatne, Riga, 1979, pp. 142-148 (in Russian).
4. Protasov, V.D., Ermolenko, A.F., Filipenko A.A., and Dimitrenko, I.P., *Mekh. komposit. materialov*, **2**, 254-261 (1980).
5. Bolotin, V.V., and Novichkov Yu.N., *Mechanics of Multilayered Structures*, Mashinostroyenie, Moscow, 1980 (in Russian).
6. Bolotin, V.V., *Mekh. polimerov*, **2**, 247-255 (1976).
7. Tamuzs, V.P., in: *Fracture of Composite Materials*, Zinatne, Riga, 1979, pp. 17-24 (in Russian).
8. Bolotin, V.V., *Mekh. kompozit. materialov*, **3**, 405-420 (1981).
9. Novozhilov, V.V., *Priklad. matematika i mekhanika*, 2(33), 212-223 (1969).
10. Rosen, B., in: *Fiber Composite Materials*, American Society for Metals, 1965, pp. 54-96.
11. Bolotin, V.V., *Mekh. polimerov*, **1**, 11-19 (1966).
12. Tikhonov, V.I., *Crossings of Random Processes*, Nauka, Moscow, 1970 (in Russian).

3 Theory of Microheterogeneous Fibrous Media

G. A. Vanin, *D. Sc. (Eng.)*

3.1 INTRODUCTION

The structure of fibrous materials is formed by a combination of a large number of fibers and of an interfiber medium, a matrix. Depending on the origin of the material, in its phases it is possible to isolate elements of heterogeneity with a higher structural level. For instance, polymer fibers are a fibrous medium where the role of fibers is taken by fibrils and the bonding medium governs interfibrillar interaction. The process of successive discretization of composites is rational up to the states where the mechanism of the phenomena studied is revealed in greater detail and where it is possible to relate in a quantitative way the introduced parameters to the experimental data on quantities under observation.

The purpose of the microheterogeneous medium theory is to predict, in a quantitative way, the changes in the average physical and mechanical properties of composites with an increase in the number of imperfections during loading using a minimum of initial parameters characterizing the properties, geometry, and imperfection of constituents. The complex structure of material and the diversity of growth modes of cracks and other imperfections present some difficulties for a precise solution of the set problem. As a consequence this solution is sought with certain restrictions often resulting in approximate estimates of the stress state. To simplify the problem formulation only such unidirectionally reinforced materials will be studied that have continuous fibers oriented strictly along the axis x_1.

The integral parts of the theory, immediately preceding stress analysis, are as follows:

(a) construction of a model of the structure;

(b) selection of governing equations for constituents;

(c) isolation of states described with a minimum number of parameters;

(d) construction of a model of interface and structural imperfections;

(e) development of methods of many-body interaction calculations;

(f) introduction of averaged quantities and the determination of the constitutive equations for the composite.

The solution of problems for microheterogeneous bodies is largely framed using and generalizing the studies carried out earlier for homogeneous fibrous media, therefore the major preceding results will be briefly presented below. A theory of highly-filled fibrous materials based on the combination of both a structure regularization method and an assumption of its homogeneous stress-strain state is proposed by the present author in [1, 2]. The allowance for fiber interaction in the simplest structures for slowly varying average stresses was provided by the introduction of doubly periodic Weierstrass functions and special functions constructed in [3]. The above assumptions permitted the general case of stress state to be represented as a superposition of three states—longitudinal shear, longitudinal tension-compression, and transverse tension and shear:

$$[\sigma_{ik}] = \begin{bmatrix} 0 & \sigma_{12} & \sigma_{13} \\ \sigma_{21} & 0 & 0 \\ \sigma_{31} & 0 & 0 \end{bmatrix} + \begin{bmatrix} \sigma_{11} & 0 & 0 \\ 0 & 0 & 0 \\ 0 & 0 & 0 \end{bmatrix} + \begin{bmatrix} 0 & 0 & 0 \\ 0 & \sigma_{22} & \sigma_{23} \\ 0 & \sigma_{32} & \sigma_{33} \end{bmatrix} \tag{1}$$

Because of the existence of a symmetry plane perpendicular to the fiber orientation the longitudinal shear state is independent of the others while the remaining two are interrelated. An exact (within the limitations imposed) solution of the problem of the transverse stress state can be found from a known solution of the problem of longitudinal tension-compression. The solution of problems for all the listed loading cases enables the average elastic constants of reinforced medium to be determined, relating the averaged components of stress tensor $\langle\sigma_{ik}\rangle$ to those of strain tensor $\langle\varepsilon_{ik}\rangle$:

$$\langle\varepsilon_{ik}\rangle = Z_{iksn}\,\langle\sigma_{sn}\rangle \tag{2}$$

Hence a relation is established between the symmetry of structure and the number of significantly different elastic moduli as well as the dependence of the constants Z_{iksn} on geometry and phase properties. The numerical calculations were mainly carried out for hexagonal (chess-board), tetragonal (square), and parallel row fiber distributions. The existence of two types of interfiber interactions was revealed: a smoothed one and one oscillating about an individual fiber. The first interaction is determined with a high accuracy in considering the interaction of an isolated fiber with the matrix and is the main contribution to the elastic moduli values and internal stress field at the relative volume fraction of fibers $v \leqslant 0.5$. The amplitude of oscillating interaction is a function of the distance between fibers and of their orientation relative to the inclusion considered. This interaction controls the increasing concentration of internal stresses with a build-up of v and provides an essential contribution to the values of moduli of highly-filled composites. Therefore, composite calculations by means of isolated fiber model are only

reliable with weak oscillating interactions. The longitudinal tension of fibrous materials owing to the transverse effects and fiber interactions is accompanied by local transverse tensile and shearing stresses [4, 5].

Further generalizations using Volterra's principle and asymptotic formulas for the reduced elastic constants resulted in the construction of constitutive equations and of explicit expressions for operators of anisotropic viscoelasticity theory under conditions of three-dimensional stress-strain state. The investigations of fibrous media with due regard for thermal phase expansion and viscoelastic matrix properties permitted the formulation of constitutive equations of anisotropic thermal viscoelasticity [5]. The components of the thermal expansion tensor of fibrous material are expressed in a simple way through the thermal and mechanical characteristics of constituent phases and through the average elastic constants of composite [2]. These relations formed the basis of the theory of curing stress initiation of composites, disregarding the chemical reactions and assuming the matrix material to be a linearly viscoelastic one [1].

In later works a number of authors investigated the properties of fibrous materials taking into account the rectilinear and curvilinear anisotropy of fibers and matrix as well as the new geometrical factors.

Using a solution of the problem of the stress state of perforated plates the authors of [6] analyzed an approximate solution of the problem of determination of average elastic moduli and the internal stress field in a transverse stress state. In so doing the above mentioned relation of the problems of longitudinal and transverse stress states was not taken into account. Another way of investigating elastic fibrous materials with a regular structure is proposed in [7]. Using the Airy stress function the authors constructed a complete solution of the problem of stress-strain state for materials with unidirectional reinforcement. They indicated not only the exact solutions but also the approximate ones and evaluated their errors. The results for an individual layer were used to describe laminated materials with varied fiber orientation in the reinforced plates.

The model of unidirectionally reinforced media is broadly applied to construct a model of materials with complex and woven structure in [7, 8], as well as in [9].

Numerous studies of reinforced materials using other methods and models can be found in [8, 10-12].

To investigate the general type of periodic structures, when the parallelogram of periods contains a finite number of arbitrarily oriented fibers, the present author proposed a solution [2] in which fiber interaction is allowed for by a general representation of the elliptic function specified by Whittaker and Watson [13], as well as

by special functions. The discovered solution made it possible to establish the dependence of averaged elastic constants on the symmetry of relative orientation of fibers and on the properties of solid and hollow fibers for a complex monoclinic structure as well as for multicomponent composites [2].

In the following works [14, 15] the solution of the problems of two-dimensional stress state of periodic media was constructed with the aid of Koiter's representation using the Weierstrass function instead of Cauchy's kernel. These solutions allow for the rectilinear anisotropy of fibers and matrix, and also cover noncircular fibers. The calculations performed indicate the strong influence of fiber anisotropy on elastic moduli, a fact not observed in experiment. The latter is explained by the absence of an ordered orientation of fiber symmetry axes in real materials.

The problems of reduced parameters determination for quasistatic diffusion processes of heat transfer and electromagnetic radiation were solved in an analogous way. The representations found allowed the study of related phenomena in reinforced media: thermoelectric, galvanomagnetic, piezoelectric, piezooptic, etc. [16].

An investigation of HF processes with elastic and electromagnetic waves was performed by constructing the solutions for individual cells with a limited number of fibers by means of special functions and subsequently averaging the wave fields [5]. The next step in the development of fibrous material theory is associated with the incorporation of imperfections into the structure. The present author suggested a method of determining reduced moduli, stress fields, and a condition of local fracture for a fibrous medium [17], [18].

The maximum stress concentration near the interface favours the initiation of equidistant cracks relative to interface planes. Using the method of asymptotic concordance proposed earlier [17] the authors of works [14, 15] constructed a solution of the longitudinal shear problem of a medium reinforced with rectilinearly anisotropic fibers allowing for the anisotropy of matrix and crack at the interface. A method of solving the problems with heterogeneous curvilinear anisotropy of fibers is suggested below.

3.2 FUNDAMENTAL PROPOSITIONS

3.2.1 When choosing the structure models and typology of imperfections it is expedient to have the experimental data on fiber distribution in the structure for the given fabrication method. In the unidirectionally reinforced glass-fiber plastic obtained by continuous drawing most of the fibers are so distributed that the angles between straight lines connecting the centres of adjacent fibers are found to be within an interval from $2\pi/7$ to $\pi/3$ [19]. Therefore, for the material considered the hexagonal packing is one of the probable.

thermodynamic equilibrium. The ensemble also includes a limiting case of a medium in which the sizes of inclusions decrease infinitely, conserving their volume fraction in the cell. Here the internal field approaches a uniform one and is totally determined by a minimum of thermodynamic parameters.

A criterion of equivalency of regular media states is introduced as follows:

(1) the group elements characterizing the symmetry of isolated volumes coincide;

(2) with an increase in the same type of parameters determining the medium state the thermodynamic potentials of these volumes acquire equal increments.

The necessity of satisfying the first condition follows from Curie's symmetry principle. The satisfaction of the second condition requires

$$\delta \langle \tilde{F} \rangle = (1/V) \sum_{j=1}^{N} \int_{V_j} \delta F_j \, dv \tag{3}$$

here $\langle \tilde{F} \rangle$ is the specific thermodynamic potential of a medium with an equivalent state, F_j is the specific thermodynamic potential of the jth component in a cell for a medium from the ensemble, V is the cell volume, V_j is the volume taken in V by the jth component. In the case of media with a great number of cracks this relation should be formulated per unit mass. It determines the average values of thermodynamic parameters for the composite when $\langle \tilde{F} \rangle$ is established for a homogeneous medium.

Let now the fibrous dielectric medium also be placed in an elec tric field $\boldsymbol{E}$. The change in free energy is described by the relation

$$dF = -s\,dT + \sigma_{ik} d\varepsilon_{ik} + \boldsymbol{E} \cdot d\boldsymbol{D} \tag{4}$$

where the commonly adopted notations are used.

To satisfy the equivalent relations one requires the equality of elements from a point symmetry group of the composite medium considered and of that chosen from the ensemble, and also the satisfaction of the following condition:

$$\delta \langle \tilde{F} \rangle = (1/V) \sum_{j=1}^{N} \int_{V_j} (-s\,dT + \sigma_{ik}\, d\varepsilon_{ik} + \boldsymbol{E} \cdot d\boldsymbol{D})\, dV \tag{5}$$

For isothermal processes, transforming the volume integrals into the surface ones and taking into account the equality

$$\boldsymbol{E} = -\operatorname{grad} \Phi \tag{6}$$

one obtains

$$\delta \langle \widetilde{F} \rangle = \langle \sigma_{ik} \rangle \delta \langle \varepsilon_{ik} \rangle + \langle \boldsymbol{E} \rangle \cdot \delta \langle \boldsymbol{D} \rangle = (1/V) \iint_{s} (\sigma_{ik} n_i \delta u_k - \Phi \boldsymbol{n} \cdot \delta \boldsymbol{D})\, ds \quad (7)$$

where n_i are the components of outer normal vector and s is the outer boundary of the cell. It is assumed that within the components and at the boundary between them the concentrated forces are absent. Therefore, the integrals over boundary surfaces cancel one another owing to the contact conditions.

If the fields are periodic,

$$\sigma_{ik}(x_m + \omega_m) = \sigma_{ik}(x_m), \quad \boldsymbol{D}(x_m + \omega_m) = \boldsymbol{D}(x_m), \quad (m = 1, 2, 3) \quad (8)$$

integration will lead to the determination of average values:

$$\langle \sigma_{ik} \rangle = (\omega_i / V) \int_{k} \int \sigma_{ik}\, ds$$

$$\langle D_k \rangle = (\omega_k / V) \int_{s_k} \int D_k\, ds \quad (9)$$

where ω_k is the size of a cell side (period) and s_k is the area of a parallelepiped face located perpendicular to the axis x_k; hence

$$\Delta\Phi(\omega_m) = \Phi(x_m + \omega_m) - \Phi(x_m) = \text{const}$$

$$\Delta u_k(\omega_m) = u_k(x_m + \omega_m) - u_k(x_m) = \text{const}$$

The average parameters corresponding to the above formulas are of the form:

$$\langle \varepsilon_{ik} \rangle = \frac{1}{2}\left[\frac{\Delta u_i(\omega_k)}{\omega_k} + \frac{\Delta u_k(\omega_i)}{\omega_i}\right], \quad \langle E_k \rangle = -\frac{\Delta\Phi(\omega_k)}{\omega_k} \quad (10)$$

The corresponding equations of state are directly established:

$$\langle \varepsilon_{ik} \rangle = \frac{1}{V} \sum_{j=1}^{N} \int_{V_j} \left(\frac{\partial F_j}{\partial \langle \sigma_{ik} \rangle}\right)_{T,\, \langle D \rangle} dV,$$

$$\langle \boldsymbol{E} \rangle = \frac{1}{V} \sum_{j=1}^{N} \int_{V_j} \left(\frac{\partial F_j}{\partial \langle \boldsymbol{D} \rangle}\right)_{T,\, \langle \varepsilon_{ik} \rangle} dV \quad (11)$$

To vary stresses the Gibbs potential is introduced:

$$d\Psi = -s\, dT + \varepsilon_{ik} d\sigma_{ik} + \boldsymbol{D} \cdot d\boldsymbol{E} \quad (12)$$

The averaging criterion proposed here guarantees the equivalent representation of thermodynamic relations both at an isolated point of the medium and for averaged quantities.

3.2.4 Methods of solving the problems of interaction between many inclusions in periodic media are considered. The regularization of single two-dimensional structures with every cell containing a single fiber is performed by the introduction of an oblique-angle system of cells with periods ω_1 and $\omega_2 = \omega_1 b e^{i\alpha}$ where $\alpha \neq 0$ is the angle between the cell boundary and the axis x_2. For hexagonal and tetragonal structures one should put $b = 1$ and $\alpha = \pi/3$, $\alpha = \pi/2$, respectively.

The plane stress state and plane strain of elastic bodies are described by complex variable functions of $z = x_2 + ix_3$ proposed by Kolosov and Muskhelishvili [21] $\varphi(z)$ and $\psi(z)$, and the problem of longitudinal shear reduces to the determination of a function $f(z)$. The stresses are related to these functions by the following expressions:

$$\begin{gathered}\sigma_{12} - i\sigma_{13} = 2Gf'(z) \\ \sigma_{33} - \sigma_{22} - 2i\sigma_{23} = 2[\bar{z}\varphi'(z) + \psi(z)] \\ \sigma_{33} + \sigma_{22} = 4 \operatorname{Re} \varphi(z), \quad \sigma_{11} = 4\nu \operatorname{Re} \varphi(z)\end{gathered} \tag{13}$$

Owing to the periodicity condition of the stressed state of the matrix:

$$\begin{gathered}f'(z + \omega_j) = f'(z), \quad \varphi(z + \omega_j) = \varphi(z) \\ \bar{\omega}_j \varphi'(z) + \psi(z + \omega_j) = \psi(z), \quad (j = 1, 2)\end{gathered} \tag{14}$$

The functions $f'(z)$ and $\varphi(z)$ are expressed in terms of elliptic functions and are proportional to the following series:

$$\varphi(z) = C_0 + \sum_{k=1}^{\infty} C_k \zeta^{(k)}(z) \tag{15}$$

where $\zeta^{(k)}(z)$ is the kth derivative of the Weierstrass ζ-function:

$$\zeta(z) = \frac{1}{z} + \sum_m \sum_n{}' \left(\frac{1}{z - P} + \frac{1}{P} + \frac{z}{P^2} \right) \quad (m, n = 0, \pm 1, \ldots) \tag{16}$$

with the prime on the summation symbol signifying that a term with $m = n = 0$ is to be dropped and

$$P = m\omega_1 + n\omega_2 \tag{17}$$

The function $\psi(z)$ is constructed according to relation (12) and is of the form:

$$\psi(z) = D_0 + \sum_{k=1}^{\infty} D_k \zeta^{(k)}(z) - \sum_{k=1}^{\infty} C_k Q^{(k)}(z) \tag{18}$$

where [3]:

$$Q(z) = \sum_m \sum_n{}' \left[\frac{\bar{P}}{(z-P)^2} - 2z\frac{\bar{P}}{P^3} - \frac{\bar{P}}{P^2} \right] \tag{19}$$

For a general structure with a cell containing N fibers the present author used the following representations [2]:

$$\begin{aligned} \varphi(z) &= C_0 + \sum_{k=1}^{N} \sum_{s=1}^{\infty} \frac{(-1)^s}{(s-1)!} C_{k,s}\zeta^{(s-1)}(z-a_k) \\ \psi(z) &= D_0 + \sum_{k=1}^{N} \sum_{s=1}^{\infty} \frac{(-1)^s}{(s-1)!} [D_{k,s}\zeta^{(s-1)}(z-a_k) - C_{k,s}\eta^{(s)}(z-a_k)] \end{aligned} \tag{20}$$

where

$$\eta(z) = \sum_m \sum_n{}' \left(\frac{\bar{P}}{z-P} + z^2\frac{\bar{P}}{P^3} + z\frac{\bar{P}}{P^2} \right) \tag{21}$$

3.2.5 The present author proposed a method of allowance for interaction of many inclusions, which reduces the problem to the solution of a set of boundary problems for regions becoming complicated in a smoothed field changing with every successive approximation [22]. According to this method in an infinite medium the surface s_0 isolates the volume V_0 composed of one or several fibers, the origin of coordinates being placed in the centre of gravity of the volume or individual inclusion, and assumes that the structure of the remaining part is obtained by means of the double- or triple-periodic translation of the volume V_0. In this approximation the volume V_0 is located in the field with the given symmetry group. For systems with the regular structure the symmetry group is known; for irregular positioning of fibers one assumes that the system outside the volume V_0 has a hexagonal structure with the highest possible symmetry group. The interaction potential is constructed in the form of the following series:

$$U_1 = U_\infty + U_0 + U_1 + \dots \tag{22}$$

where U_∞ is the field potential "at infinity" (without interaction), U_0 is the smoothed field potential, U_1 is the smoothed field potential for the volume with a complicated structure, etc.

The solution scheme for a medium with two-dimensional tetragonal symmetry is illustrated in Fig. 3.3. Every successive approxi-

mation allows for the influence of an ever increasing number of adjacent inclusions, thus improving the smoothed field and isolating its oscillating part. In each approximation the smoothed field am-

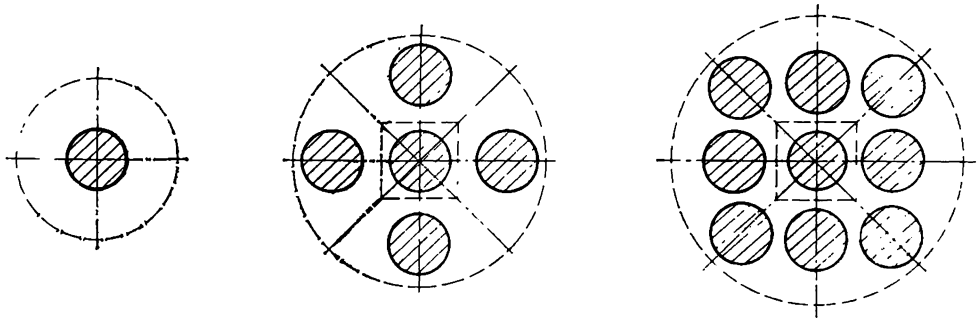

Fig. 3.3 Solution scheme

plitude is determined by the averaging. Allowing for only the first term U_0 with one inclusion in the solution permits the formulas for moduli valid to $v \approx 0.65$ to be obtained for a simple hexagonal structure.

3.3 LOCAL FRACTURES

3.3.1 Local fractures of structure precede the initiation of the critical size crack and favour its accelerated growth. The investigation of the conditions of growth and arrest of local cracks, allowing for discrete material structure, refines the redistribution of stresses in adjacent regions and reveals the sequence of new critical state occurrence inside the medium constituents. Crack initiation at the interface results in an unstable state, and, changing the stress state in a fiber, aids the initiation and growth of surface cracks within it normal to the fiber axis.

Initial imperfections in the form of voids and cracks are elongated parallel to the fibers and therefore from now on the following assumptions will be adopted:

(1) crack faces in the initial state form surfaces equidistant to the component interface surfaces or close to them; a projection of the crack boundary onto the surface perpendicular to the normal in the geometrical centre of gravity of the crack produces an ellipse with the major axis parallel to the axis of fiber and whose length exceeds by an order of magnitude that of the minor axis;

(2) crack growth does not alter the initial semi-axes ratio;

(3) crack growth resistance in the matrix and at the interface under normal tension and shear is determined by the parameters k_1, k_2 and k_{01}, k_{02}, respectively. The parameters k_{a1}, k'_{a1} and k_{a2} charac-

terize both the breaking strength of fibers along and across the axis and the longitudinal transverse shear resistance.

The evolution of brittle fracture of composites, allowing for a local crack multitude, can be reduced to the determination of an explicit dependence of Z-matrix elements in equation (2) on the parameters defining the structure, imperfections, and initial stresses.

Under loading, when the local fractures begin, the change in Z-matrix elements results in an additional redistribution of stresses not only in the vicinity of fibers but also between the layers with variously oriented fibers.

In the proposed model of fracture of unidirectionally reinforced polymers under loads slowly varying over time along fibers the following problems can be isolated:

(a) determining the zone sizes of the interface with bonds weakened owing to technological curing stresses;

(b) establishing the conditions of fracture of weakened bonds and finding the redistributions of stresses near the cracks on fiber surfaces when the phase contact fails;

(c) establishing conditions of individual fiber fracture as the above zones attain critical dimensions dependent on the imperfection distribution along the fibers;

(d) establishing conditions of the formation and growth of macrocracks within a preweakened fibrous layer.

According to X-ray diffraction data [20] the initial transverse and longitudinal crack dimensions amount to 400-600 Å and over 3000 Å, respectively. The restrictions imposed on the medium fine structure depend on the mutual proximity and symmetry of the fibers in the matrix. The last restriction becomes invalid with weak interaction between fibers.

The general case of the stable stress state of the fibrous medium can be subdivided into the sum of simplest states according to representation (1). The solutions of mixed problems are constructed by the method proposed earlier [18] where the functions to be found for the matrix are composed of functions which describe a local field near fibers and possess a point symmetry and functions which determine the interaction between inclusions with due regard of the translational symmetry of fibrous material structure.

Let $\bar{x}$ be the coordinate of a point at the interface, $L = l + l_0$ the cylindrical fiber surface, a section of which determines a continuity rupture (a crack), $\boldsymbol{u}$ the displacement vector, T_n the boundary value of stresses on a surface element with the normal $\boldsymbol{n}$. In the absence of friction bonds and with overlaying of rupture faces the functions sought satisfy the following conditions in every cell:

$$\begin{aligned} &[T_{na}\boldsymbol{n}]^+ = [T_n\boldsymbol{n}]^-, \quad \boldsymbol{u}_a^+ = \boldsymbol{u}^- \quad \text{at} \quad \bar{x} \in l \\ &[T_{na}\boldsymbol{n}]^+ = 0, \quad [T_n\boldsymbol{n}]^- = 0 \quad \text{at} \quad \bar{x} \in l_0 \end{aligned} \tag{23}$$

Here the quantities pertaining to a fiber are labelled by the subscript a, and those of the matrix are without this subscript; the subscripts plus and minus mean that the ultimate value is determined along the positive and negative directions of the normal. The relations (23)

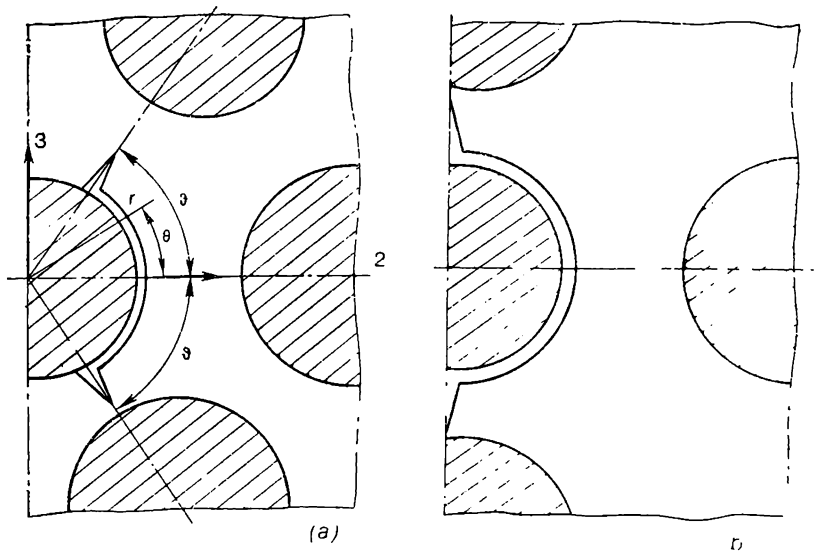

Fig. 3.4 Scheme of crack opening for (*a*) hexagonal and (*b*) tetragonal structures

and (8) are complemented by the equalities for stresses (9), the Z-matrix elements being established by (11).

For a medium with a hexagonal structure and cracks positioned symmetrically (Fig. 3.4) the first terms of the expansion of Z-matrix elements are found in an explicit form. In the case of longitudinal shear the effective shear moduli are of the form:

$$G_{12} = G\frac{2(1+v\cos\vartheta)G_a + 2\eta G - vG_a\sin^2\vartheta}{2(1-v\cos\vartheta)G_a + 2(1+v)G + vG_a\sin^2\vartheta} + \ldots$$
$$G_{13} = G\frac{2(1+v\cos\vartheta)G_a + 2\eta G + vG_a\sin^2\vartheta}{2(1-v\cos\vartheta)G_a + 2(1+v)G - vG_a\sin^2\vartheta} + \ldots \qquad (24)$$

where $\eta = 1 - v$ is the volume fraction of the matrix.

The transverse shear modulus is

$$G_{23} = G\frac{(1+\varkappa)[1+v\chi(\vartheta)]G_a + \eta(1+\varkappa_a)G}{(1+\varkappa)[1-v\chi(\vartheta)]G_a + (1+\varkappa_a)(1+v\varkappa)G} + \ldots \qquad (25)$$

Here ν is Poisson's ratio, $\varkappa = 3 - 4\nu$,

$$4\chi(\vartheta) = 4(\cos\vartheta - 2\beta\sin\vartheta)e^{-2\beta(\pi+\vartheta)} - (1+4\beta^2)^2[m(1+e^{2\beta\pi})]^{-1}\sin^4\vartheta$$
$$2\beta\pi = \ln\frac{G+\varkappa G_a}{G_a+\varkappa_a G} \qquad (26)$$

$$m(1+e^{2\beta\pi}) = 1 + (\cos\vartheta - 2\beta\sin\vartheta)\, e^{2\beta(\pi-\vartheta)}$$

The longitudinal and transverse elastic moduli are determined from equations:

$$E_1 = vE_a + \eta E + \frac{8v\eta\,(\nu_a-\nu)^2\, mGG_a}{v(1+\varkappa)\, mG_a + 2\eta\,(G_a+\varkappa_a G) - \eta\,(1+\varkappa_a)\, mG} + \ldots$$

$$E_2^{-1} = \frac{\nu_{21}^2}{E_1} + \frac{1+\varkappa}{4G}\,\frac{\varkappa G_a + (1+2v)\,[G_a + (1+\varkappa_a) G] - vG_a\Omega(\vartheta)}{(1+\varkappa)\,[1+\eta+v\lambda_1(\vartheta)]\, G_a + 2\eta\,(1+\varkappa_a)\, G} + \ldots \qquad (27)$$

$$E_3^{-1} = \frac{\nu_{31}^2}{E_1} + \frac{1+\varkappa}{4G}\,\frac{\varkappa G_a + (1+2v)\,[G_a + (1+\varkappa_a) G] - vG_a\mu(\vartheta)}{(1+\varkappa)\,[1+\eta+v\lambda_2(\vartheta)]\, G_a + 2\eta\,(1+\varkappa_a)\, G} + \ldots$$

where

$$\Omega(\vartheta) = g + m(1+e^{2\beta\pi}) + 2\varkappa(\cos\vartheta - 2\beta\sin\vartheta)\, e^{-2\beta(\pi-\vartheta)} - 0.5(1+4\beta^2)\,[2+\varkappa+g\varkappa(1+e^{2\beta\pi})^{-1}]\sin^2\vartheta$$

$$4\lambda_{1,2}(\vartheta) = 2g + 2m(1+e^{2\beta\pi}) + 4(\cos\vartheta - 2\beta\sin\vartheta)\, e^{-2\beta(\pi-\vartheta)} \pm (1+4\beta^2)\,[3+g(1+e^{2\beta\pi})^{-1}]\sin^2\vartheta$$

$$\mu(\vartheta) = g + m(1+e^{2\beta\pi}) + (1+8\beta^2)\sin^2\vartheta - 2\varkappa(\cos\vartheta - 2\beta\sin\vartheta)\, e^{-2\beta(\pi-\vartheta)} + 0.5\varkappa(1+4\beta^2)\,[1+g(1+e^{2\beta\pi})^{-1}]\sin^2\vartheta$$

$$g = (1+\varkappa_a)\, mG\,\frac{m(1+e^{2\beta\pi}) - (1+4\beta^2)\sin^2\vartheta}{2(G_a+\varkappa_a G) - (1+\varkappa_a)\, mG} \qquad (28)$$

In the formula for $\lambda_{1,2}(\vartheta)$ the upper sign is taken for $\lambda_1(\vartheta)$, and the lower one for $\lambda_2(\vartheta)$.

Poisson's ratios satisfy the following relations:

$$\nu_{21} \approx \nu_{31} = \nu + \frac{v(1+\varkappa)(\nu_a-\nu)\, mG_a}{v(1+\varkappa)\, mG_a + 2\eta\,(G_a+\varkappa_a G) - \eta\,(1+\varkappa_a)\, mG} + \ldots$$

$$\nu_{23}/E_2 = -\nu_{21}\nu_{31}/E_1 + \frac{1}{2G} \times \frac{(1+\varkappa)\, G_a + (1+\varkappa_a)(1+v\varkappa)\, G - 0.5v(1+\varkappa)\,[\Omega+\varkappa(1+4\beta^2)]\sin^2\vartheta}{(1+\varkappa)\,[1+\eta+v\lambda_1(\vartheta)]\, G_a + 2\eta\,(1+\varkappa_a)\, G} \qquad (29)$$

For small cracks $\vartheta \to 0$ and the previously found elastic constants of fibrous materials, expressed through the properties of constituents under their perfect contact, follow from the formulas given above. When $\vartheta \to \pi$ the contact between fibers and the matrix disappears.

The stresses at the crack tips are defined in terms of the average parameter derivatives; thus for longitudinal shear:

$$\sigma_{1\theta} = -\{\pi\lambda/[2\pi\rho v(1+G/G_a)]\}^{1/2} \times \{\langle\sigma_{12}\rangle\,[\partial(G/G_{12})/\partial\vartheta]^{1/2} - \langle\sigma_{13}\rangle\,[\partial(G/G_{13})/\partial\vartheta]^{1/2}\} \qquad (30)$$

Here the quantities pertaining to a fiber are labelled by the subscript a, and those of the matrix are without this subscript; the subscripts plus and minus mean that the ultimate value is determined along the positive and negative directions of the normal. The relations (23)

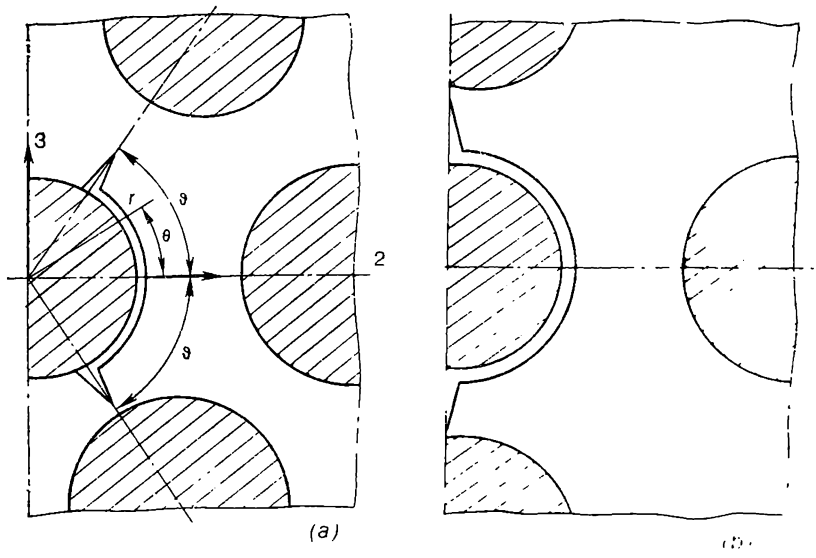

Fig. 3.4 Scheme of crack opening for (*a*) hexagonal and (*b*) tetragonal structures

and (8) are complemented by the equalities for stresses (9), the Z-matrix elements being established by (11).

For a medium with a hexagonal structure and cracks positioned symmetrically (Fig. 3.4) the first terms of the expansion of Z-matrix elements are found in an explicit form. In the case of longitudinal shear the effective shear moduli are of the form:

$$G_{12} = G\frac{2(1+v\cos\vartheta)G_a + 2\eta G - vG_a\sin^2\vartheta}{2(1-v\cos\vartheta)G_a + 2(1+v)G + vG_a\sin^2\vartheta} + \ldots$$
$$G_{13} = G\frac{2(1+v\cos\vartheta)G_a + 2\eta G + vG_a\sin^2\vartheta}{2(1-v\cos\vartheta)G_a + 2(1+v)G - vG_a\sin^2\vartheta} + \ldots \qquad (24)$$

where $\eta = 1 - v$ is the volume fraction of the matrix.

The transverse shear modulus is

$$G_{23} = G\frac{(1+\varkappa)[1+v\chi(\vartheta)]G_a + \eta(1+\varkappa_a)G}{(1+\varkappa)[1-v\chi(\vartheta)]G_a + (1+\varkappa_a)(1+v\varkappa)G} + \ldots \qquad (25)$$

Here ν is Poisson's ratio, $\varkappa = 3 - 4\nu$,

$$4\chi(\vartheta) = 4(\cos\vartheta - 2\beta\sin\vartheta)e^{-2\beta(\pi+\vartheta)} - (1+4\beta^2)^2[m(1+e^{2\beta\pi})]^{-1}\sin^4\vartheta$$
$$2\beta\pi = \ln\frac{G+\varkappa G_a}{G_a+\varkappa_a G} \qquad (26)$$

$$m(1+e^{2\beta\pi}) = 1 + (\cos\vartheta - 2\beta\sin\vartheta)\, e^{2\beta(\pi-\vartheta)}$$

The longitudinal and transverse elastic moduli are determined from equations:

$$E_1 = vE_a + \eta E + \frac{8v\eta\,(\nu_a-\nu)^2\, mGG_a}{v(1+\varkappa)\, mG_a + 2\eta\,(G_a+\varkappa_a G) - \eta\,(1+\varkappa_a)\, mG} + \ldots$$

$$E_2^{-1} = \frac{\nu_{21}^2}{E_1} + \frac{1+\varkappa}{4G}\,\frac{\varkappa G_a + (1+2v)\,[G_a + (1+\varkappa_a) G] - vG_a\Omega(\vartheta)}{(1+\varkappa)\,[1+\eta+v\lambda_1(\vartheta)]\, G_a + 2\eta\,(1+\varkappa_a)\, G} + \ldots \qquad (27)$$

$$E_3^{-1} = \frac{\nu_{31}^2}{E_1} + \frac{1+\varkappa}{4G}\,\frac{\varkappa G_a + (1+2v)\,[G_a + (1+\varkappa_a) G] - vG_a\mu(\vartheta)}{(1+\varkappa)\,[1+\eta+v\lambda_2(\vartheta)]\, G_a + 2\eta\,(1+\varkappa_a)\, G} + \ldots$$

where

$$\Omega(\vartheta) = g + m(1+e^{2\beta\pi}) + 2\varkappa(\cos\vartheta - 2\beta\sin\vartheta)\, e^{-2\beta(\pi-\vartheta)} - 0.5(1+4\beta^2)\,[2+\varkappa+g\varkappa(1+e^{2\beta\pi})^{-1}]\sin^2\vartheta$$

$$4\lambda_{1,2}(\vartheta) = 2g + 2m(1+e^{2\beta\pi}) + 4(\cos\vartheta - 2\beta\sin\vartheta)\, e^{-2\beta(\pi-\vartheta)} \pm (1+4\beta^2)\,[3+g(1+e^{2\beta\pi})^{-1}]\sin^2\vartheta$$

$$\mu(\vartheta) = g + m(1+e^{2\beta\pi}) + (1+8\beta^2)\sin^2\vartheta - 2\varkappa(\cos\vartheta - 2\beta\sin\vartheta)\, e^{-2\beta(\pi-\vartheta)} + 0.5\varkappa(1+4\beta^2)\,[1+g(1+e^{2\beta\pi})^{-1}]\sin^2\vartheta$$

$$g = (1+\varkappa_a)\, mG\,\frac{m(1+e^{2\beta\pi}) - (1+4\beta^2)\sin^2\vartheta}{2(G_a+\varkappa_a G) - (1+\varkappa_a)\, mG} \qquad (28)$$

In the formula for $\lambda_{1,2}(\vartheta)$ the upper sign is taken for $\lambda_1(\vartheta)$, and the lower one for $\lambda_2(\vartheta)$.

Poisson's ratios satisfy the following relations:

$$\nu_{21} \approx \nu_{31} = \nu + \frac{v(1+\varkappa)(\nu_a-\nu)\, mG_a}{v(1+\varkappa)\, mG_a + 2\eta\,(G_a+\varkappa_a G) - \eta\,(1+\varkappa_a)\, mG} + \ldots$$

$$\nu_{23}/E_2 = -\nu_{21}\nu_{31}/E_1 + \frac{1}{2G} \times \frac{(1+\varkappa)\, G_a + (1+\varkappa_a)(1+v\varkappa)\, G - 0.5v(1+\varkappa)\,[\Omega + \varkappa(1+4\beta^2)]\sin^2\vartheta}{(1+\varkappa)\,[1+\eta+v\lambda_1(\vartheta)]\, G_a + 2\eta\,(1+\varkappa_a)\, G} \qquad (29)$$

For small cracks $\vartheta \to 0$ and the previously found elastic constants of fibrous materials, expressed through the properties of constituents under their perfect contact, follow from the formulas given above. When $\vartheta \to \pi$ the contact between fibers and the matrix disappears.

The stresses at the crack tips are defined in terms of the average parameter derivatives; thus for longitudinal shear:

$$\sigma_{16} = -\{\pi\lambda/[2\pi\rho v\,(1+G/G_a)]\}^{1/2} \times \{\langle\sigma_{12}\rangle\,[\partial(G/G_{12})/\partial\vartheta]^{1/2} - \langle\sigma_{13}\rangle\,[\partial(G/G_{13})/\partial\vartheta]^{1/2}\} \qquad (30)$$

where ρ is the distance from the crack tip, and 2λ is the fiber diameter. The remaining components of local stresses σ_{rr}, $\sigma_{r\theta}$, $\sigma_{\theta\theta}$ are expanded into a series of the type:

$$\frac{\sqrt{\pi\lambda \sin\theta}}{\sqrt{2\pi\rho}} e^{\beta(\pi/2-\theta)}\left[A_1 \sin\left(\beta \ln \frac{\rho}{2\lambda \sin\vartheta} + \frac{\vartheta}{2}\right)\right.$$

$$\left. + B_1 \cos\left(\beta \ln \frac{\rho}{2\lambda \sin\vartheta} + \frac{\vartheta}{2}\right) + \ldots\right] \quad (31)$$

Here A_1, B_1, are dependent on ϑ, the parameters of elasticity and the average stresses $\langle\sigma_{11}\rangle$, $\langle\sigma_{22}\rangle$, $\langle\sigma_{33}\rangle$, $\langle\sigma_{23}\rangle$.

3.3.2 Some calculation results are considered. According to experiments [20] the initially observed transverse sizes of cracks ϑ at interfaces do not exceed one degree. In the case of single cracks the average values of elastic moduli of glass-fiber reinforced plastics

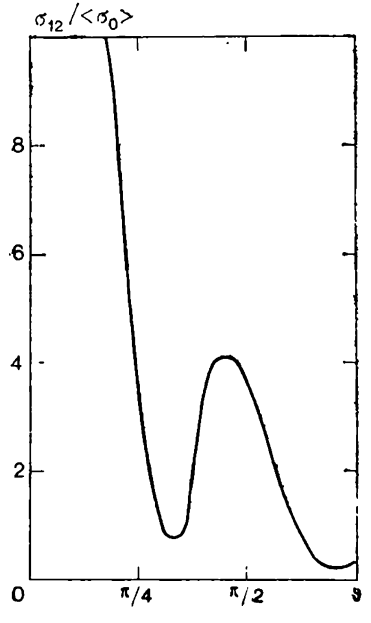

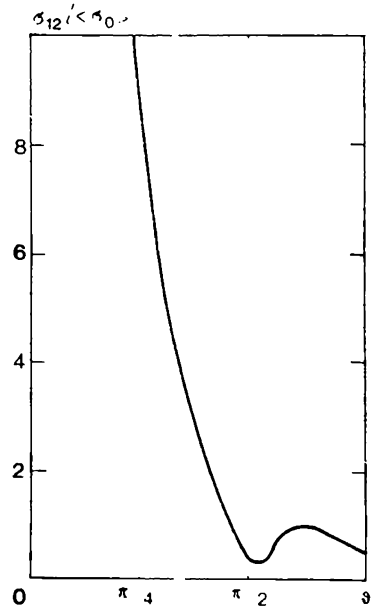

Fig. 3.5 Stress distribution at the crack tip in hexagonal structure

Fig. 3.6 Stress distribution at the crack tip in tetragonal structure

and of other fibrous materials change only by fractions of a percent, therefore these imperfections do not result in the redistribution of stresses between fibers. At $\vartheta \approx \pi/6$ a significant decrease in the moduli G_{12} and E_2 is observed. Calculations with an exact allowance for the interaction of fibers during their closing-in elucidate anomalies in the changes of stress intensity near the crack during its growth. In the case of longitudinal shear the limiting possible opening

of half-cracks for hexagonal and tetragonal fiber packings is limited by the angles $\pi/3$ and $\pi/2$ (Fig. 3.4). The curves in Figs. 3.5 and 3.6 show variation in stress intensity for structures considered at the crack tip as the crack grows along a circular arc ϑ. The barriers found guarantee crack localization at interfaces. Hexagonal packing favours the least possible delamination of fibers from the matrix in longitudinal shear.

3.3.3 Here is considered a problem of stress intensity change near a through macrocrack in a thin plate from unidirectional fibrous material under tension with an increase in the angle ϑ at interface. The mutual orientation of fibers and of the macrocrack is presented in Fig. 3.7; all fibers are uniformly delaminated from the matrix. The stress intensity in the composite is compared to that in a homogeneous orthotropic medium. Let the elastic characteristics of the homogeneous orthotropic medium correspond quantitatively to the average parameters of a fibrous medium with the perfect contact of constituents. A zone S of edge effects and of a high stress gradient near the crack faces in fibrous material is isolated where the found solutions require an amendment. The stress state is known near a macrocrack, considered as a limiting case of an elliptic hole with the major semi-axis $2a$ and with the minor semi-axis tending to zero. The normal and tangential stresses near S will be:

$$\langle\sigma_{yy}\rangle = \langle\sigma_0\rangle \frac{\sqrt{\pi a}}{\sqrt{2\pi r}} \operatorname{Re}\left[\frac{\mu_1\mu_2}{\mu_1+\mu_2} \times \left(\frac{\mu_2}{\sqrt{\cos\alpha+\mu_2\sin\alpha}} - \frac{\mu_1}{\sqrt{\cos\alpha+\mu_1\sin\alpha}}\right)\right] \tag{32}$$

$$\langle\sigma_{xy}\rangle = \langle\sigma_0\rangle \frac{\sqrt{\pi a}}{\sqrt{2\pi r}} \operatorname{Re}\left[\frac{\mu_1\mu_2}{\mu_1+\mu_2} \times \left(\frac{1}{\sqrt{\cos\alpha+\mu_2\sin\alpha}} - \frac{1}{\sqrt{\cos\alpha+\mu_1\sin\alpha}}\right)\right]$$

where r is the distance from the macrocrack tip, α the inclination angle of the surface element, μ_1 and μ_2 the parameters dependent on plate elastic constants. For the surface elements located on the crack continuation ($\alpha = 0$) the normal stresses will be

$$\langle\sigma_{yy}\rangle = \langle\sigma_0\rangle \frac{\sqrt{\pi a}}{\sqrt{2\pi r}} \sqrt{\frac{E_y}{E_x}} = \frac{k_{yy}}{\sqrt{2\pi r}} \tag{33}$$

and the tangential ones at the perpendicular surface elements equal

$$\langle\sigma_{xy}\rangle = \langle\sigma_0\rangle \frac{\sqrt{\pi a}}{\sqrt{2\pi r}} \times \frac{h}{\sqrt{4h+2\,(2h^2-2\nu_{yx}+E_yG_{xy}^{-1})^{1/2}}} = \frac{k_{xy}}{\sqrt{2\pi r}}$$

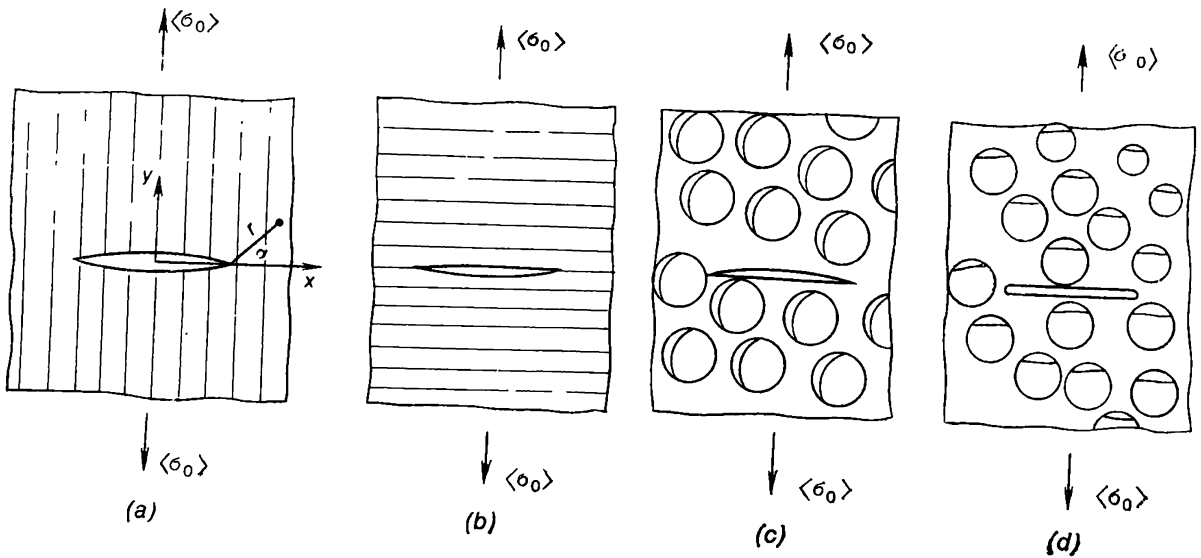

Fig. 3.7 The scheme of mutual orientations of macro- and micro-cracks in a plate of unidirectionally reinforced composite

where $h = \sqrt[4]{E_y E_x^{-1}}$. The following estimates are valid for delamination angles $\vartheta < \pi/12$:

$$E_1' \simeq E_1, \quad E_3' \simeq E_3, \quad G_{23}' \simeq G_{23}, \quad \nu_{12}' \simeq \nu_{12}, \quad \nu_{32}' \simeq \nu_{32} \tag{35}$$

(primed are elastic constants and stresses in a medium with perfect phase contact). The estimates of stresses at the macrocrack tips according to the schemes in Fig. 3.7 are given below. In formulas (33) and (34) it is adopted:

$$E_y = E_1, \quad E_x = E_2, \quad G_{xy} = G_{12}, \quad \nu_{yx} = \nu_{12} \tag{36}$$

and incorporating (35) for the state a one obtains:

$$\delta_{11}(\vartheta) = k_{11}(\vartheta) - k_{11}'(\vartheta) < 0 \tag{37}$$

i.e. a normal tension macrocrack is "blunted" upon delamination; $\delta_{11}(\vartheta)$ demonstrates the influence of cumulative fracture in the structure on averaged stress intensity. The tangential stresses of longitudinal shear at fiber boundaries increase according to the relation:

$$\sigma_{1\theta} = (k_3/\sqrt{2\pi\rho})(k_{21}/\sqrt{2\pi r}) \tag{38}$$

The next state b is determined by the relations:

$$E_y = E_3, \; E_x = E_2, \quad G_{xy} = G_{23}, \quad \nu_{yx} = \nu_{32} \tag{39}$$

and in this case the decrease in normal stresses is observed:

$$\delta_{11}(\vartheta) < 0 \tag{40}$$

In the states c and d the stress intensity of normal rupture increases, i.e.

$$\delta_{11}(\vartheta) > 0 \tag{41}$$

The weakening of interface bonds in fibrous medium under the tension of plate along fibers leads to an increase in fracture toughness; under the tension of plate across fibers the weakening of fiber-matrix interface diminishes its fracture toughness.

3.4 LOCAL FRACTURE OF HETEROGENEOUS PHASE MEDIA

3.4.1 In longitudinal shear the fracture resistance of two-component fibrous medium with cracks elongated parallel to fibers is determined by three parameters k_{02}, k_{a2}, and k_2. The first parameter characterizes fracture toughness at the interface under adhesive fracture and the others determine the cohesive fracture of fibers and matrix respectively.

The heterogeneous structure of fibers is described with the aid of heterogeneous anisotropic medium models. A local system of cylindrical coordinates r, θ is introduced whose centre is on the fiber axis (Fig. 3.4). The properties near the fiber centre differ from those at its boundaries $r = \lambda$, therefore models of media are used with cylindrical anisotropy. Hooke's law for such a medium is of the form:

$$\sigma_{1r} = G_r \frac{\partial u_a}{\partial r} + G_{r\theta} \frac{1}{r} \frac{\partial u_a}{\partial \theta}$$
$$\sigma_{1\theta} = G_{r\theta} \frac{\partial u_a}{\partial r} + G_\theta \frac{1}{r} \frac{\partial u_a}{\partial \theta} \tag{42}$$

where the displacement function $u\ (r, \theta)$ satisfies the equation:

$$G_r \frac{\partial^2 u_a}{\partial r^2} + \left(\frac{G_r}{r} + \frac{\partial G_r}{\partial r} + \frac{1}{r} \frac{\partial G_{r\theta}}{\partial \theta} \right) \frac{\partial u_a}{\partial r}$$
$$+ \left(\frac{1}{r^2} \frac{\partial G_\theta}{\partial \theta} + \frac{1}{r} \frac{\partial G_{r\theta}}{\partial r} \right) \frac{\partial u_a}{\partial \theta} + \frac{2G_{r\theta}}{r} \frac{\partial^2 u_a}{\partial r\, \partial \theta} + \frac{G_\theta}{r^2} \frac{\partial^2 u_a}{\partial \theta^2} = 0 \tag{43}$$

The dependence of shear moduli on the coordinate θ was insufficiently understood for a quantitative description to be made; to the first approximation the following expressions are suggested:

$$G_r = G_r^0 (x/x_1)^{2g} e^{(x-x_1)}, G_{r\theta} = \varkappa G_r$$
$$G_\theta = \nu^2 G_r, \quad x = \alpha r, \quad x_1 = \alpha \varepsilon \tag{44}$$

Here G_r^0, g, α, $\varkappa$, ν^2 are the constants reflecting the changes in elastic fiber properties, ε is the radius of the central region of the fiber with a homogeneous structure. The matrix material is considered a homogeneous isotropic medium with the shear modulus G, and the microstructural heterogeneity near the fibers is not taken into account.

The solution of equation (43) is constructed in the following form

$$u_a = 2 \operatorname{Re} \sum_{n>0} e^{-x+in0} x^{q_n - in\varkappa} [A_n F(a_n, b_n; x) + B_n U(a_n, b_n; x)]. \tag{45}$$

where the degenerate hypergeometric functions are introduced as:

$$F(a_n, b_n; x) = \sum_{m=0}^{\infty} \frac{(a_n)_m}{(b_n)_m} \frac{x^m}{m!}$$
$$U(a_n, b_n; x) = \frac{\pi}{\sin \pi b_n} \tag{46}$$
$$\times \left[\frac{F(a_n, b_n; x)}{\Gamma(1-q_n)\,\Gamma(b_n)} - x^{1-b_n} \frac{F(1-q_n, 2-b_n; x)}{\Gamma(a_n)\,\Gamma(2-b_n)} \right]$$

with

$$q_n = g + \sqrt{g^2 + n^2(\nu^2 - \varkappa^2)}$$
$$a_n = 1 + 2g + q_n, \quad b_n = 1 + 2g + 2q_n \tag{47}$$

The expansion coefficients in the series (45) are defined both by the component interaction conditions (23) and by the solution of the problem with mixed boundary conditions for the auxiliary piecewise holomorphic functions $X(z)$ and $Y(z)$ so that:

$$X^+(\tau) - X^-(\tau) = 0, \quad Y^+(\tau) - Y^-(\tau) = 0 \quad (\tau \in l_0)$$
$$[\sigma X(\tau) + Y(\tau)]^+ - [\sigma X(\tau) + Y(\tau)]^- = 0 \ (\tau \in l) \tag{48}$$
$$[\rho X(\tau) - Y(\tau)]^+ + [\bar{\rho} X(\tau) - Y(\tau)]^- = 0 \ (\tau \in l)$$

Here τ is the coordinate on L and σ and ρ are the complex parameters. The expansions $X(z)$, $Y(z)$ into the series by powers of Z express in an explicit form the dependence of the sought coefficients on the

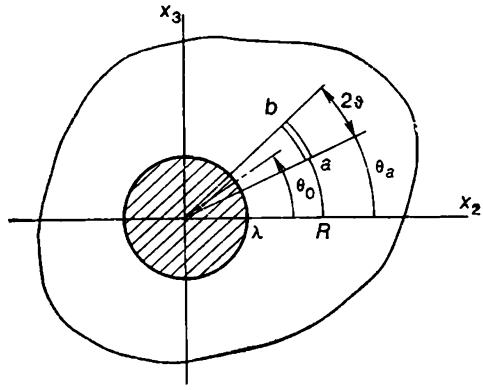

Fig. 3.8 Coordinates of crack at cohesive fracture

problem parameters. The dependence of Z-matrix elements on elastic constants and the geometry of flaws is written extremely cumbersomely and hence only special cases are investigated.

3.4.2 A numerical analysis of the solution reveals the central contribution of the first term of the series (45) on the magnitude of elastic constants at the fiber volume fraction $v < 0.6$. The succeeding expansion terms appreciably change the magnitude of critical load since they indicate the existence of a stability barrier for the hexagonal structure appearing owing to the strong interaction of fibers during their closing-in. The terms of the series have a uniform structure, therefore, to simplify and visualize the study, only the first terms of the expansion are retained in the subsequent analysis.

For materials with isotropic fibers having longitudinal shear rigidity increasing towards the side surface, one should put:

$$G_r = G_r^0 e^{x}, \quad G_\theta = G_r, \quad G_{r\theta} = 0 \tag{49}$$

The crack at distance R from the centre is opened by an angle 2ϑ and its middle part has the coordinate $Re^{i\theta_0}$, where it is taken (Fig. 3.8):

$$2\theta_0 = \theta_b + \theta_a, \quad 2\vartheta = \theta_b - \theta_a$$

The generalized Hooke's law for a fibrous medium takes the form:

$$\langle\gamma_{12}\rangle = \frac{1}{G_{12}}\langle\sigma_{12}\rangle + \frac{\mu_{23}}{G_{13}}\langle\sigma_{13}\rangle$$
$$\langle\gamma_{13}\rangle = \frac{\mu_{23}}{G_{13}}\langle\sigma_{12}\rangle + \frac{1}{G_{13}}\langle\sigma_{13}\rangle \tag{50}$$

where the first terms in the expansion of Z-matrix elements are as follows:

$$G_{12} = G\frac{h^2(\vartheta) - v^2\sin^4\vartheta\,[G_a - G + f(G_a+G)]^2}{L(\vartheta) + 8v\sin^2\vartheta\cos 2\theta_0\,[G_a - G + f(G_a+G)]\,(G_a+G)} + \cdots$$
$$G_{13} = G\frac{h^2(\vartheta) - v^2\sin^4\vartheta\,[G_a - G + f(G_a+G)]^2}{L(\vartheta) - 8v\sin^2\vartheta\cos 2\theta_0\,[G_a - G + f(G_a+G)]\,G_a+G)} + \cdots$$
$$\mu_{23} = \frac{8v\sin^2\vartheta\sin 2\theta_0\,[G_a - G + f(G_a+G)]\,(G_a+G)}{L(\vartheta) - 8v\sin^2\vartheta\cos 2\theta_0\,[G_a - G + f(G_a+G)]\,(G_a - G)} + \cdots \tag{51}$$

Here

$$f = R^2/\lambda^2,\quad x_0 = \alpha\lambda,\quad G_a = G_r^0 e^{x_0}(e^{x_0} - x_0 + 1)(1 + x_0 e^{x_0} - e^{x_0})^{-1}$$
$$L(\vartheta) = (G_a+G)^2\{16 + f^2v^2[\sin^4\vartheta - 4(1-\cos\vartheta)^2]\}$$
$$+ 2fv^2(G_a - G)^2\sin^2\vartheta(4 + \sin^2\vartheta) + v^2(G_a - G)^2$$
$$\times[\sin^4\vartheta - 4(1+\cos\vartheta)^2]$$
$$h(\vartheta) = 4(G_a+G) - 2fv(1-\cos\vartheta)(G_a+G) + 2v(1+\cos\vartheta)(G_a - G) \tag{52}$$

From the given formulas one obtains the magnitudes of the elastic constants of a reinforced medium for limiting cases free of cracking ($\vartheta = 0$) and total cohesive delamination of a fiber with a portion of the matrix ($\vartheta = \pi$). With weak fiber-matrix adhesion, when $k_{02} \ll k_2$, yet $k_{a2} > k_2$, one obtains, by means of limiting transitions $f \to 1$ from the given formulas, the dependences for average parameters in the case of materials with interface cracks. The critical shearing stresses near a symmetrical crack ($\theta_0 = 0$) are determined at

$$\langle\sigma_{13}\rangle = 0$$

If one assumes that at the next stage crack growth occurs along the same cylindrical surface (this is possible only for an angle less than a certain critical value), then stress concentration of the crack tip will be:

$$\sigma_{1n} = K(\vartheta, \theta_0)/\sqrt{2\pi\rho} \tag{53}$$

where ρ is the distance from the crack tip during its symmetrical growth, and $K(\vartheta, \theta_0)$ is the function characterizing stress intensity.

The critical average stresses will therefore be:

$$\langle\sigma_{12}^*\rangle = \frac{k_2 f}{\sqrt{2\pi\lambda}} \frac{h(\vartheta) - G_p v \sin^2\vartheta}{2G_p \cos(\vartheta/2)\sqrt{\sin\vartheta}} \tag{54}$$

where

$$G_p = G_a - G + f(G_a + G) \tag{55}$$

According to Griffith's energy criterion:

$$\langle\sigma_{12}^*\rangle = \sqrt{\frac{8\lambda\gamma}{\partial(F/G_{12})/\partial\vartheta}} = \sqrt{\frac{\gamma G}{\lambda}} \frac{h(\vartheta) - G_p v \sin^2\vartheta}{2\sqrt{G_p(G_a + G)}\cos(\vartheta/2)\sqrt{\sin\vartheta}} + \ldots \tag{56}$$

where γ is the surface energy. Relations (54) and (56) coincide within an accuracy of parameters which depend on an elastic moduli ratio. The last aspect can be of importance in the prediction of the limiting stresses for different composites and for given γ and k_2.

According to (52) with an increase in α one observes an increase in the reduced shear modulus G_a and in the stress intensity, resulting in a decrease in critical load according to the laws (54) and (56).

3.4.3 In the case of simple fracture the formulas obtained permit an approximate estimate of the conditions of an equality between cohesive and adhesive strengths of a medium, starting from the equality of critical stresses for a small crack at the interface and in a region adjacent to fiber, with all other parameters the same. Let the crack be located symmetrically ($\theta_0 = 0$) at $R = 1.1\,\lambda$ when local deviations in the mechanical properties of the matrix are damped:

$$\frac{k_{02}}{k_2} = \frac{fG_a \cos(\vartheta/2)\sqrt{\sin\vartheta_1}}{G_p \cos(\vartheta/2)\sqrt{\sin\vartheta}} \frac{h(\vartheta) - G_p v \sin^2\vartheta}{2[G_a(1 + v\cos\vartheta_1 + \eta G] - vG_a \sin^2\vartheta_1} \tag{57}$$

For glass-fiber reinforced plastics with the volume fraction of matrix

$\eta = 0.3$ $(v = 0.7)$, $G/G_a = 0.04$, $\vartheta_1 = \pi/180$

$\vartheta = \lambda\vartheta_1/R$, $f = 1.21$

one finds

$$k_{02} \sim 1.1\ k_2 \tag{58}$$

i.e. crack growth resistance under adhesive fracture should be 10% higher than under cohesive fracture. The given relation is extremely crude and should be improved by taking into account both the subsequent terms in the solution and the conditions at the

interface. The crack growth pattern in the matrix at cohesive fracture along the constant radius arc is one of the possible ones. During this crack growth it is of interest to follow the variation of reduced shear moduli. The data in Figs. 3.9 and 3.10 approximately illustrate a decrease in these parameters with an increase in ϑ given one symmetrically located crack ($\theta_0 = 0$). Curves *1* and *2* in Fig. 3.9

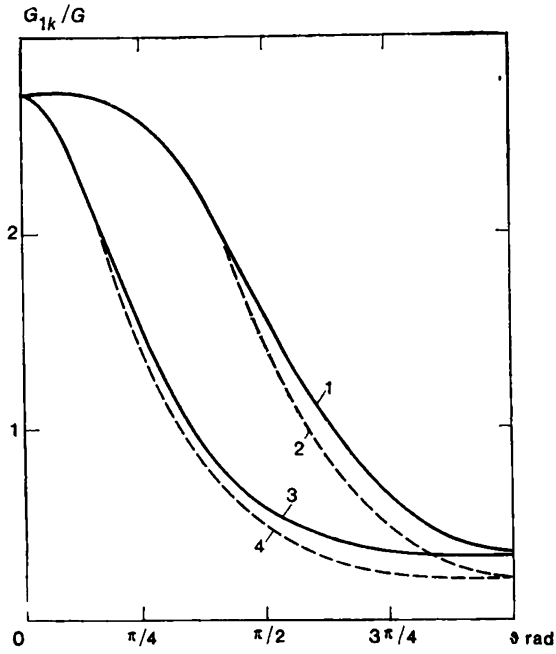

Fig. 3.9 Variation of longitudinal shear moduli at fiber volume fraction $v = 0.5$

show the variation in G_{13}/G at $v = 0.5$, $f = 1$, and $f = 1.21$. Curves *3* and *4* illustrate the drop in the ratio G_{12}/G under similar assumptions. Analogous data for $v = 0.7$ with the same notations are plotted in Fig. 3.10. Curves *1* and *2* in Fig. 3.11 illustrate variation in the side effect coefficients μ_{23} at $v = 0.7$ depending on the crack centre position θ_0 with its opening angle $\vartheta = \pi/4$ for $f = 1.21$ and $f = 1$. A variation of the same data for $v = 0.5$ is shown by curves *3* and *4*.

3.4.4 If a heterogeneous isotropic structure of fibers changes both the elastic properties and stress concentration near the crack according to relations (51) and subsequent ones, then the fiber anisotropy makes qualitative changes to the stress distribution as well as to the dependence of reduced moduli on composite properties. To be

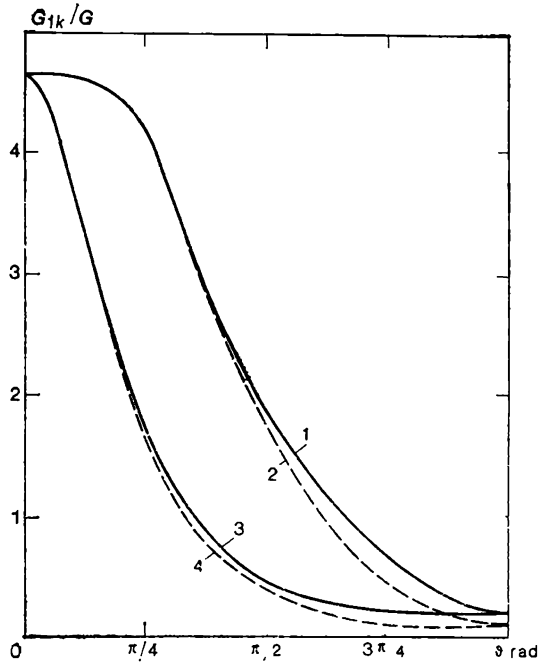

Fig. 3.10 Variation of longitudinal shear moduli at fiber volume fraction $v = 0.7$

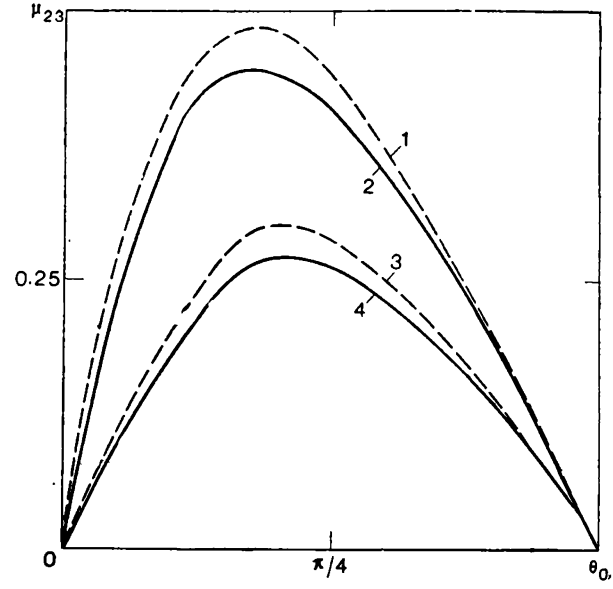

Fig. 3.11 Variation of side effect coefficient μ_{23} versus crack centre position

specific let us treat the following case:

$$G_r = G_r^{(0)} = \text{const}, \quad G_\theta = \nu^2 G_r, \quad G_{r\theta} = \varkappa G_r$$

Let the fiber core of the radius ε be isotropic. In order to avoid cumbersome formulas the relations will be given for a medium both with a crack located at random near the interface and with the low ratio $\varepsilon/\lambda \ll 1$: K

$$G_{12} = G\,\frac{4[(1+v\cos\vartheta)G_a+\eta G]^2 - v^2 G_a^2 \sin^4\vartheta}{L(\vartheta)+4vG_a(G_a+G)\sin^2\vartheta\cos 2\theta_0} + \cdots$$

$$G_{13} = G\,\frac{4[(1+v\cos\vartheta)G_a+\eta G]^2 - v^2 G_a^2 \sin^4\vartheta}{L(\vartheta)-4vG_a(G_a+G)\sin^2\vartheta\cos 2\theta_0} + \cdots \tag{59}$$

$$\mu_{23} = \frac{4vG_a(G_a+G)\sin^2\vartheta\sin 2\vartheta_0}{L(\vartheta)-4vG_a(G_a+G)\sin^2\vartheta\cos 2\theta_0} + \cdots$$

where

$$G_a = \sqrt{G_r G_\theta + G_{r\theta}^2}$$

$$L(\vartheta) = 4[(1-v^2\cos^2\vartheta)G_a^2 + 2(1+v^2\cos\vartheta)G_a G + (1-v^2)G^2] + v^2 G_a^2 \sin^4\vartheta \tag{60}$$

and the remaining notations as explained above. From the comparison of (59) with the formulas given earlier it follows that the quantity

$$\sqrt{G_r G_\theta - G_{r\theta}^2} \tag{61}$$

plays the role of reduced shear modulus of a fiber both with an arbitrary cylindrical anisotropy in shear and with an isotropic inclusion of extremely small radius. The stresses at the tip of a symmetrically positioned crack under the action of only $\langle\sigma_{12}\rangle$ are determined by a series the first term of which is:

$$\sigma_{1n} = \sum_{m>0} \sqrt{(2\sin\vartheta/\rho)^{1-2g_m}}\, K_m(\vartheta, g_m) = \sqrt{[(2\sin\vartheta)/\rho]^{1-2g_1}} \times \frac{2G_a(1+2g_1)\cos(\pi/4-g_1\pi/2)\sin(g_1+1/2)\vartheta}{2[(1+v\cos\vartheta)G_a+\eta G]-vG_a\sin^2\vartheta}\langle\sigma_{12}\rangle + \cdots \tag{62}$$

Here ρ is the distance from the crack tip along the circular arc,

$$\pi g_m \approx \{4GG_aG_{r\theta}/[(G_a+G)G_r^2]\}\,(\varepsilon/\lambda)^{\Omega_m} \tag{63}$$

$$\Omega_m = 2_m G_a/G_r$$

The occurrence of side effects in Hooke's law for the fiber owing to the presence of the constant $G_{r\theta}$ in relations (42) changes the distinctive feature of the stress state at the crack tips. To be convincing

let us give the exact formula for the parameter g_m:

$$\pi g_m = \text{arc tan} \frac{G_a G_{r\theta} (\varepsilon/\lambda)^{\Omega_m}}{G_\theta (G_a + G_{r\theta}) + G_{r\theta}^2 (\varepsilon/\lambda)^{\Omega_m}}$$

$$- \text{arc tan} \frac{G_a G_{r\theta} (G_a - G) (\varepsilon/\lambda)^{\Omega_m}}{(G_a + G)(G_a + G_\theta) G_\theta + (G_a - G) G_{r\theta}^2 (\varepsilon/\lambda)^{\Omega_m}} \tag{64}$$

from which it follows that the side effects vanish only in the case of $G_{r\theta} = 0$. With the initiation of cracks in the fiber which distort the symmetry of stress-strain equations, in the stress state of an isotropic matrix the singularity at the crack tips will be changed.

3.4.5 The critical stress state in the general case of longitudinal shear is determined by the relation obtained earlier, following from the energy criterion:

$$\frac{\langle \sigma_{12}^* \rangle^2}{a^2} + \frac{\langle \sigma_{13}^* \rangle^2}{b^2} + \frac{\langle \sigma_{12}^* \rangle \langle \sigma_{13}^* \rangle}{c^2} = 1 \tag{65}$$

If the crack begins to propagate at the tip θ_a then:

$$a^2 = \frac{8\lambda\gamma}{| (\partial/\partial\vartheta - \partial/\partial\theta_0)(F/G_{12}) |}$$

$$b^2 = \frac{8\lambda\gamma}{| (\partial/\partial\vartheta - \partial/\partial\theta_0)(F/G_{13}) |}$$

$$c^2 = \frac{4\lambda\gamma}{\left| (\partial/\partial\vartheta - \partial/\partial\theta_0) \frac{\mu_{23} F}{G_{13}} \right|}$$

where F is the area of a cell (limited by the lines connecting the centres of adjacent fibers) and if the crack begins to propagate at the tip θ_b, then

$$a^2 = \frac{8\lambda\gamma}{(\partial/\partial\vartheta + \partial/\partial\theta_0)(F/G_{12})}$$

$$b^2 = \frac{8\lambda\gamma}{(\partial/\partial\vartheta + \partial/\partial\theta_0)(F/G_{13})} \tag{66}$$

$$c^2 = \frac{4\lambda\gamma}{(\partial/\partial\vartheta + \partial/\partial\theta_0)(\mu_{23} F/G_{13})}$$

Equation (65) in the coordinates $\langle \sigma_{12}^* \rangle$, $\langle \sigma_{13}^* \rangle$ defines an ellipse whose position is determined by the value of the derivative of the Z-matrix elements.

It follows from the above exposition that in the case of longitudinal shear the Z-matrix elements totally determine the changes in the mechanical characteristics of composite and the onset of the critical stress state.

References

1. Van Fo Fy (Vanin), G.A., *Mekh. polimerov*, **6**, 61-68 (1965).
2. Van Fo Fy, G.A., *Doklady Akad. Nauk SSSR*, 166 (4), 817-820 (1966).
3. Natanson, V.Ya., *Matem. sbornik*, **42** (5), 616-636 (1935).
4. Van Fo Fy, G.A., *Structures from Reinforced Plastics*, Naukova dumka, Kiev, 1971 (in Russian).
5. Van Fo Fy, G.A., *Theory of Reinforced Materials*, Naukova dumka, Kiev, 1971 (in Russian).
6. Grigolyuk, E.I., and Filshtinsky, L.A., *Perforated Plates and Shells*, Nauka, Moscow, 1970 (in Russian).
7. Skudra, A.M., and Bulavs, F.Ya., *Structural Theory of Reinforced Plastics*, Zinatne, Riga, 1978 (in Russian).
8. Bolotin, V.V., and Novichkov, Yu.N., *Mechanics of Multilayered Structures*, Mashinostroyenie, Moscow, 1980 (in Russian).
9. Zhigun, I.G., and Polyakov, V.A., *Properties of Spatially Reinforced Plastics*, Zinatne, Riga, 1978 (in Russian).
10. Bolotin, V.V., *Mekh. polimerov*, **2**, 27-37, 1965 (in Russian).
11. Rabotnov, Yu.N., *Mechanics of Deformable Solids*, Nauka, Moscow, 1979 (in Russian).
12. Tamuzs, V.P., and Kuksenko, V.S., *Micromechanics of Polymer Material Fracture*, Zinatne, Riga, 1978 (in Russian).
13. Whittaker, E.T., and Watson, G.N., *A Course of Modern Analysis*, University Press, Cambridge, 1927.
14. Gringauz, M.G., Dolghikh, V.N., and Filshtinsky, L.A., in: *Dynamics and Strength of Machines*, vol. 26, Kharkov, 1976, pp. 16-21 (in Russian).
15. Dolghikh, V.N., and Filshtinsky, L.A., in: *Dynamics and Strength of Machines*, vol. 27, Kharkov, 1978, pp. 39-44 (in Russian).
16. Vanin, G.A., *Doklady Akad. Nauk USSR*, Kiev, **10**, 894-897 (1977).
17. Vanin, G.A., *Prikl. mekhanika*, **10**, 14-22 (1977).
18. Vanin, G.A., *Prikl. mekhanika*, **8**, 35-41 (1977).
19. Van Fo Fy, G.A., Klyavlin, V.V., and Gordienko, V.P., *Mekh. polimerov*, **2**, 282-287 (1969).
20. Orlov, L.G., Leksovskii, A.M., and Regel', V.R., in: *Physics of Strength of Composite Materials*, Proc. All-Union Seminar, RTP LIYaF, Leningrad, 1979, pp. 74-78 (in Russian).
21. Muskhelishvili, N.I., *Selected Fundamental Problems of Mathematical Theory of Elasticity*, Nauka, Moscow, 1966 (in Russian).
22. Vanin, G.A., *Doklady Akad. Nauk USSR*, Kiev, 4, 321-324, (1976).

4 Strength and Creep Micromechanics of Composites

A. M. Skudra, *D. Sc. (Eng.)*,
F. Ya. Bulavs, *Cand. Sc. (Eng.)*

4.1 INTRODUCTION

One of the main trends in the development of modern technology consists in making the best use of potential properties of the available materials. For this the features of the real performance of the materials in use under different conditions of loading should be taken into account not only qualitatively, but also quantitatively, with sufficient accuracy. This primarily concerns various types of reinforced materials finding wide application in different branches of technology.

Multidirectionally reinforced composites have laminated structure and in operating conditions they are usually under plane stress. In the process of loading unidirectionally reinforced layers with different orientations do not fail simultaneously. The fracture of individual layers does not always coincide with the overall failure of the laminate. In many cases the failure of these materials proceeds in two steps: first the material loses its continuity as a result of matrix or bond failure in the most unfavourably oriented layers; then, with a further increase of load, complete failure occurs resulting from fiber fracture.

To determine the instant of continuity loss and complete failure of the composite it is necessary to estimate the strength properties of individual unidirectionally reinforced layers with different orientations.

To simplify the design dependences the composite's physical structure is assumed to be symmetric with respect to the midplane surface.

A design model of a multidirectionally reinforced laminated composite under plane stress is shown in Fig. 4.1.

One of the features of the mechanical behaviour of composites is the dependence of their rigidity properties on loading duration. The presence of a polymeric matrix as an integral constituent, highly sensitive rheonomously to mechanical actions, causes a more or less pronounced viscoelasticity of composite materials. Unidirectionally reinforced composites in longitudinal shear and under transverse axial loading are characterized both by a distinctly pronounced creep and by an intensive stress relaxation. A similar situation is observed

with loading at an angle to the reinforcement direction. A heterogeneous structure, fiber anisotropy and markedly different rigidity characteristics of the components are the main causes of nonuniform distribution and redistribution of stresses in composites during loading. Thus, for a number of composites an increase in stress concentration in the polymeric matrix is observed during creep. This is important for the determination of composite endurance

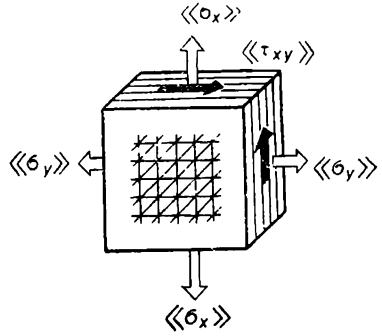

Fig. 4.1 State of stress in laminated material

under long-time loading. Similar processes occur in laminated composites composed of unidirectionally reinforced layers. The character of the redistribution of the stress field in the components of a unidirectionally reinforced layer and a laminated composite as a whole affects the intensity of creep in these materials with different types of loading. Thus, an efficient use of composites as a structural material requires the features of their stress-strain state under long-time loading to be studied and estimated.

4.2 STRENGTH MICROMECHANICS

4.2.1 Stresses in an Elementary Layer

In the general case of plane stress, shown in Fig. 4.2, stresses in the directions of the elastic symmetry of layers are determined as follows [1]:

$$\langle\sigma_1\rangle_k = (1/\Delta)\,(\langle\langle\sigma_x\rangle\rangle\, a_{1k} + \langle\langle\sigma_y\rangle\rangle\, b_{1k} + \langle\langle\tau_{xy}\rangle\rangle\, c_{1k}) \tag{1}$$

$$\langle\sigma_2\rangle_k = (1/\Delta)\,(\langle\langle\sigma_x\rangle\rangle\, a_{2k} + \langle\langle\sigma_y\rangle\rangle\, b_{2k} + \langle\langle\tau_{xy}\rangle\rangle\, c_{2k}) \tag{2}$$

$$\langle\tau_{12}\rangle_k = (1/\Delta)\,(\langle\langle\sigma_x\rangle\rangle\, a_{3k} + \langle\langle\sigma_y\rangle\rangle\, b_{3k} + \langle\langle\tau_{xy}\rangle\rangle\, c_{3k}) \tag{3}$$

The following designations are used in the above formulas:

$$a_{1k} = \cos^2\varphi_k A_{66}\,(Q^k_{11}A_{22} - Q^k_{12}A_{12}) + \sin^2\varphi_k A_{66}\,(Q^k_{12}A_{22} - Q^k_{22}A_{12}) + \sin 2\varphi_k A_{66}\,(Q^k_{16}A_{22} - Q^k_{26}A_{12})$$

$$b_{1k} = \cos^2\varphi_k A_{66}(Q^k_{12}A_{11} - Q^k_{11}A_{12}) \quad \sin^2\varphi_k A_{66}(Q^k_{22}A_{11} - Q^k_{12}A_{12}) + \sin 2\varphi_k A_{66}(Q^k_{26}A_{11} - Q^k_{16}A_{12})$$

$$c_{1k} = A_{11}A_{66}(Q^k_{16}\cos^2\varphi_k \quad Q^k_{66}\sin^2\varphi_k \quad Q^k_{16}\sin 2\varphi_k)$$

$$a_{2k} = \sin^2\varphi_k A_{66}(Q^k_{11}A_{22} - Q^k_{12}A_{12}) \quad \cos^2\varphi_k A_{66}(Q^k_{12}A_{22} - Q^k_{26}A_{12}) + \sin 2\varphi_k A_{66}(Q^k_{16}A_{22} \quad Q^k_{26}A_{12})$$

$$b_{2k} = \sin^2\varphi_k A_{66}(Q^k_{12}A_{11} - Q^k_{11}A_{12}) + \cos^2\varphi_k A_{66}(Q^k_{22}A_{11} - Q^k_{12}A_{12}) - \sin 2\varphi_k A_{66}(Q^k_{26}A_{11} - Q^k_{16}A_{12})$$

$$c_{2k} = A_{11}A_{66}(Q^k_{16}\sin^2\varphi_k \quad Q^k_{26}\cos^2\varphi_k - Q^k_{66}\sin 2\varphi_k)$$

$$a_{3k} \quad 1.2\sin 2\varphi_k A_{66}[A_{26}(Q^k_{66} \quad Q^k_{11}) \quad A_{12}(Q^k_{12} - Q^k_{22})] + A_{66}\cos 2\varphi_k (Q^k_{16}A_{22} - Q^k_{26}A_{12})$$

$$b_{3k} = 1/2\sin 2\varphi_k A_{66}[A_{11}(Q^k_{22} - Q^k_{12}) + A_{12}(Q^k_{11} - Q^k_{12})] + A_{66}\cos 2\varphi_k (Q^k_{26}A_{11} - Q^k_{16}A_{12})$$

$$c_{3k} = A_{11}A_{22}[1/2\sin 2\varphi_k (Q^k_{26} - Q^k_{16}) + \cos 2\varphi_k Q^k_{66}]$$

$$\setminus \quad A_{11}(A_{22}A_{66} - A^2_{26}) - A_{12}(A_{12}A_{66} - A_{16}A_{26}) \quad A_{16}(A_{12}A_{26} - A_{22}A_{16})$$

The quantities A_{ij} are determined by

$$A_{ij} = (1/\delta)\sum_{k=1}^{n} Q^k_{ij}h_k$$

where δ is the laminate thickness and h_k layer thickness. The rigidity

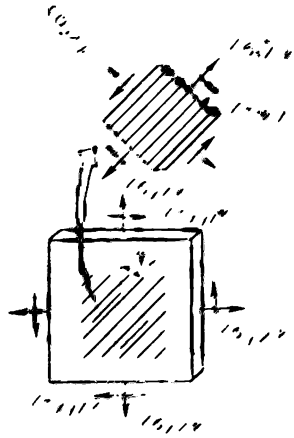

Fig. 4.2 State of stress in elementary layer

parameters of the Q^k_{ij} layer with the reinforcement angle φ_k are

$$Q^k_{11} = B_{11}\cos^4\varphi_k + 2(B_{12} + 2B_{66})\sin^2\varphi_k\cos^2\varphi_k + B_{22}\sin^4\varphi_k$$

$$Q^k_{22} = B_{11}\sin^4\varphi_k + 2(B_{12} + 2B_{66})\sin^2\varphi_k\cos^2\varphi_k + B_{22}\cos^4\varphi_k$$

$$Q_{12}^k = (B_{11} + B_{22} - 4B_{66}) \sin^2 \varphi_k \cos^2 \varphi_k + B_{12} (\sin^4 \varphi_k + \cos^4 \varphi_k)$$
$$Q_{66}^k = (B_{11} + B_{22} - 2B_{12} - 2B_{66}) \sin^2 \varphi_k \cos^2 \varphi_k + B_{66} (\sin^4 \varphi_k + \cos^4 \varphi_k)$$
$$Q_{16}^k = (B_{11} - B_{12} - 2B_{66}) \sin \varphi_k \cos^3 \varphi_k + (B_{12} - B_{22} + 2B_{66}) \sin^3 \varphi_k \cos \varphi_k$$
$$Q_{26}^k = (B_{11} - B_{12} - 2B_{66}) \sin^3 \varphi_k \cos \varphi_k + (B_{12} - B_{22} + 2B_{66}) \sin \varphi_k \cos^3 \varphi_k$$

The quantities B_{ij} are expressed in terms of the elastic constants of a layer in the principal axes orthotropy:

$$B_{11} = \frac{E_1}{1 - \mu_{12}\mu_{21}}, \quad B_{22} = \frac{E_2}{1 - \mu_{12}\mu_{21}},$$
$$B_{12} = \frac{E_1 \mu_{12}}{1 - \mu_{12}\mu_{21}}, \quad B_{66} = G_{12}$$

It follows from (1)-(3) that the unidirectionally reinforced elementary layer is in plane stress state even with simple types of loading, for example, when $\langle\langle \sigma_y \rangle\rangle = \langle\langle \tau_{xy} \rangle\rangle = 0$.

4.2.2 Fiber Fracture

To determine the strength of an elementary unidirectionally reinforced layer at fibers fracture the strain-strength criterion is used. According to this criterion fibers break if their strain reaches its ultimate value. Assuming a close fiber-matrix bond, i.e. that slippage is absent, the strain of fibers is equal to that of the reinforced composite in the direction of reinforcement $\langle e_1 \rangle$.

Separate elementary layers of a laminated material are reinforced in different directions, determined by an angle φ. Fig. 4.2, for example, shows an arbitrary kth layer. The strength criterion of this layer is:

$$\langle e_1 \rangle_k = e_{fR} \tag{4}$$

where e_{fR} is the ultimate strain of fibers in tension or compression. Substituting the expression for $\langle e_1 \rangle_k$ in (4), we obtain

$$\langle\langle e_x \rangle\rangle \cos^2 \varphi_k + \langle\langle e_y \rangle\rangle \sin^2 \varphi_k + \langle\langle e_{xy} \rangle\rangle \sin \varphi_k \cos \varphi_k = e_{fR} \tag{5}$$

The strains $\langle\langle e_x \rangle\rangle$, $\langle\langle e_y \rangle\rangle$, and $\langle\langle e_{xy} \rangle\rangle$ are determined using the theory of laminates with the condition that slippage between layers is absent. If we take into account the expressions for these strains, criterion (5) takes the form

$$\langle\langle \sigma_x \rangle\rangle (a_x \cos^2 \varphi_k + a_y \sin^2 \varphi_k + 1/2\, a_{xy} \sin 2\varphi_k) + \langle\langle \sigma_y \rangle\rangle (b_x \cos^2 \varphi_k + b_y \sin^2 \varphi_k + 1/2\, b_{xy} \sin 2\varphi_k) + \langle\langle \sigma_{xy} \rangle\rangle (c_x \cos^2 \varphi_k + c_y \sin^2 \varphi_k + 1/2\, c_{xy} \sin 2\varphi_k) = e_{fR} \tag{6}$$

Criterion (6) determines the initiation of fiber fracture in the kth layer. This criterion must be repeatedly applied to all layers with different fiber orientations. These calculations allow the determination of the layer that will fracture first, i.e. to find the critical angle φ_k. If we know the critical value of the angle φ_k and the laminate structure, using criterion (6) we can determine the overall laminate strength. The explanation is that after the fracture of the most heavily loaded fibers an avalanche failure of the whole material usually occurs as a result of a jumpwise redistribution of stresses.

Thus, criterion (6) is a generalized structural strength criterion for composites in the case when fibers fail first. The coefficients a, b and c in this criterion depend on the composite structure. They are expressed in terms of the above-given quantities A_{ij}:

$$a_x = (1/\Delta)(A_{22}A_{66} - A_{26}^2),\quad b_x = (1/\Delta)(A_{16}A_{26} - A_{12}A_{66})$$

$$c_x = (1/\Delta)(A_{12}A_{26} - A_{22}A_{16})$$

$$a_y = (1/\Delta)(A_{16}A_{26} - A_{12}A_{66}),\quad b_y = (1/\Delta)(A_{11}A_{66} - A_{12}^2)$$

$$c_y = (1/\Delta)(A_{12}A_{16} - A_{11}A_{26})$$

$$a_{xy} = (1/\Delta)(A_{12}A_{26} - A_{16}A_{22}),\quad b_{xy} = (1/\Delta)(A_{12}A_{16} - A_{26}A_{11})$$

$$c_{xy} = (1/\Delta)(A_{11}A_{22} - A_{12}^2)$$

4.2.3 Polymeric Matrix Failure

If the material failure is caused by fracture of the matrix of fiber-matrix bond the generalized strength criterion has the form

$$F(\langle\sigma_2\rangle_k;\ \langle\tau_{12}\rangle_k) = 1 \tag{7}$$

where $\langle\sigma_2\rangle_k$ and $\langle\tau_{12}\rangle_k$ are average stresses in the layer that fails first. The form of the function on the left-hand side of criterion (7) depends on the accepted failure conditions and the ratio between $\langle\sigma_2\rangle_k$ and $\langle\tau_{12}\rangle_k$.

The failure features of unidirectional composites subjected to stresses $\langle\sigma_2\rangle_k$ and $\langle\tau_{12}\rangle_k$ have been considered in [2]. If with combined tension and shear tensile failure of the polymeric matrix occurs then the function F assumes the following form

$$F(\langle\sigma_2\rangle_k,\ \langle\tau_{12}\rangle_k) = (1-\mu_m^2)\,\bar{\sigma}_r^2\,\frac{\langle\sigma_2^2\rangle_k}{(\sigma_m^+)^2} + \frac{\langle\tau_{12}^2\rangle_k}{(\tau_m^u)^2} \tag{8}$$

Formula (8) is derived on the assumption that matrix strength with combined tension and shear is determined by the energy criterion.

If failure of a unidirectionally reinforced layer, oriented at an angle φ_k, is typical of longitudinal shear, then

$$F(\langle\sigma_2\rangle_k, \langle\tau_{12}\rangle_k) = \frac{1}{2}\left(\frac{\langle\sigma_2\rangle_k}{\sigma_m^+}\right)^2 + (1+\mu_m)\left(\frac{\langle\tau_{12}\rangle_k}{\sigma_m^+}\right)^2 + \frac{\langle\sigma_2\rangle_k}{2(\sigma_m^+)^2}\sqrt{\langle\sigma_2^2\rangle_k + 4\langle\tau_{12}^2\rangle_k} \tag{9}$$

and with the combined action of compression and shear stresses

$$F(\langle\sigma_2\rangle_k, \langle\tau_{12}\rangle_k) = \frac{1}{2}\left(\frac{\langle\sigma_2\rangle_k}{\sigma_2^-}\right)^2 + (1+\mu_{21})\left(\frac{\langle\tau_{12}\rangle_k}{\sigma_2^-}\right)^2 - \frac{\langle\sigma_2\rangle_k}{2(\sigma_2^-)_k^2}\sqrt{\langle\sigma_2^2\rangle_k + 4\langle\tau_{12}^2\rangle_k} \tag{10}$$

The following designations in formulas (8)-(10) have been adopted: σ_m^+ and τ_m^u are matrix strength in tension and in shear, respectively; μ_m and μ_{21} are Poisson's ratios for the matrix and unidirectional material, respectively; $(\sigma_2^-)_k$ is transverse compression strength of unidirectionally reinforced kth layer where σ_2^- is determined by the following formula [2]:

$$\sigma_2^- = \frac{3.5\sigma_m^+}{(1+\mu_{21})\bar{\sigma}_r\sqrt{1-\mu_m^2}}$$

where $\bar{\sigma}_r$ is the structural parameter (see below).

4.2.4 Bond Failure

The strength criterion of an anisotropic material in the form of a tensor series is used to obtain an analytical expression of the F function in the case of fiber-matrix bond failure:

$$\Pi_{\alpha\beta}\sigma_{\alpha\beta} + \Pi_{\alpha\beta\gamma\delta}\sigma_{\alpha\beta}\sigma_{\gamma\delta} = 1 \tag{11}$$

Using the interface symmetry, assuming that the bonds ensuring mechanical interaction between fibers and matrix can be broken only by elongation, criterion (11) gives the following formula for F [3]:

$$F(\langle\sigma_2\rangle_k, \langle\tau_{12}\rangle_k) = \frac{\langle\sigma_2\rangle_k\bar{\sigma}_r}{\sigma_b} + \left(\frac{\langle\tau_{12}\rangle_k\bar{\tau}_{rz}}{\tau_b^u}\right)^2 \tag{12}$$

The value and the sign of the stresses $\langle\sigma_2\rangle_k$ and $\langle\tau_{12}\rangle_k$ are determined for each load from formulas (2) and (3). If the stress $\langle\sigma_1\rangle_k$ is compressive, then in formulas (9)-(12) it is with minus sign.

The parameters $\bar{\sigma}_r$ and $\bar{\tau}_{rz}$ in formulas (8) and (12) depend on the structure of the material, the volume fraction of fibers, the fiber lay-up, and the elastic properties of the fibers and the matrix. The values of these parameters are determined by the elasticity theory. Figures 4.3 and 4.4 show the dependences of these parameters on

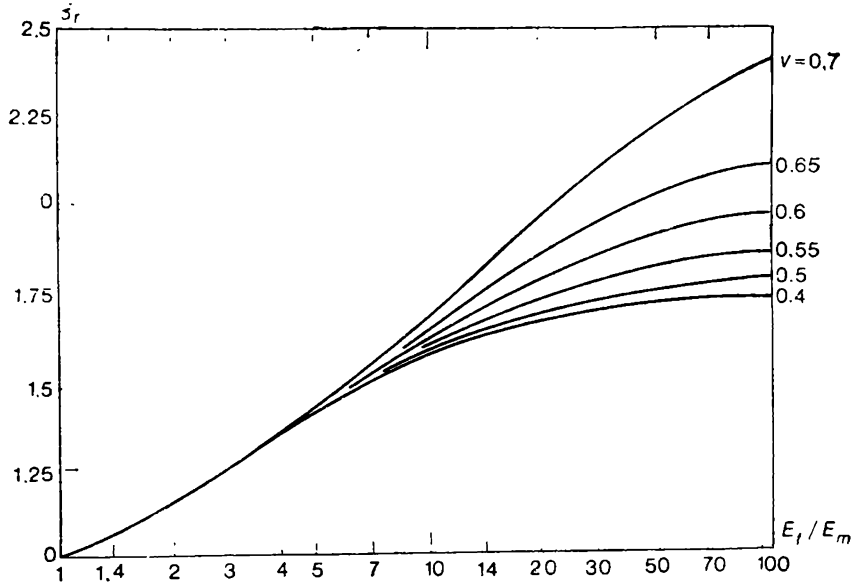

Fig. 4.3 Dependence of structural parameter $\bar{\sigma}_r$ on fiber volume fraction v and ratio between transverse elastic moduli of fibers E_f and matrix E_m

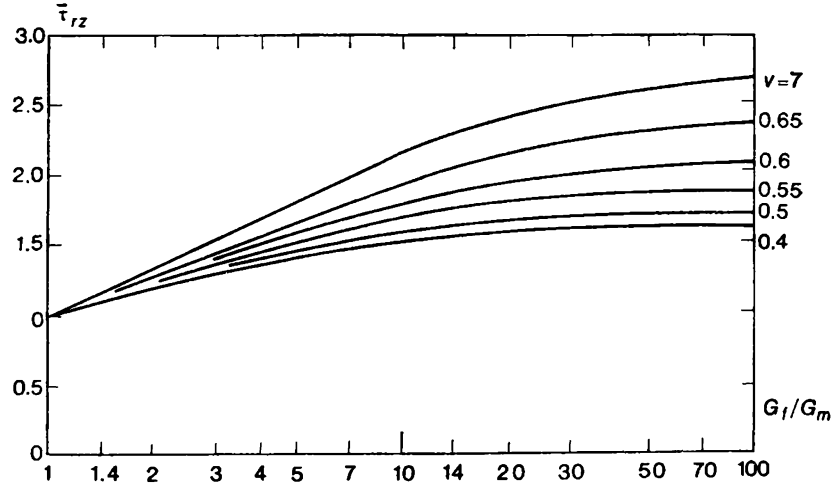

Fig. 4.4 Dependence of structural parameter $\bar{\tau}_{rz}$ on fiber volume fraction v and ratio between shear moduli of fibers G_f and matrix G_m

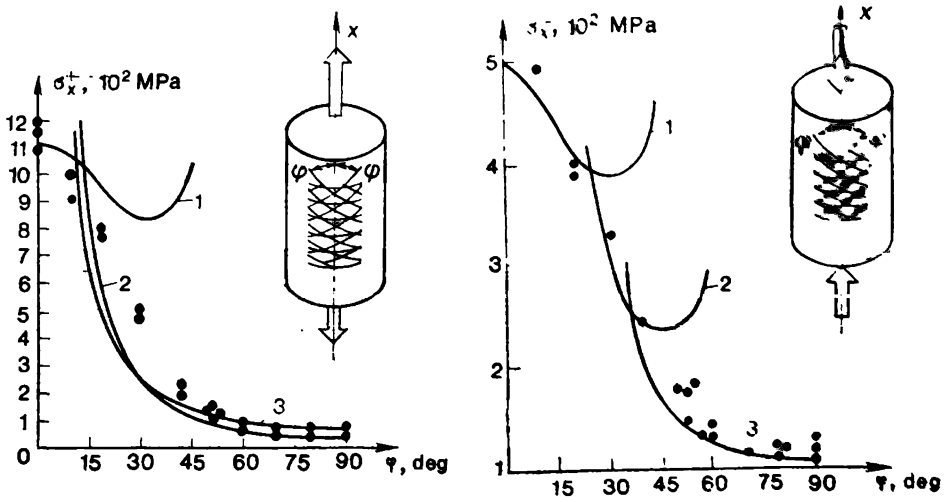

Fig. 4.5 Dependence of tensile strength on winding angle:
1—fiber failure; *2*—matrix tensile failure; *3*—matrix shear failure. The solid circles are experimental values

Fig. 4.6 Dependence of compressive strength on winding angle:
1—fiber failure; *2*—matrix shear failure; *3*—transverse compression failure. The solid circles are experimental values

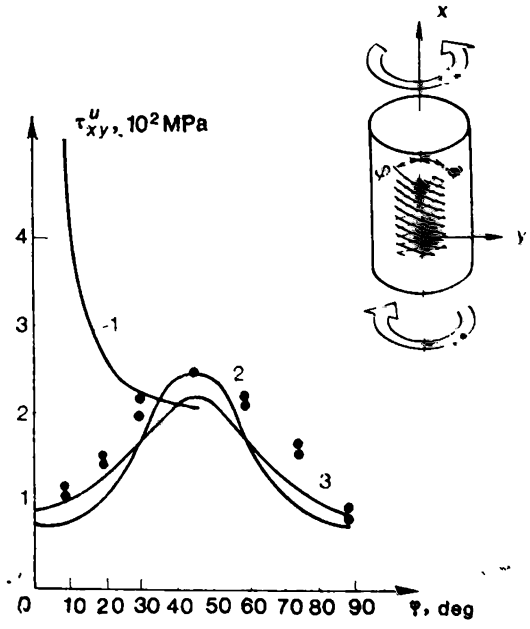

Fig. 4.7 Dependence of shear strength on winding angle:
1—fiber failure; *2*—matrix tensile failure; *3*—matrix shear failure. The solid circles are experimental values

the ratio of elastic moduli of fibers and the matrix with different volume fractions of fibers.

In formula (12) σ_b and τ_b^u denote the bond strengths in tension and in shear. These strengths are determined experimentally by the following dependences [3]:

$$\sigma_b = \sigma_2^+ \bar{\sigma}_r \tag{13}$$

$$\tau_b = \tau_{12}^u \bar{\tau}_{rz} \tag{14}$$

In these formulas σ_2^+ and τ_{12}^u denote experimentally found strengths of a unidirectional composite in transverse tension and longitudinal shear, and the parameters $\bar{\sigma}_r$ and $\bar{\tau}_{rz}$ are determined from the curves given in Figs. 4.3 and 4.4.

Figures 4.5, 4.6, 4.7 show dependences of tensile, compressive and shear strengths on the winding angle for an angle-ply reinforced fiber-glass plastic [1]. The theoretical curves are plotted according to criteria (6) and (7).

4.2.5 Biaxial Loading of an Orthogonally Reinforced Composite

The failure envelopes and curves of continuity loss for cross-ply epoxy fiber-glass plastic under biaxial loading are given in Fig. 4.8. The failure envelopes related to fiber failure are shown by solid lines, and the curves of continuity loss, related to matrix failure, by dashed lines. Criterion (6) is used to plot the ultimate strength curves, while criterion (7), taking into account formulas (8) and (9), for plotting the continuity loss curves. The working dependences, following from these criteria, were:

$$\langle\langle\sigma_x\rangle\rangle A_{22} - \langle\langle\sigma_y\rangle\rangle A_{12} = e_{fR}^{+}(A_{11}A_{22} - A_{12}^2) \tag{15}$$

$$-\langle\langle\sigma_x\rangle\rangle A_{12} + \langle\langle\sigma_y\rangle\rangle A_{11} = e_{fR}^{+}(A_{11}A_{22} - A_{12}^2) \tag{16}$$

$$\langle\langle\sigma_x\rangle\rangle A_{22} - \langle\langle\sigma_y\rangle\rangle A_{12} = e_{fR}^{-}(A_{11}A_{22} - A_{12}^2) \tag{17}$$

$$-\langle\langle\sigma_x\rangle\rangle A_{12} + \langle\langle\sigma_y\rangle\rangle A_{11} = e_{fR}^{-}(A_{11}A_{22} - A_{12}^2) \tag{18}$$

$$\langle\langle\sigma_x\rangle\rangle q_1 + \langle\langle\sigma_y\rangle\rangle q_2 = \sigma_m^+ \tag{19}$$

$$\langle\sigma_x\rangle\rangle q_3 + \langle\langle\sigma_y\rangle\rangle q_4 = \sigma_m^+ \tag{20}$$

$$\langle\langle\sigma_x\rangle\rangle q_3 - \langle\langle\sigma_y\rangle\rangle q_4 = \sigma_m^+ \tag{21}$$

$$\langle\sigma_x\rangle\rangle q_1 + \langle\langle\sigma_y\rangle\rangle q_2 = \sigma_m^+ \tag{22}$$

The notation in these formulas is as follows:

$$q_1 = \frac{B_{12}A_{22} - B_{22}A_{12}}{A_{11}A_{22} - A_{12}^2}\bar{\sigma}_r\sqrt{1-\mu_m^2}$$

$$q_2 = \frac{B_{22}A_{11} - B_{12}A_{12}}{A_{11}A_{22} - A_{12}^2}\bar{\sigma}_r\sqrt{1-\mu_m^2}$$

$$q_3 = \frac{B_{22}A_{22} - B_{12}A_{12}}{A_{11}A_{22} - A_{12}^2}\bar{\sigma}_r\sqrt{1-\mu_m^2}$$

$$q_4 = \frac{B_{12}A_{11} - B_{22}A_{12}}{A_{11}A_{22} - A_{12}^2}\bar{\sigma}_r\sqrt{1-\mu_m^2}$$

In Fig. 4.8 the numbers on some curves indicate the formulas used

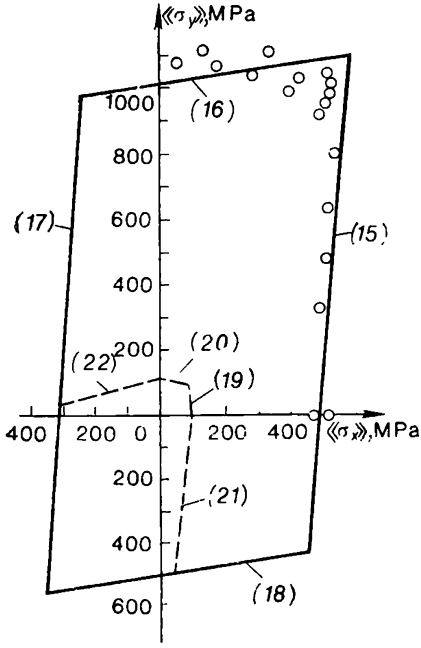

Fig. 4.8 Failure envelopes for cross-ply reinforced fiber-glass plastics. The open circles are experimental values

for their plotting. Experimental data obtained for fiber-glass plastic are also shown.

4.2.6 Combined Axial Loading and Shear of Cross-Ply Composite

Let us consider the case when a cross-ply composite is loaded in the directions parallel to reinforcement. Then some layers simultaneously subjected to the shear stresses $\langle\tau_{12}\rangle$ and the tensile stresses $\langle\sigma_2\rangle$, perpendicular to reinforcement, are in the most unfavourable conditions. The fracture mechanism of these layers depends on the ratio between the applied stresses $\langle\langle\tau_{xy}\rangle\rangle$ and $\langle\langle\sigma_x\rangle\rangle$ and the ratio between polymeric matrix strength and bond strength.

Let us consider the case when matrix strength is less than that of bond.

If the ratios $\langle\langle\tau_{xy}\rangle\rangle/\langle\langle\sigma_x\rangle\rangle$ exceed a definite value then the layer fracture is related to matrix failure in shear. In this case from criterion (7), taking account of (9), we obtain:

$$\langle\langle\tau_{xy}\rangle\rangle = \sqrt{u_1 - u_2\langle\langle\sigma_x^2\rangle\rangle - \langle\langle\sigma_x\rangle\rangle\sqrt{u_2^2\langle\langle\sigma_x^2\rangle\rangle + (2/\mu_m)\,u_1u_2}} \qquad (23)$$

where

$$u_1 = \frac{(\sigma_m^+ A_{66})^2}{(1+\mu_m)G_{12}^2}, \qquad u_2 = \left(\frac{q_5}{q}\right)^2 \frac{\mu_m A_{66}^2}{2G_{12}^2(1+\mu_m)}$$

$$q_5 = B_{22}A_{22} - B_{12}A_{12}, \quad q = A_{11}A_{22} - A_{12}^2$$

The pattern of composite failure, corresponding to criterion (23), which determines matrix shear fracture in layer b, is shown in Fig. 4.9. Following the failure of layer b shear stresses in layer a

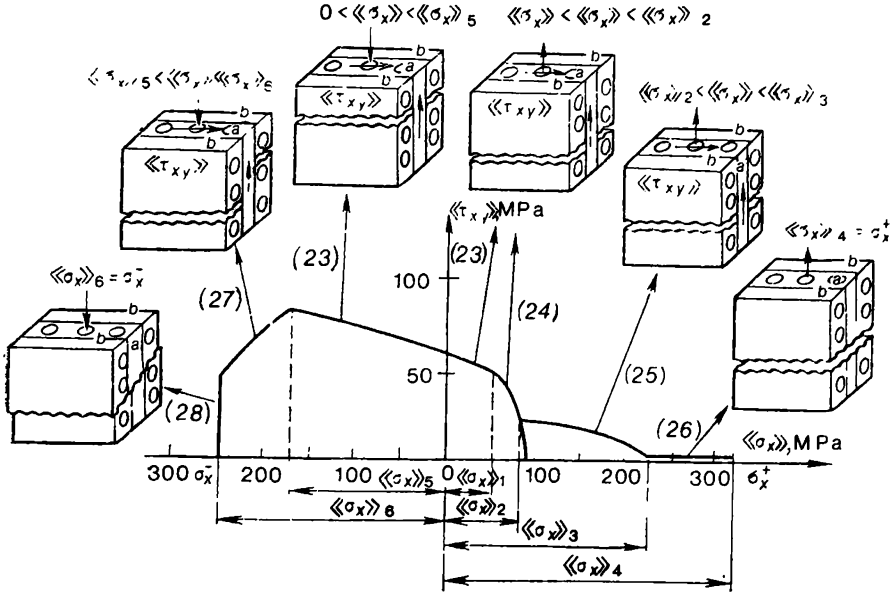

Fig. 4.9 Failure patterns and failure envelope for cross-ply reinforced fiber-glass plastics under axial loading combined with shear

increase jumpwise. With such a jumpwise increase in stresses, layer a usually fails and thus the failure of layer b practically determines the overall failure of the laminated material.

A decrease in the stress ratio $\langle\langle\tau_{xy}\rangle\rangle/\langle\langle\sigma_x\rangle\rangle$ to a definite limit causes a change in the mechanism of matrix failure in layer b, i.e. the matrix tensile failure occurs. In this case criterion (7), taking account of (8), gives

$$\langle\langle\tau_{xy}\rangle\rangle = \sqrt{u_3 - u_3u_4\langle\langle\sigma_x^2\rangle\rangle} \qquad (24)$$

where

$$u_3 = \left(\frac{\tau_m^u A_{66}}{G_{12}}\right)^2, \quad u_4 \left(\frac{q_5}{q}\right)^2 \left(\frac{\bar{\sigma}_r}{\sigma_m^+}\right)^2 (1 - \mu_m^2)$$

If the stress ratio $\langle\langle\tau_{xy}\rangle\rangle / \langle\langle\sigma_x\rangle\rangle$ does not exceed a definite limit, then the failure of layer b does not cause the simultaneous failure of layer a. Following the failure of b a considerable redistribution of stresses occurs in the laminate. Taking account of the real state of stress of layer a from criterion (7) we obtain:

$$\langle\langle\tau_{xy}\rangle\rangle = \sqrt{m_1^2 (\tau_m^u)^2 - u_5 \langle\langle\sigma_x^2\rangle\rangle} \tag{25}$$

where

$$u_5 = (1 - \mu_m^2) \left[\frac{\bar{\sigma}_r (1 - m_1) \mu_{21} E_1 \tau_m^u}{E_y \sigma_m^+}\right]^2$$

The notation in these formulas is as follows: m_1 is the ratio of the total volume of the layers reinforced in direction x to the overall volume of material; E_y is the elastic modulus of laminate in direction y; μ_{21} and E_1 are Poisson's ratio and the elastic modulus of a unidirectionally reinforced layer, respectively.

With a further increase in $\langle\langle\sigma_x\rangle\rangle$ the fibers fail as shown schematically in Fig. 4.9. In this case criterion (3) gives

$$\langle\langle\sigma_x\rangle\rangle = m_1 [vE_f + (1 - v)E_m] e_{fR}^+ \tag{26}$$

where v is the volume fraction of fibers, E_f and E_m are the elastic moduli of fibers and matrix, respectively.

It should be noted that the shape of the overall envelope to a large extent depends on the lay-up ratio of layers m_1. Thus, for example, when

$$m_1 = (1 - A)/[1 - A\ (1 - E_2/E_1)]$$

where

$$A = \sigma_m^+ / (E_1 \mu_{21} \bar{\sigma}_r e_{fR}^+ \sqrt{1 - \mu_m^2})$$

fibers fail in layer a simultaneously with the failure of the polymeric matrix in layer b.

Now let us consider the case of combined compression and shear. When the compressive stress $\langle\langle\sigma_x\rangle\rangle$ is changed from zero to some limit, criterion (23) remains valid and the stress $\langle\langle\sigma_x\rangle\rangle$ in the latter must be introduced with the minus sign.

With a further increase in the compressive stress the mechanism of layer failure changes. The failure becomes typical not of longitudinal shear, but of transverse compression. In this case from criteri-

on (7), taking account of (10), we obtain:

$$\langle\langle\tau_{xy}\rangle\rangle = \sqrt{u_6 - u_7\langle\langle\sigma_x^2\rangle\rangle} - \langle\langle\sigma_x\rangle\rangle\sqrt{u_7^2\langle\langle\sigma_x^2\rangle\rangle + (2/\mu_{21})u_6u_7} \quad (27)$$

where

$$u_6 = \frac{(\bar{\sigma_2}A_{66})^2}{(1+\mu_{21})G_{12}^2}, \quad u_7 = \left(\frac{q_5}{q}\right)^2 \frac{\mu_{21}A_{66}^2}{2G_{12}^2(1+\mu_{21})^2}$$

Criterion (27) can be applied at a change of the compressive stress $\langle\langle\sigma_x\rangle\rangle$ to the ultimate compression strength $\bar{\sigma_x}$ of a cross-ply composite in the direction of reinforcement x:

$$\bar{\sigma_x} = E_x\bar{e_{fR}} \quad (28)$$

where E_x is the elastic modulus of the cross-ply composite in direction x.

The strength envelopes plotted using formulas (23)-(28) for cross-ply (1 : 2) fiber-glass plastic are given in Fig. 4.9, numbers near the curves indicating the formulas used.

In conclusion, it should be noted that the approach described in this paper for the determination of strength of reinforced composites under combined loading by given properties of fibers and matrix and a given composite structure permits the solution of an inverse problem of the selection of the proper composite structure to provide a given strength.

The envelope in Fig. 4.9 cannot be described by the strength criteria based on average stresses. These criteria can practically describe only ellipse-like curves. Thus the strength criteria based on average stresses are of very limited applicability for composites.

4.3 CREEP MICROMECHANICS

4.3.1 Viscoelastic Properties of Components

Numerous experiments have provided evidence that polymeric matrices possess pronounced viscoelastic properties [6]. Under constant long-time loading strains in these materials can change by a factor of several times in comparison with their initial values. Thus, time is an important parameter for polymeric matrices.

Stress ranges exist for practically all polymeric matrices when they obey relations for a linear viscoelastic medium of the hereditary type [6]. In this case the physical stress-strain relationships are written in the following form:

$$2Ge_{ij}(t) = s_{ij}(t) + \int_0^t \Gamma(t-\theta)\, s_{ij}(\theta)\, d\theta \quad (29)$$

$$3K\varepsilon(t) = \sigma(t) + \int_0^t U(t-\theta)\,\sigma(\theta)\, d\theta \quad (30)$$

Here $s_{ij} = \sigma_{ij} - \sigma\delta_{ij}$ is the stress deviator, $e_{ij} = \varepsilon_{ij} - \varepsilon\delta_{ij}$ is the strain deviator, 3ε is the relative change of volume, σ is the average stress, ε is the average strain, G is the instantaneous elastic modulus of shear, and K is the instantaneous modulus of volume strain. The functions $\Gamma(t-\theta)$ and $U(t-\theta)$ characterize the rheologic properties of the material. The argument of these functions is the difference $t - \theta \geqslant 0$, i.e. equations (29) and (30) are invariant with respect to the zero time reference.

Having solved equations (29) and (30) with respect to s_{ij} and σ we obtain

$$s_{ij}(t) = 2G\left[e_{ij}(t) - \int_0^t R(t-\theta)\, e_{ij}(\theta)\, d\theta\right] \tag{31}$$

$$\sigma(t) = K\left[3\varepsilon(t) - \int_0^t V(t-\theta)\,\varepsilon(\theta)\, d\theta\right] \tag{32}$$

Here $R(t-\theta)$ and $V(t-\theta)$ are the resolvents of the kernels $\Gamma(t-\theta)$ and $U(t-\theta)$. The functions $R(t)$ and $\Gamma(t)$ must satisfy the same requirements as the kernels of creep $\Gamma(t)$ and $U(t)$.

If the kernels $\Gamma(t-\theta)$ and $U(t-\theta)$ are determined by experiment, we can calculate their resolvents. For the determination of the function $\Gamma(t-\theta)$ it is expedient to use experimentally plotted creep curves in pure shear. In this case, taking into account that $s_{ij}(t) = \tau_{12}(t) = \text{const}$, $\sigma = 0$, $e_{ij}(t) = \varepsilon_{12}(t)$ and $\varepsilon(t) = 0$, equations (29) and (30) reduce to a single equation:

$$2G\frac{\varepsilon_{12}(t)}{\tau_{12}} = G\frac{\gamma(t)}{\tau} = 1 + \int_0^t \Gamma(t-\theta)\, d\theta \tag{33}$$

If the creep function in pure shear is introduced

$$J(t) = \gamma(t)/\tau$$

then according to equation (33)

$$\Gamma(t) = G\, dJ(t)/dt \tag{34}$$

Consequently the creep kernel is obtained by differentiation of the creep function. This differentiation, for example, can be performed graphically. The discovery of an analytical expression of the function $\Gamma(t)$ reduces to approximation of the differentiated creep curves. The simplest analytical form of the creep kernel is an exponential function

$$\Gamma(t) = Ae^{-\alpha t} \quad (A > 0,\ \alpha > 0) \tag{35}$$

The merits of this form of the creep kernel are a relative simplicity of determining the constants A and α from the creep curves and that

kernel (35) permits the replacement of integral equation (29) by a first order differential equation with constant coefficients. The drawback of kernel (35) is that the presence of only two arbitrary constants does not always permit a high accuracy of creep curve approximation to be obtained over a wide time range. To increase approximation accuracy, the kernels in the form of a sum of exponents are frequently taken:

$$\Gamma(t) = \sum_{i=1}^{n} A_i e^{-\alpha_i t} \tag{36}$$

The presence of two or three terms of series (36) provides a high accuracy of approximation. An increasing number of parameters, however, complicates the mathematical apparatus when using these kernels. Kernels with a weak singularity at material loading are therefore used for the best description of the creep properties of the material in the short-time range. This implies that the function $\Gamma(t-\theta)$ tends to infinity as $t \to \theta$, corresponding to an infinite high material strain rate at the first instant after application of load. The second requirement of these kernels is prompted by the necessity of finiteness of the integral $\int_0^\infty \Gamma(t-\theta)\, d\theta$*. According to this condition the kernel $\Gamma(t-\theta)$ singularity must be weak, i.e. the kernel must be a Duffing kernel [6]:

$$At^{-\alpha}, \quad 0 < \alpha < 1 \tag{37}$$

It should be noted that in this case the creep curve is described by a power function, which increases indefinitely with an increasing argument. Thus, the Duffing kernel can be used only for materials with unstable creep strain, i.e. with a zero modulus of long-time elasticity.

For materials with a finite modulus of long-time elasticity A. R. Rzhanitsyn [4] suggested the following functions as a creep kernel

$$\Gamma(t) = Ae^{-\alpha t}t^{-\alpha}, \quad 0 < \alpha < 1 \tag{38}$$

The fractional-exponential functions in the form of the series

$$\Gamma(t) = \Im\alpha(-\beta, t) = \sum_{n=0}^{\infty} \frac{(-\beta)^n t^{(1+\alpha)\, n} t^{\alpha}}{\Gamma_0(1+n)(1+\alpha)} \tag{39}$$

* The expression $\eta_\tau = 1 + \int_0^\infty \Gamma(t-\theta)\, d\theta$ is the relation between the strain of steady-state creep $\gamma(t \to \infty)$ and short-time strain $\gamma(t \to 0)$. Here η_τ is called the characteristic of creep degree of the material in shear.

suggested by Yu. N. Rabotnov [6] is widely applied as the creep kernel of polymeric materials. The power alternating series (39) converges (although relatively slowly) at any finite $\beta > 0$ for all values of the argument $t > 0$.

The function $U(t)$ is determined similarly, but from experiments with hydrostatic pressure. It should be noted, however, that for polymeric matrices a volume change is practically elastic. Consequently, equations (30) and (32) reduce to the relation of the linear elasticity theory $3K\varepsilon = \sigma$. Thus, the rheonomous properties of polymeric materials in the linear range of strain are determined only by one creep kernel (of relaxation). The function $\Gamma(t)$, or $R(t)$, determined from shear tests, can be used as this kernel. But it can be a time function determined under other types of loading as well. Thus, for example, it is simpler technically to carry out creep tests under axial loading. In this case strain in the direction of loading is determined by the expression

$$\varepsilon_1(t) = D(t)\sigma_1 \tag{40}$$

where the creep function under axial loading is

$$D(t) = (1/E)\left[1 + \int_0^t K(t-\theta)\, d\theta\right] \tag{41}$$

A question arises concerning the kind of interrelation between the creep kernels and hence between the creep functions in shear and under axial loading. For polymeric materials this interrelation is found from the condition that the volume change is elastic.

As a result of some transformations we find that

$$\Gamma(t-\theta) = \frac{3}{2(1+\mu)} K(t-\theta) \tag{42}$$

where μ is Poisson's ratio of the material.

In solving volume problems of viscoelasticity for isotropic materials, the question arises of determining the time variations transverse to the loading direction. According to the condition of volume elastic change under long-time static loading the kernel of transverse creep $K_2(t-\theta)$ is expressed in terms of the creep kernel under axial loading:

$$K_2(t-\theta) = \frac{1}{2\mu} K(t-\theta) \tag{43}$$

Applying (43) we find the following relation between creep functions longitudinally and transversely with respect to the loading direction

$$D_2(t) = -\frac{1}{2} D(t) + \frac{1-2\mu}{2E} \tag{44}$$

Thus, the strain of an isotropic linearly viscoelastic material under triaxial long-time static stress is determined by the following dependence

$$\varepsilon_1(t) = D(t)\left(\sigma_1 - \frac{\sigma_2+\sigma_3}{2}\right) + \frac{1-2\mu}{2E}(\sigma_2+\sigma_3) \tag{45}$$

For practically any polymeric matrix a range of stresses is found where the stress-strain relations are linear. Occasionally, however, for example, at elevated temperatures, as well as under stresses approaching ultimate values, nonlinear stress-strain relations are

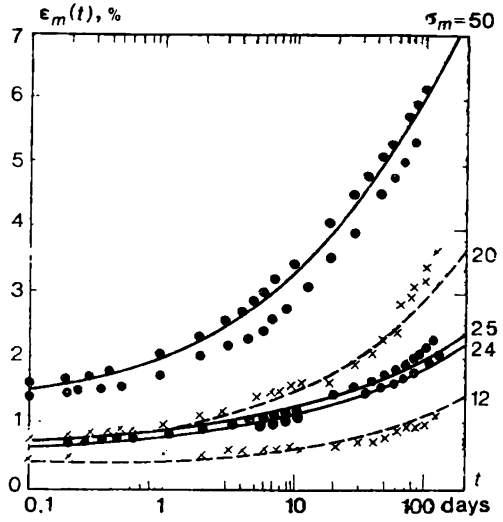

Fig. 4.10 Creep curves for epoxy matrix in tension (solid lines) and compression (dashed lines). The solid circles and crosses are experimental values

to be found. For a number of polymeric matrices nonlinearity changes with loading duration, i.e. neither the similarity condition nor the similarity of isochronous creep curves are confirmed. Figure 4.10 shows the creep curves of an epoxy matrix in uniaxial tension and compression under isothermic conditions $T = 294°K$. It is expedient to describe creep curves by the use of the rheological equation in the form

$$\varepsilon_m(t) = (1/E_m)\left[\sigma_m(t) + k_m\sigma_m^3(t) + \int_0^t K_m(t-\theta)\{\sigma_m(\theta) + [d_m + (k_m - d_m)e^{-\varkappa_m\theta}]\,\sigma_m^3(\theta)\}\,d\theta\right] \tag{46}$$

where the creep kernel $K_m(t-\theta)$ characterizes creep in the linear strain zone (as a rule, it is the zone of low load levels) and the three parameters k_m, d_m and $\varkappa_m$ permit the nonlinear behaviour of the polymeric matrix to be taken into account. The subscript m denotes the characteristics describing the matrix. It is convenient to take a sum of exponents as a creep kernel:

$$K_m(t-\theta) = \sum_{j=1}^{n} C_{mj} \exp[-\alpha_{mj}(t-\theta)]$$

It should be noted that for polymeric matrices when $n = 2$ or $n = 3$ for practical purposes sufficient accuracy is achieved. The solid and

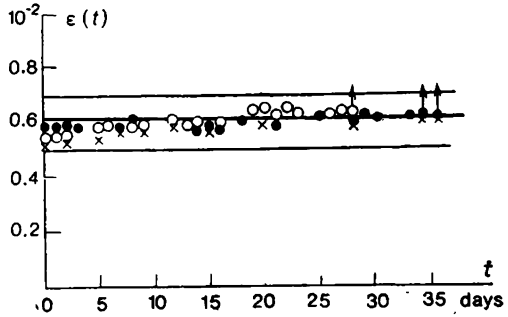

Fig. 4.11 Experimental creep curves for boron fibers under tensile stress $\sigma = 2.72 \cdot 10^3$ MPa

dashed creep curves in Fig. 4.10 are plotted according to dependence (46) when $n = 3$ and the following values of the parameters are taken:

$C_{m1} = 0.57$, $C_{m2} = 0.028$, $C_{m3} = 0.0106$, $\alpha_{m1} = 2$ (days)$^{-1}$,

$\alpha_{m2} = 83 \cdot 10$ (days)$^{-1}$, $\alpha_{m3} = 7.14 \cdot 10^3$ (days)$^{-1}$,

$k_m^+ = 0.35 \cdot 10^{-3}$ (MPa)$^{-2}$, $d_m^+ = 0.54 \cdot 10^{-2}$ (MPa)$^{-2}$,

$k_m^- = 0.104 \cdot 10^{-4}$ (MPa)$^{-2}$, $d_m^- = 0.61 \cdot 10^{-3}$ (MPa)$^{-2}$,

$\varkappa_m^+ = 0.4$ (days)$^{-1}$, $\varkappa_m^- = 0.55$ (days)$^{-1}$.

The superscripts + and − denote the characteristics of tension or compression, respectively.

The above statements on the rigidity properties of polymeric matrix under long-time loading can also be applied to the reinforcing fibers. But unlike polymeric matrices, fibers used in structural composites have relatively small creep. Such fibers as boron, carbon and glass practically do not change their rigidity properties during loading. Experimental creep curves for boron fibers under long-time tensile stress are illustrated in Fig. 4.11. The vertical arrows show the instants of fiber fracture.

If boron, carbon or glass fibers have practically no creep and can be considered as elastic, for organic fibers this premise can be quite erroneous. According to the results of [5] Kevlar-49 fibers possess creep properties. The results of creep analysis of high-strength organic threads impregnated with a polymeric matrix come to the same conclusion. In this case creep strains make up 50-60% of elastic ones.

4.3.2 Creep of Unidirectional Composites

4.3.2.1 Loading in the Direction of Reinforcement

In solving elastic boundary-value problems for models in the form of coaxial cylinders under uniaxial loading in the reinforcement direction, it is established that stresses in directions perpendicular to reinforcement make up a negligible fraction of stresses in the reinforcement direction. Thus, for fiber-glass and carbon-fiber plastics the ratio of transverse stresses to longitudinal ones is not larger than 0.1. If we consider that for practical applications the influence of transverse effects can be neglected, the conclusion can be drawn that stresses in the direction of reinforcement in the polymeric matrix and fibers are proportional to their elastic moduli. Since such reinforcing fibers as glass, carbon and boron practically do not creep, we can consider that respective composites under longitudinal load also practically do not creep, while stresses in fibers throughout loading remain practically constant.

To estimate the stress-strain state of components of organic-fiber plastics and of the whole material a set of equations must be solved presenting the laws of component straining, the condition of strain compatibility and the equilibrium equation. This problem has been solved [6] with the use of fractional-exponential (39) and exponential functions as creep kernels of the polymeric matrix and fibers. The conclusion can be drawn that strains of a unidirectional composite under long-time loading in the reinforcement direction are practically determined only by the properties of the fibers. During creep, stresses in the fibers practically do not change, and in the polymeric matrix relaxation of stresses occurs.

4.3.2.2 Longitudinal Shear

The longitudinal shear of a unidirectional composite is the stress under which the viscoelastic properties of composite material are most pronounced. The problem of determining the rigidity properties of composites in longitudinal shear, when geometry, volume fraction, and properties of the components are taken into account, reduced to the solution of a boundary-value problem for a doubly periodic model of a binary medium. But this solution

leads to great mathematical complexity and its practical application is restricted. Therefore, for the determination of the main characteristics of the stress-strain state of a unidirectional composite in longitudinal shear we use an approximation based on the methods of calculations for laminated media. Thus, deformation of a repeated composite element is identified with the combined deformation of a package of infinitely thin layers parallel to the loading plane.

The analysis of shear stress distribution in layers has shown that they change monotonically from layer to layer, reaching a maximum value in layers with maximum fiber content.

The stress concentration factor, i.e. the ratio between the maximum and the average values of stresses, depends both on the volume ratio of the components and the ratio of their shear moduli.

In boron plastics the stress concentration ($G_f/G_m \approx 100$) is reached at large volume fractions of fibers; for organic-fiber plastics, with $G_f/G_m \approx 2$, the maximum stresses are only 10-20% higher than average ones.

Owing to the viscoelasticity of the polymeric matrix (fibers are considered as transverse isotropic and elastic) redistribution of stresses in the material components occurs in the process of long-time loading.

The main characteristic of creep in composites with linearly strained polymeric matrices is an increase in the stress concentration factor over time. Time variation of the stress concentration factor for fiber-glass plastics and organic-fiber plastics are given in Fig. 4.12. An increase in stress concentration is more pronounced in organic-fiber plastics and enhances with an increasing level of polymeric matrix creep.

In a nonlinearly strained polymeric matrix the stress concentration decreases over time. If this decrease is negligible for materials reinforced with transverse isotropic fibers, for example, organic plastics, then for boron plastics with a volume fraction of fibers of 60%, it is 25%.

Fig. 4.13 shows changes in the stress concentration factor over time for an epoxy boron plastic at different levels of average stress. Curve *1* is for material with a linearly strained polymeric matrix.

Thus, it follows that in the process of creep of composites in longitudinal shear a significant change in the strained state of the components occurs. Therefore with a long-time constant average stress the plastic components are strained under the conditions of alternating stress field. This circumstance complicates the creep analysis of composites, taking into account their structure geometry, volume fraction and rheological properties of their components. The stress field analysis in the material components and of the features of its redistribution over time has made possible the use, within

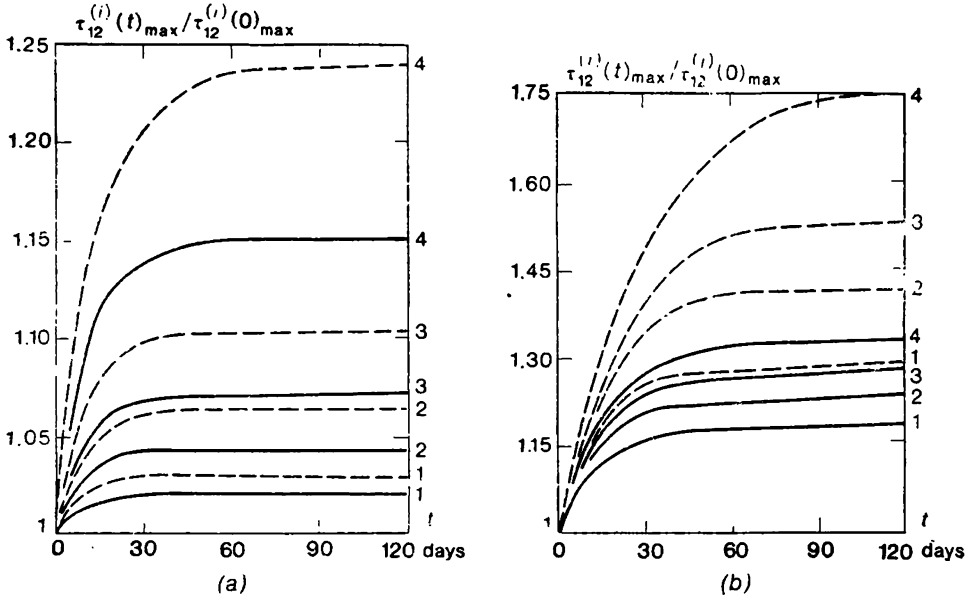

Fig. 4.12 Time variation of stress concentration factor in longitudinal shear of (*a*) fiber-glass plastics and (*b*) organic plastics. The solid lines correspond to matrix creep degree $\eta_{m\tau} = 3$, and the dashed lines, to $\eta_{m\tau} = 10$. Curves *1* to *4* correspond to composites with volume fraction $v = 0.3, 0.5, 0.6, 0.7$

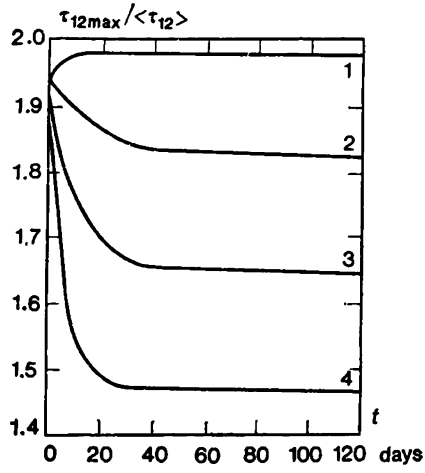

Fig. 4.13 Variation of stress concentration factor for epoxy boron plastics at different levels of average stresses:
1—$\langle\tau_{12}\rangle = 5$ MPa; *2*—$\langle\tau_{12}\rangle = 12.5$ MPa; *3*—$\langle\tau_{12}\rangle = 25$ MPa; *4*—$\langle\tau_{12}\rangle = 50$ MPa

the design model, of the assumption that for a repeated material element there is a plane parallel to the plane of loading in which shear stresses in the process of creep are practically constant. Thus, if one considers the strain in this plane equal to the strain of the whole composite the problem is significantly simplified. The point is that in this case creep strain of the composite is determined as a sum of strains of fibers and polymeric matrix under long-time constant shear stress τ_{m12}. The value of τ_{m12} depends both on the average stress $\langle\tau_{12}\rangle$ and on the strain characteristics and volume fraction of the components. This value is determined by

$$\tau_{m12} = \frac{G_f}{G_{12}}\left[1 - \frac{1-\eta_{12}}{1-\eta_{m\tau}}\left(1 - \frac{G_m}{G_{frz}}\right)\right]\langle\tau_{12}\rangle \tag{47}$$

where $\eta_{m\tau}$ and η_{12} are the characteristics of the degree of shear creep of the polymeric matrix and composite, respectively. If $\eta_{m\tau}$ is determined by

$$\eta_{m\tau} = \frac{J_m(t)\,|_{t\to\infty}}{J_m(t)\,|_{t\to 0}}$$

then η_{12} in the linear strain zone is determined by the ratio of moduli of composite longitudinal shear, corresponding to strain of short-time loading and strain of steady-state creep. Thus we have

$$\eta_{12} = \frac{1+(2/c_1)\sqrt{v/\pi}\,[(2/\sqrt{1-c_1^2})\arctan\sqrt{(1+c_1)\cdot(1-c_1)}-\pi/2]-2\sqrt{v/\pi}}{1+(2/c_2)\sqrt{v/\pi}\,[(2/\sqrt{1-c_2^2})\arctan\sqrt{(1+c_2)\cdot(1-c_2)}-\pi/2]-2\sqrt{v/\pi}}\,\eta_{m\tau}$$

where

$$c_1 = 2\sqrt{v/\pi}\,[1-(1/G_f)\,J_m^{-1}(t)\,|_{t\to 0}]$$

$$c_2 = 2\sqrt{v/\pi}\,[1-(1/G_f)\,J_m^{-1}(t)\,|_{t\to\infty}]$$

The shear strain of composite is determined by

$$\langle\gamma_{12}(t)\rangle = v_\omega\gamma_f + (1+v_\omega)\,\gamma_m = [v_\omega/G_f + (1-v_\omega)J_m(t)]\tau_{m12} \tag{48}$$

where v_ω is the parameter characterizing the ratio between fibers and matrix in the plane of stress τ_{m12} action. The parameter v_ω is found from

$$v_\omega = \left(1 + \frac{1-\eta_{12}}{\eta_{12}-\eta_{m\tau}}\,\frac{G_m}{G_f}\right)^{-1}$$

According to (48), and taking into account (47), the creep curve of a unidirectional composite in longitudinal shear is determined by

$$\langle\gamma_{12}(t)\rangle = s_{66}(t)\;\langle\tau_{12}\rangle \tag{49}$$

where $s_{66}(t)$ is the creep function of the composite in longitudinal shear:

$$s_{66}(t) = \frac{1}{G_{12}}\,\frac{1-\eta_{12}}{1-\eta_{m\tau}}\left[\frac{\eta_{12}-\eta_{m\tau}}{1-\eta_{12}} + G_m J_m(t)\right] \tag{50}$$

The shear modulus, G_{12}, of composite is found experimentally or by the structural theory of reinforced media.

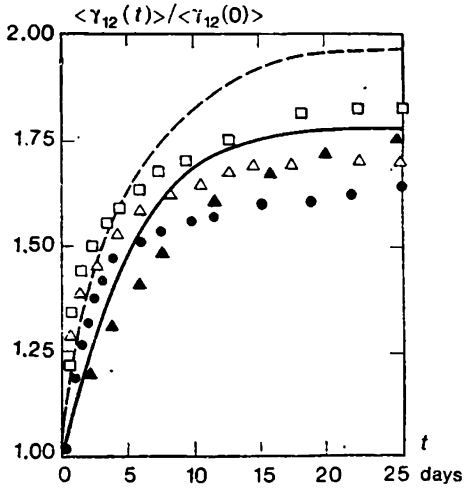

Fig. 4.14 Creep curves for epoxy glass plastics in longitudinal shear

Experimental creep curves for epoxy fiber-glass plastic obtained within shear stresses from 15 to 24 MPa are shown in Fig. 4.14. The dashed line is the creep curve of the polymeric matrix, the solid line is plotted according to (49), and the solid curve illustrates the experimental data.

4.3.2.3 Transverse Loading

In order to find the stress-strain state of the structural elements of unidirectional composites under long-time transverse loading, we must solve a volume boundary-value problem for the heterogeneous binary medium. However, at present we do not know such a practically applicable solution, therefore an approximation method of calculation is suggested, permitting the solution in an explicit form to be obtained. To find the characteristics of distribution and redistribution of stresses in the components under composite transverse loading, we use a repeated element of the doubly periodic structure of unidirectional composite as a design model shown in Fig. 4.15.

The section method is applied here, i.e. hypothetical section by planes parallel to that of reinforcement and to the direction of action of the transverse external loading. Thus, the repeated element is divided into an arbitrary number of parallel layers, the thickness of the latter decreasing with an increase in the number of sections.

The parameter v_ω varies from layer to layer and, according to Fig. 4.15, is determined by expression $v_\omega = (r_f/l) \cos \omega$. In the limiting case, when layers contain only polymeric matrix, $v_\omega = 0$.

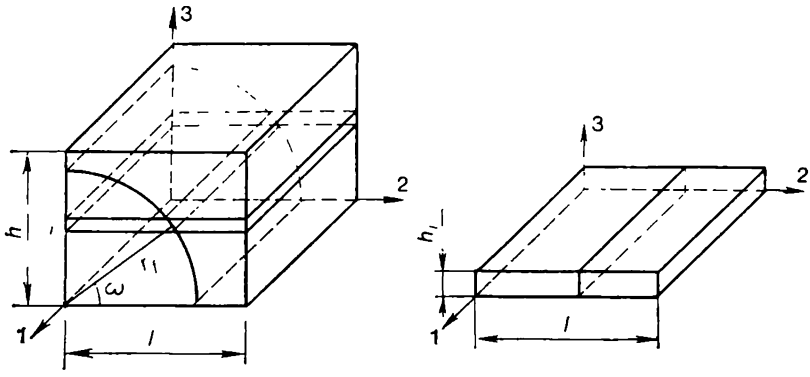

Fig. 4.15 Model of unidirectional composite

When formulating a set of equations to determine the stress-strain state of the repeated element, subjected to creep under transverse loading, the following starting hypotheses are used:

(1) all element layers of the repeated element are deformed together, i.e. their strains in the loading direction are equal:

$$(1 - v_\omega)\varepsilon^\omega_{m2}(t) + v_\omega \varepsilon^\omega_{f2}(t) = \langle \varepsilon_2(t) \rangle \tag{51}$$

where $\varepsilon^\omega_{m2}(t)$, $\varepsilon^\omega_{f2}(t)$ are the respective strains of matrix and fibers in the layer corresponding to the angle ω (Fig. 4.15);

(2) strains of fibers and matrix in the direction of reinforcement are equal

$$\varepsilon^\omega_{m1}(t) = \varepsilon^\omega_{f1}(t) = \varepsilon^\omega_{m1}(t) = \mu_{21} \langle \varepsilon_2(t) \rangle \tag{52}$$

and in many cases, for example, for high-modulus anisotropic reinforcing fibers, it is expedient to use the condition

$$\mu_{21} = 0$$

(3) section planes of the repeated element remain plane throughout the deformation:

$$\varepsilon^\omega_{m3}(t) = \varepsilon^\omega_{f3}(t) \tag{53}$$

(4) matrix and fibers are deformed together and the equilibrium equation holds:

$$(1 - v_\omega)\sigma^\omega_{m3}(t) + v_\omega \sigma^\omega_{f3}(t) = 0 \tag{54}$$

(5) stresses in the direction of loading in different elementary layers in matrix and fibers are similar and on average equal the

external applied stress:

$$\sigma_{m2}^{\omega}(t) = \sigma_{f2}^{\omega}(t) = \sigma_2^{\omega}(t) \tag{55}$$

$$(r_f/h) \int_0^{\pi/2} \sigma_2^{\omega}(t) \cos\omega \, d\omega + (1 - r_f/h)\, \sigma_{m2}(t) = \langle \sigma_2(t) \rangle \tag{56}$$

where $\sigma_{m2}(t)$ is stress in the nonreinforced part of the estimated element;

(6) matrix is a linear isotropic viscoelastic material, and fibers are a transverse isotropic elastic material

$$\varepsilon_{mj}^{\omega}(t) = S_{mjl}\left[\sigma_{ml}^{\omega}(t) + \int_0^t K(t-\theta)\, \sigma_{ml}^{\omega}(\theta)\, d\theta\right] \tag{57}$$

$$\varepsilon_{fj}^{\omega}(t) = S_{fjl}\sigma_{fl}^{\omega}(t) \qquad j,\ l = 1,\ 2,\ 3 \tag{58}$$

where S_{mjl}, S_{fjl} are the compliance coefficients of matrix and fibers, respectively, and $\varepsilon_{mj}^{\omega}$, $\varepsilon_{fj}^{\omega}$, σ_{ml}^{ω}, σ_{fl}^{ω} are the strains and stresses in matrix and fibers in the layer, corresponding to ω = const.

As a result of the solution of the set of equations (51)-(58) regularities of stress variation in the composite components and average strains under the long-time constant average stress $\langle \sigma_1 \rangle$ are found. It should be noted that while solving this set some mathematical difficulties may be encountered, associated with the chosen creep kernel of the matrix. Therefore, it is recommended to use the simplest functions as creep kernels, namely, exponential ones. With some loss of accuracy for short-time loading, it is possible to obtain explicit results accurate for long-time loading.

An analysis of the obtained results has shown that the composite components under uniaxial transverse loading are in a three-dimensional state of stress. The direction of the maximum main stress coincides with that of loading. The two other principal stresses are roughly equal and compose about half of the stress maximum value. Analogous results for boron plastic by the method of finite elements in elasticity have been obtained by Foye [7]. This ratio of stress components is maintained throughout the whole loading cycle.

As with longitudinal shear, with transverse loading the stress concentration increases over time. This process is more intensive for composites with anisotropic fibers than for those with isotropic fibers. Thus, for carbon-fiber plastic the factor of maximum stress concentration, with 50% fraction of fibers, changes in the process of creep from 1.18 at the time of loading to 1.42 when steady-state strain is reached. For fiber-glass plastic the corresponding values of stress concentration factor are 1.63 and 1.75. An increase in stress concentration over time is also caused by the growth of the creep

degree of polymeric matrix. The maximum stress concentration factor for carbon plastic with the matrix creep degree of 4 is 20% higher than that for a similar material with matrix creep degree of 2.

On the basis of stress stability the deformation law of a unidirectional composite under long-time transverse loading is established in a certain layer

$$\langle \varepsilon_2 (t) \rangle = v_\omega \varepsilon_f + (1 - v_\omega)\, \varepsilon_m$$

where ε_f is the elastic strain of fibers under three-dimensional stress and ε_m is the matrix strain determined by the deformation law under

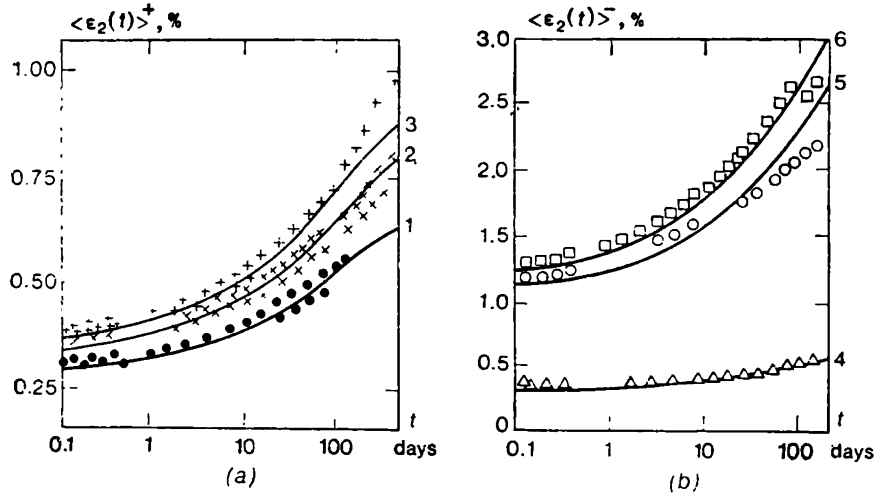

Fig. 4.16 Creep curves for organic plastics in (*a*) transverse tension and (*b*) compression for the following stress values:
1—$\langle \sigma_2 \rangle^+ = 12$ MPa; *2*—$\langle \sigma_2 \rangle^+ = 14$ MPa; *3*—$\langle \sigma_2 \rangle^+ = 15$ MPa; *4*—$\langle \sigma_2 \rangle^- = 14$ MPa; *5*—$\langle \sigma_2 \rangle^- = 46.4$ MPa; *6*—$\langle \sigma_2 \rangle^- = 50$ MPa

long-time static stress. After a number of transformations the following expression is obtained

$$\langle \varepsilon_2 (t) \rangle = s_{22} (t)\ \langle \sigma_2 \rangle \tag{59}$$

where

$$s_{22} (t) = \frac{1}{E_2} \frac{1-\eta_2}{1-\eta_m} \left[\frac{\eta_2 - \eta_m}{1-\eta_2} + E_m D (t) \right] \langle \sigma_2 \rangle \tag{60}$$

The modulus of transverse elasticity, E_2, is determined either by experiment, or from the structural theory of reinforced materials. The characteristic of the degree of plastic transverse creep, η_2, is determined by an expression similar to η_{12} if G is replaced by E and the function $J(t)$ by $D(t)$.

The creep curves for an organic-fiber plastic in tension and compression are given in Fig. 4.16 for three levels of stresses. The agreement between experimental and theoretical curves is satisfactory.

4.3.3 Creep in Laminates

In real structures composites are usually used in the form of balanced laminated materials consisting of alternating unidirectionally reinforced layers with different orientations. As a result of simultaneous deformation of all the layers non-uniform stress distribution among layers develops, the stresses redistributing over time. A widely used quasi-elastic method of solution of viscoelastic problems for laminates [8, 9], as well as the method of averaging the

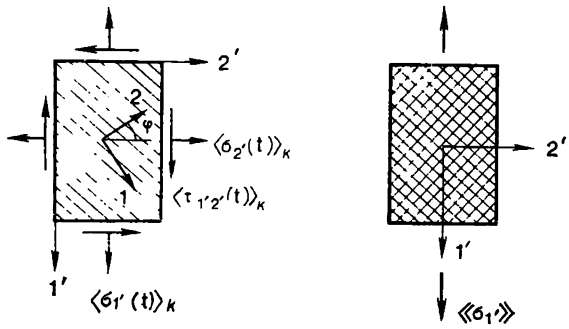

Fig. 4.17 Stress-strain state of unidirectional reinforced layer with arbitrary orientation

components of elastic matrices or compliance of different layers, is based on an assumption of permanent stress field in these materials.

Let us consider the stress-strain state of an arbitrarily oriented unidirectionally reinforced layer, loaded with stresses varying over time $\langle\sigma_{1'}(t)_k\rangle$, $\langle\sigma_{2'}(t)_k\rangle$, $\langle\tau_{1'2'}(t)_k\rangle$ (Fig. 4.17). In the matrix form of description we introduce the notation

$$\langle\tau_{1'2'}(t)_k\rangle = \langle\sigma_{6'}(t)_k\rangle, \quad \langle\tau_{12}(t)_k\rangle = \langle\sigma_6(t)_k\rangle$$

$$\langle\gamma_{1'2'}(t)_k\rangle = \langle\varepsilon_{6'}(t)_k\rangle, \quad \langle\gamma_{12}(t)_k\rangle = \langle\varepsilon_6(t)_k\rangle$$

In this case stresses along the axes of elastic symmetry of a unidirectionally reinforced layer are determined by

$$[\langle\sigma_j(t)4\rangle_k] = [T_k]\,[\langle\sigma_p(t)\rangle_k], \quad j = 1', 2', 6'; \quad p = 1, 2, 6. \tag{61}$$

The transformation matrix has the form

$$[T_k] = \begin{bmatrix} \cos^2\varphi_k & \sin^2\varphi_k & \sin 2\varphi_k \\ \sin^2\varphi_k & \cos^2\varphi_k & -\sin 2\varphi_k \\ -1/2\sin 2\varphi_k & 1/2\sin 2\varphi_k & \cos 2\varphi_k \end{bmatrix}$$

The deformation law of a unidirectionally reinforced layer in the case of the plane stress state in the axes of elastic symmetry is written

as follows

$$[\langle \varepsilon_i(t)\rangle_k] = [S_{ij}^{(k)}]\,[\langle \sigma_j(t)\rangle_k] + \int_0^t [S_{ij}^{(k)} K_{ij}^{(k)}(t-\theta)]\,[\langle \sigma_j(\theta)\rangle_k]\,d\theta \qquad (62)$$

where S_{ij} are the coefficients of compliance, $K_{ij}(t-\theta)$ are the creep kernels characterizing the properties of a unidirectionally reinforced layer in the axes of elastic symmetry.

Strains of unidirectional composite at an angle to the axes of elastic symmetry are determined by

$$[\langle \varepsilon_o(t)\rangle_k] = [T_k]^{-1}\,[\langle \varepsilon_i(t)\rangle_k],\quad o = 1', 2', 6';\ i = 1, 2, 6 \qquad (63)$$

Solving equations (61)-(62) together we obtain the deformation law of a unidirectionally reinforced layer at an angle to the axes of elastic symmetry:

$$[\langle \varepsilon_o(t)\rangle_k] = [S_{op}^{(k)}]\,[\langle \sigma_p(t)\rangle_k] + \int_0^t [S_{op}^{(k)} K_{op}^{(k)}(t-\theta)]\,[\langle \sigma_p(\theta)\rangle_k]\,d\theta \qquad (64)$$

where

$$[S_{op}^{(k)}] = [T_k]^{-1}\,[S_{ij}^{(k)}]\,[T_k]$$
$$[S_{op}^{(k)} K_{op}^{(k)}(t-\theta)] = [T_k]^{-1}\,[S_{ij}^{(k)} K_{ij}^{(k)}(t-\theta)]\,[T_k] \qquad (64a)$$
$$i, j = 1, 2, 6;\ p, o = 1', 2', 6'$$

The creep kernels of unidirectional composite in the axes of elastic symmetry $K_{ij}(t-\theta)$ can be determined both by experiment and by calculation proceeding from the properties of the components.

On the basis of dependences (64) we obtain expressions for the determination of creep strains of arbitrarily oriented unidirectionally reinforced material under plane stress.

For the determination of the stress-strain state of a laminated composite under plane long-time loading the following assumptions are made:

(1) strains of individual layers are equal to strains of the whole laminate

$$\langle\langle \varepsilon_o(t)\rangle\rangle = \langle \varepsilon_o(t)\rangle_k,\quad o = 1', 2', 6' \qquad (65)$$

(2) average stresses in composite are equal to the averaged stresses of individual layers

$$[\langle\langle \sigma_p(t)\rangle\rangle] = \sum_1^n m_k\,[\langle \sigma_p(t)\rangle_k],\quad p = 1', 2', 6' \qquad (66)$$

where m_k is the specific volume of the kth layer;

(3) the deformation law of an arbitrarily oriented unidirectionally reinforced layer has the form (64).

The set of equations (64)-(66) determines the stress-strain state of a laminated composite under long-time plane loading. To solve this set of equations it is expedient to use the Laplace transform. Then from (64) and (66), and taking (65) into account we obtain:

$$[\langle\langle\bar{\varepsilon}_o(p)\rangle\rangle] = [S_{op}^{(k)}(1+\bar{K}_{op}^{(k)}(p)][\langle\bar{\sigma}_p(p)\rangle_k] \tag{67}$$

$$[\langle\langle\bar{\sigma}_p(p)\rangle\rangle] = \sum_1^n m_k[\langle\bar{\sigma}_p(p)\rangle_k], \quad o,\ p=1',\ 2',\ 6' \tag{68}$$

where $\langle\langle\bar{\varepsilon}_o(p)\rangle\rangle$, $\langle\langle\bar{\sigma}_p(p)\rangle\rangle$, $K_{op}^{(k)}(p)$ and $\langle\bar{\sigma}_p(p)\rangle_k$ are Laplace representations of the corresponding functions.

From (67) we obtain expressions determining the stress state of an arbitrary unidirectionally reinforced layer of the laminated composite at given deformations:

$$[\langle\bar{\sigma}_p(p)\rangle_k] = [S_{op}^{(k)}(1+\bar{K}_{op}^{(k)}(p))]^{-1}[\langle\langle\bar{\varepsilon}_o(p)\rangle\rangle], \quad o,\ p=1',\ 2',\ 6' \tag{69}$$

In its turn dependence (68), taking account of (69), establishes the relationship between representations of external stresses and strains which, in the general case, determines creep and stress relaxation of the laminated composite:

$$[\langle\langle\bar{\sigma}_p(p)\rangle\rangle] = [\sum_1^n m_k[S_{op}^{(k)}(1+\bar{K}_{op}^{(k)}(p))]^{-1}][\langle\langle\bar{\varepsilon}_o(p)\rangle\rangle] \tag{70}$$

hence

$$[\langle\langle\bar{\varepsilon}_o(p)\rangle\rangle] = [\sum_1^n m_k[S_{op}^{(k)}(1+\bar{K}_{op}^{(k)}(p))]^{-1}]^{-1}[\langle\langle\bar{\sigma}_p(p)\rangle\rangle] \tag{71}$$

It should be noted that the solution of Eqs. (70), (71), even with the simplest creep kernels (exponential), is a very complicated problem. However, for a number of materials and particular cases of loading this problem can be significantly simplified if account is taken of the characteristics related to the properties of the components and the geometry of orientation of the unidirectionally reinforced layers. For example, in materials reinforced with fibers of boron, carbon and glass, strain in the direction of fibers can be considered with high accuracy as elastic [89] and only viscoelastic properties must be taken into account under transverse loading and in longitudinal shear.

We can take as an example a symmetrically reinforced binary composite with layers oriented at angles $\pm\varphi$ to the axes of elastic symmetry, $m_1 = m_2 = 0.5$, loaded along one of the symmetry axes (e.g., along 1') with the stress $\langle\langle\sigma_1'\rangle\rangle$ constant over time (Fig. 4.17). The condition $\langle\langle\varepsilon_{6'}\rangle\rangle = 0$ follows from this material orthotropic symmetry. Considering dependences (69) in an expanded form, it is possible to show that for layers oriented at angles $+\varphi$ and $-\varphi$ to

the symmetry axes the stresses $\langle\sigma_1'(t)\rangle_1 = \langle\sigma_1'(t)\rangle_2$, $\langle\sigma_2'(t)\rangle_1 = \langle\sigma_2'(t)\rangle_2$, and $\langle\tau_{1'2'}(t)\rangle_1 = -\langle\tau_{1'2'}(t)\rangle_2$. And when dependence (66) is taken into account we obtain $\langle\sigma_{1'}(t)\rangle_{1,2} = \langle\langle\sigma_{1'}\rangle\rangle$, $\langle\sigma_{2'}(t)\rangle_1 = \langle\sigma_{2'}(t)\rangle_2 = 0$ and $\langle\tau_{1'2'}(t)\rangle_1 + \langle\tau_{1'2'}(t)\rangle_2 = 0$. Hence, for the determination of the viscoelastic behaviour of the considered material the set of equations (67) must be solved taking into account the above-mentioned conditions. Now this set has the form

$$\begin{aligned}
\langle\langle\bar{\varepsilon}_{1'}(p)\rangle\rangle &= \bar{S}^{(k)}_{1'1'}\langle\langle\sigma_{1'}\rangle\rangle(1/p) + \bar{S}^{(k)}_{1'6'}\langle\bar{\tau}_{1'2'}(p)\rangle_k \\
\langle\langle\bar{\varepsilon}_{2'}(p)\rangle\rangle &= \bar{S}^{(k)}_{1'2'}\langle\langle\sigma_{1'}\rangle\rangle(1/p) + \bar{S}^{(k)}_{2'6'}\langle\bar{\tau}_{1'2'}(p)\rangle_k \qquad (72)\\
0 &= \bar{S}^{(k)}_{1'6'}\langle\langle\sigma_{1'}\rangle\rangle(1/p) + \bar{S}^{(k)}_{6'6'}\langle\bar{\tau}_{1'2'}(p)\rangle_k
\end{aligned}$$

where, taking (64a) into account,

$$\begin{aligned}
\bar{S}^{(k)}_{1'1'} &= S^{(k)}_{11}[1+\bar{K}^{(k)}_{11}(p)]\cos^4\varphi + S^{(k)}_{22}[1+\bar{K}^{(k)}_{22}(p)]\sin^4\varphi \\
&\quad + \{2S^{(k)}_{12}[1+K^{(k)}_{12}(p)] + S^{(k)}_{66}[1+K^{(k)}_{66}(p)]\}\sin^2\varphi\cos^2\varphi \\
\bar{S}^{(k)}_{1'2'} &= \{S^{(k)}_{11}[1+\bar{K}^{(k)}_{11}(p)] + S^{(k)}_{22}[1+\bar{K}^{(k)}_{22}(p)] \\
&\quad - S^{(k)}_{66}[1+\bar{K}^{(k)}_{66}(p)]\}\sin^2\varphi\cos^2\varphi \\
&\quad + S^{(k)}_{12}[1+\bar{K}^{(k)}_{12}(p)](\cos^4\varphi + \sin^4\varphi) \\
\bar{S}^{(k)}_{1'6'} &= \{2[S^{(k)}_{11}[1+\bar{K}^{(k)}_{11}(p)]\cos^2\varphi - S^{(k)}_{66}[1+\bar{K}^{(k)}_{66}(p)]\sin^2\varphi] \\
&\quad - [2S^{(k)}_{12}[1+\bar{K}^{(k)}_{12}(p)] + S^{(k)}_{66}[1+\bar{K}^{(k)}_{66}(p)]] \\
&\quad \times(\cos^2\varphi - \sin^2\varphi)\}\sin\varphi\cos\varphi \\
\bar{S}^{(k)}_{2'6'} &= \{2[S^{(k)}_{11}[1+\bar{K}^{(k)}_{11}(p)]\sin^2\varphi - S^{(k)}_{66}[1+\bar{K}^{(k)}_{66}(p)]\cos^2\varphi] \\
&\quad + [2S^{(k)}_{12}[1+\bar{K}^{(k)}_{12}(p)] + S^{(k)}_{66}[1+\bar{K}^{(k)}_{66}(p)]] \\
&\quad \times(\cos^2\varphi - \sin^2\varphi)\}\sin\varphi\cos\varphi \\
\bar{S}^{(k)}_{6'6'} &= 4\{S^{(k)}_{11}[1+\bar{K}^k_{11}(p)] - 2S^{(k)}_{12}[1+\bar{K}^{(k)}_{12}(p)] + S_{22}[1+\bar{K}^{(k)}_{22}(p)]\} \\
&\quad \times\sin^2\varphi\cos^2\varphi + S^{(k)}_{66}[1+\bar{K}^{(k)}_{66}(p)](\cos^2\varphi - \sin^2\varphi)^2 \qquad (73)
\end{aligned}$$

From the last equation of set (72) we obtain for the kth layer

$$\langle\bar{\tau}_{1'2'}(p)\rangle_k = -\frac{\bar{S}^{(k)}_{1'6'}}{\bar{S}^{(k)}_{6'6'}}\frac{\langle\langle\sigma_{1'}\rangle\rangle}{p} \qquad (74)$$

The composite strains are determined by the first two equations of set (72):

$$\begin{aligned}
\langle\langle\bar{\varepsilon}_{1'}(p)\rangle\rangle &= \left(\bar{S}^{(k)}_{1'1'} - \frac{\bar{S}^{(k)2}_{1'6'}}{\bar{S}^{(k)}_{6'6'}}\right)\frac{\langle\langle\sigma_{1'}\rangle\rangle}{p} \\
\langle\langle\bar{\varepsilon}_{2'}(p)\rangle\rangle &= \left(\bar{S}^{(k)}_{1'2'} - \frac{\bar{S}^{(k)}_{1'6'}\bar{S}^{(k)}_{2'6'}}{\bar{S}^{(k)}_{6'6'}}\right)\frac{\langle\langle\sigma_{1'}\rangle\rangle}{p}
\end{aligned} \qquad (75)$$

Let us consider the creep of a symmetrically reinforced fiberglass plastic. We consider only the viscoelastic properties of a unidirectionally reinforced layer under transverse loading and in longitudinal shear, i.e. we accept that $K_{11}^{(k)}(t-\theta) = K_{12}^{(k)}(t-\theta) = 0$. In choosing the corresponding creep kernels in the form of the exponents $K_{22}^{(k)}(t-\theta) = C_{22}e^{-\alpha_{22}(t-\theta)}$ and $K_{66}^{(k)}(t-\theta) = C_{66}e^{-\alpha_{66}(t-\theta)}$ it is simple to perform the inverse Laplace transform of dependence (74)

$$\langle\tau_{1'2'}(t)\rangle_k = -(S_{1'6'}^{(k)}/S_{6'6'}^{(k)}) \times \left\{1 - \sum_{l=1}^{2} [P_1(P_l)/P_l P_2(P_l)]\,(1-e^{P_l t})\right\}\langle\langle\sigma_{1'}\rangle\rangle \qquad (76)$$

where P_l are the roots of equation $P^2 + b_1 P + b_2 = 0$

$$P_1(P_l) = (a_1 - b_1)P_l + a_2 - b_2,\quad P_2(P_l) = 2P_l + b_1$$

$$a_1 = \frac{1}{S_{1'6'}^{(k)}}[S_{1'6'}^{(k)}(\alpha_{22}+\alpha_{66}) - 2C_{22}S_{22}^{(k)}\sin^3\varphi\cos\varphi - C_{66}S_{66}^{(k)}(\cos^2\varphi - \sin^2\varphi)\sin\varphi\cos\varphi]$$

$$a_2 = \frac{1}{S_{1'6'}^{(k)}}[S_{1'6'}^{(k)}(\alpha_{22}+\alpha_{66}) - 2C_{22}\alpha_{66}S_{22}^{(k)}\sin^3\varphi\cos\varphi - C_{66}\alpha_{22}S_{66}^{(k)}(\cos^2\varphi - \sin^2\varphi)\sin\varphi\cos\varphi]$$

$$b_1 = \frac{1}{S_{6'6'}^{(k)}}[S_{6'6'}^{(k)}(\alpha_{22}+\alpha_{66}) + 4C_{22}S_{22}^{(k)}\sin^2\varphi\cos^2\varphi + C_{66}S_{66}^{(k)}(\cos^2\varphi - \sin^2\varphi)^2]$$

$$b_2 = \frac{1}{S_{6'6'}^{(k)}}[S_{6'6'}^{(k)}\alpha_{22}\alpha_{66} + 4C_{22}\alpha_{66}S_{22}^{(k)}\sin^2\varphi\cos^2\varphi + C_{66}\alpha_{22}S_{66}^{(k)}(\cos^2\varphi - \sin^2\varphi)^2]$$

Expressions for determining the values of $S_{op}^{(k)}$, $o, p = 1', 2', 6'$ are obtained from (73) if one assumes $K_{ij}^{(k)}(p) = 0$, $i, j = 1, 2, 6$.

Strains of laminate in the directions 1′ and 2′ are determined from the first two equations of (72):

$$\langle\langle\varepsilon_{1'}(t)\rangle\rangle = \left\{S_{1'1'}^{(k)} + \frac{C_{22}S_{22}^{(k)}}{\alpha_{22}}(1-e^{-\alpha_{22}t})\sin^4\varphi + \frac{C_{66}S_{66}^{(k)}}{\alpha_{66}}\sin^2\varphi\cos^2\varphi\,(1-e^{-\alpha_{66}t}) + S_{1'6'}^{(k)}\langle\tau_{1'2'}(t)\rangle_k\frac{1}{\langle\langle\sigma_{1'}\rangle\rangle} - 2\frac{S_{1'6'}^{(k)}}{S_{6'6'}^{(k)}}S_{22}^{(k)}\sin^3\varphi\cos\varphi\Phi_{22}(t)\right.$$

5 Polymeric Composites with Reinforced Matrix

G. M. Gunyaev, D. Sc. (Eng.),
B. V. Perov, D. Sc. (Eng.)

5.1 PRODUCTION METHODS AND STRUCTURE OF MATRIX-REINFORCED COMPOSITES

One of the most important directions of improvements of the service properties of polymeric composites is an increase in rigidity and strength of the matrix. This problem is solved by the production of new matrices and by modification of the existing ones and also by the directed control of processes of interaction at the fiber-matrix interface.

Recent studies [1, 2] have shown that the mechanical properties of polymeric matrices can be considerably improved by reinforcement with short fibers or whiskers of high modulus and high strength.

This method of production of composites with a reinforced matrix appears to be very interesting, since the physical and mechanical properties of the polymeric matrix are substantially improved, with practically no changes in its chemical base. The introduction in composites of short fibers with different physical properties other than those of the basic (continuous) fibers permits such characteristics as heat conduction and electric conductivity, dielectric permittivity and loss factor to be governed. Filling the polymeric matrix with short fibers improves its elastic and strength characteristics proportionally (up to a certain limit) to the amount of fibers and their mechanical characteristics. In turn, this favours an increase in strain resistance of composites subjected to interlaminar shear, compression and loading in a direction different from that of the orientation of continuous fibers. An especially marked improvement of the mechanical characteristics of composites is achieved by the reinforcement of their matrix with whiskers, the properties of the latter being given in Table 5.1.

The geometrical dimensions of short fibers affect the efficiency of matrix reinforcement, the mechanical properties of composites and the uniformity of their distribution in the interfiber space. The fiber length must be comparable with the diameter (thickness) of the structural elements of the basic reinforcing fibers and for composites based on glass, organic or carbon fibers to be equal to approximately $(1\text{-}2)\cdot 10^{-4}$ m. Since for the efficient matrix reinforcement the ratio $l/d \approx 100$ must be maintained, the diameter of a short fiber must not exceed $2\cdot 10^{-6}$ m. Therefore for these purposes "thin" fractions of whiskers are most useful.

Table 5.1. Physical and Mechanical Characteristics and Dimensions of Whiskers Used for Whiskerization [3, 4]

Whiskers	γ, kg/m³	σ, MPa	E, GPa	$d \cdot 10^{-6}$, m	$l \cdot 10^{-3}$, m
Sapphire (α-Al_2O_3)	3.9	6000-10000	590	2.5-4.0	5.0-10.0
β-rutile (TiO_2)	4.0	3000-5000	380	0.5-2.5	0.3-2.0
Aluminium nitride (AlN)	3.3	4000-6000	320	4.0-6.0	5.0-8.0
Silicon carbide (SiC)	3.2	5000-7000	420	3.0-5.0	7.0-10.0
Silicon nitride (Si_3N_4)	—	3000-4000	340	0.5-2.5	2.5-4.0

Several methods of the introduction of short fibers into the matrix filling the interspace between continuous fibers are used in the production of composites:

— alternation in laying up basic fibers with filler layers of short fibers, for example, mats;

— precipitation of short fibers and whiskers from aerosol on the basic fibers;

— whisker growth on the surface of some types of fibers during high temperature gas-phase reactions [4, 5]. The last two methods are called whiskerization.

The introduction of mats and paper of short fibers between layers of basic fibers is simple from the technological point of view. The control of the ratio between short and continuous fibers is achieved by choosing the thickness of the fillers to be combined. This method, however, has a restricted application for local strengthening of composites, for example, in places of bolt or rivet joints. With this method, uniform and random distributions of short fibers between different continuous fibers cannot be achieved, since mats and paper of short fibers are characterized by disorientation only in the layer plane, and fibers oriented normally to the surfaces of layers are practically absent and as a result the reinforced matrix is anisotropic.

Precipitation of whiskers and short fibers on the basic fibers is done from aerosols or their suspension. In whiskerization of reinforcing fillers of woven structure the use is made of precipitation from a suspension with whiskers in a weakly concentrated solution of the matrix material [6]. The required degree of whiskerization is reached by a change of concentration in pulp of its amount on filtration through fabric. The character of whisker distribution in interfiber space varies with increasing whiskerization. For small values of the degree of whiskerization the normal orientation of whiskers perpendicularly to the fabric plane and their penetration between individual threads are typical. With an increased amount of precipitated whiskers they are now to be found in the fabric plane. Figure 5.1 gives

the dependence of the relative strength τ^*_{xz}/τ_{xz} and relative shear moduli G^*_{xz}/G_{xz} and G^*_{xy}/G_{xy} in interlaminar shear of glass-fabric laminate on the degree of its filling with AlN whiskers precipitated from suspension on the glass fabric. Clearly strength in interlaminar shear depends on the diameter of whiskers, increasing with their decreasing thickness, since it simplifies penetration of whiskers into the fabric structure. The graph of the function $\tau^*_{xz}/\tau_{xz} = f(v_w)$ has a maximum, the latter with decreasing thickness of whiskers shifts

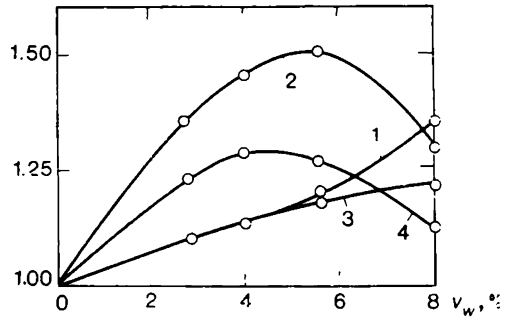

Fig. 5.1 Dependence of relative strength τ^*_{xz}/τ_{xz} (curves *2*, *4*) and relative shear moduli G^*_{xz}/G_{xz} and G^*_{xy}/G_{xy} (curves *1*, *3*) for epoxy glass plastic in interlaminar shear on volume fraction of AlN whiskers with diameter $2 \cdot 10^{-6}$ m (*1*, *2*) and $20 \cdot 10^{-6}$ m (*3*, *4*) precipitated from suspension onto cord glass fabric. The circles are experimental values

towards their larger content. When a small degree of composite filling with whiskers is reached, the rate of modulus G^*_{xz} growth decreases and that of modulus G^*_{xy} increases. It is caused by a change in the orientation of whiskers by their predominant location in the plane of the layer of the basic fibers.

Whiskerization from aerosols occurs on the passage of resin-coated yarns, threads or tapes through a chamber containing a suspension of short fibers or whiskers in air. Electrification through electrostatic repulsion owing to friction in a fluidized bed layer results in the fibers and whiskers being distributed randomly over the surface of the basic fiber during precipitation. The quality of orientation can be improved on whiskerization in an electrostatic field [7]. The density of distribution of precipitated fibers and whiskers is determined by their dimensions, concentration in aerosol, rate of fiber passage through the precipitation chamber and on the intensity of the electric field. Practically all kinds of reinforcing fillers, irrespective of the filler nature, can be subjected to whiskerization from aerosol.

Thin fractions of short fiber whiskers, for example, β-rutile, are most suitable for precipitation. On whiskerization from aerosol, whiskers are distributed uniformly and randomly in the matrix

between individual threads or yarns, not penetrating the space between fibers. The absence of the favoured orientation of short fibers in the composite matrix on whiskerization from aerosol results in their having the same values of shear moduli G^*_{xz} and G^*_{xy} (Fig. 5.2).

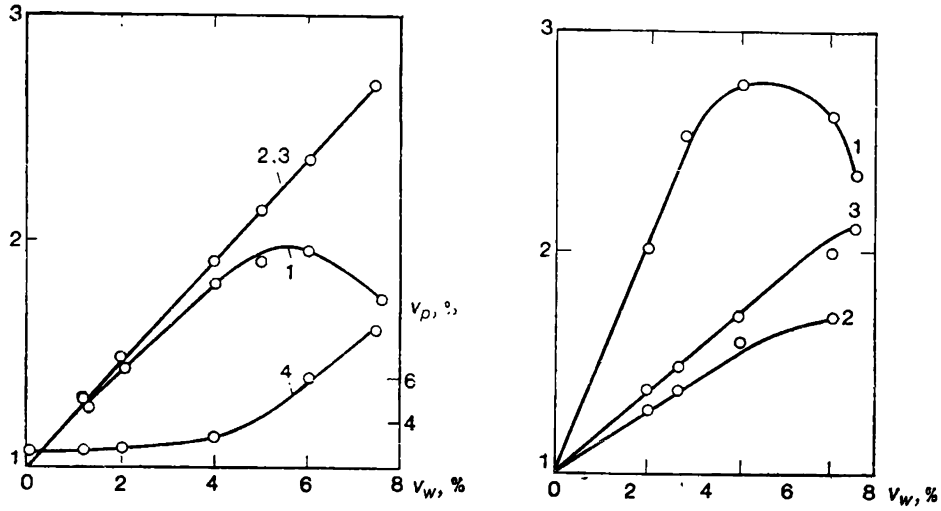

Fig. 5.2 Dependence of relative strength τ^*_{xz}/τ_{xz} (curve *1*) and relative shear moduli G^*_{xz}/G_{xz} (curve *2*) and G^*_{xy}/G_{xy} (curve *3*) in interlaminar shear, and also of void content v_p (curve *4*) for epoxy organic fiber composite, on volume fraction of β-rutile whiskers precipitated from aerosol onto aramide thread. The circles are experimental values

Fig. 5.3 Dependence of relative strength τ^*_{xz}/τ_{xz} (curve *1*) and relative shear moduli G^*_{xz}/G_{xz} (curve *2*) and $G^*_{yz}\,G_{yz}$ (curve *3*) for epoxy carbon plastic on volume fraction of Si_3N_4 whiskers grown on the surface of carbon fibers from gas phase. The circles are experimental values

The curve $\tau^*_{xz}/\tau_{xz} = f(v_w)$ passes through a maximum, the appearance of the latter being connected with an increase in composite void content when the optimal volume fraction of short fibers is exceeded.

The method of whisker growing on the surface of reinforcing fibers can be used in whiskerization of carbon and refractory fibers: SiC, Si_3N_4, Al_2O_3, and others. In this case continuous fibers are placed in a high temperature chamber supplied with a mixture of the agents required for the formation of whiskers from the gas phase, and their growth by the "vapour-liquid-solid phase" mechanism [4]. The formation time of whiskers, their dimensions and the density of their distribution over the surface of individual fibers are determined by the nature of the fiber-substrate and whiskers and by the conditions of their growth (composition of gas medium, temperature,

pressure, duration of the process). For example, only several minutes are required for the formation of SiC crystals on a high modulus carbon fiber with a temperature in the reaction chamber of 1650-1900°C [5].

In fiber whiskerization from the gas phase a porous coat of silicon carbide is formed on the fiber surface that increases the specific surface causing an increase in the strength, bonding between whiskerized fibers and the matrix.

Changes in relative interlaminar strength and shear moduli of carbon laminated plastics based on carbon tape whiskerized with Si_3N_4 are shown in Fig. 5.3. With increasing degree of whiskerization modulus G^*_{yz} rises sharply while there is only a slight increase in modulus G^*_{xz}, which is caused by a selective direction of whisker orientation. During their growth whiskers orientate normally to the surface of fibers, reinforcing the matrix in the *yz* plane. The occurrence of a maximum on the curve describing the dependence of τ^*_{xz} on the degree of whiskerization is explained by an increase in composite void content owing to a decrease in forming pressure during specimens preparation. The necessity of pressure decrease is to avoid damaging "soft" carbon fibers on their contact with hard faceted whiskers.

In a number of cases, as can be seen in Table 5.2, with increasing whiskerization of carbon fibers their strength decreases because of oxidation processes and changes of fiber structure at high temperature heating.

The method employed to introduce whiskers into the composite determines its physical structure and properties (Table 5.3). Only in the case of whiskerization from the gas phase are whiskers uniformly distributed over the whole matrix volume in the space between elementary fibers and rigidly bonded with them. In the other cases whiskers are uniformly distributed in the space between fiber strands (or threads, yarns) where an interlayer of the matrix material exists and interfiber space in individual yarns and threads remains unreinforced and is filled with the usual matrix material.

Depending on the method of whiskerization, whiskers can be randomly distributed throughout the composite matrix (in precipitation from aerosol) or in the transverse planes (in growing from the gas phase or introduction of paper layers). Random distribution of whiskers leads to a simultaneous increase in material shear moduli in all three planes. These moduli in a given case are determined not only by the volume fraction of the whole reinforcement (basic fibers + + whiskers), but also by the elastic properties of whiskers.

At random distribution of whiskers in one plane, perpendicular or parallel to the direction of fibers, the shear modulus of composite in this plane increases to a greater extent than in all other directions. In particular, shear moduli in the two other planes increase slightly,

Table 5.2. Effect of the Degree of Fiber Whiskerization with SiC on the Mechanical Characteristics of Carbon Fibers and Corresponding Epoxy Composites [2, 5]*

Characteristics of fibers			Characteristics of composite						
Degree of fiber whiskerization, %	σ, MPa	$E \cdot 10^{-3}$, MPa	Volume fraction in composite, %		γ, kg/m^3	σ^*_{xb}, MPa	σ^*_{xc}, MPa	$E^*_x \cdot 10^{-3}$, MPa	τ^*_{xz}, MPa
			Whiskers	Voids					
0	2190±420	279	0	4.0	1.4	1000	400	130	40
2.5	2250±360	273	1.25	5.3	1.46	730	700	170	54
3.3	1990±300	304	2.5	5.7	1.43	750	780	175	65
4.2	1860±410	294	3.4	6.9	1.5	720	700	170	61

*Subscripts b and c mean bending and compression.

Table 5.3. Effect of the Method of Whiskerization of Carbon Yarns on the Characteristics of Epoxy Composites

Method of whiskerization*	E^*_x/E_x	E^*_y/E_y	E^*_z/E_z	G^*_{xy}/G_{xy}	G^*_{xz}/G_{xz}	G^*_{yz}/G_{yz}	σ^*_x/σ_x	σ^*_y/σ_y	σ^*_z/σ_z	τ^*_{xy}/τ_{xy}	τ^*_{xz}/τ_{xz}	τ^*_{yz}/τ_{yz}
Introduction of a paper layer from SiC whiskers	1.0	2.4	1.0	2.5	1.1	1.1	0.98	2.1	1.1	1.9	1.3	1.2
Precipitation of TiO_2 whiskers from aerosol	1.0	1.4	1.6	1.7	1.65	1.7	0.96	1.57	1.48	1.55	1.6	1.64
Growing of SiC whiskers from gas phase	1.05	1.5	1.65	1.3	1.4	1.9	0.82	1.83	1.88	1.2	2.5	1.15

*Volume fraction of whiskers is 2.5 to 3.0%.

since an increase in their values is determined not by the properties of whiskers, but by their fraction [1].

Thus, the composite characteristics in shear and under loading in a direction different from that of the orientation of basic fibers, depend on the method of whiskerization and are determined by the properties of the reinforced matrix.

5.2 CHARACTERISTICS OF WHISKER-REINFORCED MATRIX

To determine the characteristics of composites based on whiskerized fibers, it is necessary to have information on the mechanical characteristics of the reinforced matrix in at least two forms of orientation of whiskers: unidirectional and random in the plane (or random in the volume).

The introduction of whiskers into the polymeric matrix increases its elastic and strength characteristics proportionally to the volume fraction and values of the mechanical characteristics of whiskers [3], as can be seen from the data provided in Table 5.4.

Table 5.4. Effect of Whisker Distribution on the Characteristics of Epoxy Matrix

Characteristics	Whisker distribution in matrix			
	Random (plane) $v_w = 11$ %		Unidirectional $v_w = 25$ %	
	Si_3N_4	TiO_2	TiO_2	SiC
E_x^*, GPa	165	22	78	120
σ_x^*, MPa	193	102	490	880

The efficiency of reinforcement depends on the geometrical dimensions of the whiskers and their distribution in the matrix. There exists a minimum critical volume (amount) of whiskers introduced into the matrix. When the amount of whiskers is smaller than v_w^c the effect of reinforcement is not manifested.

The minimum critical volume

$$v_w^c = \left[1 + \frac{(1 + l_w^c/l_w)\,\sigma_w}{\sigma_m - \sigma_m'}\right]^{-1} \qquad (1)$$

depends on the geometrical dimensions and strength of whiskers. In formula (1) σ_m and σ_m' are respectively matrix strength and stresses in it at fracture of whiskers, σ_w is the strength of whiskers, l_w is their length and l_w^c is the critical length of whiskers.

For epoxy matrices, reinforced with thin fractions of whiskers of silicon carbide and nitride, aluminium nitride and titanium dio-

xide v_w^c equals 1.6-2% [3]. At a degree of filling above v_w^c, the strength and elastic characteristics of reinforced matrices increase proportionally, as shown in Fig. 5.4.

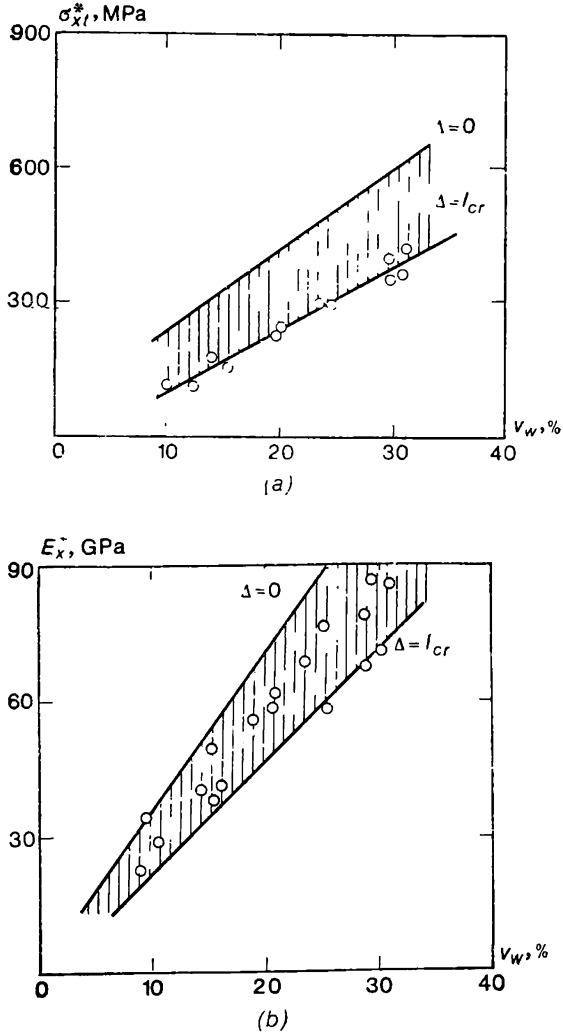

Fig. 5.4 Dependence of (*a*) strength and (*b*) elastic modulus in tension on volume fraction of whiskers for unidirectional composites. The circles are experimental values

According to [8] the strength and elastic modulus in the longitudinal direction for composites based on short unidirectional fibers are expressed in terms of the parameters of fiber and matrix taking into account the weakening of the cross-section of the composite at the fiber ends (on ineffective segments $l_w^c/2$ long) and the gap Δ be-

tween the fiber ends:

$$\sigma_1^* = \sigma_w v_w [1 - (l_w^c + 2\Delta)/2l_w] + \sigma_m' v_m$$
$$E_1^* = E_w v_w [1 - (l_w^c + 2\Delta)/2l_w] + E_m v_m \quad (2)$$

The factor in square brackets characterizes the influence of the length of reinforcing fibers. The effect of this factor on the characteristics of epoxy matrices, matrices reinforced with TiO_2 whiskers (σ_w = 1580 MPa, E_w = 400 GPa, d_w = $2.5 \cdot 10^{-6}$ m) is shown in Table 5.5.

Table 5.5. Effect of Values of l_w/l_w^c, Δ/l_w^c and v_w on the Characteristics of Epoxy Matrix

l_w/l_w^c	Δ/l_w^c	v_w	σ_1^*, MPa	E_1^*, MPa
2.5	1.0	3.2	116	24.5
2.5	0.4	25	297	70
6.5	1.2	28	295	70.3

The values of other elastic constants of the uniaxial whisker reinforced matrix can be determined by the formulas given in [6]:

$$E_2^* = \frac{1+v_w}{1-v_w} E_m, \quad G_{12}^* = \frac{1+v_w}{1-v_w} G_m$$
$$\nu_{12}^* = \nu_m (1 - v_w) + \nu_w v_w \quad (3)$$

In the case of the isotropic whisker reinforced polymeric matrix its elastic constants increase (Fig. 5.5), reaching optimal values at a considerably smaller filling than with the use of continuous fibers [3]. This is explained by the difficulty of achieving a close packing of short fibers containing whiskers of polygonal shape with a wide range of lengths and diameters. The introduction of whiskers with a random distribution into the matrix in quantities of 10-12% (corresponding to their optimal content in the interfiber space of a composite with whiskerized fibers) causes a sharp increase in the matrix characteristics (Table 5.6). For example, the elastic modulus in tension is 5-7 times greater, the shear modulus 5-6 times, the tensile strength 3-4 times. On filling the epoxy matrix with whiskers the character of the σ-ε curves changes, the initial modulus and the length of the initial linear segment of the curve increase, strength increases and ultimate elongation decreases. However, the ultimate work of fracture, characterized as an area below the σ-ε curve is higher for filled polymers. On 3% filling of epoxy resin with β-rutile whiskers the stress intensity factor K_{1c} increases to 2.5%, cracking

resistance rises and simultaneously specific work of damage and resistance to the development of viscoelastic strains under long-time static load increase, while creep decreases [9]. The values of these

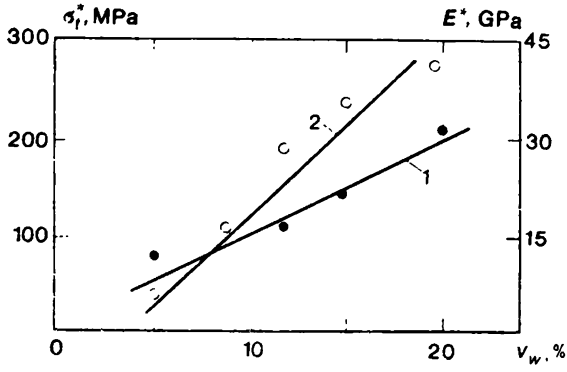

Fig. 5.5 Dependence of strength (curves *1*, solid circles) and elastic modulus (curves *2*, open circles) for epoxy resin in (*a*) tension and (*b*) shear on volume fraction of Si_3N_4 whiskers of in-plane random orientation. The open and solid circles are experimental values

parameters for an unreinforced epoxy matrix and a matrix reinforced with β-rutile whiskers are presented in Table 5.7.

With a random packing of whiskers parallel to one plane, for example, the *xy* plane, the reinforced matrix can be considered as transverse isotropic in this plane. Then the matrix stiffnesses can be determined from computational expressions for a laminate with unidirectional whisker-reinforced layers oriented at angles 0 and $\pm\pi/3$. In cases when the degree of matrix filling with whiskers is less than 15%, formulas to calculate the elastic properties of the matrix with a random distribution of fibers (ignoring the value of

Table 5.6. Mechanical Characteristics of Epoxy Whisker-Reinforced Matrix [1, 2]

Reinforcing element	Volume fraction of reinforcing element	γ^* kg/m³	$E^* \cdot 10^3$, MPa	σ^*, MPa	$G^* \cdot 10^{-3}$, MPa	τ^*, MPa	ν^*, MPa
TiO_2 whiskers	13.0	1.55	20	220	7.1	68	0.29
Si_3N_4 whiskers	11.1	1.40	16.5	193	6.1	50	0.32
AlN whiskers	11.5	1.41	18	221	6.2	52	0.31
Unreinforced matrix	—	1.23	3.2	56	1.25	34	0.35

the product of Poisson's ratios) have the following form [1]:

$$E^*_{mx} = E^*_{my} = B_{xx} - B^2_{xy}/B_{yy},\ \nu^*_{myx} = B_{xy}/B_{xx}$$

$$G^*_{mxy} = 1/2\, G^*_{12} + 1/8\, (E^*_1 + E^*_2 - 2\nu_{21}E^*_2) \qquad (4)$$

where

$$B_{xy} = 3/4\nu^{*2}_{12}E_2 + 1/8\, (E^*_1 + E^*_2 - 4G^*_{12})$$

$$B_{xx} = B_{yy} = 3/8\, (E^*_1 + E^*_2) + 1/4\, (\nu^{*2}_{12}E^*_2 + 2G^*_{12})$$

Table 5.7. Effect of Matrix Reinforcementwith β-Rutile Whiskers on the Characteristics of Epoxy Matrix

Characteristics	Unrenforced matrix	Matrix reinforced with 3% of β-rutile
Fracture toughness, N/mm$^{3/2}$	41	51
Specific work of damage at $\varepsilon = 2\%$, 10^{-4} J/mm²	0.15	0.4
Elongation at stress of 30 MPa during 1000 h, %	2.8	1.7

The values of the elastic constants E^*_1, E^*_2, G^*_{12}, and ν^*_{21} are determined from formulas (2) and (3).

At a random distribution of whiskers over the volume of the polymeric matrix, its elastic characteristics are also calculated from formulas (4) and the similar characteristics of a unidirectional layer are calculated from (2) and (3), but at the volume fraction of whiskers equal to 1/3 of their total content in the matrix [1].

With temperature rise the effect of matrix reinforcement owing to its filling with whiskers increases. The data given in Table 5.8 show that the ratios of the elastic moduli and ultimate strength in bending and shear of the reinforced matrix to those of the unreinforced matrix increase from 1.6-1.7 to 2.45-2.75 at heating from 20°C

Table 5.8. Changes of Relative Characteristics of Epoxy Matrix Reinforced with β-Rutile Whiskers on Heating [1, 6]

Characteristics	Temperature, °K				
	293	373	423	473	523
Elastic modulus in tension, E_m^*/E_m	1.75	2.4	2.7	2.75	2.45
Bending strength, σ_m^*/σ_m	1.6	1.95	2.25	2.2	2.0
Shear strength, τ_m^*/τ_m	1.6	1.8	2.1	2.45	2.35

to the glass-transition temperature, then they begin to decrease. Whisker reinforcement of epoxy matrices results in an increase in their strain heat resistance, apparent glass-transition temperature and in a decrease in the rate of the mechanical properties fall with temperature rise.

5.3 MECHANICAL CHARACTERISTICS OF REINFORCED-MATRIX COMPOSITES

On the basis of experimental data and theory the characteristics of composites can be represented in the form of functions of matrix characteristics, including interfacial adhesion strength τ_a and σ_a: elastic moduli E_x^*, E_y^*, E_z^*, G_{xy}^*, $G_{yz}^* = f(E_m, G_m)$; tensile strength in the direction of fibers $\sigma_{xt}^* = f(\tau_m, \tau_a, E_m)$; resistance to static tensile fatigue in the direction of fibers $\sigma_{xt}^* = f(\sigma_m, W, K_{Ic})$; tensile strength in the direction perpendicular to the orientation of fibers $\sigma_{yt}^* = f(\sigma_a, \tau_a, \sigma_m)$; strength in interlaminar shear $\tau_{xz}^* = f(\tau_a, \tau_m)$; compression strength in the direction of fibers $\sigma_{xc}^* = f_i(\sigma_m, \sigma_a, \tau_m, \tau_a)$.

The introduction of whiskers into the polymeric matrix leads to a significant increase in its elastic moduli, ultimate strength, cracking resistance, ultimate work of fracture W^*, temperature stability and other characteristics, while reinforcement of the matrix filling the interfiber space results in the reinforcement of the whole composite as well.

Experimental data given in Table 5.9 [2, 6] clearly show an increase in mechanical characteristics (except tensile strength) of fiber-glass,

Table 5.4. Mechanical Characteristics of Epoxy Composites with Reinforced or Unreinforced Substrates*

Composite	Filler	Features and method of introduction of filler	σ_a^*, MPa	σ_{at}^*, MPa	σ_{ac}^*, MPa	σ_{cc}^*, MPa	$E_a \cdot 10^{-3}$, MPa	$G_{ac} \cdot 10^{-3}$, MPa
Fiber-glass plastic	Satin fabric	Precipitation of Al_2O_3 from suspension	600 950	300 420	42 54	250 370	38 53	2.4 2.7
	Tape	Precipitation of TiO_2 from suspension	1900 1500	250 280	360 [illegible]	332 [illegible]	64 [illegible]	2.8 3.4
Carbon plastic	Tape	Si_3N_4 growing	1180 1020	49 80	600 [illegible]	37 64	113 [illegible]	3.2 4.9
	Tape	SiC growing	1260 [illegible]	18 24	460 780	26 67	165 172	3.8 5.0
	Fabric	Precipitation of TiO_2 from suspension	1400 [illegible]	11 28	360 430	250 41	190 190	2.7 3.2
Organic plastic	Thread	Precipitation of TiO_2 from suspension	150 145	22 29	220 320	270 44	12 34	2.4 2.8

* Subscripts b, t and c mean bending, tension and compression, respectively.

carbon and organic plastics as a result of the reinforcement of the epoxy matrix with whiskers introduced in various ways.

The elastic characteristics of composites based on whiskerized fibers are calculated by the technique used for three-dimensionally reinforced plastics [1] and involving calculations of the elastic characteristics for the reinforced matrix and composite taking into account the properties of a modified matrix.

Calculations of the elastic characteristics of unidirectional composites, taking into account the averaged characteristics of the matrix are made using the known formulas given in [10]. The elastic constants of the matrix found in these dependences are replaced by those of the reinforced matrix determined by experiments or calculated from formulas (4). The character of random distribution of whiskers in the matrix (depending on the method of composite production) is also taken into account. Expressions for the elastic characteristics of a composite, reinforced with whiskerized fibers in the x-axis direction, are [1]:

$$
\begin{aligned}
&E_x^* = E_{mx}^*(1-v_f) + E_f v_f \\
&E_y^* \quad E_z^* = \frac{[1+(n_x-1)v_f]E_f}{[v_f+n_z(1-v_f)][1+(n_x-1)v_f]-(n_x\nu_{mzx}^*-\nu_f)^2(1-v_f)v_f} \\
&\nu_{zx}^* = \nu_{yx}^* = \nu_{mzx}^*(1-v_f) + \nu_f v_f \\
&G_{yz}^* = 0.5E_f[v_f(1-\nu_f)+n_z(1+\nu_{mzy}^*)(1-v_f)]^{-1} \\
&G_{xy}^* = G_{xz}^* = G_{mxz}^* \frac{n_{xz}(1-v_f)+1-v_f}{n_{xz}(1-v_f)+1+v_f}
\end{aligned}
\tag{5}
$$

where $n_x = E_f/E_{mx}^*$, $n_z = E_f/E_{mz}^*$, $n_{xz} = G_f/G_{mxz}^*$ and v_f is the volume fraction of the basic fibers (less whiskers).

High strength and rigidity under loading at an angle to the orientation of basic fibers are typical of composites with a reinforced matrix. In the case of angle ply laminates with whiskerized fibers the calculation of the elastic characteristics of composites is made using formulas obtained for laminated media of a similar physical structure, the elastic constants of the unidirectional ply being determined by taking into account the properties of the reinforced matrix.

Figure 5.6 shows the dependence of the elastic characteristics on the angle of antiphase disorientation of layers of epoxy carbon plastic based on carbon tapes and the same tapes whiskerized by whisker growing. A satisfactory agreement between the calculated and experimental values is seen as well as a decreased sensitivity to disorientation of layers of composites with the reinforced matrix. At the antiphase disorientation of the base fibers by $\pm 15°$, the elastic modulus of whiskerized carbon plastic decreases by 7% and for a material similar in composition without whiskers by 20%. A decreased sensitivity of composites with the reinforced matrix to such structural

defects as waviness, twist and disorientation of fibers is caused by a significant decrease in the anisotropy parameter E_f/G_m of materials based on whiskerized fibers [2].

Short-time tensile strength of composites with an increasing degree of matrix reinforcement with whiskers monotonously decreases to some critical volume fraction, and once this is reached the rate of strength decrease rises sharply. It is caused by various factors

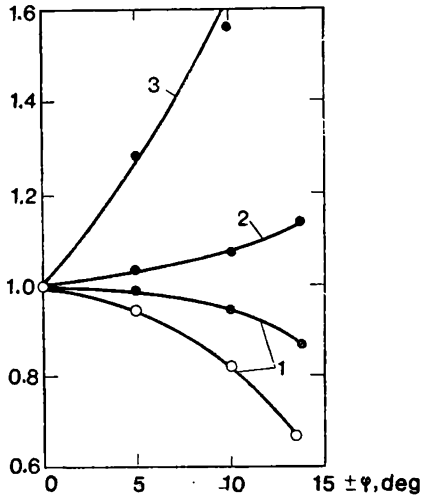

Fig. 5.6 Dependence of relative characteristics of carbon plastic on the angle of antiphasal disorientation of layers:
$1-E_{x\varphi}/E_{x0}$; $2-E_{y\varphi}/E_{y0}$; $3-G_{xy_\varphi}/G_{xy0}$. The solid circles are experimental values for whiskerized fibers, the open circles, for unwhiskerized fibers

and depends on the method of introducing the whiskers into the matrix. In growing whiskers on the fiber surface through high temperature gas-phase reactions the reinforcing fibers are weakened [5], the degree of resin impregnation decreases, and as a result the degree of interfacial contact and the degree of composite filling decrease. On precipitation from aerosol the whiskers reinforce the matrix only in the space between individual yarns or threads, and as a result the mechanism of composite failure changes. In this case not a fiber but a strand of fibers (thread or yarn) is the element of reinforcement; individual fibers do not split and brittle failure of the material takes place.

Long-time strength of composites, for example, of carbon plastics, increases with an increase in matrix filling with whiskers, achieving a maximum at a volume fraction of 2.5-3%. Having close values of short-time static tensile strength, corresponding to the starting points on the axis of the dependence $\sigma^*_{x\tau} = f(\tau)$ (Fig. 5.7), carbon plastic with the reinforced matrix (2.5% of β-rutile whiskers) loses in 100 h

its bearing strength by 11%, while carbon plastic with the unreinforced matrix loses it by 35% [9]. The introduction of whiskers into the matrix changes its bearing strength and viscoelastic properties, affecting the mechanism and intensity of processes of failure in the course of time, transfer of forces and redistribution of stresses between the components. In particular, this can be clearly seen by comparing the values of the parameter determining material life-time, the area below the σ-ε curve of the matrix. Since composite tensile strength

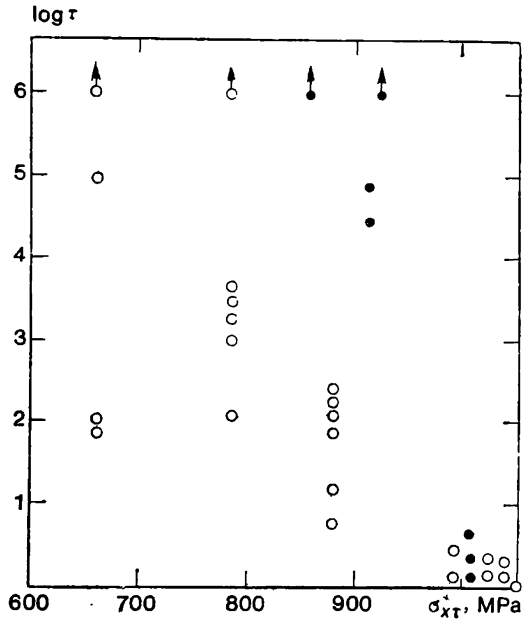

Fig. 5.7 Time variation of strength for carbon plastics under permanent load. The solid circles are experimental values for whiskerized fibers, the open circles, for unwhiskerized fibers (τ — sec.)

is determined by a maximum strain of fibers, practically independent of the conditions of loading and time, the ultimate work of fracture of the reinforced matrix increases by 40-45% at elongation of ε = = 0.7%. A higher failure resistance of the filled matrix is almost not realized during a short-time action of stresses, but it can be marked under long-time static loading. The introduction of randomly distributed whiskers into the interfiber space of composites increases the total surface of interface in the material, changes the conditions of stress redistribution owing to the formation of new centres of microcrack initiation and inhibits the development of microcracks, thus drastically slowing the development of microfracture in stressed volumes.

For the further development of cracks encountering hard particles, either an additional energy is required (an increase in the applied stress), or a longer time of damage accumulation under the action of permanent load.

The higher the content of whiskers, the greater the number of obstacles, the latter inhibiting the development of cracks which break the integrity of the composite. However, the volume of whiskers introduced into the matrix should be determined by taking into consideration the fact that the ultimate strain of the filled matrix must be 1.5-2 times higher than that of the basic reinforcing fibers.

The strength of fiber composites in interlaminar shear, transverse tension and compression is directly proportional to the matrix strength and adhesive strength bond with the reinforcing fibers. The interrelation between longitudinal compressive strength and transverse tensile strength with interlaminar shear strength [11] is observed.

The introduction of whiskers into the matrix filling the interfiber space in composites, whiskerization of yarns, tapes, fabrics from aerosol and suspensions contribute to an increase of composite strength in interlaminar shear, transverse strength in tension and compression owing to an increase of elastic modulus of the matrix as well as its adhesion and cohesion strength (in the case of whiskerization from the gas phase).

When whiskers are not distributed uniformly throughout the matrix volume but concentrate in the space between fiber strands composite failure is more likely to occur resulting from the cohesion mechanism. It is caused by the imbalance in the stiffness of the reinforced matrix between fiber strands and that of the unreinforced matrix within strands. In this case strength in interlaminar shear and transverse tension are found from the following formulas [11]:

$$\tau_{xz}^{*} = \tau_{mxz}^{*}(1 - v_p^{2/3})\left\{1 - \left[\frac{v_f(1+v_m)}{v_{f\max}}\right]^{1/2}\right\}$$
$$\sigma_{y}^{*} = \sigma_{my}^{*}(1 - v_p^{2/3})\left\{1 - \left[\frac{v_f(1+v_m)}{v_{f\max}}\right]^{1/2}\right\} \qquad (6)$$

where v_m is the volume fraction of the unreinforced matrix, $v_{f\max}$ is the maximum volume fraction of continuous fibers and v_p is the void content.

At an optimum fraction of whiskers of 3-4%, the ultimate strength of composites in shear increases 2.5 to 3 times, in compression 1.8 to 2.2 times, and in transverse tension 1.5 to 2 times.

Thermal stability of the reinforced matrix is crucial for thermal stability of polymeric composites. With an increasing glass-transition temperature of the matrix and its heat resistance, the rate of decrease in composites thermostability diminishes on the segment of the curve confining the region below the glass-transition tempera-

ture. The higher the strength and elastic characteristics of matrix after heating, the greater thermostability of the composites on its base. This explains the increase in thermostability of reinforced-matrix composites on heating (the appropriate data are given in Table 5.10).

With rise in temperature the effect of whisker reinforcement is more pronounced. The maximum reinforcement of composites is

Table 5.10. Effect of Epoxy Matrix Reinforcement with β-Rutile Whiskers on the Properties of Composites on Heating

Composite	Temperature of tests, K	$\sigma^*_{xb}\ \sigma_{xb}$	τ^*_{xz}/τ_{xz}	G^*_{xy}/G_{xy}	E^*_x/E_x	G^*_{xz}/G_{xz}
Carbon plastic	293	0.96	2.1	1.6	1.0	1.6
	373	—	2.5	1.9	—	—
	473	1.3	3.1	2.3	1.4	1.9
	523	—	2.9	2.4	—	—
	553	—	2.7	2.2	—	—
Fiber-glass plastic	293	0.98	2.3	1.7	1.05	1.5
	473	1.3	2.4	2.3	1.24	1.7

achieved at temperatures somewhat higher than that of glass-transition of the unfilled matrix [12]. Strength and elastic modulus in interlaminar shear increase from 2 to 3 and from 1.6 to 2.4 times, respectively.

The results presented in this paper of research into the enhancement of composite service properties through modification of polymeric matrices by the introduction of whiskers indicate the originality and efficiency of this method. It should be noted that it can also be applied to nonpolymeric matrices.

References

1. Zhigun, I.G., and Polyakov, V.A., *Properties of Three-Dimensionally Reinforced Plastics*, Zinatne, Riga, 1978 (in Russian).
2. Gunyaev, G.M., *Structure and Properties of Polymeric Fibrous Composites*, Khimia, Moscow, 1981 (in Russian).
3. Gunyaev, G.M., and Sorina, T.G., *Plastich. Massy*, **11**, 13-15 (1971).
4. *Whisker Technology* (A.P. Levitt, ed.), Wiley, New York, 1970.
5. Dergunova, V.S., Davidov, Yu.A., Gunyaev, G.M., Kilin, V.S., Sorina, T.G., Surgucheva, A.I., Moskalenko, A.G., Lunin, A.P., in: *Whiskers and Thin Films*, VPI, Voronezh, 1975, pp. 373-379 (in Russian).
6. Gunyaev, G.M., Zhigun, I.G., Sorina, T.G., Yakushin, V.A., *Mekh. Polimerov*, **3**, 492-501 (1973).
7. Sorina, T.G., Braverman, B.G., Surgucheva, A.I., *Plastich. Massy*, **4**, 17-18 (1978).

formulation of such constitutive equations of an anisotropic solid which could be used in the structural design following the determination of specific material parameters to be used in the equations. This branch is in fact a bridge between the classical mechanics of deformable solids and composite mechanics.

A peculiar feature of the bridge should be noted. The ground on which it is to be erected depends on a particular problem. This can be a unidirectional composite layer, multilaminar structure, etc. In each case the analysis scale (micro or macro) is conditioned by the relative positions of the levels.

These peculiarities of composites and composite mechanics are inherent in composites with polymeric as well as metal matrix.

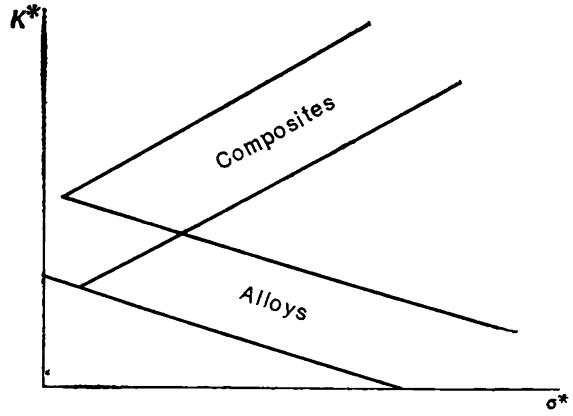

Fig. 6.1 Schematic representation of relationship between strength σ^* and fracture toughness K^* for alloys and composites

However, to define a specific matrix identifies a problem, too. It appears that problems, important for mechanics of reinforced plastics (e.g., hereditary effects, shear characteristics, etc.), become not so important for metal-matrix composites where other problems emerge into the foreground (peculiarities of plastic deformation, in particular, near the micro- and macroflaws, creep strength, etc.).

In the present review much attention is paid to problems and results important for metal-matrix composites. Wherever possible attempts are undertaken to carry out an analysis at the structural and phenomenological levels, bearing in mind that the results of both types of analysis have their own application: micromodels produce information necessary to choose a proper (if not optimum) structure as well as to reveal the nature of structurally noncontradictory phenomenological relationships which, in turn, can be used directly in the design of structures.

6.2 EFFECTIVE ELASTIC CHARACTERISTICS

There are numerous papers dedicated to the calculation of effective elastic moduli (the micromechanical approach) and to the experimental determination of elastic properties (the phenomenological approach). We shall therefore restrict ourselves only to some remarks.

1. A purely elastic behaviour of composites is observed rather seldom. In the case of metal-matrix composites the yield stress of a matrix is reached at relatively low composite stresses. Since in that case $0.1 \leqslant E_m/E_f \leqslant 1$ the transition of the matrix into plastic state substantially changes the tangent and secant moduli of the composite. The nonlinear deformation of the matrix is not so essential for fiber reinforced plastics since here $5 \cdot 10^{-3} \leqslant E_m/E_f \leqslant 10^{-1}$. In both cases the damage accumulation in a composite (such as cracking of fibers, matrix or interface) also lowers the tangent modulus, this effect being very considerable.

2. In the case of quasi-homogeneous materials such as conventional structural alloys the question of error resulting from the use of effective elastic characteristics can only arise at very high stress gradients. The question should be raised much more often in the case of real structures of fibrous composites [1].

3. The direct calculation of elastic moduli of a composite presents some difficulties because of the scarcity and inadequacy of the information on the elastic properties of composite constituents, which is, apparently, conditioned by two reasons. Firstly, the behaviour of the constituents in the composite differs from that under their loading separately because of specific features in the monomer polymerization on the developed fiber surface, chemical interaction of the metal matrix with the fiber material and other processes of physical-chemical interaction. Secondly, when testing separate fibers it is practically impossible to measure certain fiber moduli (e.g., those responsible for transverse fiber strain). Both these circumstances result in the necessity of measuring the moduli of the constituents when testing composites of a certain standard. The standard structure should, in part, feature regularity: deviation from a doubly periodic configuration may substantially affect the computed moduli and, as a consequence, the result of determination of the elastic properties of the constituents, too.

Now, to give an example, we will show the results of measuring the elastic moduli of a typical metal-matrix composite, boron-aluminium, and a fairly uncommon sapphire-molybdenum model composite tested to evaluate the longitudinal Young's modulus of sapphire fibers over a wide temperature range.

The elastic properties of boron-aluminium composites have been investigated in detail by Kiiko and Spiridonov [2], who performed

the measurements by three methods: detecting the elastic wave propagation velocities (the ultrasonic method), measuring the natural frequency of specimen oscillations (the resonance method), and recording the static stress-strain curve (the static method).

To obtain the complete components set of the elastic modulus tensor of a heterogeneous anisotropic body in the ultrasonic test it is necessary to measure the velocities of longitudinal, shear (transverse) and quasi-longitudinal (quasi-transverse) waves over a certain frequency range. The velocities of the last-mentioned waves are equal to each other along the definite directions of an anisotropic (e.g., orthotropic) body. Following the corresponding velocity measurements the well-known Christoffel equations [3] yield all the moduli.

The ultrasonic equipment used in [2] enables the measurement of the time difference in ultrasonic waves propagation through a circuit with and without a specimen. The frequency dependences of the velocities of longitudinal ($c_{l,11}$, $c_{l,22}$, $c_{l,33}$), transverse ($c_{s,23}$, $c_{s,31}$, $c_{s,12}$) and quasi-longitudinal ($c_{q,n}$) waves are shown in Figs. 6.2 to 6.4, where the specimen orientation is also indicated (subscripts l, s, q relate to the longitudinal, transverse, and quasi-longitudinal waves, respectively, the first subscript figure indicating displacement direction, the second one, as well as n, the wave propagation direction). The axis x_1 here and below is directed along the fibers. A pronounced difference in the velocities $c_{l,22}$ and $c_{l,33}$ indicates the deviation of fiber packing from the square one in the specimen cross-section. The dispersion of longitudinal waves is small. The velocities of longitudinal and transverse waves in an aluminium alloy are about $6 \cdot 10^3$ m/s and $3 \cdot 10^3$ m/s, respectively, and in the boron fibers (if one takes them as isotropic) they should be about $15 \cdot 10^3$ m/s and $7 \cdot 10^3$ m/s, respectively. Since characteristic size λ of the boron-aluminium structure is 0.1-0.2 mm the wavelengths in a composite and in each of its constituents exceed by more than an order of magnitude the value of λ, and an appreciable dispersion is not to be anticipated.

The velocity values and the dispersion nature are, by and large, the same in all three directions of quasi-longitudinal wave propagation, forming in pairs angles of 45° with the elastic symmetry axes (quasi-longitudinal and quasi-transverse waves in an orthotropic body coincide in these directions).

The transverse waves traveling across the fiber direction reveal significantly lower dispersion when the displacements are directed along the fibers than in the case with the displacements directed across the fibers (e.g., for subscripts s,12 and s,23).

With a frequency tending to zero the dispersion should vanish. Extrapolating the curves $c(f)$ at $f = 0$ yields the velocity values which (in terms of the Christoffel equation) produce the effective elas-

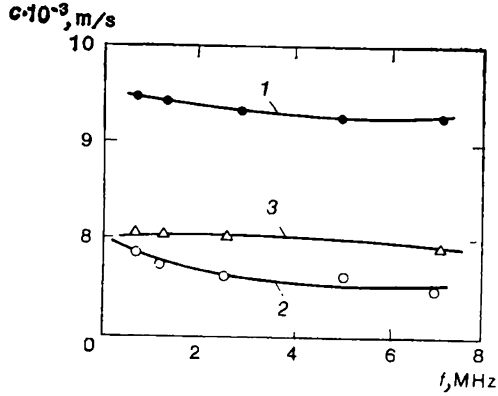

Fig. 6.2 Frequency dependence of longitudinal wave velocity for boron-aluminium composite:
●—$c_{l,11}$; ○—$c_{l,22}$; △—$c_{l,33}$[2]

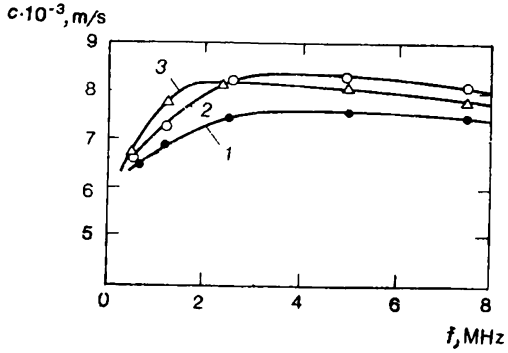

Fig. 6.3 Frequency dependence of quasi-longitudinal wave velocity for boron-aluminium composite:
●—$c_{q,n}$; ○—$c_{q,m}$; △—$c_{q,k}$ [2]

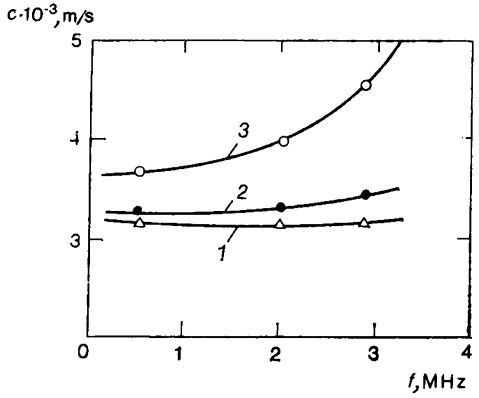

Fig. 6.4 Frequency dependence of transverse wave velocity for boron-aluminium composite:
●—$c_{s,13}$; ○—$c_{s,23}$; △—$c_{s,12}$[2]

Table 6.1. Elastic Characteristics of Boron-Aluminium Composite ($v_f = 0.5$)

Elastic characteristics obtained by ultrasonic method

$C_{ij} \cdot 10^{-4}$, MPa		Elastic moduli $E, G \cdot 10^{-4}$, MPa		Poisson's ratio	
C_{11}	22.5	E_1	21.8	ν_{12}	0.105
C_{22}	15.5	E_2	15.2	ν_{21}	0.151
C_{33}	15.9	E_3	15.7	ν_{13}	0.0973
C_{44}	3.20	G_{23}	3.20	ν_{31}	0.136
C_{55}	2.56	G_{31}	2.56	ν_{23}	0.00529
C_{66}	2.49	G_{12}	2.49	ν_{32}	0.00514
C_{12}	2.38				
C_{13}	2.20				
C_{23}	0.31				

Elastic characteristics obtained by other methods

Method	$E_1 \cdot 10^{-4}$, MPa	$E_2 \cdot 10^{-4}$, MPa	ν_{12}	ν_{21}
Static	20.9	10.6	0.110	0.226
Resonance	19.4	11.6	—	—
Calculated estimate	22.5	11.8	—	—

tic characteristics of the unidirectional boron-aluminium composite given in Table 6.1.

The same table gives the values of elastic moduli obtained by measuring the natural frequencies and static stress-strain curves. Note that some discrepancy is observed between the values of moduli obtained by different methods.

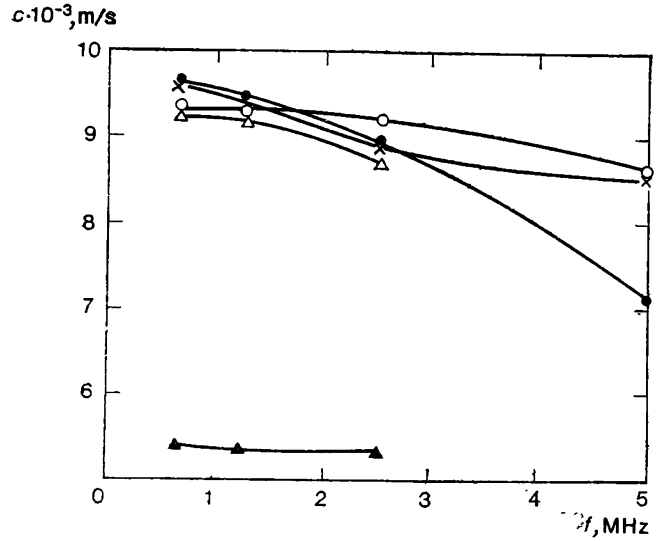

Fig. 6.5 Frequency dependence of longitudinal wave propagation velocity for boron-aluminium bidirectional composite with angle θ between the directions of reinforcement (the direction of wave propagation coincides with the bisector of θ):
○—θ = 0; ●—θ = 10°; ×—θ = 20°; △—θ = 45°; ▲—θ = 90° [2]

The results of measuring longitudinal wave velocities in the laminate are given in Fig. 6.5. The largest dispersion is observed in angle-ply specimens, the smallest, in cross-ply and unidirectional specimens.

It is interesting to compare now the values of E'_{1111} obtained in experiment (x'_1 is the bisector direction of an acute angle between

Table 6.2. The Results of Comparison between E'_{1111} and $\widetilde{E}'_{1111}$

θ, deg	0	10	20	45	90
$E'_{1111}\cdot 10^{-4}$, MPa	21.8	23.7	23.2	21.4	7.20
$\widetilde{E}'_{1111}\cdot 10^{-4}$, MPa	22.5	22.4	21.7	17.4	12.9

the fiber orientations) with the computed values of $\widetilde{E}'_{1111}$ obtained by transformation of the components $\widetilde{E}_{ijkl}$ for a unidirectional composite with $v_f = 0.5$ (see Table 6.1). The comparison is shown in

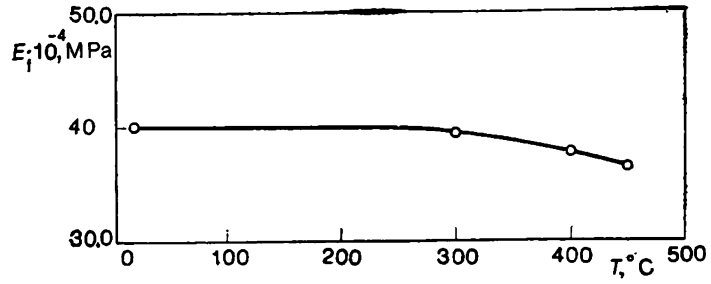

Fig. 6.6 Temperature dependence of longitudinal Young's modulus for boron fibers (data by E. G. Golofast)

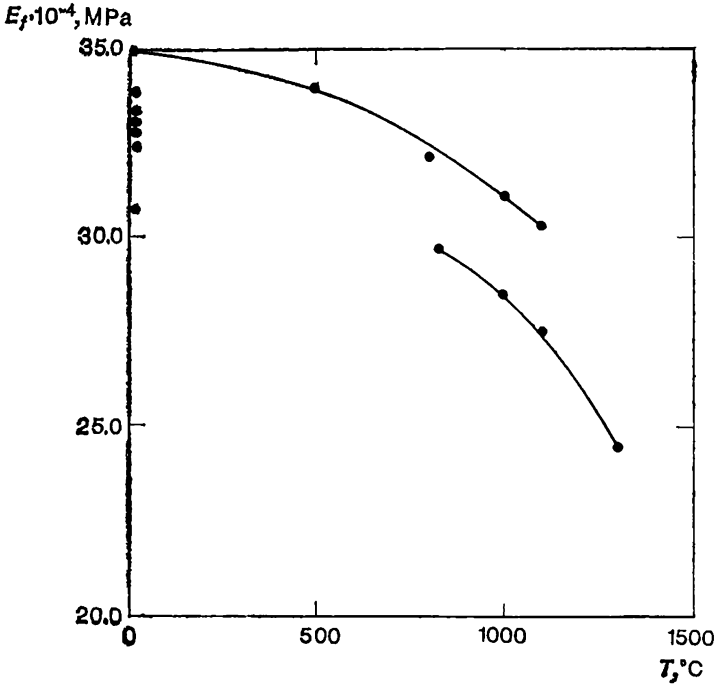

Fig. 6.7 Temperature dependence of longitudinal Young's modulus for sapphire fibers. The points joined by line are for fibers from the same batch (data by V. I. Kaz'min)

Table 6.2; note that at $\theta = 90°$ the two results differ substantially.

In conclusion we show the temperature dependence of the longitudinal Young's modulus of boron and sapphire fibers, obtained by measuring the natural frequencies of boron-aluminium and sapphire-

molybdenum specimens with various fiber volume fractions (Figs. 6.6 and 6.7). Note that the temperature dependence of the elastic modulus of boron fibers over a range between room temperature and 450°C proved to be very weak.

6.3 INELASTIC BEHAVIOUR

It is now evident that the inelasticity of composites could be a result of both the inelasticity of its constituents and accumulation of various structural damages under loading. Here we shall briefly discuss the behaviour of composites with inelastic constituents, leaving the analysis of inelasticity resulting from damage to the next section.

6.3.1 Elastic-Plastic Behaviour of a Composite

The micromechanics of an elastic-plastic composite can be formulated in the most general way. Thus, Yu. N. Rabotnov [4] has proposed a general method of constructing the limiting surfaces and investigating the elastic-plastic state of a composite structure. The composite structure in Rabotnov's formulation is a structure S obtained as a result of spatial superposition of m simple structures S_r ($r = 1, 2, \ldots, m$) with at least some common elements. All the possible composites, polycrystalline materials and structurally anisotropic elements, strengthened plates and shells, are examples of such structures.

State of a simple structure is described by two n-space vectors: that of internal forces $\mathbf{Q}_r$ and that of generalized strains $\mathbf{q}$. There takes place the law of elasticity $\mathbf{q} = \mathbf{A}_r\mathbf{Q}_r$, the limiting condition $\Phi_r(\mathbf{Q}_r) = k_r^2$ and the associated flow rule. Hence we have

$$\dot{\mathbf{q}}^{(p)} = \dot{\mathbf{q}} - \mathbf{A}_r\dot{\mathbf{Q}}_r = \lambda \operatorname{grad} \Phi_r = \lambda\,(\partial\Phi_r/\partial\mathbf{Q}_r)$$

Here $\mathbf{A}_r$ is the symmetric matrix, Φ_r is the scalar function, k_r and λ are constants, $\mathbf{q}^{(p)}$ is the vector of generalized plastic strains.

The vector $\mathbf{Q} = \sum_{r=1}^{m} \mathbf{Q}_r$, defined in n-dimensional space which contains all the vectors $\mathbf{Q}_r$, is called the vector of internal forces in the structure S.

An initial yield locus is evaluated and an elastic-plastic state as well as a limiting state of the two-component structure ($m = 2$) are analyzed in [4]. Since some metal-matrix composites can be simulated by a structure with one ideal plastic and one elastic constituent (metal-brittle fiber composite) we will reproduce here the evaluation of an initial yield locus and the analysis of the elastic-plastic behaviour.

the fiber orientations) with the computed values of $\widetilde{E}'_{1111}$ obtained by transformation of the components $\widetilde{E}_{ijkl}$ for a unidirectional composite with $v_f = 0.5$ (see Table 6.1). The comparison is shown in

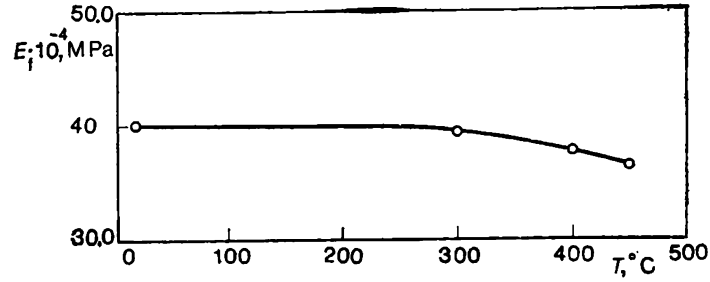

Fig. 6.6 Temperature dependence of longitudinal Young's modulus for boron fibers (data by E. G. Golofast)

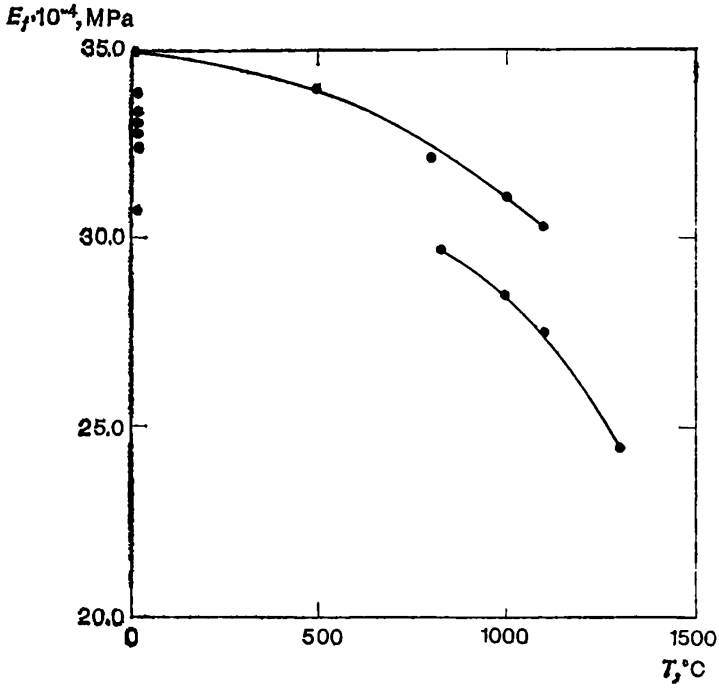

Fig. 6.7 Temperature dependence of longitudinal Young's modulus for sapphire fibers. The points joined by line are for fibers from the same batch (data by V. I. Kaz'min)

Table 6.2; note that at $\theta = 90°$ the two results differ substantially.

In conclusion we show the temperature dependence of the longitudinal Young's modulus of boron and sapphire fibers, obtained by measuring the natural frequencies of boron-aluminium and sapphire-

molybdenum specimens with various fiber volume fractions (Figs. 6.6 and 6.7). Note that the temperature dependence of the elastic modulus of boron fibers over a range between room temperature and 450°C proved to be very weak.

6.3 INELASTIC BEHAVIOUR

It is now evident that the inelasticity of composites could be a result of both the inelasticity of its constituents and accumulation of various structural damages under loading. Here we shall briefly discuss the behaviour of composites with inelastic constituents, leaving the analysis of inelasticity resulting from damage to the next section.

6.3.1 Elastic-Plastic Behaviour of a Composite

The micromechanics of an elastic-plastic composite can be formulated in the most general way. Thus, Yu. N. Rabotnov [4] has proposed a general method of constructing the limiting surfaces and investigating the elastic-plastic state of a composite structure. The composite structure in Rabotnov's formulation is a structure S obtained as a result of spatial superposition of m simple structures S_r ($r = 1, 2, \ldots, m$) with at least some common elements. All the possible composites, polycrystalline materials and structurally anisotropic elements, strengthened plates and shells, are examples of such structures.

State of a simple structure is described by two n-space vectors: that of internal forces $\mathbf{Q}_r$ and that of generalized strains $\mathbf{q}$. There takes place the law of elasticity $\mathbf{q} = \mathbf{A}_r\mathbf{Q}_r$, the limiting condition $\Phi_r(\mathbf{Q}_r) = k_r^2$ and the associated flow rule. Hence we have

$$\dot{\mathbf{q}}^{(p)} = \dot{\mathbf{q}} - \mathbf{A}_r\dot{\mathbf{Q}}_r = \lambda \operatorname{grad} \Phi_r = \lambda\,(\partial\Phi_r/\partial\mathbf{Q}_r)$$

Here $\mathbf{A}_r$ is the symmetric matrix, Φ_r is the scalar function, k_r and λ are constants, $\mathbf{q}^{(p)}$ is the vector of generalized plastic strains.

The vector $\mathbf{Q} = \sum_{r=1}^{m} \mathbf{Q}_r$, defined in n-dimensional space which contains all the vectors $\mathbf{Q}_r$, is called the vector of internal forces in the structure S.

An initial yield locus is evaluated and an elastic-plastic state as well as a limiting state of the two-component structure ($m = 2$) are analyzed in [4]. Since some metal-matrix composites can be simulated by a structure with one ideal plastic and one elastic constituent (metal-brittle fiber composite) we will reproduce here the evaluation of an initial yield locus and the analysis of the elastic-plastic behaviour.

Assuming the equality of the vectors $\mathbf{q}$ in the substructures (constituents) we then have in an elastic state:

$$\mathbf{q} = \mathbf{A}_1\mathbf{Q}_1 = \mathbf{A}_2\mathbf{Q}_2$$
$$\mathbf{Q} = \mathbf{Q}_1 + \mathbf{Q}_2 = (\mathbf{A}_1^{-1} + \mathbf{A}_2^{-1})\,\mathbf{q} = \mathbf{C}^{-1}\mathbf{q} \tag{1}$$
$$\mathbf{Q}_1 = \mathbf{C}\mathbf{A}_1^{-1}\mathbf{Q}, \quad \mathbf{Q}_2 = \mathbf{C}\mathbf{A}_2^{-1}\mathbf{Q}$$

The yield stress of the structure is reached when at least one of the following conditions is met:

$$\Phi_1(\mathbf{C}\mathbf{A}_1^{-1}\mathbf{Q}) = k_1^2, \quad \Phi_2(\mathbf{C}\mathbf{A}_2^{-1}\mathbf{Q}) = k_2^2 \tag{2}$$

The surfaces given by Equation (2) can be either embedded one into another or intersect. In either case we assume that at first a loading radius intersects the first surface. (In this analysis the second surface will never be reached.)

In an elastic-plastic state we have

$$\dot{\mathbf{q}} = \lambda\,(\partial\Phi_1/\partial\mathbf{Q}_1) + \mathbf{A}_1\dot{\mathbf{Q}}_1 = \mathbf{A}_2(\dot{\mathbf{Q}} - \dot{\mathbf{Q}}_1) \tag{3}$$

Excluding $\mathbf{q}$ from Equation (3) we obtain:

$$\dot{\mathbf{Q}}_1 = \mathbf{A}_2(\mathbf{A}_1 + \mathbf{A}_2)^{-1}\,\dot{\mathbf{Q}} - \lambda\,(\mathbf{A}_1 + \mathbf{A}_2)^{-1}(\partial\Phi_1/\partial\mathbf{Q}_1) \tag{4}$$

Besides, the condition $\Phi_1(\mathbf{Q}_1) = k_1^2$ yields

$$(\partial\Phi_1/\partial\mathbf{Q}_1)^{-1}\,\dot{\mathbf{Q}}_1 = 0$$

Substituting here Equation (4) we evaluate λ as:

$$\lambda = \frac{(\partial\Phi_1/\partial\mathbf{Q}_1)^{-1}\,\mathbf{A}_2(\mathbf{A}_1 + \mathbf{A}_2)^{-1}\,\dot{\mathbf{Q}}}{(\partial\Phi_1/\partial\mathbf{Q}_1)^{-1}(\mathbf{A}_1 + \mathbf{A}_2)^{-1}\,\partial\Phi_1/\partial\mathbf{Q}_1} \tag{5}$$

It is shown in [4] that the flow rule obtained is the conventional law of translational hardening, i.e. under loading the initial flow surface is transposed within the internal forces space parallel to itself.

If the volume fraction of a reinforcing constituent is small, heterogeneities of the stress-strain fields in the composite structural elements appear to be insignificant from the standpoint of the elastic-plastic behaviour of the composite. However this case is observed in practice relatively infrequently. With an increase in the fiber volume fraction the field heterogeneities become significant (this follows, in part, from the results of the corresponding numerical solution: see, for example, [5]) and the problem of evaluating approximate mechanical models emerges because of the unwieldiness of the exact calculation procedure.

One such model is suggested in [6]. The model uses the method of thin cross-sections: a typical representative element of the volume containing a fiber and a matrix (owing to symmetry it is sufficient

to take, for example, only a quarter of an elementary cell) is divided into plane elements and in each element the fiber and the matrix are bound by a certain elastic element (Fig. 6.8), such that the rigidity matrix ($\mathbf{A}_2$ in Rabotnov's model) is modified by substituting component $\tilde{a}_{11}^{(2)} = \alpha a_{11}^{(2)}$ for component $a_{11}^{(2)}$ (the axes are indicated in Fig. 6.8). At $\alpha = 1$ the strains ε_3 of the fiber and the matrix are the same, and at $\alpha = \infty$ the components σ_3 in the fiber and the matrix are equal to zero. All intermediate cases are realized by the choice of a proper value of α on the basis of experiment. An example given in [6], namely the stress-strain curves of a boron-aluminium composite along the x_2-axis, is shown in Fig. 6.9. Comparing these data with experiment the author of [6] recommends $\alpha = 11$.

6.3.2 Creep

It can be easily shown using creep as an example that an analysis of the strain characteristics of a composite should include the process of damage accumulation.

In fact, the simplest case of the deformation of a composite with brittle fibers and a creeping matrix under a constant load provides such an example.

Let a fiber be strained elastically (the fiber Young's modulus is E_f) up to the stress σ_f^* when the fiber breaks simultaneously at all the defect points spaced at a distance of l_f. The strength of fiber segments between two defects will for the time being be considered infinite. The constitutive equation of the matrix material will be taken as

$$\dot{\varepsilon} = \varepsilon_m (\sigma''/\sigma_m)^m + \dot{\sigma}''/E_m \tag{6}$$

where σ'' is the stress in the matrix, σ_m, m, and ε_m are creep constants.

Assuming the condition $\dot{\varepsilon}' = \dot{\varepsilon}''$ and adding to it the equilibrium equation (σ' are the stresses in the fibers)

$$\sigma = \sigma' v_f + \sigma'' v_m, \tag{7}$$

leads to the time-dependent stress in the matrix as

$$\sigma'' = \sigma_0'' \left[1 + \varepsilon_m \frac{m-1}{v^{(m)}} \left(\frac{\sigma_0''}{\sigma_m} \right)^{m-1} \frac{E_m}{\sigma_m} t \right]^{1/(1-m)} \tag{8}$$

where

$$v^{(m)} = 1 + v_m E_m / v_f E_f, \quad v^{(f)} = 1 + v_f E_f / v_m E_m$$

and $\sigma_0'' = \sigma/(v_m v^{(f)})$ is the initial stress in the matrix. At $t \to \infty$ $\sigma'' \to 0$, and as a consequence $\sigma' \to \sigma/v_f$. Hence, if

$$\sigma/v_f < \sigma_f^* < \sigma/(v_f v^{(m)})$$

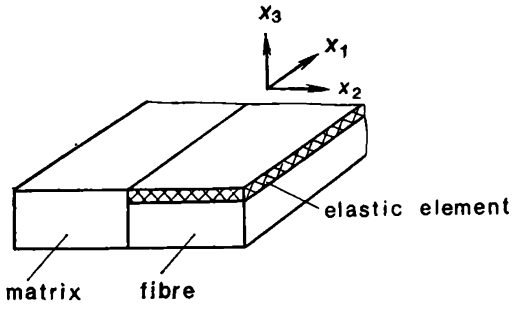

Fig. 6.8 Representative element of Dymkov's model [6]

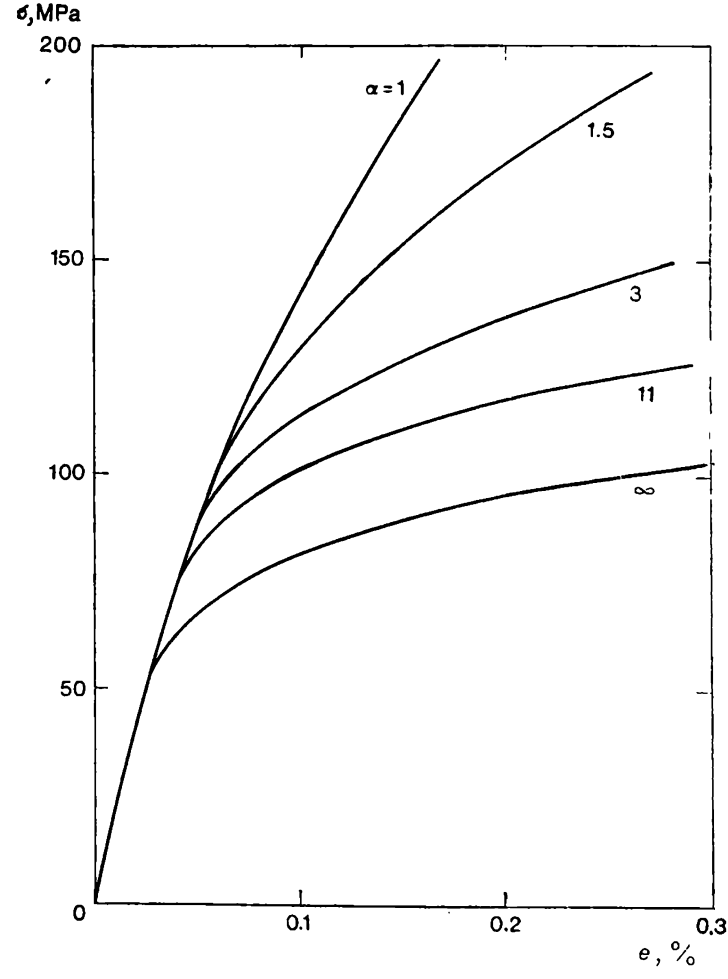

Fig. 6.9 Calculated transverse stress-strain curves for boron-aluminium composites [6]

where $\sigma/v_f v^{(m)}$ is the initial stress in the fiber, then at a certain instant $t^* > 0$ the fiber will fail and the matrix will be reinforced by short fibers if l_f is sufficiently small.

The composite creep rate will change abruptly: the matrix inelasticity results in a change of the fiber damage degree.

The above example is important not only as an illustration of the effect of composite structure damage (having a real physical form) on material rigidity (creep rate), but it also has an independent significance in estimating the creep rate of a composite with continuous brittle fibers. The question has been considered in detail by the present author in [7] allowing for the continuous changeover of composite structure from an initial to a steady-state one with a definite average fiber length. In that calculation the scale dependence of the fiber strength follows Weibull's distribution.

6.4 COMPOSITE FAILURE UNDER SHORT-TIME STATIC LOADING

Since the present review is concerned with metal-matrix composites only, the subject of the present section will be composites of two types: brittle fibers—metal matrix and ductile metal fiber—ductile metal matrix. An analysis of the failure mechanisms of such composites results in a three-component composite, i.e. brittle fibers—ductile metal fibers—metal matrix.

6.4.1 Strength of a Metal-Metal Composite

Assume that a composite consists of two metals having stress-strain curve equations which can be written in terms of true stress s and logarithmic strain e as $f(s, e) = 0$. Assuming Poisson's ratio to be known one obtains the usual stress-strain equation, namely, $F(\sigma, e) = 0$. Longitudinal strains of the composite constituents are taken to be equal. Then the stress-strain curve is given by

$$\sigma = \sigma'(e)\, v_f + \sigma''(e)\, v_m \tag{9}$$

The condition of stability in tension (the onset of necking), when applied to (9) with known functions $F_f(\sigma, e)$ and $F_m(\sigma, e)$ and assuming an ideal bond at the interface, yields

$$v_f \frac{\partial F_f/\partial e}{\partial F_f/\partial \sigma} + v_m \frac{\partial F_m/\partial e}{\partial F_f/\partial \sigma} = 0 \tag{10}$$

which gives ultimate values σ^* and e^* for the composite.

The idea of simultaneous necking of the fibers and the matrix is brought in [8] to result comparable with experiment. The dependen-

ces of σ^* and e^* on the fiber volume fraction are obtained in the form:

$$\sigma^* = \lambda_f \sigma_f^* v_f + \lambda_m \sigma_m^* v_m \tag{11}$$

$$v_f = \left[1 + \beta \frac{e^* - e_f^*}{e_m^* - e^*} (e^*)^{e_f^* - e_m^*} \right]^{-1} \tag{12}$$

here

$$\beta = \frac{\sigma_f^*}{\sigma_m^*} \frac{(e_m^*)^{e_m^*}}{(e_f^*)^{e_f^*}} \frac{\exp e_f^*}{\exp e_m^*}$$

$$\lambda_r = (e^*/e_r^*)^{e_r^*} \exp (e_f^* - e^*)$$

where $r = f$ or m (the fiber or the matrix).

Comparison of Eq. (11) and Eq. (12) with experiment can be found in [8], yet most convincing experimental data in favour of this model's

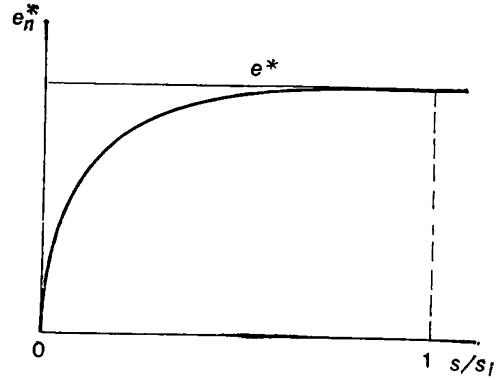

Fig. 6.10 Dependence of ultimate strain e^* on strength s^* of the fiber-matrix interface for composite, following qualitatively from the experiments by Ochiai and Murakami [15].

validity were obtained by Murakami and Ochiai [9]. In their experiments the interfacial strength has been changed to a large degree (the estimates are only qualitative) and it has been thus discovered that a large weakening of the bonding does not considerably affect the value of e^*.

A complete theory of the ultimate state of a metal-metal composite should include as a parameter a quantity relative to the bonding strength of the interface. Clearly, in the case of nonideal bonding at $e_f^* < e_m^*$, the ultimate elongation e_n^* will be such that $e_f^* \leqslant e_n^* \leqslant e^*$. The experiments by Murakami and Ochiai show that a dependence of e_n^* on parameter s describing the interfacial strength and changing from 0 to s_i should be as shown schematically in Fig. 6.10.

Note that the experimental data by Igata *et al.* (see, for example, [10]) are within the scheme proposed.

6.4.2 Fracture Toughness of a Metal-Metal Composite

Let us make another essential assumption remaining in the framework of the above model, namely, that the work of fracture G (such as $K^2 = GE$, for instance, in the case of an isotropic body) is linearly connected with ultimate strain e^* of the material in tension, and, if one changes the value of e^* without changing the

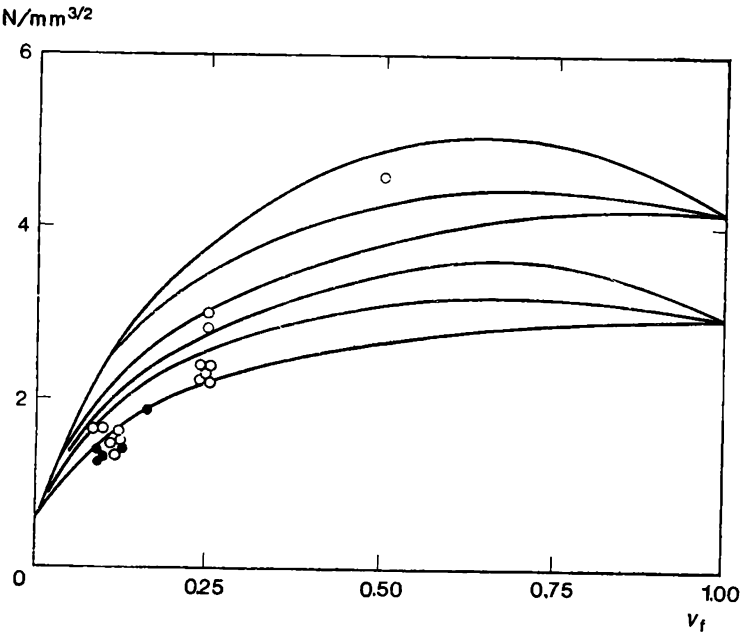

Fig. 6.11 Calculated and experimental dependences of fracture toughness for steel-aluminium composites. The open circles are data from [11], the solid circles, from [12]

structure and other physical-chemical characteristics of the material, then the work of fracture will change proportionally to e^*.

If now the constituents of the composite, considered in the preceding section, are characterized by quantities G_f and G_m of the fracture work, then G for the composite will be obtained by mere summation

$$G = G_f\ (e^*/e_f^*)\ v_f + G_m\ (e^*/e_m^*)\ v_m + \Delta G_{fm} \qquad (13)$$

where ΔG_{fm} is associated with the energy dissipation resulting from friction, delamination and other processes at the fiber-matrix interface.

In the case of sufficiently ductile constituents the value of ΔG_{fm} may, apparently, be neglected. In any case the experimental data obtained with the steel-aluminium composite [11] are adequately described by Eq. (15) assuming $\Delta G_{fm} = 0$.

Note that when describing the composite behaviour the values of both G_f and G_m are assumed to be known. In fact, the value of G_m can be obtained comparatively easily, but wire fracture toughness G_f can be only found by testing the wire-containing composites.

In the example of calculated and experimental dependences K^* (v_f) for steel-aluminium composites shown in Fig. 6.11 note that the curves K^* (v_f) with a well pronounced maximum are quite possible.

Since the fracture mechanism changes at $e_f^* \to 0$ formula (13) becomes invalid. The fracture mechanism at the macrocrack tip for this case will be considered below (Section 6.4.4).

6.4.3 Strength of a Brittle-Fiber Composite

Let us consider a failure model [13-15] based essentially on well-established experimental facts, namely, the possibility of two extreme failure mechanisms. The first model is cumulative fiber breaking and the second one is of the weakest link type, when the first fiber break results in composite failure. The first possibility is visualized in the observation of longitudinal sections of failed specimens (corresponding micrographs are given in [14] for boron-aluminium composites and in [16] for sapphire-molybdenum composites). As for the second possibility, certain indirect data, in particular, recording of acoustic emission signals in the process of specimen loading, leave no doubts as to the possible realization of the mechanism. The remaining necessary assumptions will be made below.

If the first possible failure mechanism takes place, then the fibers break at points where the stress (non-uniform with the onset of fiber breaking, as discussed in the preceding section) reaches the local strength value σ_f^*. Fiber breaking continues until within a composite band of critical length l^* at least one break on each fiber appears and the possibility emerges of separating the specimen into two parts by the shear along the fiber-matrix interface. (The length l^* is such that $\langle \sigma_f^* (l^*) \rangle / (2\tau^*) = l^*/d$, where τ^* is the ultimate shear stress at the interface.) The average ultimate composite stress in this case will obviously be

$$\langle \sigma_1^* \rangle = \alpha \langle \sigma_f^* (l^*) \rangle v_f + \sigma_m^* v_m \tag{14}$$

Here σ_m^* can be taken equal to the ultimate matrix strength, though a more rigorous model should somewhat correct the value, being equal to average matrix stress in the above-discussed failure situation; the factor α $(1/2 \leqslant \alpha \leqslant 1)$ is determined by stress distribution along the fibers (including the fact that the value of $\langle \sigma_f^* (l^*) \rangle$ depends on the stress distribution along the fibers), fiber length distribution in the limiting state, etc.

In failure of the weakest link type it is possible to take the following expression for average ultimate stress:

$$\langle \sigma_2^* \rangle = \langle \sigma_f^* (L) \rangle v_f + \sigma_m' v_m \qquad (15)$$

where L is the total fiber length within the whole volume of a constant cross-section composite rod in tension, and σ_m' is matrix stress at the moment of the first fiber break.

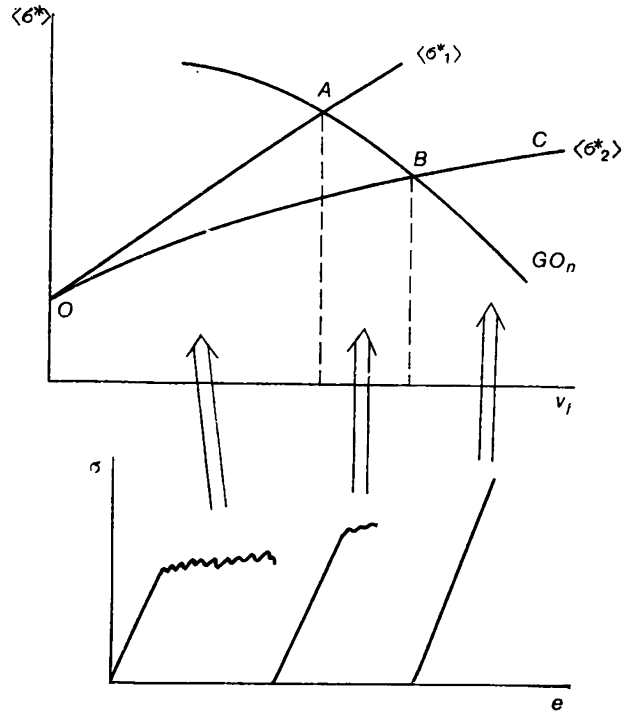

Fig. 6.12 Dependence of average strength on fiber volume fraction for brittle-fiber composite and a schematic representation of stress-strain curves

Now assume that for a particular composite the dependences of $\langle \sigma_1^* \rangle$ and $\langle \sigma_2^* \rangle$ on v_f are located in the $\langle \sigma^* \rangle$, v_f plane, as schematically shown in Fig. 6.12.

To understand when a particular failure mechanism takes place, let us introduce the idea of specific microcracks of the length nd (n is the number featuring the fiber packing quality in a transverse cross-section). In the case of an ideal packing $n = 1$; when deviating from the ideal packing the value of n rises; e.g. for pair-by-pair packing of all fibers $n = 2$ and the break of a fiber from a pair is immediately followed by the formation of a microcrack of the length $2d$ (if the interface does not arrest the microcrack propagation).

Now in the $\langle\sigma^*\rangle$, v_f plane it is possible to draw the curve GO_n corresponding to the Griffith-Orowan ultimate stress for an anisotropic material characterized by the fracture work $G(v_f)$ and containing the noninteracting microcracks of the length nd:

$$\sigma = \sqrt{GC/(\lambda\, nd)} \tag{16}$$

where C is the known combination of elastic characteristics of an anisotropic body, and λ is the constant which depends on the reinforcement geometry (on the type of stress state).

The dependence of average composite strength on fiber volume fraction is now given by the curve $OABC$ (Fig. 6.12) which may be nonmonotonical. In the region OA the failure takes place with a total localization of fiber breaks; in the region BC the first fiber break results in the composite failure; in the region AB the partial localization of fiber breaks takes place.

It should be noted, that, firstly, the relative position of the curves $\langle\sigma_1^*\rangle$ and $\langle\sigma_2^*\rangle$ in Fig. 6.12 can be different, in particular, the second curve can pass above the first one at small v_f; secondly, the position of the point A is of special importance (since along the segment OA a favourable type of failure persists) and with an increase in the values of $\alpha < \sigma_f^*$ (l^*) the point A shifts to the left; thirdly, the real composite behaviour is somewhat aggravated by initial stresses in the components.

The question of strength scatter appears to be of importance. Along the segment OA the strength scatter is small, while along the segments AB and BC the composite strength scatter is nearly equal to the fiber strength scatter. Therefore, it can be large enough and make it difficult to trace the curve $OABC$ in all the experiments. (Indeed, a real $\langle\sigma^*\rangle$-v_f curve should be smooth without inflections at the points A and B.) A large strength scatter as well as a small increment in average scatter strength necessitate controlling the point A along the segment ABC, namely, removing it into a region of large values of v_f. Possibilities of doing this will be discussed below (in Section 6.4.5).

Figs. 6.13 and 6.14 are examples of the σ^*-v_f relationships, obtained for boron-aluminium and sapphire-molybdenum composites, which qualitatively confirm the foregoing scheme.

This scheme relies on Griffith's energy approach to the estimate of a limiting state of a cracked body. An alternative approach is used in [17]. The results of the appropriate calculations, using both Monte-Carlo method to determine a set of random situations in the strength distribution of the brittle fibers and an approximate evaluation of the fiber load concentration in the vicinity of a fiber break, yield qualitatively the same $\langle\sigma^*\rangle$-v_f dependence as that in Fig. 6.12.

Note that the fiber breaking in the interval OA (accumulation of damage whose nature can be established in a simple way) results in

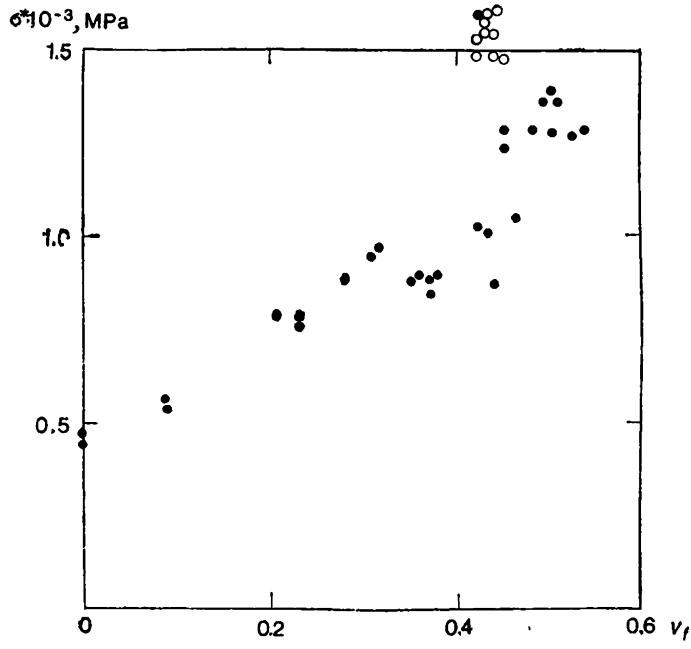

Fig. 6.13 Dependence of strength on fiber volume fraction for boron-aluminium composite. The solid circles are for boron-aluminium composite, the open circles, for boron-aluminium composite with 6% addition of steel wire [26]

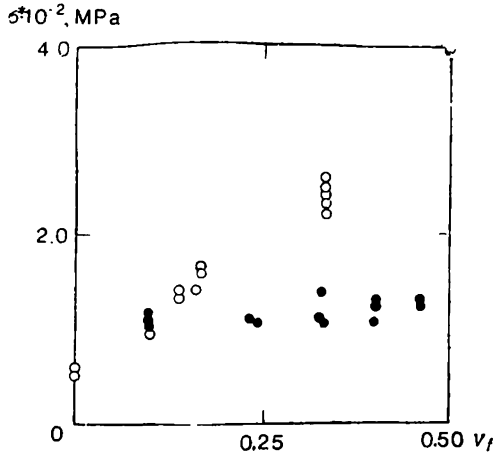

Fig. 6.14 Dependence of strength on fiber volume fraction for sapphire-molybdenum composite. The open circles are for fiber diameter 50 μm, the solid circles, for 200 μm

physically nonlinear material behaviour (Fig. 6.12) which is an illustration of the general situation mentioned above (Section 6.3). The quantitative analysis of such behaviour has been performed, e.g. in [17].

Finally, it should be noted that the composite behaviour description within the model accepted here is specific not only for metal-matrix composites. While there has been no systematic testing of the model in the case of reinforced plastics, many publications reveal a characteristic maximum on the σ^*-v_f curve, though shifted to a region of high fiber volume fractions.

6.4.4 Fracture Toughness of a Brittle-Fiber Composite

The fracture toughness of fibrous structures containing brittle constituents is in the final analysis the decisive factor in the evaluation of the prospects of fibrous composites and as such it deserves a close analysis.

6.4.4.1 Experimental Fundamentals

The possibility of producing composite structures with a fracture toughness exceeding that of individual constituents was

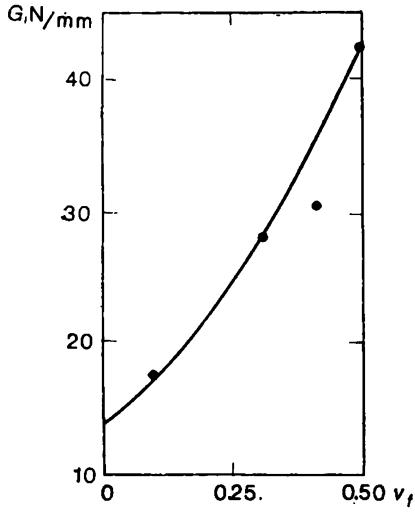

Fig. 6.15 Work of fracture of boron-aluminium composite versus volume fraction of brittle boron fibers

established experimentally long ago. It is this fact that influenced the extensive application of reinforced plastics: the high strength of reinforcement along with its low density is attained when using brittle substances with ionic and covalent bonds [18].

The high fracture toughness of the metal-metal composites analyzed in Section 6.4.2 was not unexpected. What might be surprising is the presence of a maximum on the curve K^* (v_f).

As to the fracture toughness of composites with brittle fibers and a metal matrix, after the experiments by Kelly and Cooper, who had observed a decrease in the work of fracture of tungsten-copper composites with an increase in the volume fraction of tungsten wire, in the given case the dependence of such a kind seemed to be typical. If this conclusion had turned out to be valid, then the prospects of the practical use of metal-matrix composites would be thought of as extremely limited.

However experiments with boron-aluminium composites [15, 19] have shown (and this is somewhat unexpected) that the work of fracture of metal-matrix composite can increase with the volume fraction of brittle fibers (Fig. 6.15). Qualitatively, the fact could be explained by the expansion of the fracture zone at the macrocrack tip as a result of breaking of brittle fibers characterized by a strength scatter. (In the composites tested by Kelly and Cooper the tungsten wire had seemingly much less strength scatter compared to boron fibers.)

6.4.4.2 A Micromechanical Model [20]

Let us evaluate the size of a cracking zone at the macrocrack tip using a simple model. Let a plane semi-infinite heteroge-

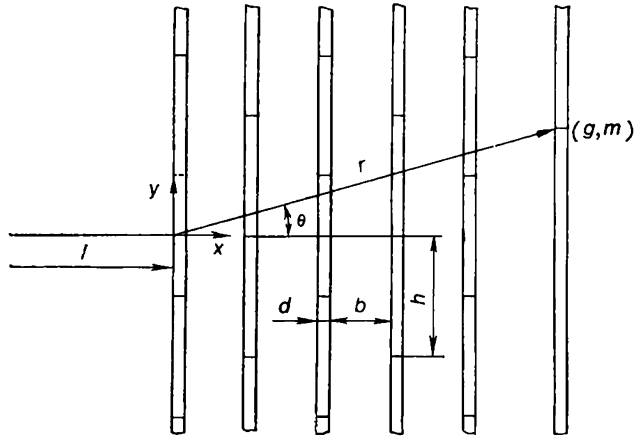

Fig. 6.16 Plane model of composite with a regular system of defects on fibers

neous medium (Fig. 6.16) be composed of alternate layers (constituents), one of which contains such orderly located defects that if the stress σ_y at a defect point of the layer reaches the value σ^*,

then a microcrack arises here. Let the microcrack length be always equal to d (that means that it cuts a layer as a whole but never passes into an adjacent layer (e.g., as a result of local plastic deformation of a layer of the second kind). Consider for simplicity the case of elastically isotropic layers with equal elastic moduli, i.e. the composite as a whole appears to be elastically isotropic.

Imagine that all defects (g, m), where g is a defect number on a fiber and m is a fiber number (see Fig. 6.16), located within a finite region, including a priori the sought cracking region, are opened in a sense that each microcrack defect produces an elastic field. Further we shall treat each microcrack (defect) as placed in the macrocrack field and in the fields of adjacent microcracks, i.e. write the stress at point (g, m) in the following dimensionless form:

$$\sigma(g, m) = \frac{\sigma_0 \sqrt{l}}{\sqrt{2\pi(1+\mu)}} \varphi(g, m) \tag{17}$$

Here all the stresses are normalized via stress σ^* and the crack length l via dimension b (Fig. 6.16):

$$\varphi(g, m) = \frac{(1+\xi)^{3/2}(3\xi-2)}{2\sqrt{2}\xi}$$

$$\xi = (1+\eta^2)^{1/2}, \quad \eta = (g/m)[h/(b+d)] = (g/m) v_f \chi$$

$$v_f = d/(b+d), \quad \chi = h/d, \quad \mu = d/b$$

The condition for defect (k, s) to appear in the cracking zone is as follows

$$\psi(k, s) = \sigma(k, s) + \Delta\sigma(k, s) + \sigma_0 \geqslant 1 \tag{18}$$

Here the equality sign corresponds to the defect position on the cracking zone boundary. The value of $\sigma(k, s)$ is given by Eq. (17).

Let us write the expression for $\Delta\sigma(g, m)$ on defect (g, m) as follows

$$\Delta\sigma_*(g, m) = \varkappa_{ij} \Delta\sigma_{g+i, m+j}(g, m)$$

where $i, j = \pm 1$ (summation is carried out over the recurring subscripts) and $\varkappa_{ij} = 1$, if point $(g + i, m + j)$ is in the cracking zone, and $\varkappa_{ij} = 0$ in the opposite case.

It is possible to find $\Delta\sigma_{g+i, m+j}$ assuming that microcracks are to be found in a heterogeneous stress field, but this results in rather complicated calculations. Therefore, allowing for the fact that in the general case $d < b$ and assuming the interrelation of only the adjacent defects, for simplicity we consider the macrocrack field as locally heterogeneous, so that

$$\Delta\sigma_{g+i, m+j}(g, m) = \frac{\sigma_0 \sqrt{l}}{2\pi} \sqrt{\frac{\mu}{1+\mu}} \varphi(g+i, m+j) \varphi(i, j)$$

If point (k, s) lies in the cracking zone, then, since the boundary configuration is a priori unknown, inequality (18) yields a set of inequalities:

$$\psi^t (k, s) \geqslant 1$$

with each term being determined by its own set of $\varkappa_{ij}^l$. To determine the boundary one should test all possible alternatives $\varkappa_{ij}^t = 0$, $\varkappa_{rs}^t = 1$.

The exhaustive search of the alternatives with an increase of σ_0 has been carried out in [20] with the aid of a computer yielding cracking zones of the type provided as an example in Fig. 6.17. It might

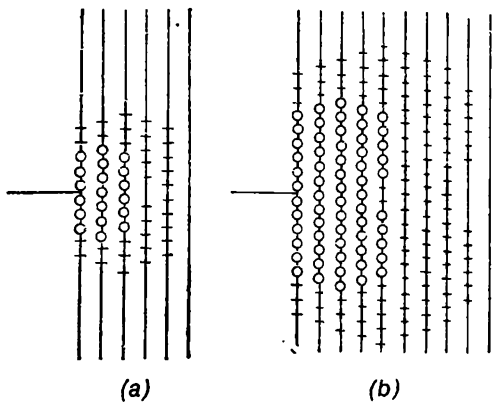

Fig. 6.17 Two examples of microcracking zone at the macrocrack tip. The open circles are from calculation with no account of microcrack interaction. $\chi = 6$, $l = 25°$, $v_f = 0.1$, $\sigma_0 = 0.20$ (*a*) and 0.25 (*b*)

be noted that the assumption on the interaction of adjacent microcracks substantially enlarges the cracking zone compared to that obtained assuming $\Delta\sigma (k, s) = 0$ (i.e. with the absence of microcrack interaction). The calculation gives the relation of maximum number n of the microcracks in a "fiber" to applied stress σ_0.

A limiting size of the cracking zone, i.e. a size attained when the zone starts growing in the direction of the macrocrack propagation only, can be obtained if one prescribes a definite value of the energy dissipation to each fibre break. Then it is possible, for example, to assume

$$G = G_m (1 + \nu n)$$

where G_m is the matrix contribution to the work of fracture of the composite associated with a single fiber break at the macrocrack plane, n is the maximum number of breaks of a single fiber, ν is a constant, $\nu < 1$.

Therefore we can have an equation for limiting stress σ_0, namely

$$G_m [1 + \nu n (\sigma_0)] = \sigma_0^2 l/E$$

which follows from the well-known Irwin's relationship.

Qualitative conclusion following from the calculation (with $\sigma^* = 1500$ MPa) illustrated in Fig. 6.18 can be formulated as follows.

1. The fracture toughness of composite K^* as a function of the fiber volume fraction v_f can be both monotonically decreasing ($\chi = 26$ in Fig. 6.18) and have a maximum at a certain fiber volume fraction ($\chi = 8$, $\chi = 10$). Within the given model an infinite increase of K^*

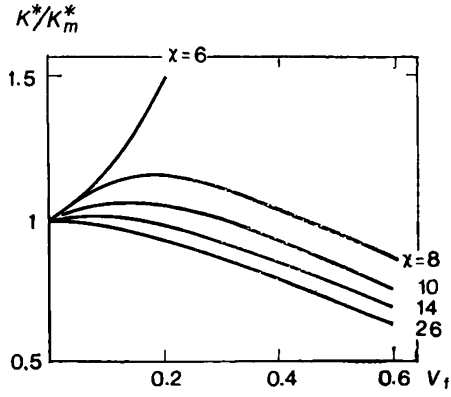

Fig. 6.18 Dependence of fracture toughness on model structural parameters. $K_m^* = 3$ kN/mm$^{3/2}$, $l = 250$

is possible at sufficiently small χ, suitable for a material not influenced by a crack up to a certain length. The behaviour of the model qualitatively fits the above-cited experiments on boron-aluminium (small χ) and tungsten-copper (large χ) composites.

2. With an increase in the crack length the value of K^* tends to be a constant, which can be taken as a specific one for a material. However the crack length required may appear to be too large for an appropriate experiment to be carried out.

3. Matrix fracture toughness exerts a very strong influence on composite fracture toughness. If a composite structure is seen as an amplifier of matrix fracture toughness K_m^*, then this amplifier appears to be a nonlinear one.

4. Composite fracture toughness depends substantially on the fiber strength revealed on the length of the order of the critical one (the average distance between the fiber defects failing in an experiment).

5. Fracture toughness of a composite structure depends on many factors, which, on the one hand, create possibilities of controlling

composite fracture toughness and, on the other hand, cause a substantial scatter of experimental data. The last aspect is illustrated in [19].

6.4.4.3 A Phenomenological (Macromechanical) Fracture Model of a Composite Element with a Macrodefect

Bearing in mind the importance of evaluating macrodefect influence on the limiting load of a composite element let us consider an alternative macromechanical approach to the problem, aiming first of all at the possibility of a rapid estimation of the behaviour of a fabricated composite structure. As with the majority of similar well-known attempts (Irwin's correction for crack length, the proposal in [21], etc.) the approach discussed here [22] is based on the introduction of a characteristic linear dimension.

Let a nonloaded composite body contain a crack of a length equal to $2l$. Under loading of the body a fracture zone originates near the crack tip. Let us assume that the effect of the zone on the crack is a change of its curvature radius at the dangerous point. Let us further assume that the crack in the loaded body transforms into an elliptical hole, having at the dangerous point a curvature radius of a certain value r^* specific for a given material at the moment of fracture. Let us consider that at fracture the local strength σ^* of the material at the crack tip is reached. Neglecting changes of the elastic properties of the composite in the fracture zone we use the well-known solution of Lekhnitskii [23] for a problem of an orthotropic plate with an elliptical hole subjected to tension by stress σ at infinity and obtain for ultimate stress $\tilde{\sigma}$

$$\sigma^*/\tilde{\sigma} = 1 + [(p+q)/pq]\sqrt{l/r^*} \tag{19}$$

where p and q are the constants depending on the material elastic parameters.

Equation (19) contains two parameters (σ^* and r^*) which have to be determined by experiment. In the $1/\tilde{\sigma}$, $\sqrt{l}$ coordinates this is an equation of a straight line with its ordinate intercept at $(1/\tilde{\sigma})$ and a slope which determines the values of constants r^* and σ^*.

Hence the first checking of the validity of the above assumptions is the linear dependence $1/\tilde{\sigma}$ on $\sqrt{l}$ to be obtained by experiment. Numerous experimental data are presented in [22] showing the dependence of $1/\tilde{\sigma}$ on $\sqrt{l}$ to be in fact linear and, in particular, for the boron-aluminium composite it is presented in Fig. 6.19. It is of interest to note that the values of σ^* obtained in this way are always larger than the values of average strength of smooth specimens

of the same material, this fact being simply interpreted by size effect ideas.

It is possible in a natural way to generalize the above assumption confirmed by experimental data, namely, to assume that for defects of an arbitrary shape with the curvature radius at the danger point being less than a critical one the onset of fracture must correspond

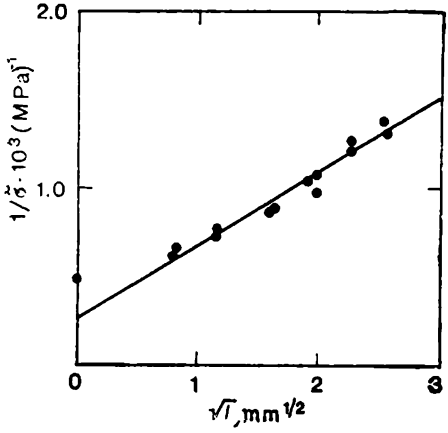

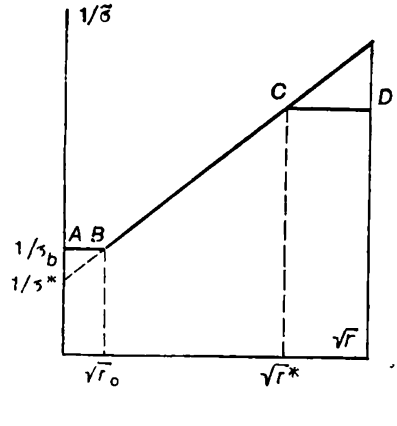

Fig. 6.19 Linear dependence of $1/\tilde{\sigma}$ on $\sqrt{l}$ for unidirectiona lboron-aluminium plates with a central hole. The experimental data by Averbuch and Hahn [24]. The stress $\tilde{\sigma}$ is corrected for finite plate width

Fig. 6.20 Scheme of determination of ultimate stress $\tilde{\sigma}$ for composite plate with a circular hole

to a "transformation" of an initial hole into one (the latter can be chosen as an elliptical hole) whose curvature radius at the danger point is equal to the critical one; at the same time the stress at the danger point reaches the value of σ^*. Thus, a plate made of a particular material will equally respond to all defects with identical sizes and curvature radii at the danger point less than critical, hence in the case of such defects one can again use Eq. (19).

When loading a plate with a central circular hole of radius r the above considerations result in a relationship between $1/\tilde{\sigma}$ and $\sqrt{r}$ as shown schematically in Fig. 6.20. There the segment BC corresponds to the straight line (19) and the slope of this line is related to the value of r^*, the point A corresponds to the strength of a specimen without a hole. The plateau at $r > r^*$ corresponds to the elastic behaviour of the plate and to its fracture upon attaining the ultimate strength σ^* at the danger point according to the elastic solution.

If the radius of the hole is small enough ($r < r_0$) the failure will not necessarily take place in the vicinity of the hole. Local strength

at the "danger" point may be higher than the stress at this point and the failure condition will be satisfied at another point.

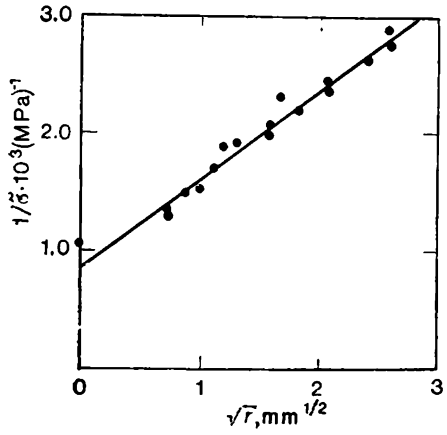

Fig. 6.21 Dependence of $1/\tilde{\sigma}$ on $\sqrt{r}$ for unidirectional boron-aluminium plates with a circular hole. The experimental data by Broockman and Sierakowski [25]. The stress $\tilde{\sigma}$ is corrected for finite plate width

Experimental data for boron-aluminium composite, treated in accordance with the scheme presented, are given in Fig. 6.21.

6.4.5 An Improved Composite

Let us return to the dependence of the average strength of brittle-fiber composites on the fiber volume fraction (a schematic illustration is shown in Fig. 6.12, two specific examples can be seen in Figs. 6.13 and 6.14). It is not difficult to see the desirability of point A being shifted to larger fiber volume fractions when the tensile strength of a designed composite should be as large as possible.

There are several ways of achieving this objective. For example, one may improve the quality of the fiber packing and so lower the value of n in Eq. (16) and in this way gain a larger admissible fiber volume fraction. (Clearly, in the case of a high-strength composite an increase of the fiber volume fraction beyond that at point A is not expedient.) This method is related to an evident limit because $n \geqslant 1$.

The second possibility of controlling the position of point A arises if one uses a matrix with a larger value of G. This possibility substantially increases if one bears in mind the dependence $K^*(v_f)$ of the metal-metal composite (Section 6.4.2, Fig. 6.11). Adding into the matrix of a brittle fiber composite a certain sufficiently small number of high-strength ductile fibers one can substantially increase

the matrix fracture work and, in so doing, shift point A (Fig. 6.12) to the right, to raise average composite strength under conditions of a small strength scatter [26]. The idea was verified with boron-aluminium composites, now called improved ones (the relevant illustration is given in Fig. 6.13).

6.4.6 Compressive Strength

Owing to the possible plastic deformation of a metal matrix the well-known assessments of the ultimate stresses in the plane elastic models of a composite (see, for example [27, 28], etc.) do not yield good results for metal-matrix composites.

In [29, 30] a model is suggested for analysing the stability of a fiber system embedded in a ductile matrix. The values of the energy

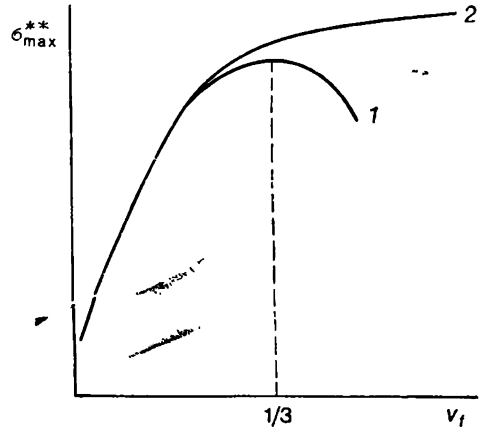

Fig. 6.22 Schematic representation of composite compressive strength versus fiber volume fraction:
1—experimental; *2*—model behaviour

are compared for a straight compressed beam and that being converted to a "broken" state with the two shear bands not changing the distance between the beam ends. Comparison shows that after a certain stress value the "broken" beam configuration proves to be energetically beneficial. However a jump-like transition into this state involves overcoming a barrier which proceeds via bending, i.e. an initial beam imperfection is increased under loading. Fig. 6.22 schematically illustrates the dependences $\sigma^{**}_{max}(v_f)$, given by the model and obtained in experiments. As seen, at $v_f \geqslant 1/3$ the discrepancy proves to be qualitative. Yet this is of no special importance if the stability of the fiber system is significant (compressive strength) and an increase in the fiber volume fraction above 1/3 is not advis-

able; if the stability of a structural element as a whole is decisive an increase in the volume fraction of the high-modulus fiber is efficient irrespective of the above discrepancy.

The critical stress σ^{**} of the compressed composite beam of sufficiently high rigidity will be less than the value σ^* of Euler's stress, so that

$$\frac{\sigma^{**}}{\sigma^*} = \left[1 + \frac{\pi}{2}\frac{a_0}{h}\frac{h}{l}\frac{\sigma^*}{\sigma_m^*}\frac{1}{v_m}\right]^{-1}$$

where h and l are the thickness and length of the beam, a_0 is the amplitude of an initial imperfection, and σ_m^* is the yield stress of the matrix material.

The ultimate compressive stress of a composite is shown to be such that

$$\sigma_{max}^{**} \sim E_f^{1/3} (\sigma_m^*)^{2/3}$$

Within the model it is achieved at $v_f = 1/3$ and a certain value of ratio h/l.

The value of a_0/h depends on the quality of the fabrication process. In particular, for composite plates fabricated under laboratory conditions $a_0/h \approx 0.05$ in the case of a steel-aluminium composite and $a_0/h = 0.10$ in the case of a boron-aluminium composite.

The deviation of fiber orientation from the uniaxial compression direction is accompanied by a decrease in the critical compressive stresses. The relevant experimental data are given in [30, 31].

6.5 CREEP STRENGTH

The consideration of creep strength of a continuous-fiber composite is a natural extension to the creep analysis of the composite (Section 6.3.2); a fiber strength distribution, e.g., Weibull's, is to be introduced into the model. Besides, by analogy with the above short-time failure (Section 6.4.4) it is to be assumed that the redistribution of stresses between elastic fibers and a creeping matrix will be accompanied by either immediate composite failure after a first fiber break at the weakest point (if the fiber volume fraction is sufficiently large), or the fragmentation of fibers into segments. In the second case we move to a short-fiber composite with a matrix in pure shear [32, 33]. The failure of the material in creep should, naturally, proceed along the interface between rigid fibers and a creeping matrix. Since in the model composite the distribution of shears along the fiber is uniform it is only natural to take as a failure criterion a certain critical value γ^* reached by the shear strain. In the case of the step-by-step fracture of the elements after reaching γ^* the composite creep curve contains, apart from the steady-state stage, an accelerated creep stage.

If all stages of the creep are present the composite rupture time will be

$$t_* = (A/\sigma)^{m-1} + (B/\sigma)^{m(\beta+1)}$$

Here β is a constant in Weibull's distribution of fiber strength and the expressions for the parameters A and B are not written here because of their unwieldiness [7].

6.6 FATIGUE

Hitherto the primary emphasis in studying fatigue of metal-matrix composites was placed on the purely phenomenological description of the fatigue of certain materials, sometimes accompanied by microscopic observations of the failure process. A survey of such works is given in [34]. Below we shall describe the fatigue fracture of metal laminates and metal-matrix composites and attempt to construct a model as the basis for a computer simulation. The comparison of simulation results with those of physical experiments can yield the determination of necessary parameters and use of the model in design.

6.6.1 Laminates

Here the simplest composites are dealt with, elastic homogeneous and isotropic materials having heterogeneities in the form of weak interfaces between the layers. Such structures can be fabricated by various techniques (diffusion bonding, glueing, etc.); the most convenient one is the diffusion bonding of a stack of thin sheets which provides simple variations of the interface strength, e.g. by varying the processing time at constant temperature and pressure.

The fatigue strength of the material depends on the interlaminar bonding strength (diffusion bonding time), with this dependence curve possessing a maximum [35]. This appears to be a very interesting fact. The experimental data obtained [35], i.e. micrographs of specimens after cyclic loading, permit the following model of the process to be suggested.

Let us imagine an interface with a nonideal bond in the form of an "island" structure in which areas of ideal bonding alternate with areas where the bonding is completely absent, so that free surfaces are present at the interface (Fig. 6.23). Both interfaces and surfaces carry a certain amount of flaws initiating fatigue cracks. Let some hierarchy of flaws exist being conditioned by the succession of the amplitudes ΔK of the stress intensity factor so that $\Delta K_1 > \Delta K_2 > > \Delta K_3 > \ldots$, with this hierarchy changing, in the general case,

over time because of changes of the stress state and the occurrence of new free surfaces owing to delamination.

Since the fatigue crack growth rate dl/dN is related in a nonlinear fashion to the quantity ΔK, a crack initiated by the most pronounced flaw with value $\Delta K = \Delta K_1$ (let it be crack *1* in Fig. 6.23) will quickly surpass in growth all other cracks, intersect the layer and approach the interface. Then it may either intersect it, falling on a

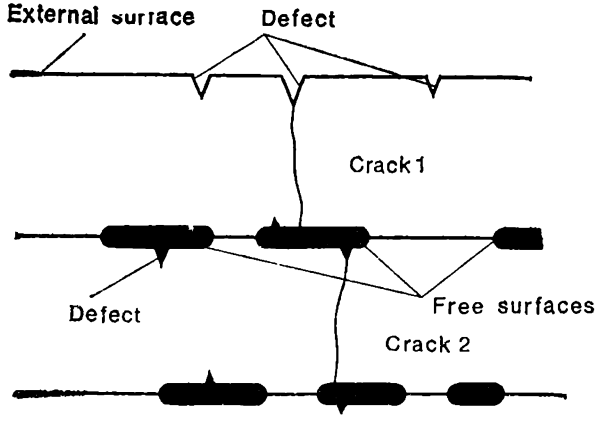

Fig. 6.23 Pattern of fatigue racture of laminated material with a nonideal interlaminar bond

strong bond area, or be arrested if the discontinuity area "catches" the crack tip (as crack *2* in Fig. 6.23), or, finally, it may delaminate the interface if the stress at the tip of the surface crack-discontinuity, that has fallen into the field of fatigue crack, proves to be sufficient for this. If the first version takes place, the crack will penetrate the next layer; if the second one, then crack *2* will begin to propagate at another flaw corresponding to $\Delta K = \Delta K_2$; in the third case delamination occurs.

An attempt at numerical simulation according to the above model demonstrated the possibility of comparing the model with physical experiment on a qualitative basis; the relevant data are presented in [13].

6.6.2 Fibrous Composites—Experimental Fundamentals

We shall discuss the main results of an experiment performed to elucidate the features of composite fatigue failure that could be a basis for a micromechanical model to be used in computer simulation [36]. This work contains a detailed description of exper-

iments as well as results obtained. Here we shall restrict ourselves to the only illustration, Fig. 6.24. In a composite with a small fiber volume fraction the fatigue process is influenced by crack propagation in the matrix. The fast growth of fatigue strength is observed at small fiber volume fraction in a composite having a foiled matrix (Fig. 6.24), this resulting from fatigue crack arrest by weak interfaces within the matrix volume. The fiber type (brittle or ductile) is here of no significance. The parameters of fiber strength are also

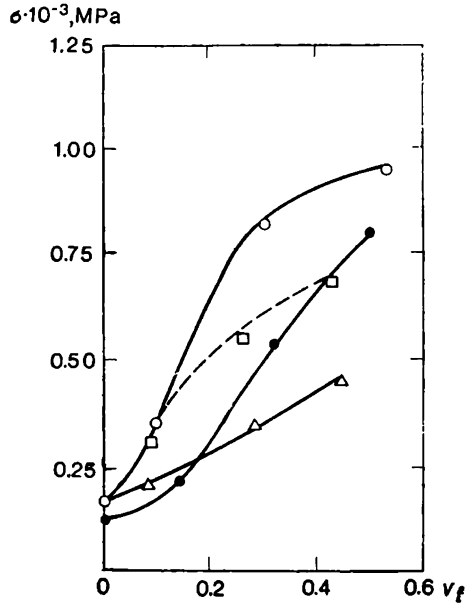

Fig. 6.24 Dependence of average composite fatigue bending strength on fiber volume fraction. Specimens have been tested up to $N = 10^6$; the fracture criterion at fixed amplitude of the free end of cantilever specimen is the drop in natural frequency by 5%. The largest stress in specimen at the first cycle is plotted on the ordinate. ○ and □ for two batches of boron-aluminium composite with a foiled matrix differing in boron fiber quality; ●, boron-aluminium composite with a plasma-sprayed matrix; △, steel-aluminium composites

of no importance (two batches of the boron-aluminium composite in Fig. 6.24). The fiber elastic modulus is of most importance since the value of the ratio of elastic moduli of the components determines stress values in the matrix.

At large fiber volume fraction fiber breaking plays the decisive role. The brittle fiber breaks at a certain point, which may be of the "fatigue" or "instant" type and may initiate a chain breaking process in the vicinity of its own plane as a result of stress redistribution between the fibers and the matrix. Under favourable conditions the

process might be delayed, for example, after the first break. In the case of ductile fibers the crack intersects both the matrix and fibers approximately in the same cross-section; as a rule, multiple cracking takes place here.

6.6.3 Fibrous Composites—a Calculational Model

Consider the case of cantilever composite beam oscillations. Let us divide the beam into plane elements (Fig. 6.25) and

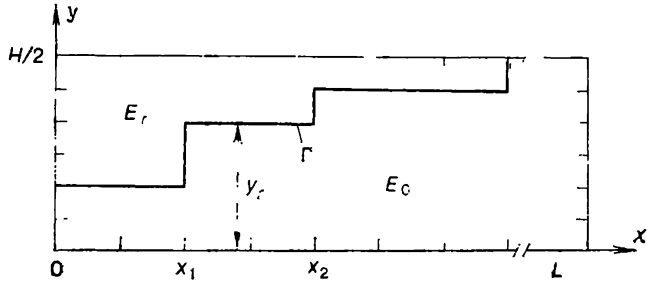

Fig. 6.25 Cantilever beam with fatigue damage zones

choose the height of each element to be equal to the layer thickness, and the length to be such a maximum possible magnitude so that only a single crack can possibly be initiated within an element. The following types of crack damages in the element are possible

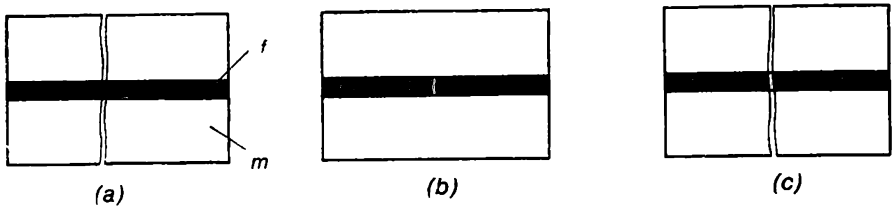

Fig. 6.26 Fatigue damage modes of a composite element

(Fig. 6.26): matrix cracking (case *a*), fiber break (case *b*), whole element rupture (case *c*). The effective Young's modulus in an initial state of an element is

$$E_0 = E_f v_f + E_m v_m$$

and in a state related to fatigue by one of the above types:

$$E_r = \alpha_f E_f v_f + \alpha_m E_m v_m$$

where $\alpha_f = 1$, $\alpha_m = 1/2$ if the matrix fails, $\alpha_f = 1/2$, $\alpha_m = 1$ if the fiber fails, $\alpha_f = \alpha_m = 1/2$ if the crack intersects a whole element.

Let us introduce the damage measure ω of an element ij (i is the layer number, j is the column number) such as in an initial state $\omega = 0$, and in a broken state $\omega = \omega_r^* = (E_0 - E_r)/E_0$, i.e.

$$\omega_1^* = \frac{1+\varkappa/2}{1+\varkappa},$$

$$\omega_2^* = \frac{1/2+\varkappa}{1+\varkappa},$$

$$\omega_3^* = 1/2$$

Here $\varkappa = E_m v_m / E_f v_f$ for the fracture of matrix, fibers and structure element as a whole, respectively.

Assume the transition of an element from the initial state into the broken one to proceed in a stepwise manner, either through the nucleation of an internal crack, or crack growth from an adjacent (in the given column) element into the element considered.

The kinetics of cracks nucleation is described by the damage accumulation equation:

$$d\omega/dN = \mu_n (\sigma/\sigma_n)^n \qquad (20)$$

where μ_n, σ_n, and n are phenomenological constants, σ is the stress amplitude, N is the cycle number.

The kinetics of crack growth is described by an equation of Paris's type:

$$dl/dN = \mu_m (\Delta K/\Delta K_m)^m \qquad (21)$$

where m, ΔK_m, μ_m are constants, ΔK is an amplitude of stress intensity factor.

At any arbitrary instant (or after any number of cycles) there is, in the beam longitudinal cross-section (Fig. 6.25), contour Γ separating a region with the initial modulus E_0 from a damaged region with the modulus E_r. The beam has the rigidity EI, which can be changed in a stepwise manner along axis x. The equation of the beam oscillations on each interval of a constant rigidity will as usual be

$$EI \frac{\partial^4 v}{\partial x^4} + \mu \frac{\partial^2 v}{\partial t^2} = 0$$

where

$$EI = E_0 I_0 [1 - \omega_r^* (1 - \xi^3)]$$

$\xi = y_r/H$, μ is the beam mass per unit length, I_0 is the beam moment of inertia.

The boundary conditions are at $x = 0$: $v = v' = 0$; at $x = x_1, x_2, \ldots, x_n$: $v_+ = v_-$, $v'_+ = v'_-$, $Q_+ = Q_-$, $M_+ = M_-$; at $x = L$: $v'' = v''' = 0$.

The method of calculation is as follows. At the first stage a value of the initial natural frequency of the beam and a distribution of stresses over the elements are to be determined (any point of the element can be taken as the reference point). Then it is necessary to find the number of cycles ΔN_1 to fracture of the most heavily loaded element, i.e. to accumulation of the magnitude ω_r^* in the element (a particular damage mechanism should be accepted which can be corrected afterwards). The next step is the determination of the

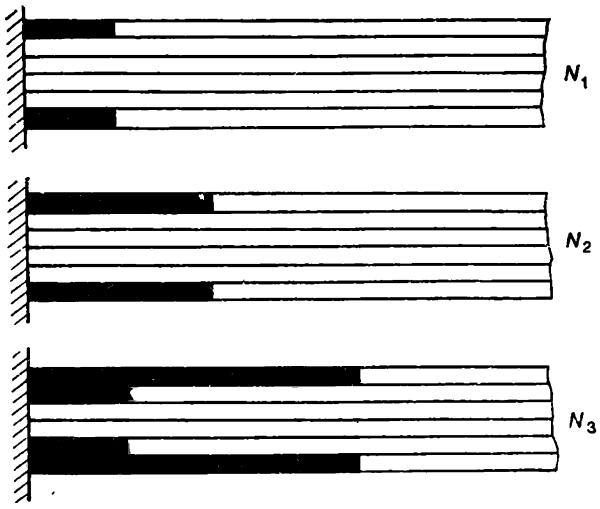

Fig. 6.27 Growth of damage zones in model composite during fatigue fracture ($\omega_r^* = \omega_1^*$, $n = 0.5$)

damage increment in all the elements (or in a particular part of them). Then one finds a new value of the natural frequency of the beam.

The next stage is also of principal importance. Let us introduce a probability s of the crack passing into an adjacent element. If as a result of computer realization of the proper stochastic process the crack propagates into the adjacent element, then at the next step it is necessary to compare the number of cycles to fracture of an element according to Eq. (21) with that to fracture of an element through damage accumulation according to Eq. (20). The quantity ΔN_2 is controlled by the minimum number of cycles to fracture of an element.

The procedure is then repeated. After a specimen fracture condition is satisfied (e.g. a given drop in the natural frequency is achieved) the calculation of the dependence f/f_0 on N terminates and the value of N^* is recorded.

The final step of the calculation is the determination of the parameters σ_n, n, ΔK_m, m, s, comparing the results of simulation and experiment. As an example the results of the calculation are given

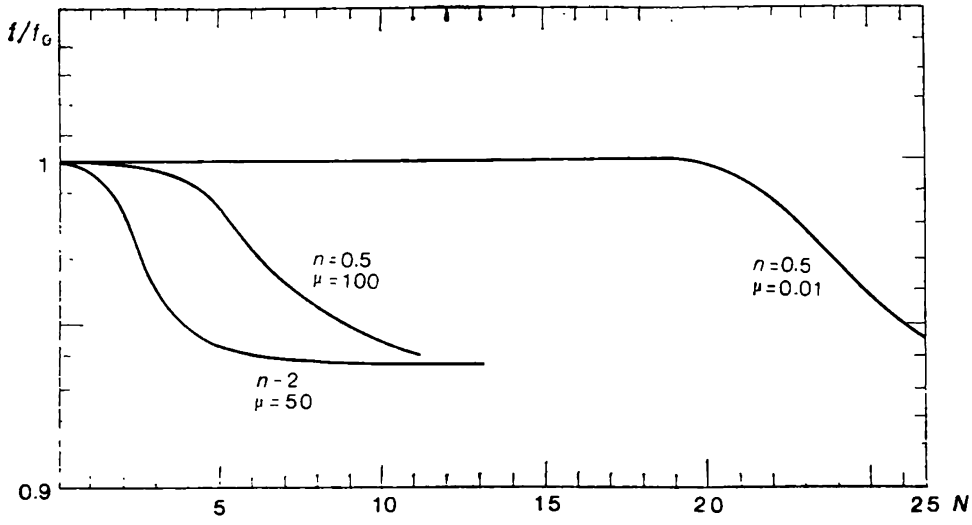

Fig. 6.28 Decrease in natural frequency of model composite with the number of loading cycles

in Figs. 6.27 and 6.28 (at $s = 0$) for the boron-aluminium composite with a small fiber volume fraction which fails because of the matrix cracking. A picture of the damage zone development is shown in Fig. 6.27 and the typical dependences f/f_0 on N at different values of n and μ can be seen in Fig. 6.28.

References

1. Mileiko, S.T., and Rabotnov, Yu.N., *Uspekhi mekh.*, **3** (1), 3-55 (1980).
2. Kiiko, V.M., and Spiridonov, L.S., *Mekh. kompozit. materialov*, **4**, 615-619 (1981).
3. Rabotnov, Yu.N., *Mechanics of Deformable Solids*, Nauka, Moscow, 1979 (in Russian).
4. Rabotnov, Yu.N., in: *Problems of Hydrodynamics and Mechanics of Continua* Nauka, Moscow, 1969, pp. 411-416 (in Russian).
5. Adams, D.F., in: *Composite Materials*, vol. 2, *Mechanics of Composite Materials* (G.P. Sendeckyj, ed.), Academic Press, New York and London, 1974 pp. 86-168.
6. Dymkov, I.A., in: *The V All-Union Conference on Composite Materials Paper Abstracts*, Izd. MGU, Moscow, 1981 (in Russian).
7. Mileiko, S.T., in: *Mechanics of Deformable Bodies and Structures*, Mashinostroyenie, Moscow, 1975, pp. 294-297 (in Russian).
8. Mileiko, S.T., *J. Mater. Sci.*, **4**, 974-977 (1969).
9. Ochiai Sh., and Murakami, Y., *J. Mater. Sci.*, **15**, 1798-1803 (1980).

10. Igata, N., Kohiyama, A., and Hata, S., in: *Composite Materials* (E.M. Sokolovskaya, ed.), Moscow University Press, Moscow, 1979.
11. Archangelskaya, I.N., and Mileiko, S.T., *J. Mater. Sci.*, **11**, 356-362 (1976).
12. Gerberich, W.W., *J. Mater. Sci.*, **5**, 283-294 (1970).
13. Mileiko, S.T., in: *Fracture of Composite Materials* (G. Sih, V. Tamuzs, eds.), Sijthoff and Noordhoff, Alphen aan den Rijn, The Netherlands, 1979, pp. 3-12.
14. Mileiko, S.T., Sorokin N.M., and Zirlin, A.M., *Mech. polimerov*, 5, 840-842 (1973).
15. Mileiko, S.T., Sorokin, N.M., and Zirlin, A.M., in: *Proc. ICCM-1*, vol. 1, AIME Publ., New York, 1976, pp. 562-575.
16. Mileiko, S.T., and Kaz'min, V.I., *Mech. komposit. materialov*, **4**, 723-726 (1979).
17. Kop'ev, I.M., and Ovchinskii, A.S., *Fracture of Fiber-Reinforced Metals*, Nauka, Moscow, 1978 (in Russian).
18. Kelly, A., *Strong Solids*, Clarendon Press, Oxford, 1973.
19. Mileiko, S.T., Sorokin, N.M., and Zirlin, A.M., *Mech. polimerov*, 6, 1010-1017 (1976).
20. Mileiko, S.T., and Suleimanov, F.Kh., *Mech. komposit. materialov*, **3**, 421-425 (1981).
21. Whitney, J.M., and Nuismer, R.J., *J. Compos. Mater.*, **8**, 253-265 (1974).
22. Mileiko, S.T., Khokhlov, V.K., and Suleimanov, F.Kh. *Mech. komposit. materialov*, **2**, 358-362 (1981).
23. Lekhnitski, S.G., *Theory of Elasticity of an Anisotropic Body*, Mir Publishers, Moscow, 1981.
24. Averbuch, J., and Hahn, H.T., *J. Compos. Mater.*, **13**, 82-107 (1979).
25. Broockman, E.C., and Sierakowski, R.L., *Fibre Sci. and Technology*, **12**, 1-10 (1979).
26. Mileiko, S.T., Sorokin, N.M., Arkhangelskaya, I.N., and Zirlin, A.M., *Matériau composite à matrice métallique*, Brevet d'invention de République Francaise N° 7802689, N° de publication: 2 416 270, 25-7-1980.
27. Rosen, B.W., in: *Fiber Composite Materials*, American Society for Metals, 1965.
28. Chang, W.-Yi., and Testa, R.B., *J. Compos. Mater.*, **3**, 58-80 (1969).
29. Mileiko, S.T., and Khvostunkov, A.A., *Zhurn. prikl. mech. i techn. fiz.* **4**, 155-160 (1971).
30. Mileiko, S.T., and Khvostunkov, A.A., *Kovové materiály*, **12**, 205-214 (1974).
31. Mileiko, S.T., Sorokin., N.M., and Zirlin, A.M., *Probl. prochn.*, **11**, 45-48 (1974).
32. Mileiko, S.T., *J. Mater. Sci.*, **5**, 254-261 (1970).
33. Mileiko, S.T., *Probl. prochn.* **7**, 3-10 (1971).
34. Hancock, J.R., in: *Composite Materials*, vol. 5, *Fracture and Fatigue* (L.J. Broutman, ed.), Academic Press, New York and London, 1974.
35. Anishchenkov, V.M., and Mileiko, S.T., *Doklady Akad. Nauk. SSSR*, **241**, (5), 1068-1069 (1978).
36. Mileiko, S.T., and Anishchenkov, A.M., *Mech. kompozit. materialov*, **3**, 409-417 (1980).

7 Deformation and Failure of Fibrous Composites with Brittle Polymeric Matrix under Plane Stress

N. A. Alfutov, *D. Sc. (Eng.)*,
P. A. Zinov'ev, *Cand. Sc. (Eng.)*

7.1 INTRODUCTION. MAIN APPROACHES TO DESCRIPTION OF THE BEHAVIOUR OF MULTILAYER COMPOSITES

There are many publications on the behaviour of multilayer composites. Conventionally the analysis of the stress-strain state for these materials has been carried out using the linear theory of elasticity of an anisotropic body [1], while one of the phenomenological criteria has been used for the determination of their bearing strength [2-5]. In recent years there has been an increase in the number of works (several of them will be cited below) in which the effects of the behaviour of multilayer composites have been found experimentally, namely the effects not described within the framework of the conventional approach. Above all they include nonlinearity of stress-strain curves, qualitative alteration of the curve character and the failure mode with changing material structure and type of stressed state, different behaviour of material in tension and compression as well as under the first and subsequent loadings. It has been established that in polymeric-matrix composites these phenomena are caused by the processes of matrix cracking, nonlinearity of matrix stress-strain curves, and by changes in the structural parameters of the material under strain (i.e. by the effects of geometric nonlinearity on the structural level—"structural nonlinearity"). A rigorous description of the above-mentioned phenomena is a very difficult problem. Nevertheless, a number of useful results have been obtained with the application of approximate phenomenological models, successfully describing some manifestations of these effects. While not claiming exhaustiveness or a strict adherence to chronological order we shall mention some papers representative of this trend.

The basis of the existing models of the behaviour of multilayer laminates is the model of the behaviour of a unidirectional laminate. One of the simplest approaches is as follows. Experimental curves are determined for tension of the unidirectional material along fibers, normally to them, and for in-plane shear. The curves are approximated in one way or another and then used as the starting data for the computer program, simulating step by step loading of a multilayer composite.

At each step of loading in accordance with the current stress-strain state of each layer the corresponding values of rigidity characteristics are taken from the stress-strain curves [6-9]. The basis of this method is the assumption that strains in tension-compression along fibers, normally to fibers and in shear are mutually independent. This assumption becomes particularly problematical when stresses reach their ultimate values on at least one of the stress-strain curves. Another difficulty with this approach is that the behaviour of a unidirectional laminate incorporated in the multilayer composite differs from that of an isolated sample layer tested for the determination of the required curves. Thus, the initiation of the very first main crack in an isolated layer causes its fracture, while in a layer of the multilayer composite this instant marks only the beginning of crack formation in the layer [10]. The duration of this process along the axis of strain can substantially exceed the ultimate strain of an isolated layer. Therefore when the ultimate stresses are reached on the curve, following the initial segment of the curve, the latter being thoroughly established by experiment and accurately approximated numerically, a fictitious segment of the curve with a negative value of tangent modulus must be added [6, 8, 9].

The results of the time-consuming operations of recording and approximating the real stress-strain curve on the first segment can come to nothing because of an arbitrary choice of the value of the negative tangent modulus on the second segment. In [11-14] nonlinear effects (above all in shear) are considered by means of the introduction of some additional terms into the physical stress-strain relations in analytical form.

Another approach to the simulation of crack formation in multilayer composites was developed somewhat earlier [15, 16]. It is considered that before an isolated unidirectional layer reaches its ultimate stresses it may be assumed as linear-elastic. The available experimental data show that this assumption is in accord with the behaviour of present-day polymeric matrix composites. The onset of the layer limit state is determined using one of the phenomenological strength criteria [15-19]. If longitudinal stress (along fibers) has not reached the layer ultimate longitudinal strength then the matrix is considered to have failed. It is shown in [20] that following the emergence of a first system of cracks, crack formation in the layer matrix does not stop. With further loading, stresses in the layer are close to the level corresponding to the beginning of crack formation. At this stage the tangent moduli of the layer elasticity E_2 (in the direction normal to the fibers) and G_{12} (shear modulus) have zero values. It is considered, as opposed to the works of the first trend, that the beginning of crack formation irrespective of its cause changes the stress-strain behaviour both in shear and in the direction normal to fibers. Zero values of the moduli E_2 and G_{12} result in a

singular stress-strain matrix for multilayer composites. Hence, in some works [18, 19] these moduli assume small arbitrary positive values. The computational procedure is then simplified, but some composites (primarily angle-ply laminates) acquire an unreal possibility of being infinitely strained.

K. Kawata [21] was apparently the first to pay attention to the fact that a change in the modulus E_2 must be related to the sign of stress σ_2 acting across the fibers. If σ_2 is negative (the layer is transversely compressed) then at initiation of cracks caused by shear stress there is no reason for the value of E_2 to change.

A more general model (taking into account K. Kawata's suggestion in particular) was developed in [22]. Its main points are described in Section 7.2 of this paper.

In constructing current strain models, both the available results of the structural theory and merely heuristic ideas on the behaviour of composites can be considered. However, it is experimental data that are the basis for their improvement. The results of experimental studies are dealt with to a greater or lesser extent in a large number of well-known papers. Here, in the main, we will mention those papers in which the structure of materials, the type of loading and the equipment used permitted the stage of nonlinear deformation of composites also to be studied.

The results of tension tests on plane specimens of fiber glass or carbon plastics are given in [7, 9, 11, 12, 13, 15, 17, 23, 24]. It is known [25] that in testing such specimens "the effect of cut filaments" occurs which causes stress concentration on the free ends of the specimens. Hence, the results described in these papers (particularly concerning the strength of the studied structures) must be looked at with a certain caution. Experiments on tube specimens were carried out by the authors of [18, 21, 26-33]. In spite of a great many publications the volume and quality of information on strain behaviour and fracture of contemporary materials is obviously insufficient. The reason, probably, is that tests with tube specimens are very labour-intensive, expensive and time-consuming. Therefore, most of the papers referred to report the results of isolated experiments to investigate the behaviour of some occasionally available structures of the materials under study, usually only breaking loads being recorded. Only some papers [27, 29, 31, 33] give strain curves obtained in tests with tube specimens. In many publications we do not find a complete set of initial data required for an analysis of the experimental results. Therefore the results of a series of experiments on biaxial tension of fiber-glass plastic tube specimens of eight different structures are presented in Section 7.3 of this paper. A parallel analysis of experimental and theoretical data is also given.

7.2 FAILURE MODEL OF MULTILAYER COMPOSITES

7.2.1 Accepted Strength Criterion of a Layer

A unidirectional layer is considered to be linearly elastic up to failure. Its strains ε_1, ε_2, γ_{12} can be determined if we know stresses σ_1, σ_2, τ_{12} applied to the layer and layer stiffness characteristics E_1, E_2, G_{12}, ν_{12}. Directions 1 and 2 are for the axes of Cartesian coordinates in the layer plane, axis 1 being directed along fibers.

In some papers it was noted that stress-strain curves of a unidirectional material (in particular, in shear) could not be completely linear. The real stress-strain curves can be taken into account in computational algorithms, but, as correctly pointed out by the authors of [13], in many cases the results of taking into account nonlinearity do not justify the effort expended.

A layer remains elastic when the following conditions are fulfilled

$$F_{-1} \leqslant \sigma_1 \leqslant F_{+1}, \quad F_{-2} \leqslant \sigma_2 \leqslant F_{+2}, \quad | \tau_{12} | \leqslant F_{12} \cdot \tag{1}$$

Here F_{+1}, F_{+2} are the ultimate strengths along fibers and transverse to them, respectively; F_{-1}, F_{-2} are similar characteristics in compression, F_{12} is ultimate in-plane shear strength.

Conditions (1) determine an ultimate surface in the shape of a rectangular parallelepiped in the coordinates σ_1, σ_2, τ_{12}. When an isolated layer reaches any of the mentioned ultimate strengths, it means that the bearing strength is completely exhausted. We consider that conditions (1), in addition to their obvious simplicity, have a number of appreciable advantages in comparison with many possible alternative strength criteria, namely:

—accuracy of approximation of the experimental data known to the authors even in the worst case is not inferior to that reached when other criteria are used;

—the criterion clearly indicates the cause of bearing strength exhaustion, which is convenient for constructing models of the layer behaviour following the first fracture;

—many studies have determined that fracture mechanisms of a unidirectional layer with different natures (rupture of fibers, matrix fracture, break of matrix-fiber adhesion bond, buckling of fibers, etc.) can take place; under these conditions the representation of the strength surface even in the shape of a simple rectangular parallelepiped is more physically convincing than its approximation by a smooth surface [34].

7.2.2 Layer Behaviour in Multilayer Composites

If a unidirectional laminate is part of a multilayer composite, then with the onset of ultimate stresses F_{+2} and/or F_{12} only the beginning of crack formation in the polymeric matrix can be indicated, not resulting in the exhaustion of bearing strength of the whole multilayer composite containing differently oriented unidirectional layers. Thus, in addition to the two natural states of a unidirectional composite—the initial (monolithic composite) and the final (failed composite)—there is a group of intermediate states, the composite with cracks in the polymeric matrix.

In its turn in this group we can distinguish a group of composite states involving open cracks (faces of cracks are separated) and a group involving closed cracks (faces of cracks are joined). It is believed that the transition from one group of states to another is determined by the sign of stress σ_2. When σ_2 is positive cracks are open, when it is negative (compression) they are closed. According to the model, four composite states differing in the combination of signs of

Table 7.1. Stiffnesses of Unidirectional Layer in Multilayer Composite

Monolithic composite	Nonmonolithic composite						Complete failure of composite $\sigma_1 = F_{+1}$ or $\sigma_1 = F_{-1}$ and/or $\sigma_2 = F_{-2}$
	open cracks $\sigma_2 > 0$				closed cracks $\sigma_2 < 0$		
	$\bar{\varepsilon}_2 < \bar{\varepsilon}_2^*$	$\bar{\varepsilon}_2 = \bar{\varepsilon}_2^*$, $\Delta\bar{\varepsilon}_2 < 0$		$\bar{\varepsilon}_2 < \bar{\varepsilon}_2^*$			
	$\lvert\gamma_{12}\rvert < \lvert\gamma_{12}^*\rvert$	$\lvert\gamma_{12}\rvert = \lvert\gamma_{12}^*\rvert$, $\lvert\Delta\gamma_{12}\rvert > 0$				$\lvert\gamma_{12}\rvert < \lvert\gamma_{12}^*\rvert$	
E_1	E_1	E_1	E_1	E_1	E_1	E_1	0
E_2	$\tilde{E}_2$	0	0	$\tilde{E}_2$	E_2	E_2	0
G_{12}	$\tilde{G}_{12}$	$\tilde{G}_{12}$	0	0	0	$\tilde{G}_{12}$	0
ν_{12}	ν_{12}	ν_{12}	ν_{12}	ν_{12}	ν_{12}	ν_{12}	0

the strain increments $\Delta\varepsilon_2$ and $\Delta\gamma_{12}$ are distinguished in the "open-crack" group while in the "closed-crack" group there are two states differing in the sign of the shear strain increments $\Delta\gamma_{12}$.

Thus, depending on the sign of the stresses σ_2 the values of the strains ε_2 and γ_{12} and the sign of their increments, the column matrix of layer-stiffness characteristics takes on one of possible eight values given in Table 7.1. There $\bar{\varepsilon}_2 = \varepsilon_2 + \nu_{12}\varepsilon_1$, and the asterisk means the maximum value of the parameter during the whole history of loading.

The layer-stress-strain curves for the described model, transverse to fiber and in shear, are represented in Fig. 7.1.

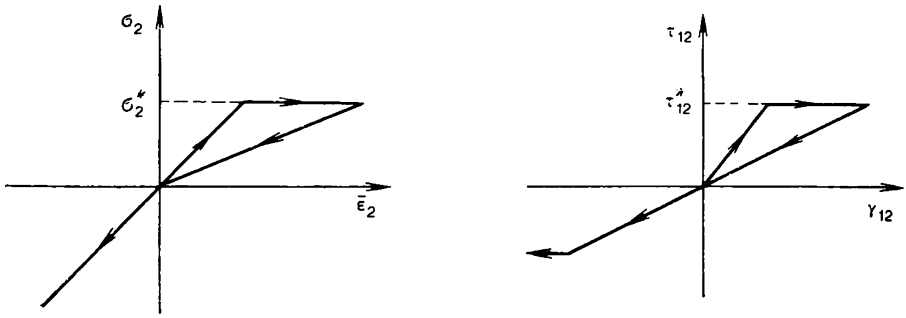

Fig. 7.1 Behaviour of unidirectional layer in multilayer composite (a model)

Unloading is considered to proceed without residual strain. The elastic moduli at the unloading stage are

$$\tilde{E}_2 = \frac{\sigma_2^*}{\varepsilon_2^* - \nu_{12}^2 \sigma_2^* / E_1} \tag{2}$$

$$\tilde{G}_{12} = \left| \frac{\tau_{12}^*}{\gamma_{12}^*} \right| \tag{3}$$

σ_2^* and τ_{12}^* correspond to the stress level at which the process of matrix fracture starts. They can have the following values

$$\sigma_2^* \leqslant F_{+2} \quad \text{when} \quad |\tau_{12}^*| = F_{12} \tag{4}$$

$$|\tau_{12}^*| \leqslant F_{12} \quad \text{when} \quad \sigma_2^* = F_{+2} \tag{5}$$

If the conditions $\sigma_1 = F_{+1}$ or $\sigma_1 = F_{-1}$ and/or $\sigma_2 = F_{-2}$ are fulfilled in at least one layer, it is considered to be sufficient for complete failure of the multilayer composite. As experiments have shown, this is true at least for composites with a small number (2 to 3) of groups with differently oriented layers.

Note also that the mentioned composite states may be considered as unrelated to structural ideas on the development of cracks formation if the curves in Fig. 7.1 are considered a phenomenological model of deformation.

7.3 RESULTS OF EXPERIMENTAL STUDIES

Figure 7.2 schematically shows a typical stress-strain curve for an angle-ply composite under loading, unloading and repeated loading. The main purpose of the experiments was to study,

depending on the composite's structure and mode of stress-strain state, the following:
—stiffness characteristics on the initial linear segment of the stress-strain curve (denoted by *1* in Fig. 7.2);

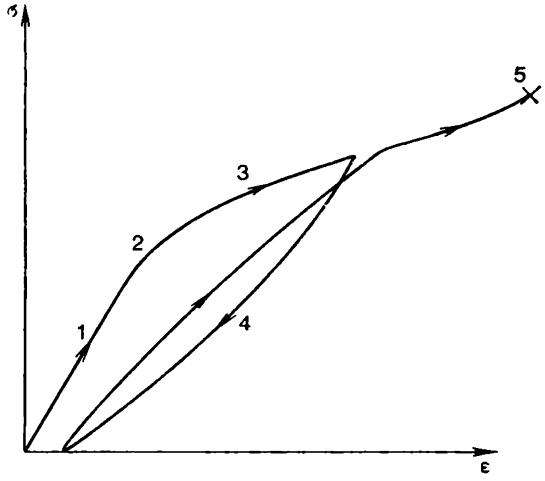

Fig. 7.2 Hypothetical stress-strain curve of multilayer composite

—conditions of the appearance of "the first ply failure"—the kink on the curve (*2*);
—composite stiffness following the initial loading (*3*);
—behaviour under unloading and repeated loading (*4*);
—conditions of complete exhaustion of composite bearing strength (*5*).

7.3.1 Experimental Technique

It is expedient to carry out tests of multilayer polymeric composites using cylindrical (tube) specimens. Specimens of this shape permit a given mode of plane stress state to be obtained owing to the combination of internal (or external) pressure, axial tension (or compression) force and torsional moment. In addition, use of tube specimens eliminates the effect of cut filaments. In this paper only data on biaxial tension are given.

Studies were carried out with fiber-glass plastic, which is a typical and wide-spread polymeric composite. The specimen inner diameter was 72 mm and the wall thickness was 0.67 or 1.0 mm, consisting of two or three pairs of layers of an angle-ply composite. The length of the working portion of the specimen must be sufficient for the edge effect, occurring near testing machine clamps, not to spread to the region of measurements. Preliminary calculations [35] performed by the method of finite elements [36] have shown that at a chosen

diameter-to-thickness ratio with the length of the working portion being 200 m, uniform momentless stressed state is provided in the specimen middle portion 60 mm long—the region of measurement.

Specimens were prepared by the method of "wet" helical winding of a tape of glass filaments, moistened with epoxy resin. Specimen pressurizing was provided by a rubberized fabric. Special measures were taken to ensure stability of the processing parameters at all stages of specimen preparation.

A wide set of angle-ply laminates involving such lay-up angles as $[\pm 30°]$, $[\pm 45°]$, $[\pm 50°]$, $[\pm 55°]$, $[\pm 60°]$, $[\pm 75°]$ were studied experimentally. In addition, $[+30°/-30°/90°]$ and $[0°/90°_2]$ specimens were tested.

A special testing unit provided specimen tests at five versions of the ratio between circumferential σ_y and axial σ_x stresses $\sigma_y/\sigma_x =$ $= 1/0$, $2/1$, $1/1$, $1/2$ and $0/1$. Thus, altogether 40 types of tests were carried out differing in the composite lay-up and/or in the stressed state. In each case not less than three (and frequently five or more) specimens were tested. The results given below were obtained by averaging the available data. Some tests, for example testing the $[\pm 30°]$ specimen at $\sigma_y/\sigma_x = 2/1$ and the $[\pm 60°]$ specimen at $\sigma_y/\sigma_x =$ $= 1/2$, were formally of the same type and they were used for cross checking the results.

Strains in tests were measured by special strain gauges with a working range of 10 per cent. Axial strains were measured with a gauge length 60 mm, while circumferential strains were calculated from the measured values of the specimen perimeter change.

7.3.2 Uniaxial Tension

Two types of composite tests on uniaxial tension were conducted: tension in the circumferential direction ($\sigma_y/\sigma_x = 1/0$) and axial tension ($\sigma_y/\sigma_x = 0/1$). Depending on the reinforcement angle three versions of exhaustion of composite bearing strength are possible, which are well identified in the graph of ultimate stresses given in Fig. 7.3. Each version has its own form of the stress-strain curve.

With a change in the angle φ within 0 to 20° composite fracture is caused by rupture of fibers. When the angles φ are smaller than about 4°, the stress-strain curve is linear up to fracture. This conclusion follows from a theoretical analysis and has not been verified experimentally. According to calculations, in circumferential tension of specimens with reinforcement angles of $\pm 75°$ (corresponding to the angle $\varphi = 15°$ in Fig. 7.3), when $\sigma_y = 520$ N/mm^2 the process of crack formation starts in the matrix, since shear stresses τ_{12} reach their ultimate value $\tau_{12} = F_{12}$. The modulus G_{12} becomes zero and E_2 remains constant since $\sigma_2 < 0$ and a kink is observed on the curve

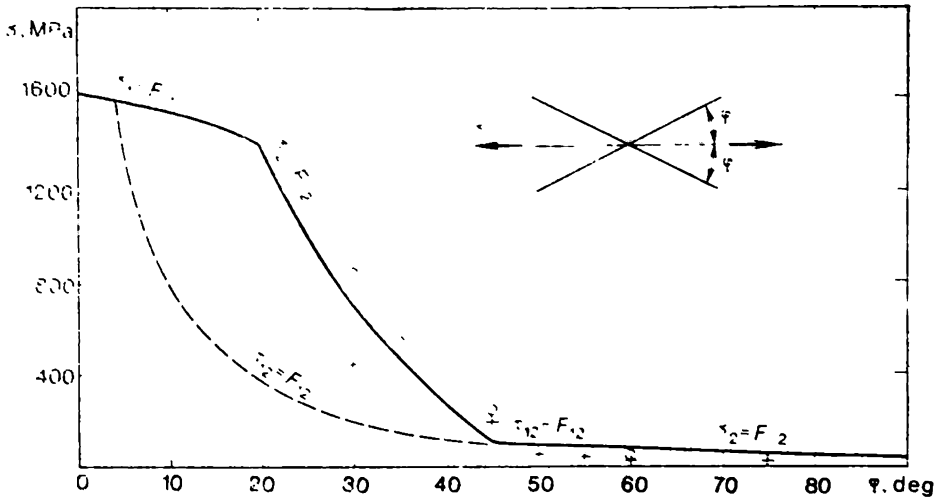

Fig. 7.3 Bearing strength of fiber-glass plastic versus reinforcement angle in uniaxial tension. Experimental data (average values) are plotted by the circles (circumferential tension) and by the crosses (axial tension); calculated data are shown by the solid curve (ultimate strength) and by the dashed curve (loss of integrity—the first ply failure)

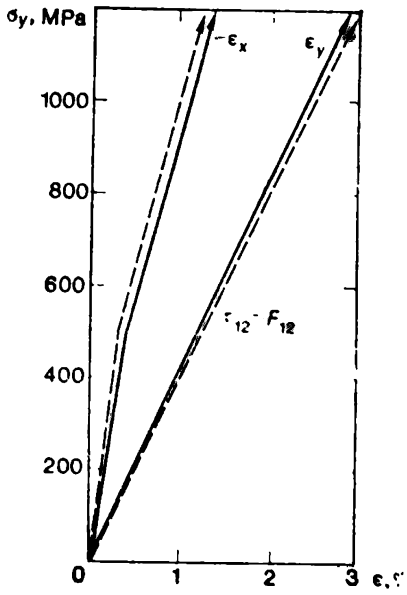

Fig. 7.4 Stress-strain curves for fiber-glass plastic with reinforcement angles $\pm 75^\circ$ ($\sigma_y/\sigma_x = 1/0$): experiment (solid lines) and calculation (dashed lines)

(see Fig. 7.4). Stress-strain curves of this type are characteristic of composites with reinforcement angles $4° < \varphi < 20°$. Arrows in Fig. 7.4 and in the following figures indicate that only a part of the stress-strain curve is given. The value of cracking load can be

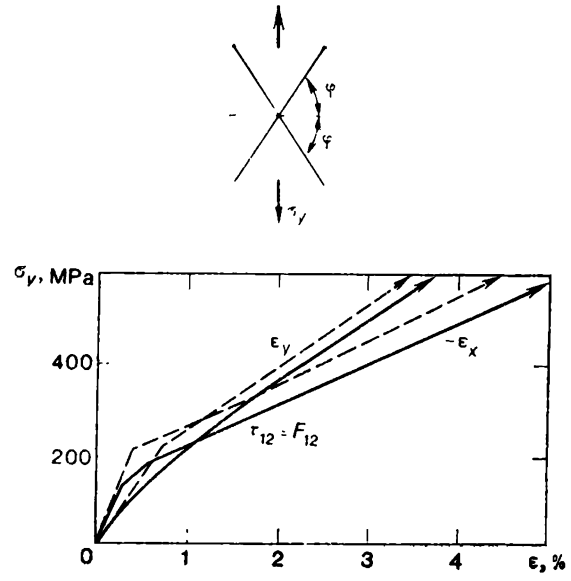

Fig. 7.5 Stress-strain curves for fiber-glass plastic with reinforcement angles $\pm 60°$ ($\sigma_y/\sigma_x = 1/0$): experiment (solid lines) and calculation (dashed lines)

determined from the graph of ultimate stresses in Fig. 7.3 and in similar figures which follow.

In the angle range $20° < \varphi < 45°$ the process of composite bearing strength exhaustion proceeds in two stages:

—at $\tau_{12} = F_{12}$ the composite loses its integrity and a change of its stiffness follows;

—composite failure is caused by compression of unidirectional layers in the direction perpendicular to reinforcement ($\sigma_2 = F_{-2}$).

Stress-strain curves typical of this angle range are represented in Figs. 7.5 and 7.6. They differ, first of all, by a marked nonlinearity. Tension in the circumferential direction of a specimen with the reinforcement angle of $\pm 60°$ ($\varphi = 30°$ in Fig. 7.3) features the effect of a sharp change in the ratio between annular and axial strains. If on the initial segment according to calculations the ratio $-\varepsilon_x/\varepsilon_y$ equals 0.67, as a result of crack formation in the matrix it reaches a value of 1.4 (Fig. 7.5). The theoretical model as a whole well describes the mentioned phenomenon. The greatest discrepancy between calculations and experiment is observed at kinks of the theoretical

curve. It is caused by a piecewise linear approximation of the stress-strain curves for a unidirectional laminate taken to construct the model.

Note an appreciable difference in the ultimate values of σ_y in circumferential tension of specimens with $\varphi = \pm 60^\circ$ and σ_x in axial tension of specimens with $\varphi = \pm 30^\circ$ (formally these tests are of the same type and correspond to $\varphi = 30^\circ$ in Fig. 7.3). In the second case delamination occurred beginning in the edge region of the specimen. The corresponding stress (shown in Fig. 7.3 by a cross for $\varphi = 30^\circ$) is ultimate for the specimen, but not for the composite.

Stress-strain curves of a composite with $\varphi = \pm 45^\circ$ resemble in appearance those of ductile metals (Fig. 7.6) and differ in principle

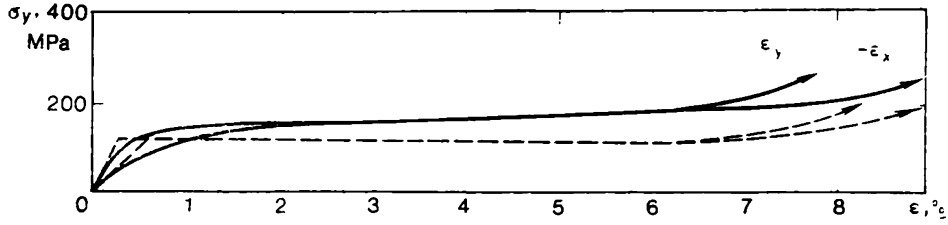

Fig. 7.6 Stress-strain curves for fiber-glass plastic with reinforcement angles $\pm 45^\circ$ (σ_y $\sigma_x = 1$ 0): experiment (solid lines) and calculation (dashed lines)

from a stress-strain curve, for example, for $\pm 75^\circ$ in circumferential tension (Fig. 7.4). The composite made up of layers whose ultimate strain does not exceed 2 to 3 percent is deformed without failure to the level of 8 to 9 percent. At the final stage of deformation an increase in composite stiffness (or tangent modulus) caused by a change of the reinforcement angles (i.e., "structural nonlinearity") is manifested

Results of uniaxial tension tests for structures in the range $5^\circ < \varphi < 45^\circ$ show that a simple attribution of zero values to stiffness of a layer G_{12} and E_2 can result in large calculation errors. In this case the ultimate loading of the composite corresponds to the dashed line in Fig. 7.3, while an unlimited "yield plateau" appears on the stress-strain curves, which would correspond to the level of about 220 MPa in Fig. 7.5.

Over the angle range $45^\circ < \varphi < 90^\circ$ loss of composite integrity results in its bearing strength exhaustion unrelated to specimen separation into different parts. In this range of structures, composites are also highly deformable. But, unlike the previous range when integrity is lost, no load increase is observed on experimental curves and in a number of cases (see, for example, Fig. 7.7) the load drops. Obviously this form of bearing strength exhaustion can be treated as a manifestation of the instability of deformation. According to the

model, axial tension of composites over the range of reinforcement angles $45° < \varphi < 90°$ after loss of integrity ($\sigma_2 > 0$, $E_2 = G_{12} = 0$) takes place under permanent load, which is also considered to be ultimate.

The described data are qualitatively in good agreement with results obtained on uniaxial tensile flat specimens of fiber-glass plastic

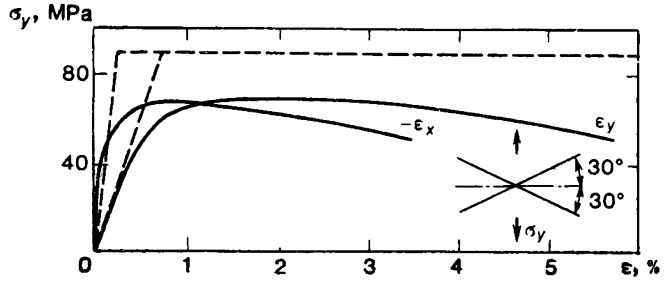

Fig. 7.7 Stress-strain curves for fiber-glass plastic with reinforcement angles $\pm 30°$ ($\sigma_y/\sigma_x = 1/0$): experiment (solid lines) and calculation (dashed lines)

[11, 37] and carbon plastic [24]. In the latter paper stress-strain curves under unloading and repeated loading are given. The authors' data on deformation under unloading of tube specimens (not given in this paper) are quantitatively also in good agreement with the results described in [24], and as a whole they satisfactorily confirm an assumption on the smallness of residual strains which underlies the theoretical model.

7.3.3 Biaxial Tension of Angle-Ply Composites

The structures under study were subjected to biaxial tension at $\sigma_y/\sigma_x = 2/1$, 1/1, 1/2. The ultimate stresses corresponding to tests at $\sigma_y/\sigma_x = 1/2$ are plotted in the graph of ultimate stresses for formally similar tests at $\sigma_y/\sigma_x = 2/1$. In Fig. 7.8 a real reinforcement angle is substituted for the complementary angle $90° - \varphi$. As a result for ultimate stresses of angle-ply structures at $\sigma_y/\sigma_x = 2/1$, characteristic of pressure vessels, in the range of reinforcement angles $30° < \varphi < 60°$ experimental data were obtained for φ with an interval of 5°.

Over the whole range of angles 0° to 90° loss of composite integrity is observed, but only in the range $45° < \varphi < 60°$ does it not result in the exhaustion of composite bearing strength.

To understand composite behaviour in biaxial tension the idea of the "equilibrium" angle of reinforcement is of great importance, when under the action of a given system of loads a uniform tension

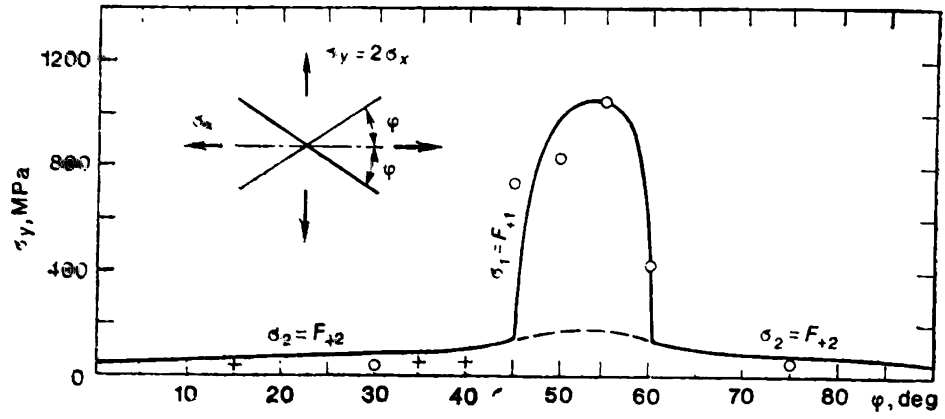

Fig. 7.8 Bearing strength of fiber-glass plastic versus reinforcement angle under biaxial loading. Experimental data (average values) are plotted by the circles (at $\sigma_y/\sigma_x = 2/1$) and by the crosses (at $\sigma_y/\sigma_x = 1/2$); calculated data are shown by the solid line (ultimate strength) and by the dashed line (loss of integrity)

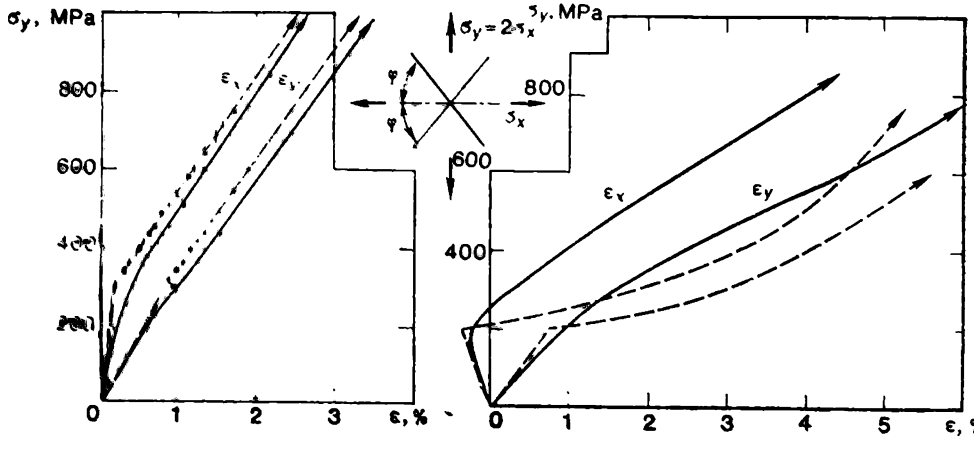

Fig. 7.9 Stress-strain curves for fiber-glass plastic with reinforcement angles $\pm 30°$ and $\sigma_y/\sigma_x = 2/1$: experiment (solid lines) and calculation (dashed lines)

Fig. 7.10 Stress-strain curves for fiber-glass plastic with reinforcement angles $\pm 30°$ and $\sigma_y/\sigma_x = 2/1$: experiment (solid lines) and calculation (dashed lines)

of composite ($\varepsilon_x = \varepsilon_y = \varepsilon_1 = \varepsilon_2$) takes place, while shear stresses τ_{12} are zeros [20]. For $\sigma_y/\sigma_x = 2/1$ the equilibrium angle is close to 55°. Theoretical and experimental stress-strain curves for the composite with such a structure (Fig. 7.9) have two characteristic segments: with the initial stiffness (at $\sigma_y < 200$ N/mm^2) and with a decreased stiffness (in calculations $\sigma_2 = F_{+2}$, $E_2 = 0$). The structure of the composite to some extent rearranges itself approaching the equilibrium one, and with further deformation increments of shear strains $\Delta\gamma_{12}$ proportional to a change of the difference $\varepsilon_y - \varepsilon_x$ are practically absent. Failure is followed by rupture of fibers and occurs under maximum stresses for this mode of tests.

Of substantially more complicated appearance is the stress-strain curve of a fiber-glass plastic with the reinforcement angles $\varphi = \pm 50°$, shown in Fig. 7.10 (the reinforcement angle in comparison with the previous example is changed by only 5°). Up to the level $\sigma_y \approx \approx 200$ MPa deformation is similar to that for $\varphi = \pm 55°$, but it sharply changes following the start of the matrix fracture process. The axial strain ε_x decreases and then changes its sign. The theoretical curves correctly describe the character of strain, but the condition of an instantaneous change of the tangent modulus G_{12} from the initial value to zero is found to be too rigorous in this case. The elastic modulus E_2, unlike the previous example, maintains its initial value in calculations, since immediately after the start of crack formation in the matrix (the reason is that $\sigma_2 = F_{+2}$) release of stresses σ_2 occurs and the "unloading" modulus $\widetilde{E}_2$ equals the initial E_2. Note that a reversal of the sign of increments of different components of strain and stress tensors (and even of the sign of the components proper) at a continuous load increase is characteristic of many cases of loading.

The loss of matrix continuity in the angle ranges $0° \leqslant \varphi < 45°$ and $60° < \varphi \leqslant 90°$ results in the exhaustion of specimen bearing strength. Typical stress-strain curves for composites of this group are given in Fig. 7.11.

For $\sigma_y/\sigma_x = 1/1$ the "equilibrium" angle of reinforcement is $\pm 45°$. The strains ε_x and ε_y are identical (Fig. 7.12). Loss of matrix continuity ($\sigma_2 = F_{+2}$) causes only a slight change in the tangent modulus on the theoretical stress-strain curve, the latter being close to the experimental one. Material failure is followed by rupture of fibers at $\sigma_y = \sigma_x \approx 800$ MPa.

Deviation from the equilibrium structure drastically changes the character of stress-strain curves. When $\varphi = \pm 50°$ (Fig. 7.13) the curves are substantially nonlinear. Following the first ply failure, circumferential strains reverse their signs. The theoretical curves have the same characteristic features as the experimental ones. Loading ends with rupture of fibers, both theory and experiment giving the same value of the breaking load $\sigma_y = \sigma_x \approx 680$ MPa (Fig. 7.14).

Specimens with reinforcement angles beyond the range $37° < \varphi < 53°$ lose their bearing strength without rupture of fibers. An example of such a curve is given in Fig. 7.15. The theoretical value of the ultimate load is somewhat smaller than the experimental one, but the theoretical model reflects correctly the deformation character and loss of bearing strength.

The stress-strain curves for a composite with a more complicated structure of reinforcement [30° —30°/90°] are much "smoother" (see Figs. 7.16 and 7.17). It is characteristic of materials reinforced in

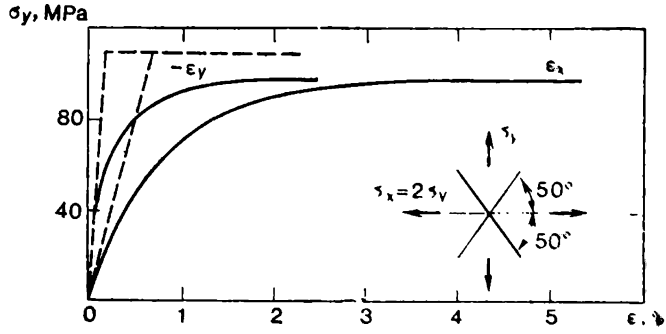

Fig. 7.11 Stress-strain curves for fiber-glass plastic with reinforcement angles $\pm 50°$ and $\sigma_y/\sigma_x = 1/2$: experiment (solid lines) and calculation (dashed lines)

three or more directions. The [30° —30° 90°] composite is quasi-isotropic in the elastic range. However, when the material behaviour is inelastic, no similarity of uniform-type strain curves in Figs. 7.16 and 7.17 is observed. No complete symmetry of the ultimate state envelopes with respect to the ray $\sigma_y = \sigma_x$ is observed either (see Fig. 7.18). The theoretical stress-strain curves and estimates of this composite bearing strength are in good agreement with experimental results. The same conclusion can be made for the results of the behaviour analysis of the $[0°/90°_3]$ composite (see Fig. 7.19).

Further information on the results of the series of experiments described in Section 7.3.1 can be found in [38]. For calculations the following initial data were taken: $E_1 = 46\,500$, $E_2 = 7000$, $G_{12} = 7000$ MPa, $\nu_{12} = 0.25$, $F_{+1} = 1600$, $F_{-1} = -500$, $F_{+2} = 40$, $F_{-2} = -200$, $F_{12} = 60$ MPa.

7.4 DISCUSSION AND CONCLUSIONS

The behaviour of multilayer composites made up of almost elastic unidirectional layers is frequently extremely complicated. Stress-strain curves of the composite can strongly alter their appearance depending on the composite structure and the

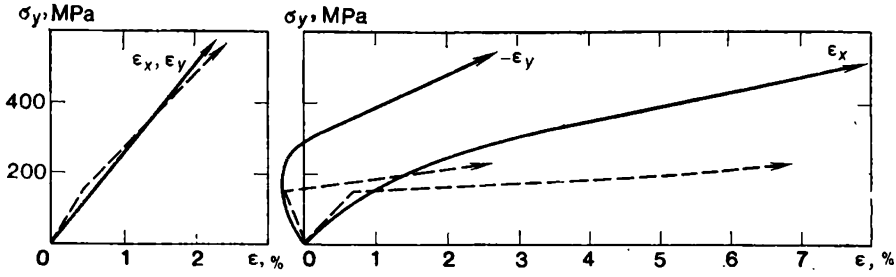

Fig. 7.12 Stress-strain curves for fiber-glass plastic with reinforcement angles $\pm 45°$ and $\sigma_y/\sigma_x = 1/1$: experiment (solid lines) and calculation (dashed lines)

Fig. 7.13 Stress-strain curves for fiber-glass plastic with reinforcement angles $\pm 50°$ and $\sigma_y/\sigma_x = 1/1$: experiment (solid lines) and calculation (dashed lines)

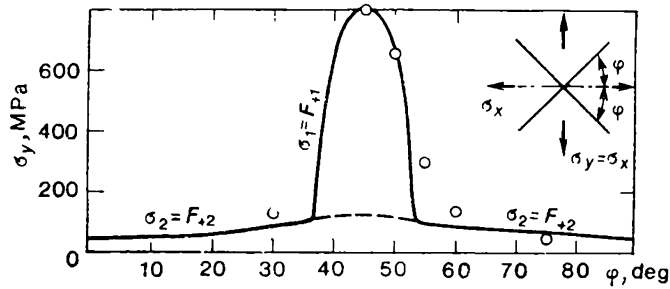

Fig. 7.14 Bearing strength of fiber-glass plastic versus reinforcement angle under biaxial loading $\sigma_y/\sigma_x = 1/1$. Experimental data (average values) are plotted by the circles; calculated data are shown by the solid line (ultimate strength) and by the dashed line (loss of integrity)

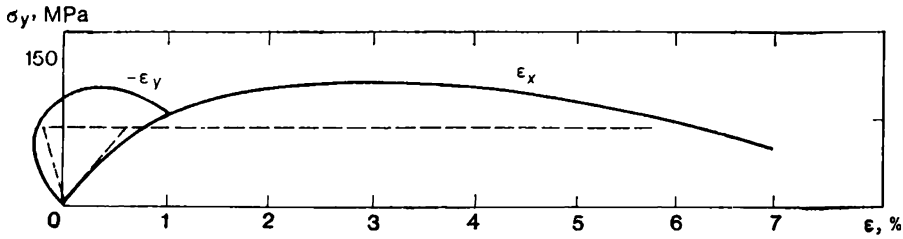

Fig. 7.15 Stress-strain curves for fiber-glass plastic with reinforcement angles $\pm 60°$ ($\sigma_y/\sigma_x = 1/1$): experiment (solid lines) and calculation (dashed lines)

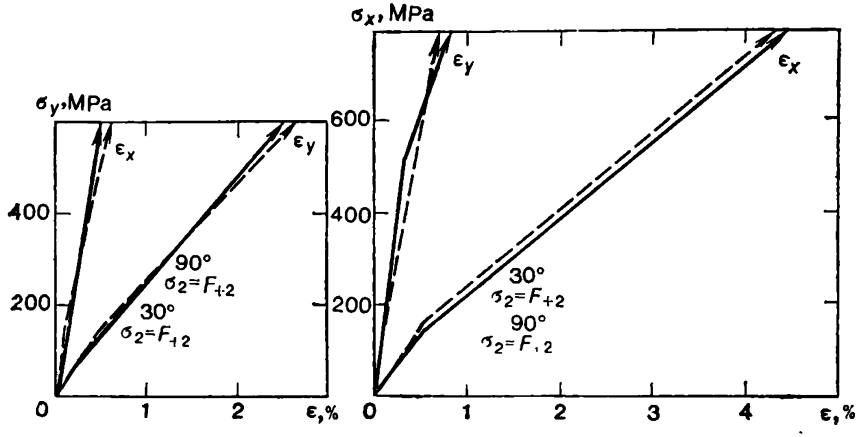

Fig. 7.16 Stress-strain curves for [30°/—30°/90°] fiber-glass plastic at $\sigma_y/\sigma_x = 2/1$: experiment (solid lines) and calculation (dashed lines)

Fig. 7.17 Stress-strain curves for [30°/—30°/90°] fiber-glass plastic at $\sigma_y/\sigma_x = 1/2$: experiment (solid lines) and calculation (dashed lines)

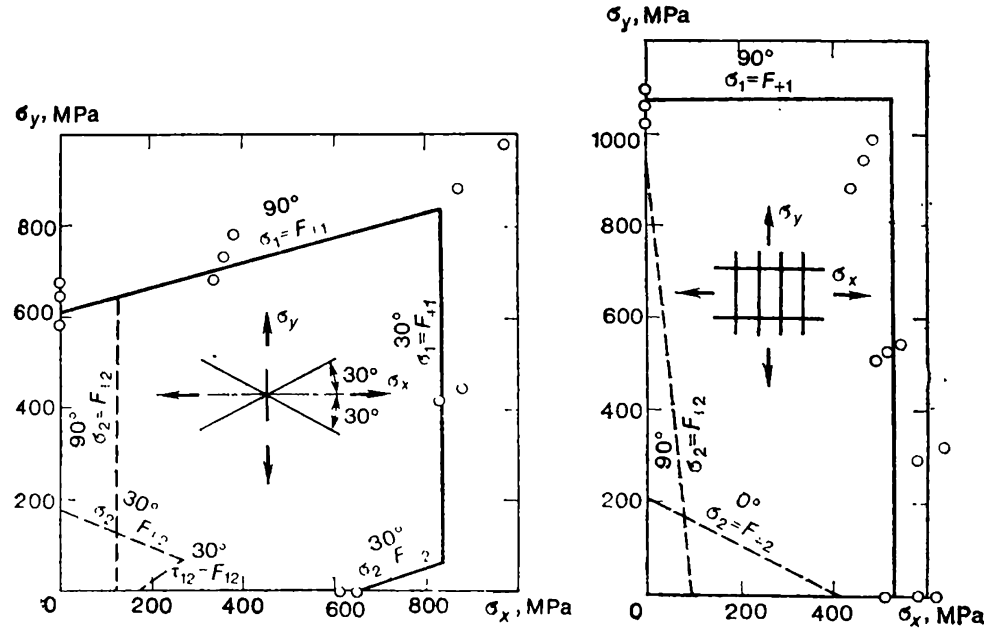

Fig. 7.18 Failure envelopes of quasi-isotropic fiber-glass plastic. Experimental data (average values) are plotted by circles, calculated data are shown by the solid lines (ultimate strength) and by the dashed lines (loss of integrity)

Fig. 7.19 Failure envelopes of cross-ply [0°/90°] fiber-glass plastic. Experimental data are plotted by the circles, calculated data are shown by the solid lines (ultimate strength) and by the dashed lines (loss of integrity)

mode of the stressed state; strength can also change from very high to very low values. In a number of cases (closeness to the equilibrium structure) composites show almost strict linearity in their behaviour and sometimes the curves in their appearance more resemble stress-strain curves of metals with developed ductile properties. The last case can complement a series of vivid examples of D. Drucker [39] showing the possibility of qualitative transformation of the component properties in composites.

The ultimate strains of the multilayer composite can by several times exceed those of layers. High compliance of many structures is not only a disadvantage of composites of this type. In many cases the effects of "pseudoplasticity" can be turned to advantage by engineers.

We consider that the experimental data presented in this paper are of interest in their own right and can be used as the basis for new theoretical developments. However, acceptable results on predictions of strength and deformability for materials with different structures of reinforcement have been also obtained with the fairly simple model described in the paper. The main features of models which have proved successful are as follows:

—taking account of the influence of stresses σ_2 on the behaviour of a layer during crack formation;

—taking account of the possibility of unloading with respect to strains or stresses even with a continuous load increase;

—taking account of one of the effects of "structural nonlinearity"—reinforcement angle change with deformation;

—simplicity (and hence greater reliability) of the determination of the initial data required for the model application.

These features, obviously, must to some extent be inherent in any model designed for the description of the multilayer composite behaviour in a wide range of composite structures and modes of loading.

As noted, three main reasons determine the nonlinearity of stress-strain curves: nonlinear properties of the matrix, crack formation and changes of the geometrical parameters of the composite structure. Certainly, in the experiments performed it was impossible to distinguish the effect of each of the factors mentioned. Nevertheless, they are distinguished in the theoretical model. Here, nonlinearity of the behaviour up to the first cracking is neglected. The considered structural nonlinearity is marked at large shear strains (about 5 percent and more). Under these conditions, by and large, satisfactory agreement between most experimental and theoretical curves can be considered as an indirect indication that the predominant factor is crack formation in the polymeric matrix.

The "angularity" of the model, and piecewise linear character of many curves do not always correspond well to the real processes of deformation. This shortcoming can be overcome or at least dimin-

ished. But improvement of the model (for example, by introducing nonzero tangent moduli following the first ply failure, approximation of layer stress-strain curves by smooth curves) might require a nonequivalent increase in initial information.

A more serious shortcoming of contemporary models is that they do not permit generalizations for a three-dimensional case to be made, i.e. in fact they are not the theories of medium. Greater attention should also be paid to specific forms of exhaustion of the composite bearing strength, unrelated to fiber rupture.

References

1. Lekhnitskii, S.G., *Theory of Elasticity of an Anisotropic Body* (transl. from the revised 1977 Russian edition), Mir Publishers, Moscow, 1981.
2. Goldenblat, I.I., and Kopnov, V.A., *Criteria of Strength and Plasticity of Structural Materials*, Mashinostroyenie, Moscow, 1968 (in Russian).
3. Ashkenazi, E.K., and Ganov, E.V., *Anisotropy of Structural Materials*, Mashinostroyenie, Moscow, 1972 (in Russian).
4. Malmeister, A.K., Tamuzh, V.P., Teters, G.A., *Strength of Polymeric and Composite Materials*, Zinatne, Riga, 1980 (in Russian).
5. Wu, E.M., in: *Composite Materials*, vol. 2, *Mechanics of Composite Materials* (G.P. Sendeckyj, ed.), New York and London, Academic Press, 1974, pp. 353-431.
6. Petit, P.H., and Waddoups, M.E., *J. Composite Materials*, 3, Jan., 2-19 (1969).
7. Amijima, S., and Adachi, T., *Science and Eng. Review of Doshisha Univ.*, 16 (3-4), 147-167 (1975).
8. Sandhu, R.S., *J. of Aircraft*, 13, (2), 104-111 (1976).
9. Pesoshnikov, E.M., Tajrova, L.P., Popov, B.G., *Izvestiya VUZov. Mashinostr.*, 11, 8-12 (1979).
10. Vasil'ev, V.V., Dudchenko, A.A., Elpatievskii, A.N., *Mekh. Polimerov*, 1, 144-147 (1970).
11. Rotem, A., and Hashin, Z., *J. Composite Materials*, 9, Apr., 191-206 (1975).
12. Rabotnov, Yu.N., Gunyaev, G.M., Kuznetsova, M.A., Makhmutov, I.M., Stepanychev, E.I., *Mekh. polimerov*, 1, 49-53 (1976).
13. Tsai, S., and Hahn, H., in: *Inelastic Behavior of Composite Materials* (C. Herakovich, ed.), ASME, New York, 1975.
14. Eckold, G.C., Leadbetter, D., Soden, P.D., Griggs, P.R., *Composites*, Oct., 243-246 (1978).
15. Tsai, S.W., and Azzi, V.D., *AIAA J.* 4, (2), 296-301 (1966).
16. Vasil'ev, V.V., and Elpatievskii, A.N., *Mekh. polimerov*, 5, 915-920 (1967).
17. Andrienko, V.M., Dushin, M.I., Tolstoborov, E.P., Ermolaev, A.M., Nedoinov, P.N., Toruteva, N.D., *Trudy TsAGI*, 1815, 3-30 (1977).
18. Rowlands, R., in: *Inelastic Behavior of Composite Materials* (C. Herakovich, ed.), ASME, New York, 1975.
19. Lemoine, L., *AIAA Paper*, 1565 (1978).
20. Obraztsov, I.F., Vasil'ev, V.V., Bunakov, V.A., *Optimum Design of Composite Shells of Revolution*, Mashinostroyenie, Moscow, 1977 (in Russian).
21. Kawata, K., in: *Mech. Behav. Mat. Proc., Int. Conf. Mech. Behav. Mat.*, 5, 146-155, Tokyo, 1972.
22. Zinov'ev, P.A., and Tarakanov, A.I., in: *Use of Plastics in Machine Building, Sb. Trudov MVTU im. Baumana*, 16, 72-80, 1978 (in Russian).
23. Gunyaev, G.M., Zhigun, I.G., Dushin, M.I., Vorontsov, I.A., Yakushin, V.A., Rumyantsev, A.F., *Mekh. Polimerov*, 6, 1019-1027 (1974).

24. Zinov'ev, P.A., Pesoshnikov, E.M., Popov, B.G., Tairova, L.P., *Mekh. Kompoz. Materialov*, 2, 241-245 (1980).
25. Tarnopol'skii, Yu.M., and Kintsis, T.Ya., *Methods of Static Tests of Reinforced Plastics*, Khimia, Moscow, 1975 (in Russian).
26. Uemura, M., and Yamawaki, T., in: *Proc. 9th Int. Conf. Space Technol. and Sci.*, 215-223, Tokyo, 1971.
27. Craddock, J.N., Zak, A.R., Majerus, J., *J. Composite Materials*, 11, 204-211 (1977).
28. Rabotnov, Yu.N., Danilova, I.N., Polilov, A.N., Sokolova, T.V., Karpeikin, M.S., Vainberg, M.V., *Mekh. Polimerov*, 2, 219-225 (1978).
29. Hull, D., Legg, M.I., Spenser, B., *Composites*, Jan., 17-24 (1978).
30. Soden, P.D., Leadbetter, D., Griggs, P.R., Eckold, G.C., *Composites*, Oct., 247-250 (1978).
31. Spenser, B., and Hull, D., *Composites*, Oct., 263-270 (1978).
32. Jones, M.J.C., and Hull, D., *J. Materials Sci.*, 14, 165-174 (1979).
33. Zinov'ev, P.A., Tarakanov, A.I., Fomin, B.Ya., in: *Use of Plastics in Machine Building*, *Sb. Trudov MVTU im. Baumana*, 18, 82-88, 1981 (in Russian).
34. Biderman, V.L., in: *Strength Analysis*, Issue 11, Mashinostroyenie, Moscow, 1965, pp. 3-30 (in Russian).
35. Zinov'ev, P.A., Tarakanov, A.I., Fomin, B.Ya., in: *Proceed. XII All-Union Conf. Theory of Shells and Plates*, Izd. Erevan Univ., 2, 157-163, Erevan, 1980 (in Russian).
36. Alfutov, N.A., Zinov'ev, P.A., Tarakanov, A.I., in: *Sb. NTO im. Akad. A.N. Krylova*, Issue 239, Sudostroyenie, Leningrad, 1976, pp. 137-142 (in Russian).
37. Ishai, O., and Lavengood, R.E., *Isr. J. of Technology*, 8, (1-2), 101-109 (1970).
38. Zinov'ev, P.A., Tarakanov, A.I., Fomin, B.Ya., in: *Use of Plastics in Machine Building*, *Sb. Trudov MVTU im. Baumana*, 19, 1982 (in Russian).
39. Drucker, D., in: *Inelastic Behavior of Composite Materials* (C. Herakovich, ed.), ASME, New York, 1975.

8 Technological Problems in Composite Winding Mechanics

Yu. M. Tarnopol'skii, *D. Sc. (Eng.)*,
G. G. Portnov, *Cand. Sc. (Eng.)*,
A. I. Beil', *Cand. Sc. (Eng.)*

8.1 INTRODUCTION

Winding is one of the most widely used production methods for fibrous composites with polymeric matrix [1]. The history of winding mechanics in the USA is presented in [2]. An important stage in the evolution of winding mechanics is associated with the study of an essential aspect of composites—turning a semifinished product (prepreg) into a finished product. The engineering mechanics of winding has been vigorously developed by Soviet scientists. It is necessary to mention V. L. Biderman [3], V. V. Bolotin and his colleagues (their contributions are reviewed in [4-8]), V. V. Vasil'ev [9, 10] and V. D. Protasov with his associates [11-15]. The kinetics of the curing stage has been investigated and described by N. S. Enikolopov [16]. The contributions of these authors have been reviewed in [17-20]; the test methods for wound materials have been generalized in [21].

The winding of composites essentially differs from the winding of conventional materials (wire, electric cables, ropes, threads, paper, fabrics, magnetic tape, etc.) in that the former is a method of transforming a prepreg into a monolithic material. Besides, the prepreg has extremely low strength and stiffness in the radial direction. To obtain a monolithic material it is necessary to build up a certain interlaminar pressure by tension winding or by applying extra pressure (to layer after layer or to the product as a whole), this technological parameter being controlled only during prepreg winding.

The winding is generally followed by heating, polymerization at an elevated temperature, cooling and removal from the mandrel (if the mandrel is not an integral part of the finished product). A heat buildup in the prepreg is accompanied by thermal expansion of the prepreg and the mandrel, a decrease in stiffness in the radial direction, filtration, partial relaxation of the stresses generated during winding. In the process of polymerization strength and stiffness in the radial direction increase and physicochemical shrinkage takes place. Thick-walled products are mainly made from hot-cured resins, because polymerization of cold-cured resins involves heat release which results in uncontrolled self-heating and in higher physicochemical shrinkage. The cooling is accompanied by joint thermal contraction of the product and the mandrel and by an increase in stiff-

ness and strength in the radial direction. On cooling the product may separate from the mandrel at a certain temperature. If this does not occur, the mandrel is removed.

Throughout the whole technological process physical-mechanical properties and the stress-strain state change substantially. Therefore, a universal (but very complex) rheological model is practically inapplicable to such a material. The engineering solution involved the

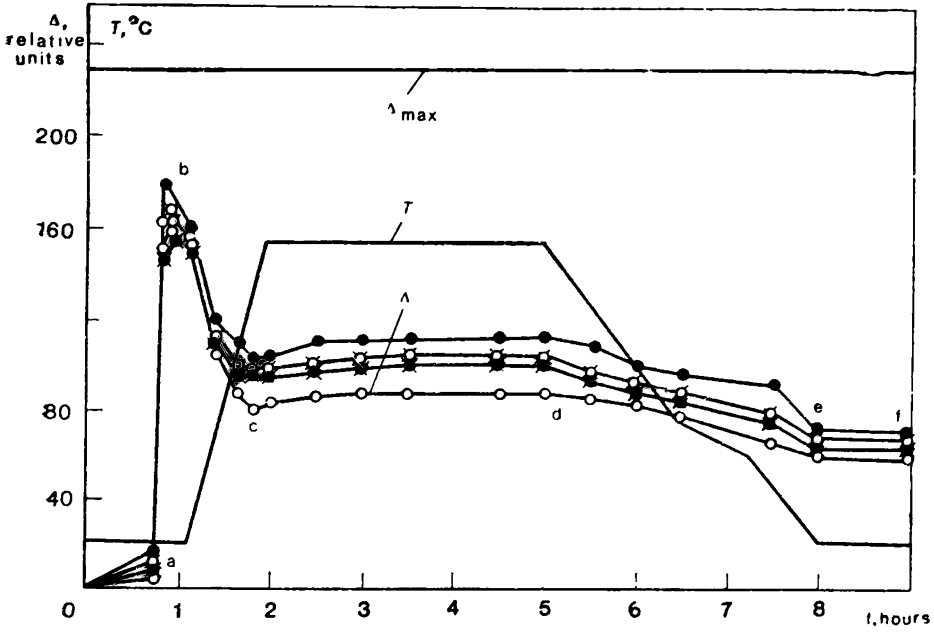

Fig. 8.1 Time variation of pressure Δ at four points of tensometric mandrel during fabrication of a ring from 20 circuits of GFRP by winding under pretensioning of $\sigma_\theta^0 = 200$ MPa:

a-b—winding; *b-c*—heat buildup; *c-d*—polymerization; *d-e-f*—cooling; Δ_{max}—the maximum allowable strain of an absolutely rigid tape during winding; *T*—molding temperature. The circles are experimental values [22]

division of the product mechanical history into several stages (including the operational one) in accordance with the technological process stages. In each stage, the mechanical behaviour of the material may be described by its rheological law. Abrupt changes in the material characteristics are observed at interstage points. Various simplifying hypotheses may be assumed concerning these points, for example, a hypothesis about the heredity of stress state or some more complex hypothesis which generally may be referred to as a hypothesis about the heredity of stress-strain state. The division into stages was convenient because it allowed a series of simplifications to be employed for each stage which are inappropriate for description of the entire process.

Experiments with tensometric mandrels, allowing the kinetics of pressure variation in all stages to be studied, have served as a starting point for the development of an engineering theory (Fig. 8.1). During polymerization, pressure on the mandrel is constant and as such it is of special interest. This approach allows different versions of the theory of initial stresses to be developed in which, by applying the hypothesis about summation of stress states in each stage, the polymerization stage has been omitted. An original approach has been proposed in [3], allowing the calculation of stress increments

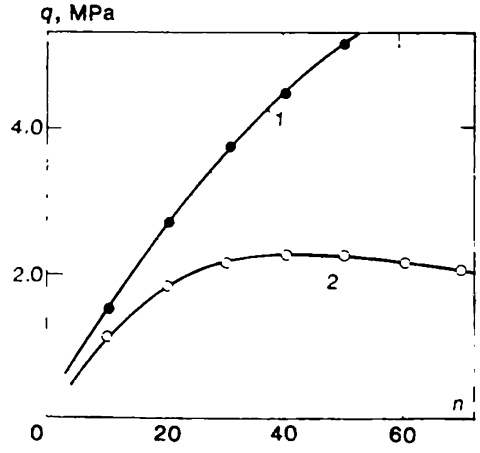

Fig. 8.2 Pressure q on mandrel versus the number n of circuits during winding:
1—nickel tape; *2*—GFRP prepreg [23]

caused by the jump in stiffness-based characteristics. This is essential for analyzing the effect of the jump in characteristics at interstage points. Experiments with tensometric mandrels allowed the composite winding to be distinguished from the winding of conventional materials (Fig. 8.2): a great deal of pressure from the newly wound circuits is not transferred onto the mandrel. This phenomenon is associated with essential anisotropy of the material and, in particular, with high compliance across compressed fibers. It is natural that the first problem to be dealt with is the evaluation and description of the elastic characteristics of a prepreg.

8.2 WINDING STAGE

8.2.1 Anisotropy of Prepregs

To describe analytically the winding process it is necessary to know the stiffness-based characteristics of the prepreg. Properties along a tape or yarn are fiber-dependent and are described by Hooke's

law with sufficient accuracy [24]. Across the fibers the prepreg is characterized by high compliance. The data available in the literature on static compression of prepreg layer packages are presented in Fig. 8.3.

Notwithstanding some conventionality owing to the lack of a unique elaborate technique, the test results indicate convincingly the

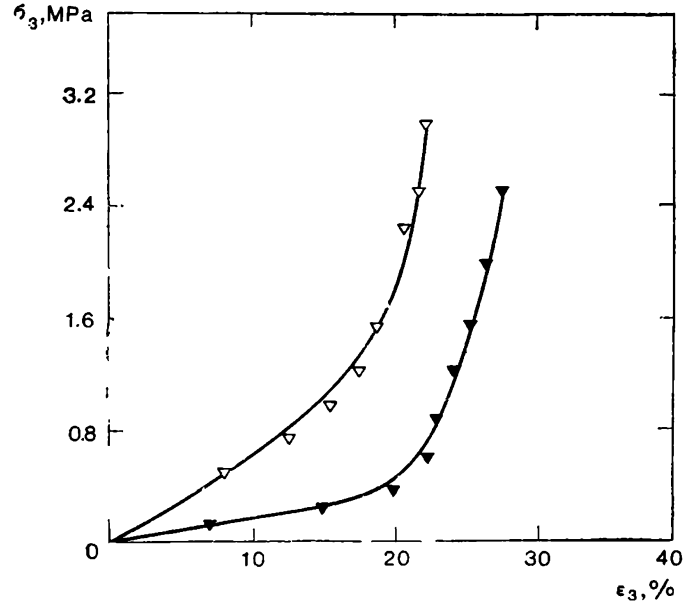

Fig. 8.3 σ_3-ε_3 curves under transverse compression of layer packages of polyester prepreg: the open triangles, at 20°C; the solid triangles, at 100°C [25]

essential nonlinearity of σ_3-ε_3 curves, caused by volume contraction of the package and formation of a monolithic material.

The anisotropy ratio, characterized by $\beta = \sqrt{E_1/E_3}$ where E_1 is Young's modulus along the fibers and E_3 is the tangent modulus in transverse compression of the prepreg, changes over a wide range, depending on the matrix state, composition, temperature, fiber properties, and load level: $4 \leqslant \beta \leqslant 200$.

Thus composite prepregs may be conceived as materials with exceptionally well-defined anisotropy and essentially nonlinear in the direction perpendicular to the reinforcing fibers.

During winding, the matrix material tends to irreversible creep. However, since interlaminar shear stresses are minimum and the prepreg undergoes volume contraction during transverse compression, the viscous-flow state of the polymeric matrix results from its filtration from regions where interlaminar pressure is high to those

where it is low. One should differentiate between microfiltration resulting from the local gradients of interlaminar pressure due to the presence of voids and macrofiltration resulting from the gradient of macrostresses transverse to the fibers. The local pressure gradients realized in small volumes are comparatively large and they cause fast microflows of the matrix material. Their average macroflow is

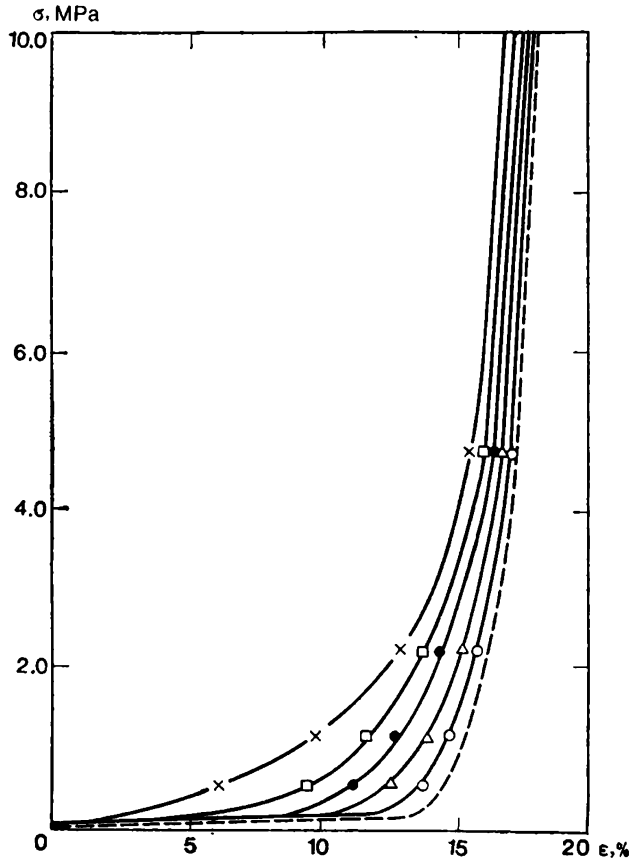

Fig. 8.4 Isochrones of creep under transverse compression for layer packages of polyester prepreg at 20°C:
×—t = 0.75; □—t = 1.5; ●—t = 2.5; △—t = 4; ○—t = 16 min and ——— $t \to \infty$

equal to zero. Microfiltration stops comparatively quickly and short-time creep during volume contraction of the prepreg is mainly ascribed to it.

Isochronous creep curves for polyester glass-fiber plastic prepreg are presented in Fig. 8.4. Note three characteristic traits of the family of isochrones: they are similar, essentially nonlinear and lie within a narrow band of values. They show that σ_3-ε_3 curves may be employed in the calculations. Analogous conclusions follow from

the creep data for uncured wound glass-fiber reinforced plastics (GFRP) produced by a "wet" technique [26].

Macrofiltration proceeds comparatively slowly and, in many cases, contributes little to nonuniform deformation of the material resulting from variation of the reinforcement coefficient. However, since the nonuniformity, as a rule, is low in the finished product and maint ly attributed to nonuniform volume compaction preceding the onse- of polymerization, then, in many cases, the consideration of macrofiltration in stressed state analysis is of no importance.

8.2.2 A Linearly Elastic Ring Model

8.2.2.1 Description of the Model

Many problems of winding mechanics have been verified with the simplest model of wound products—the ring. The model allows the main rheological features of composite prepregs to be taken into account along with the basic structural feature of wound products — the absence of radially oriented fibers. Analysis of the ring model contributes to an understanding of the winding phenomena.

Knowledge of the interrelations between the parameters of tension winding (or extra compression) and stress-strain fields allows estimation and effective control of:

(a) the distribution of interlaminar pressure between circuits, which, in turn, defines the degree of integrity and quality of the finished product;
(b) pressure on the mandrel which should not exceed the critical buckling pressure of thin-walled mandrels or the strength of thick-walled mandrels;
(c) the distribution of filament tensioning within the wound body; as a rule, during winding of subsequent layers the passing of fibers from the region of pretensioning into the region of compression up to critical buckling stresses is undesirable, since it leads to zones of drops in strength;
(d) the postwinding distribution of stresses, constituting the main component of initial technological stresses;
(e) the final configuration of the finished product.

According to the ring model the winding process involves successive mounting of thin circular layers initially onto a mandrel and afterwards onto each other under tension equal to the tension of a wound tape. Let us consider the linearly elastic ring model of winding. During winding under low or very high tension, the model describes the process qualitatively.

At the moment the outer radius R of a successive circuit being wound is on the current radius, the stresses on the radius are equal to

$$\sigma_r = 0, \quad \sigma_\theta = \sigma_\theta^0 \tag{1}$$

where σ_θ^0 is the stress preset by a tensioning device. The stresses change with pressure on each of the successive circuits

$$\Delta\sigma_r = -\sigma_\theta^0 h/R = -\sigma_\theta^0 \chi/\rho \quad \text{at } \rho = b_k \tag{2}$$

where χ, ρ, b_k are the layer thicknesses, actual and outer radii, expressed as a fraction of the inner radius R_i. All linear values, including displacements, are expressed below as fractions of the inner radius. When determining the stress increments $\Delta\sigma_r$ and $\Delta\sigma_\theta$ the already wound ring is considered a macrouniform, cylindrically orthotropic body and on the boundary with a ring-type or disk-type mandrel (of the same width) the conditions of compatibility of radial stresses and displacements are realized or, which is the same, the conditions are preset for a composite ring as follows

$$\Delta u_r = \Delta\varepsilon_\theta|_{\rho=1} = \gamma\Delta\sigma_r a_{\theta\theta} \quad \text{at} \quad \rho = 1 \tag{3}$$

where γ is the relative compliance of the mandrel. For an isotropic mandrel with characteristics E_m, ν_m and outer-to-inner radii ratio b_m

$$\gamma = -\frac{E_\theta}{E_m}\left(\frac{1+b_m^2}{1-b_m^2} + \nu_m\right) \tag{4}$$

An equation of the axisymmetric problem for a cylindrically orthotropic ring [27] is obtained by the subsequent substitution of an equilibrium equation

$$\sigma_\theta = \sigma_r + \rho\, d\sigma_r/d\rho \tag{5}$$

into Hooke's law in the form of the stress-strain relation

$$\begin{aligned} \varepsilon_r &= a_{rr}\sigma_r + a_{r\theta}\sigma_\theta \\ \varepsilon_\theta &= a_{\theta r}\sigma_r + a_{\theta\theta}\sigma_\theta \end{aligned} \tag{6}$$

where a_{rr}, $a_{\theta\theta}$, $a_{r\theta} = a_{\theta r}$ are elements of compliance matrix of the material to be wound, and then the result obtained being substituted into the equation of compatibility of strains

$$\varepsilon_r = \varepsilon_\theta + \rho\, d\varepsilon_\theta/d\rho \tag{7}$$

we arrive at

$$\rho^2 \frac{d^2\Delta\sigma_r}{d\rho^2} + 3\rho \frac{d\Delta\sigma_r}{d\rho} + (1-\beta^2)\Delta\sigma_r = 0 \tag{8}$$

Here, $\beta^2 = a_{rr}/a_{\theta\theta}$. Its solution takes the form:

$$\Delta\sigma_r = C_1\rho^{\beta-1} + C_2\rho^{-\beta-1} \tag{9}$$

/here constants C_1 and C_2 are determined from boundary conditions 2), (3). The final result has the following form

$$\Delta\sigma_r(\rho, b_k) = -\sigma_\theta^0(b_k)\frac{\eta\rho^{\beta-1}+\rho^{-\beta-1}}{\eta b_k^{\beta}+b_k^{-\beta}}\chi$$

$$\Delta\sigma_\theta(\rho, b_k) = -\sigma_\theta^0(b_k)\beta\frac{\eta\rho^{\beta-1}-\rho^{-\beta-1}}{\eta b_k^{\beta}+b_k^{-\beta}}\chi \qquad (10)$$

$$\Delta u(\rho, b_k) = -a_{\theta\theta}\sigma_\theta^0(b_k)\left[(\beta-\nu_{r\theta})\eta\rho^{\beta}+(\beta+\nu_{r\theta})\rho^{-\beta}\right]\frac{\chi}{(\eta b_k^{\beta}+b_k^{-\beta})}$$

vhere

$$\beta = (\beta+\gamma+\nu_{r\theta})/(\beta-\gamma-\nu_{r\theta})$$

$$\nu_{r\theta} = -a_{r\theta}/a_{\theta\theta}$$

Stresses and displacements in a completely wound ring having the elative outer radius b are summed up as follows

$$\sigma_r(\rho, b) = \Delta\sigma_r(\rho, \rho+\chi) + \Delta\sigma_r(\rho, \rho+2\chi) + \ldots + \Delta\sigma_r(\rho, b)$$

$$\sigma_\theta(\rho, b) = \sigma_\theta^0(\rho) + \Delta\sigma_\theta(\rho, \rho+\chi) + \Delta\sigma_\theta(\rho, \rho+2\chi) + \ldots + \Delta\sigma_\theta(\rho, b) \qquad (11)$$

$$u_r(\rho, b) = \Delta u_r(\rho, \rho+\chi) + \Delta u_r(\rho, \rho+2\chi) + \ldots + \Delta u_r(\rho, b)$$

Since χ is very small, it is reasonable for a great number of circuits o substitute summation by integration

$$\sigma_r(\rho, b) = -(\eta\rho^{\beta-1}+\rho^{-\beta-1})A(\rho, b)$$

$$\sigma_\theta(\rho, b) = \sigma_\theta^0(\rho) - \beta(\eta\rho^{\beta-1}-\rho^{-\beta-1})A(\rho, b) \qquad (12)$$

$$u_r(\rho, b) = -a_{\theta\theta}\left[(\beta-\nu_{r\theta})\eta\rho^{\beta}-(\beta+\nu_{r\theta})\rho^{-\beta}\right]A(\rho, b)$$

$$A(\rho, b) = \int_{\rho}^{b}\sigma_\theta^0(y)(\eta y^{\beta}+y^{-\beta})^{-1}\,dy$$

For some winding programs $\sigma_\theta^0(\rho)$, an integral in the right-hand side of (12) may be obtained analytically in a closed form either in a fast-converging series [25, 28], or numerically. In the latter case, a direct use of the discrete equations (10), (11) is effective.

The approach used by V. V. Vasil'ev [29] assumes that the stress $\sigma_\theta(b_k, b_k)$ in the current outer kth circuit is not equal to the stress

$\sigma_\theta^0(b_k)$ generated by the tensioning device. The value of $\sigma_\theta(b_k)$ i obtained from the energy balance $W_0 = W_1 + W_2$, where W_0 i the potential energy of the tape extended under stress σ_θ^0 and of length equal to that of the respective circuit; W_1 is the increment o deformation energy in the system consisting of the earlier wound cir cuits and the mandrel; W_2 is the energy remaining in the last cir cuit. Expressions of W_0 and W_2 are trivial, W_1 is obtained as $W_1 = \sigma_\theta(b_k, b_k)\,\Delta u_r(b_k, b_k)/2b_k$ using (10), where $\sigma_\theta^0(b_k)$ is substituted by $\sigma_\theta(b_k, b_k)$. As a result we obtain

$$\sigma_\theta(b_k, b_k) = \sigma_\theta^0(b_k)\left[1 + \frac{\chi}{b_k}\left(\beta\frac{\eta b_k^{2\beta}-1}{\eta b_k^{2\beta}+1} - \nu_{r\theta}\right)\right]^{-1/2} \qquad (13$$

The order of deviation of $\sigma_\theta(b_k, b_k)$ from $\sigma_\theta^0(b_k)$ is determined by the order of magnitude $\rho\chi/b_k$, which may reach 10^{-3} to 10^{-1}. In a physical sense, the two approaches differ in that the tension approach [23] corresponds to the winding without friction between the last layer and the preceding one, but the energy approach [29], to the winding with an infinitely large friction coefficient. Evidently, the actual situation is an intermediate case. Note that, as follows from (13), the winding constant tension according to the energy approach corresponds to the winding with slowly decreasing tension according to the tension approach. At $\chi \to 0$, both approaches coincide; therefore, the tension approach will be employed further.

8.2.2.2 Pressure on the Mandrel

The dependence of the relative pressure on the mandrel $q/\sigma_\theta^0 = -\sigma_r(1, b)/\sigma_\theta^0$ during winding under constant tension on the relative ring dimensions is presented in Fig. 8.5. The pressure on the mandrel increases nonlinearly with thickness of the wound product, approaching asymptotically a certain ultimate value. This ultimate value $q_\infty = -\sigma_r(1, b \to \infty)$ and the ring thickness, at which it is practically reached, are drastically reduced with an increase in the anisotropy ratio β of the material. For an absolutely rigid mandrel ($\eta = 1$)

$$q_\infty/\sigma_\theta^0 = \frac{2}{\beta}\left(\alpha_0 + \frac{\alpha_1}{\beta} + \frac{\alpha_2}{\beta^2} + \ldots + \frac{\alpha_n}{\beta^n} + R_n\right)$$

$$\beta > 1, \quad R_n < 1/[\beta^n(\beta-1)] \qquad (14)$$

where

$$\alpha_0 = \frac{\pi}{4} < \alpha_1 = G < \alpha_2 = \frac{\pi^3}{32} < \alpha_3$$

$$= 0.98894455\ldots < \alpha_4 = \frac{5\pi^4}{1536} < \ldots < 1$$

(Here, G is Katalan's constant.) The mandrel compliance further reduces the pressure transfer, especially at the initial stage of wind-

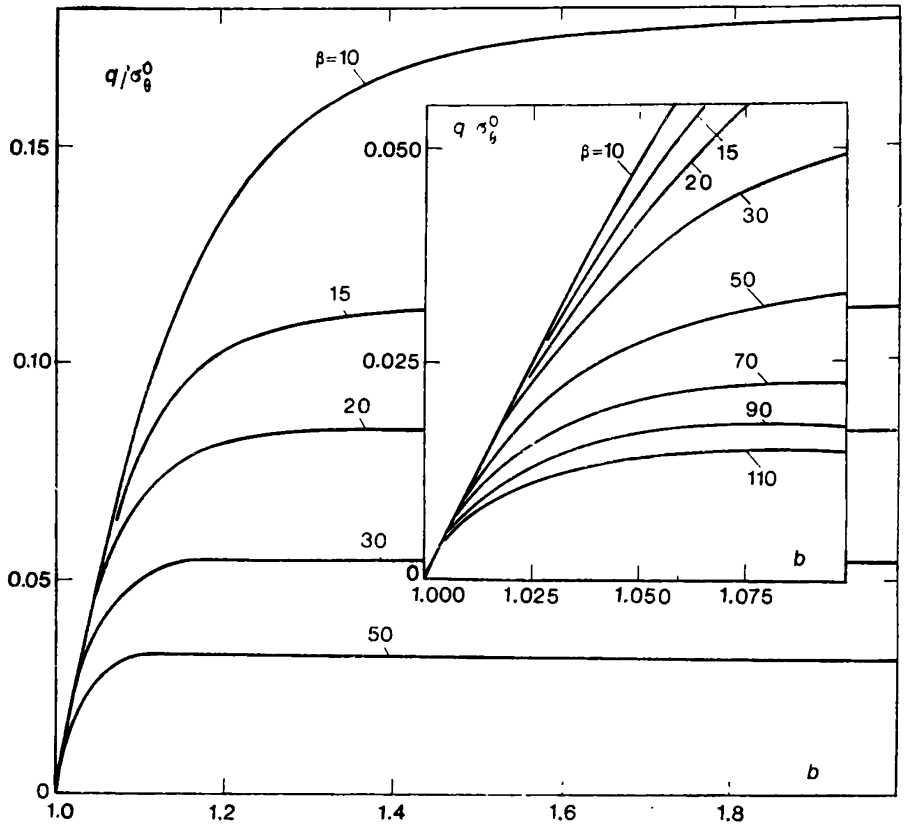

Fig. 8.5 Pressure on a rigid mandrel q (in fractions of stress σ_θ^0 in wound tape) versus current relative outer radius b of ring at various anisotropy ratios β

ing. At high anisotropy ratios ($\beta \geqslant 30$) the mandrel compliance effect over the actual range $0 \leqslant \gamma \leqslant 10$ is inessential.

8.2.2.3 Stress Distribution

Since the winding with constant tension is the most widely used fabrication method, a detailed analysis of stress-strain state in this case is of great practical importance. Fig. 8.6 presents the diagrams of stresses σ_r and σ_θ for winding under constant pressure σ_θ^0. Note that the circumferential stresses are essentially nonuniform throughout the cross-section. Moreover, there is a region in which the stresses change sign.

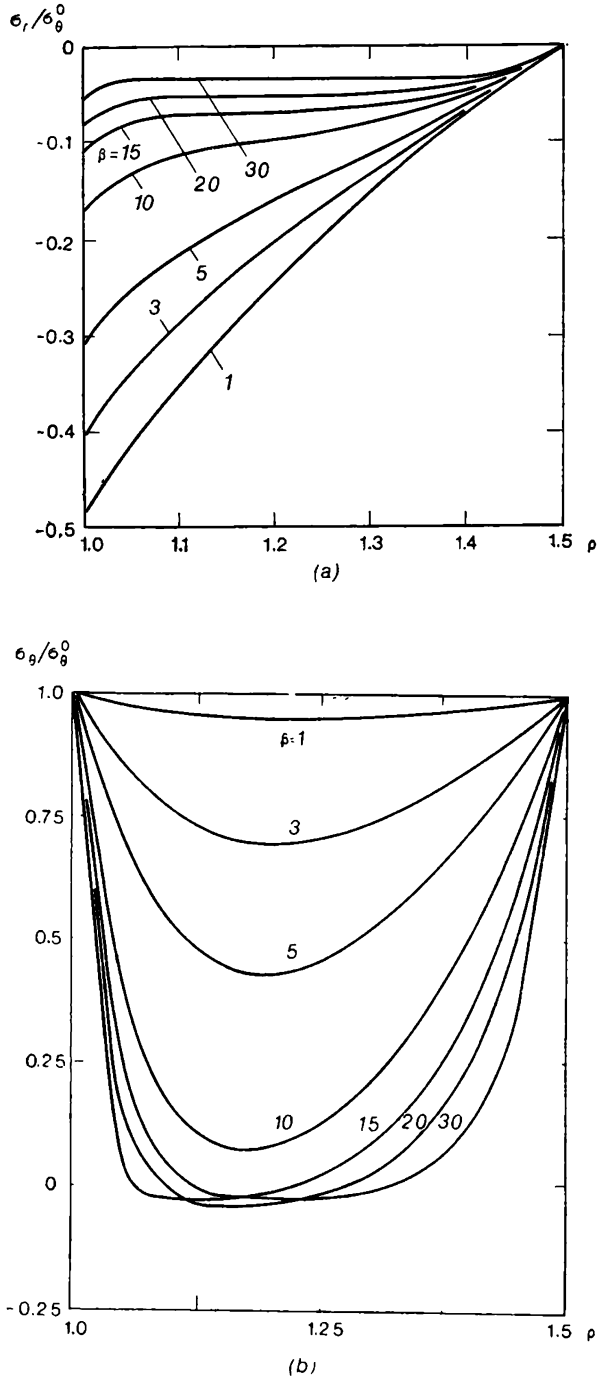

Fig. 8.6 Diagrams of (*a*) radial and (*b*) circumferential stresses during winding under constant tension σ_θ^0 onto a rigid mandrel for rings with relative dimensions b 1.5 at various anisotropy ratios β of prepreg

Since under conditions of processing the fibers can carry only tensile load, the transition from the state of pretensioning to that of compression is fraught with the danger of distortions (waviness). In Fig. 8.7 shown are combinations of the parameters b and β at which the initially preset tensioning vanishes during winding onto

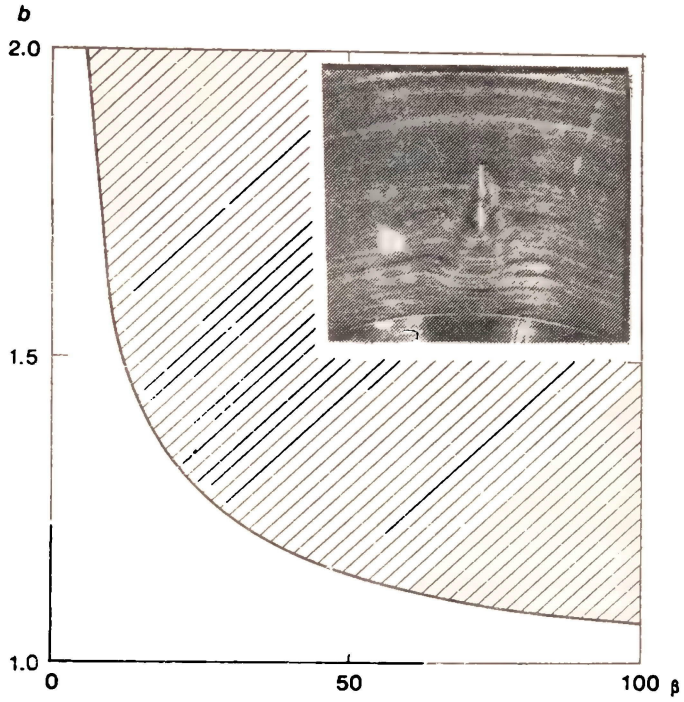

Fig. 8.7 Dependence of maximum relative ring dimensions b, for which pretensioning is still partly preserved, on anisotropy ratio β. The photo shows distortion of circuits in the prepreg during winding

a rigid mandrel. If the winding is accomplished at combinations of the parameters falling within the dashed area in Fig. 8.7, then fiber waviness is possible. In this, the material properties become uncertain and the calculation of stresses and displacements according to the above model would be incorrect.

The winding varying tension is of particular interest. Let us compare stress distribution in circuits for different programs $\sigma_0^0(\rho)$ ensuring the same pressure on the mandrel. The winding programs with tension decreasing or passing through a minimum results, after relieving pressure on the boundary with the mandrel, in undesirable tensile initial stresses, the latter together with thermoelastic initial stresses of the same sign may induce cracking in the wound product. During the programmed winding with a tension minimum the distor-

tion of circuits may occur. The winding under increasing tension allows greater compensation for radial thermoelastic stresses, but the programmed winding with a tension maximum allows prevention of distortions.

8.2.2.4 Evaluation of Ring Dimensions by Taking into Account the Compressibility of a Prepreg

By taking into account the large radial strains of the product during tension winding it is useful to know the dependence of the actual ring dimensions on the number of circuits. By integrating ε_r over the ring thickness using formulas (12) and summing up with the expression $u_r(1, b)$, we can obtain

$$\Delta b(b) = -\beta a_{\theta\theta} \int_1^b \sigma_\theta^0(y)\,[(\eta y^{2\beta} - 1)/(\eta y^{2\beta} + 1)]\,dy \qquad (15)$$

For high values of β at $b > 1.1$ formula (15) for the winding under constant tension may be approximated by a simple expression with a small error

$$\Delta b(b) \approx -a_{\theta\theta}\sigma_\theta^0\left[\beta(b-1) - \ln\frac{\eta+1}{\eta}\right] \qquad (16)$$

It follows from (16) that, if the winding tension is near to the breaking tension ($a_{\theta\theta}\sigma_\theta^0 \sim 0.01$), the change in the outer radius is comparable to the ring thickness. In this case, the use of the mathematical means, employed above and based on the theory of low strains, becomes not quite correct.

8.2.3 A Nonlinearly Elastic Ring Model

8.2.3.1 A Piecewise Linear Approximation

A linearly elastic ring model taking into account the most important factor—the anisotropy of deformation properties—allows the correct prediction of a number of basic features of composite winding, in particular, the essential nonlinearity of the mandrel pressure versus the number of circuits. However, the model ignores another important factor—the nonlinearity of the transverse compression curve σ_r-ε_r. The effect of nonlinear dependence of the mandrel pressure on tension during winding has been repeatedly confirmed in experiments [30-33]. In all cases, the relative pressure on the mandrel (i.e. in fractions of tension) did not remain constant, as in the linearly elastic model, but increased with tension (Fig. 8.8).

The effect may be explained only by characteristic stiffening of the prepreg (Fig. 8.3) in the transverse direction with the rise in

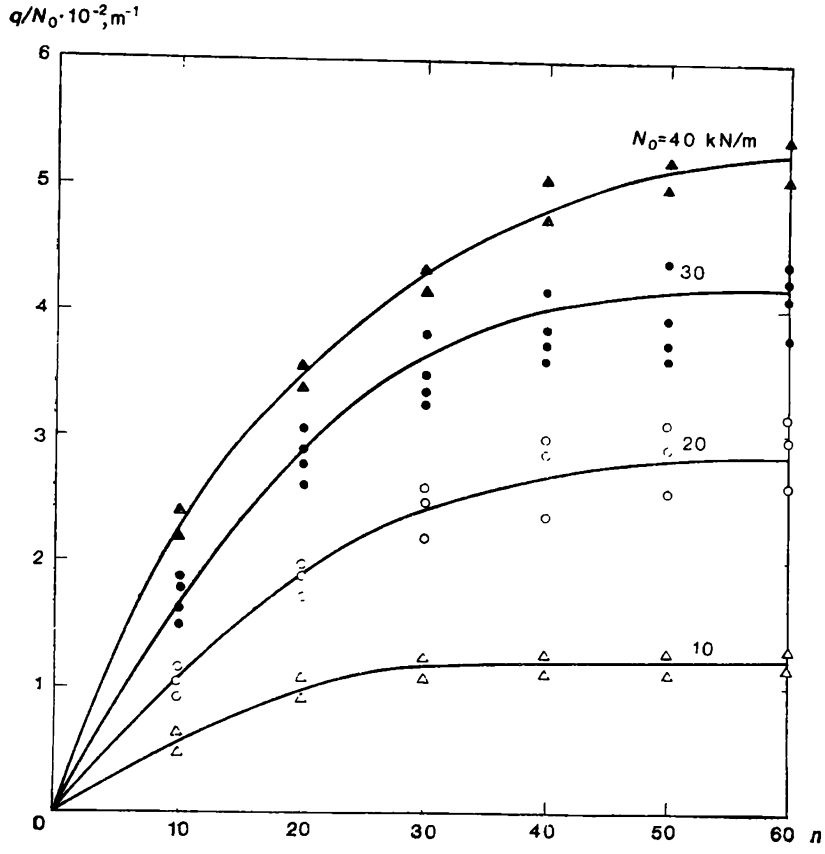

Fig. 8.8 Relative pressure on mandrel q/N_0 versus the number of circuits n during winding under varying tension N_0. The circles and triangles are experimental values [33]

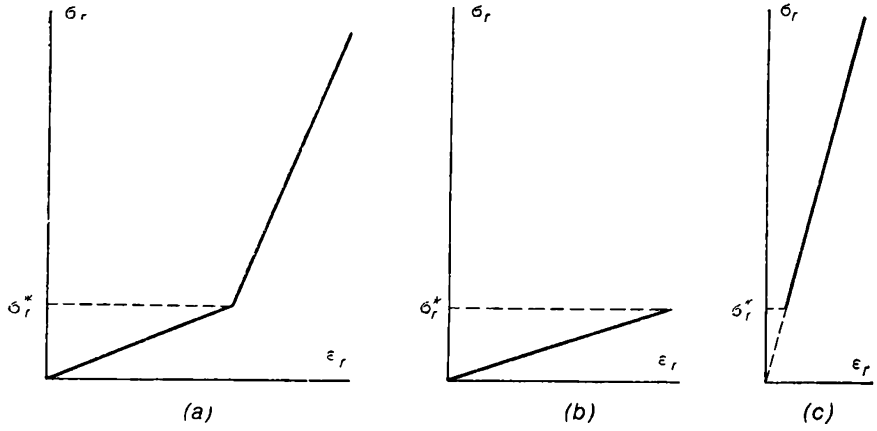

Fig. 8.9 Deformation law for (*a*) prepreg transverse compression and (*b*, *c*) its approximation over different ranges of tension variation

radial stresses. A nonlinear compression curve of the prepreg layer package to the first approximation may be approximated by a piecewise linear relationship (Fig. 8.9). The approximation, while introducing some error, allows the description of a wide spectrum of curves by a minimum number of parameters. For prepregs of structural composites, the characteristics fall within the following ranges: the limit of proportionality $|\sigma_r^*| = 0.5\text{-}2.0$ MPa, anisotropy ratio $\beta = \sqrt{E_\theta/E_r}$, evaluated via tangent modulus E_r, is 30-200 before the limit of proportionality and 4-50 beyond the limit of proportionality. Note that the stresses in the order of σ_r^* correspond to mean stresses during winding of large-scale structures, and this indirectly indicates the necessity of using the nonlinear theory in the calculations.

Early in the winding, the radial stresses are low and the process is described by a linearly elastic model with the anisotropy ratio $\beta = \lambda$ corresponding to the initial portion of the σ_r-ε_r curve. At $|\sigma_r^*| > q_\infty$ the winding of a product of any thickness is described by the linearly elastic theory with an anisotropy ratio β corresponding to the initial portion of the σ_r-ε_r curve. A second variant, where the limit of proportionality is not reached, is the winding of thin-walled products. In this case, the pressure on the mandrel is evaluated from above as σ_0^0 $(b - 1)$. If the value is less than $|\sigma_r^*|$, one has to employ the linearly elastic model with $\beta = \lambda$.

In a wound ring, the absolute value of radial stresses must monotonously decrease from the mandrel towards the outer radius. Otherwise (in case of local extremum or plateau), there is a region of compressive stresses on the diagram of σ_θ related to that of σ_r through an equilibrium equation. This is inadmissible. In the piecewise linear approximation of σ_r-ε_r curve the ring may have either uniform stiffness-based properties (if stresses near the mandrel do not exceed the limit of proportionality) or nonuniform ones (if $|\sigma_r(1, b)| > |\sigma_r^*|$). If the inner circular region with the anisotropy ratio $\beta = \omega$ is comparable in size to the outer region with the anisotropy ratio $\beta = \lambda$, the linearly elastic model is inapplicable. If the regions differ appreciably in size, it is possible to employ the linearly elastic model with the anisotropy ratio $\beta = \lambda$ or $\beta = \omega$, respectively.

8.2.3.2 Design Equations

Let at the instant the interface between the two regions of a composite ring is a circle with the relative radius $\rho = x$ an infinitesimal change in the external pressure dp be applied. In this case stress increments may be formally written in the following form

$$\frac{d\sigma_r}{dp} = \frac{\partial \sigma_r}{\partial p}\bigg|_{x=\text{const}} + \frac{\partial \sigma_r}{\partial x}\bigg|_{p=\text{const}} \cdot \frac{dx}{dp} \qquad (17)$$

This means that upon loading a ring with pressure accompanied by the interface move towards the outer radius, the stress increment may be presented as a sum of stress increments in a composite ring with a stationary interface and stress increments resulting from material replacement in a thin strip dx between the preceding and following interface positions at fixed boundary conditions. Owing to continuity of strains and stresses at the inflection point the second term in (17) is negligible.

Stress analysis in a composite anisotropic ring is given in [27]. In the given case the problem differs in what is being registered in increments and it satisfies somewhat different boundary conditions, analogous to (2) and (3):

$$\begin{aligned} d\sigma_r &= -\frac{1}{\rho}\sigma_\theta^0\, db \quad \text{at} \quad \rho = b \\ d\varepsilon_\theta &= \gamma\, d\sigma_r/E_\theta \quad \text{at} \quad \rho = 1 \end{aligned} \tag{18}$$

Formulas of stress and displacement increments in the kth ring have the form [27]

$$\begin{aligned} d\sigma_r^{(k)} &= \frac{dq_{k-1}c_k^{\beta_k+1}}{1-c_k^{2\beta_k}}\left[\left(\frac{\rho}{b_k}\right)^{\beta_k-1} - \left(\frac{\rho}{b_k}\right)^{-\beta_k-1}\right] \\ &\quad - \frac{dq_k}{1-c_k^{2\beta_k}}\left[\left(\frac{\rho}{b_k}\right)^{\beta_k-1} - c_k^{2\beta_k}\left(\frac{\rho}{b_k}\right)^{-\beta_k-1}\right] \\ d\sigma_\theta^{(k)} &= \beta_k \frac{dq_{k-1}c_k^{\beta_k+1}}{1-c_k^{2\beta_k}}\left[\left(\frac{\rho}{b_k}\right)^{\beta_k-1} + \left(\frac{\rho}{b_k}\right)^{-\beta_k-1}\right] \\ &\quad - \beta_k \frac{dq_k}{1-c_k^{2\beta_k}}\left[\left(\frac{\rho}{b_k}\right)^{\beta_k-1} + c_k^{2\beta_k}\left(\frac{\rho}{b_k}\right)^{-\beta_k-1}\right] \\ du^{(k)} &= \frac{dq_k b_k c_k^{\beta_k+1}}{E_\theta^{(k)}(1-c_k^{2\beta_k})}\left[(\beta_k - \nu_{r\theta}^{(k)})\left(\frac{\rho}{b_k}\right)^{\beta_k} + (\beta_k + \nu_{r\theta}^{(k)})\left(\frac{\rho}{b_k}\right)^{-\beta_k}\right] \\ &\quad - \frac{dq_k b_k}{E_\theta^{(k)}(1-c_k^{2\beta_k})}\left[(\beta_k - \nu_{r\theta}^{(k)})\left(\frac{\rho}{b_k}\right)^{\beta_k}\right. \\ &\quad \left. + (\beta_k + \nu_{r\theta}^{(k)})\, c_k^{2\beta_k}\left(\frac{\rho}{b_k}\right)^{-\beta_k}\right] \end{aligned} \tag{19}$$

where b_k is the relative outer radius of the kth ring.

$(b_0 = 1,\ b_1 = x,\ b_2 = b)$, $c_k = b_{k-1}/b_k$, $\beta_k = \sqrt{E_\theta^{(k)}/E_r^{(k)}} = \sqrt{a_{rr}/a_{\theta\theta}^{(k)}}$.

In the given case, the two elastic characteristics in the rings are equal: $E_\theta^{(1)} = E_\theta^{(2)} = E_\theta$, $\nu_{r\theta}^{(1)} = \nu_{r\theta}^{(2)} = \nu_{r\theta}$. The last equality is necessary

for single-valued determination of strains ε_r under radial stress $\sigma_r = \sigma_r^*$ in complex stress state, when $\sigma_\theta \neq 0$. Pressure increments dq_k on the surfaces of individual constituent rings are equal to:

$$dq_2 = (1/b)\,\sigma_\theta^0\,db$$

$$dq_1 = 2\lambda\,(\eta x^{2\omega} - 1)\,\{[(\lambda+\omega)\,\eta x^{2\omega} - (\lambda-\omega)]\,(x/b)^{1-\lambda} + [(\lambda-\omega)\,\eta x^{2\lambda} - (\lambda+\omega)]\,(x/b)^{1+\lambda^2}\}^{-1}\,dq_2 \qquad (20)$$

$$dq_0 = [(\eta+1)/(\eta x^{\omega-1} + x^{-\omega-1})]\,dq_1$$

where

$$\eta = \eta(\omega).$$

By passing over to small finite differences it is possible for a given pitch to use the above relations with the interface radius $a_1 = x$ borrowed from the preceding pitch. The increment in the interface radius Δx is obtained from the following considerations. Stresses σ_r on the moving interface are constant and equal to the limit of proportionality. Mathematically, it means that the derivative of σ_r in the direction $\rho = x$ equals zero, whence by passing over to finite differences we obtain

$$\Delta x = -\frac{\Delta\sigma_r\,|_{\rho=x}}{(\partial\sigma_r/\partial\rho)_{\rho=x}} = -\frac{\Delta\sigma_r\,|_{\rho=x}\cdot x}{\sigma_\theta\,|_{\rho=x} - \sigma_r^*} \qquad (21)$$

The sequence of calculations is as follows. Up to a certain value of $b = b^*$ the winding is accomplished at stresses not exceeding the limit of proportionality. When using a discrete form of the ring model (10), (11) the value of b^* is determined directly, but while using a continuous form (12) b^* is determined by successive approximations [25]. Following the determination of stresses and displacements at $b = b^*$ and $x = 1$, the first interface radius is calculated according to (21) and stress and displacement increments, according to (19), (20). At overall stresses the new interface radius is calculated, etc. The approach is reminiscent of Euler's numerical solution of differential equations; the same refers to the analysis of its accuracy. The latter may be improved by double scaling or by employing a technique similar to Adams-Bashforth's with construction of the initial portion by Krylov's method.

8.2.3.3 Numerical Results

The dependencies of the mandrel pressure (in fractions of constant tension σ_θ^0) on the outer radius, calculated both according to the linear theory with the anisotropy ratios $\beta = \lambda$ and $\beta = \omega$ and according to the nonlinear theory at various tensions, are presented in Fig. 8.10. Qualitatively, the situation is similar to the experimentally observed one (Fig. 8.8).

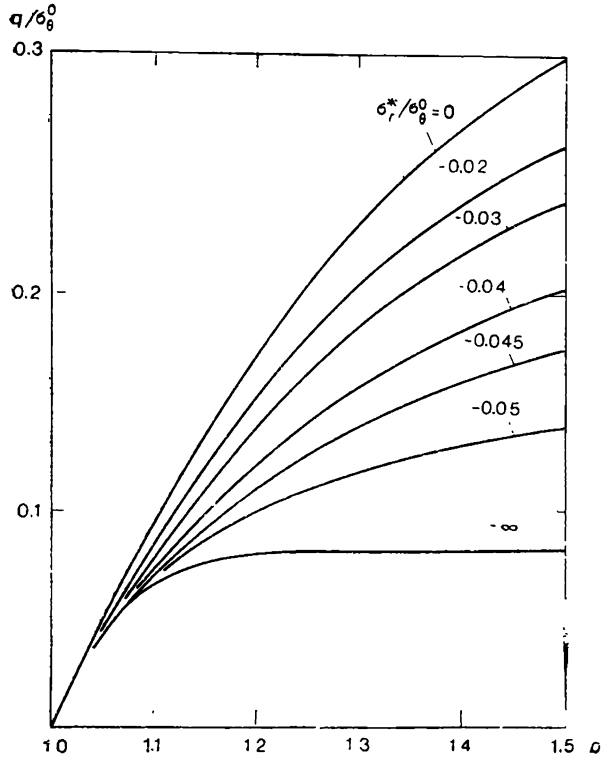

Fig. 8.10 Relative pressure on mandrel q/σ_θ^0 versus relative ring dimensions b at various tensions specified by the parameter $\sigma_r^*/\sigma_\theta^0$ ($\lambda = 20$, $\omega = 5$)

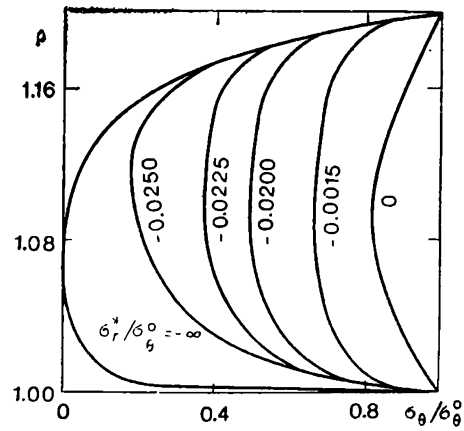

Fig. 8.11 Diagrams of relative circumferential stresses during winding under various tensions ($\lambda = 40$, $\omega = 5$)

It has been established that the value of tension substantially affects the diagrams of circumferential stresses (Fig. 8.11). A series of calculations using the developed program allowed the area of application of each of the three winding models to be numerically

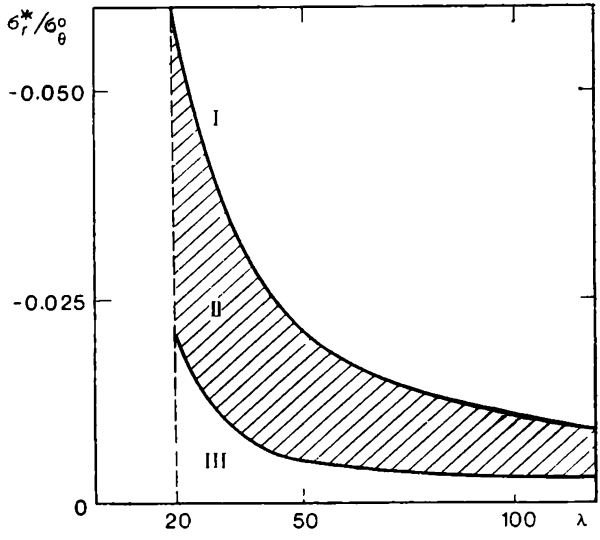

Fig. 8.12 Areas of application of three theoretical variants in description of winding:
I—linear theory with $\beta = \lambda$; II—nonlinear theory; III—linear theory with $\beta = \omega$. Boundaries are set at $\omega \leqslant 0.25$

estimated: two linear models with the anisotropy ratio $\beta = \lambda$ or $\beta = \omega$ and a nonlinear one. The calculations have shown that, if the anisotropy ratios λ differ from ω by four or more times, the area of application of the nonlinear winding model is governed by only two parameters $\sigma_r^*/\sigma_\theta^0$ and $\beta = \lambda$. In Fig. 8.12 the respective areas for the winding onto a rigid mandrel are given.

8.3 MECHANICS OF POSTWINDING TECHNOLOGICAL STAGES

8.3.1 A Linearly Thermoelastic Problem for an Anisotropic Ring

To understand the basic features relevant to heat build-up and cooling it is useful to analyze in detail the simplest linearly elastic problem for a cylindrically orthotropic ring [34-39]*. Ther-

* Presentation of this section is in keeping with the papers by V. V. Bolotin and K. S. Bolotina [34, 35].

moelastic stresses are mainly caused by the fact that if the strains of thermal expansion do not satisfy the kinematic restrictions extra strains appear associated with the stresses and of such magnitude that the overall strains satisfy the restrictions. For a ring, the equation of strain compatibility (7) serves as such a restriction. Substitution of Duhamel-Neumann's law

$$\begin{aligned} \varepsilon_r &= \alpha_r \Delta T + a_{rr}\sigma_r + a_{r\theta}\sigma_\theta \\ \varepsilon_\theta &= \alpha_\theta \Delta T + a_{\theta r}\sigma_r + a_{\theta\theta}\sigma_\theta, \\ a_{r\theta} &= a_{\theta r} \end{aligned} \tag{22}$$

into the equation of strain compatibility (7) with the subsequent elimination of σ_θ by means of the equilibrium equation (5) leads to

$$\rho^2 \frac{d^2\sigma_r}{d\rho^2} + 3\rho \frac{d\sigma_r}{d\rho} + (1-\beta^2)\sigma_r + \frac{(\alpha_\theta - \alpha_r)\Delta T}{a_{\theta\theta}} + \rho \frac{d(\alpha_\theta \Delta T)}{d\rho} = 0 \tag{23}$$

As a rule, the temperature field early in the process and at its end is uniform, i.e. $\Delta T = \text{const}$. For a homogeneous ring, the equation (23) is solved as follows:

$$\sigma_r = C_1\rho^{\beta-1} + C_2\rho^{-\beta-1} + D \tag{24}$$

where

$$D = (\alpha_\theta - \alpha_r)\,\Delta T/(a_{rr} - a_{\theta\theta}) \tag{25}$$

By substituting (24) into the equilibrium equation (5) the formula for circumferential stresses is obtained

$$\sigma_\theta = C_1\beta\rho^{\beta-1} - C_2\beta\rho^{-\beta-1} + D \tag{26}$$

It follows from (24), (26), and (22) that the displacements are expressed as

$$u_r = a_{\theta\theta}(\beta - \nu_{r\theta})\,C_1\rho^\beta - a_{\theta\theta}(\beta + \nu_{r\theta})\,C_2\rho^{-\beta} + a_{\theta\theta}(1 - \nu_{r\theta})\,D \tag{27}$$

Let us consider two sets of boundary conditions:

$$\begin{aligned} &\text{(a)}\ \sigma_r = 0 \text{ at } \rho = b,\ \sigma_r = 0 \text{ at } \rho = 1 \\ &\text{(b)}\ \sigma_r = 0 \text{ at } \rho = b,\ \sigma_\theta = \sigma_r(\gamma + \nu_{r\theta}) + E_\theta(\alpha_m - \alpha_\theta)\Delta T \\ &\qquad \text{at } \rho = 1 \end{aligned} \tag{28}$$

corresponding to (a) free or (b) simultaneous with the mandrel heating or cooling. Here, α_m is a complex coefficient covering the thermophysical and elastic properties of the mandrel and its dimensions, and is being equal to the ratio of translation of the mandrel outer surface (in fractions of its outer radius, i.e. the inner radius of the

product) to the temperature difference causing the translation. For an isotropic ring mandrel, α_m coincides with the thermal expansion coefficient of the mandrel material (provided there is a uniform temperature field in the mandrel body). The following constants correspond to the boundary conditions (28)

$$\text{(a)}\quad C_1 = D\frac{1-b^{\beta+1}}{b^{2\beta}-1}, \qquad C_2 = D\frac{b^{\beta+1}-b^{2\beta}}{b^{2\beta}-1}$$

$$\text{(b)}\quad C_1 = -\frac{D(\psi+\eta b^{\beta+1})+\zeta}{\eta b^{2\beta}+1}, \qquad C_2 = \frac{D(\psi-b^{1-\beta})+\zeta}{\eta b^{2\beta}+1}b^{2\beta} \tag{29}$$

where η is determined by (10) while ψ and ζ from

$$\psi = \frac{1-\gamma-\nu_{r\theta}}{\beta-\gamma-\nu_{r\theta}}$$

$$\zeta = \frac{E_\theta(\alpha_\theta-\alpha_m)\Delta T}{\beta-\gamma-\nu_{r\theta}} \tag{30}$$

Let us analyze the relationships obtained. In the case of free cooling (heating) the maximum radial stresses are attained on the radius

$$\rho^* = b^{1/2}\left[\frac{b^\beta-b}{b^{\beta+1}-1}\,\frac{\beta+1}{\beta-1}\right]^{1/2\beta} \tag{31}$$

The level of thermoelastic stresses increases with thickness. In rings with very thick walls (at $b \to \infty$) the maximum stresses are

$$\sigma_{r\,\max} = D, \quad \sigma_{\theta\,\max}(1) = D(1+\beta)$$

$$\sigma_{\theta\,\max}(b) = D(1-\beta) \tag{32}$$

In contrast to isotropic rings, the stresses are generated by uniform variation in temperature. On cooling, the radial stresses are tensile, on heating—compressive. The level of radial tensile stresses, as follows from (32) and (25), may exceed the ultimate transverse tensile strength. In thick-walled rings, on free cooling-heating, the displacements of the inner and outer ring surfaces have opposite signs.

Similar limiting estimates in the case of joint (together with the mandrel) thermoelastic deformation have the following form

$$\sigma_{r\,\max}(1) = \frac{E_\theta(\alpha_\theta-\alpha_m)\Delta T}{\beta+\gamma+\nu_{r\theta}} + \frac{D(1+\beta)}{\beta+\gamma+\nu_{r\theta}}$$

$$\sigma_{\theta\,\max}(1) = -\frac{\beta E_\theta(\alpha_\theta-\alpha_m)\Delta T}{\beta+\gamma+\nu_{r\theta}} + \frac{D(1+\beta)(\gamma+\nu_{r\theta})}{\beta+\gamma+\nu_{r\theta}} \tag{33}$$

$$\sigma_{\theta\,\max}(b) = D(1-\beta)$$

Note the important role of the term associated with the difference in coefficients of linear thermal expansion.

8.3.2 A Variant of the Theory of Initial Stresses

With winding of a preheated tape onto a preheated mandrel the stage of preheating is eliminated from the design scheme. The invariability of mandrel pressure during polymerization (Fig. 8.1) allows us to assume that the stress state does not vary in this stage [35]. Therefore, the stresses on the basis of the hypothesis about the heredity of the stress state can be considered a sum of three constituents: stresses brought about during winding (Section 8.2), stresses resulting from simultaneous cooling of the product and the mandrel (Section 8.3.1), and stresses as a result of relieving the final pressure on the mandrel:

$$\sigma_r = \frac{q_m}{b^{2\beta}-1}\left(\rho^{\beta-1} - b^{2\beta}\rho^{-\beta-1}\right)$$
$$\sigma_\theta = \frac{\beta q_m}{b^{2\beta}-1}\left(\rho^{\beta-1} + b^{2\beta}\rho^{-\beta-1}\right) \qquad (34)$$

where q_m is the negative pressure, equal to the sum of the postwinding stress σ_r (1, b) and the stress σ_r (1) caused by simultaneous cooling of the product and the mandrel and calculated by (24) and (29).

To calculate the most popular manufacturing version of winding of an unheated tape onto a cold mandrel, the stage of heat buildup must be considered. The theoretical description of the process of heat buildup is complicated by the fact that mere consideration of the effects of elasticity and thermal expansion leads to results directly opposed to experimental ones: on heat buildup, resulting from a higher coefficient of linear thermal expansion of the mandrel compared to that of the composite, as well as from the anisotropy of linear thermal expansion of the composite (with the rise in temperature the outer radius in the thick-walled rings must move outward, the inner radius—inward) pressure on the mandrel should increase. In practice, however, a significant fall is observed (Fig. 8.1).

This contradiction can be explained only by neglecting a sharp increase in the deformability of composites with a rise in temperature. In [3] an approach has been proposed allowing the effect of variation in the radial Young's modulus E_r (radial compliance a_{rr}) on stress-strain state to be taken into account. The free strain ε_r^0 is presented as a sum of the thermal strain and that caused by variation in a_{rr} from its initial value a_{rr} (T_1), to its finite one a_{rr} (T_2):

$$\varepsilon_r^0 = \alpha_r (T_2 - T_1) + \sigma_r (T_1)\,[a_{rr}(T_2) - a_{rr}(T_1)] \qquad (35)$$

where σ_r (T_1) is the postwinding stress (before the jump of a_{rr}).

The use of Hooke's law (for stress increments caused by heat buildup)

$$\Delta\varepsilon_r = \Delta\varepsilon_r^0 - a_{rr}(T_2)\,\Delta\sigma_r$$
$$\Delta\varepsilon_\theta = \alpha_\theta \Delta T + a_{\theta\theta}\Delta\sigma_\theta \tag{36}$$

by taking into consideration expression (35) in the problem about heating of a ring connected with the mandrel yields

$$\Delta\sigma_r = \frac{(\alpha_m - \alpha_\theta)\,\Delta T}{a_{\theta\theta}(\varkappa - \gamma - \nu_{r\theta})} \frac{\rho^{\varkappa-1} - b^{2\varkappa}\rho^{-\varkappa-1}}{\eta b^{2\varkappa}+1} + \frac{Y(b)\,(\eta\rho^{\varkappa-1}+\rho^{-\varkappa-1})}{2\varkappa\,(\eta b^{2\varkappa}+1)} - \frac{Y(\rho)}{2\varkappa\rho^{\varkappa+1}}$$
$$\Delta\sigma_\theta = \frac{(\alpha_m - \alpha_\theta)\,\Delta T\varkappa}{a_{\theta\theta}\,(\varkappa - \gamma - \nu_{r\theta})} \frac{\rho^{\varkappa-1} + b^{2\varkappa}\rho^{-\varkappa-1}}{\eta b^{2\varkappa}+1} + \frac{Y(b)\,(\eta\rho^{\varkappa-1}-\rho^{-\varkappa-1})}{2\,(\eta b^{2\varkappa}+1)} + \frac{Z(\rho)}{2\rho^{\varkappa+1}} \tag{37}$$

where

$$Y(\rho) = \int_1^\rho [(\alpha_r - \alpha_\theta)\,\Delta T/a_{\theta\theta} + (\varkappa^2 - \mu^2)\,\sigma_r(\xi)]\,(\xi^\varkappa - \rho^{2\varkappa}\xi^{-\varkappa})\,d\xi$$

$$Z(\rho) = \int_1^\rho [(\alpha_r - \alpha_\theta)\,\Delta T/a_{\theta\theta} + (\varkappa^2 - \mu^2)\,\sigma_r(\xi)]\,(\xi^\varkappa + \rho^{2\varkappa}\xi^{-\varkappa})\,d\xi$$

and $\varkappa = \beta(T_2)$, $\mu = \beta(T_1)$, $\eta = \eta(\varkappa)$

The terms describing Poisson's effect have been omitted because they cancel themselves out for a ring.

Polymerization and cooling may be described by the same relations as those for the heat buildup, with the exception that instead of thermal shrinkage $\alpha\Delta T$ physicochemical shrinkage ε^* enters the relations for the polymerization process.

The use of the above approach allows the requirement of continuous variation to be satisfied not only of stresses but also of strains in models of production processes. More stringent and also more complex variants of the theory of initial stresses are given in [4-6 and 40-42].

8.3.3 Experimental Data on Initial Stresses

Let us consider the diagrams of initial stresses σ_r^i (Fig. 8.13) for thick-walled glass-fiber reinforced plastic (GFRP) and carbon-fiber reinforced plastic (CFRP) rings [43, 44]. Those stresses are dangerous because they are of an order of transverse tensile strength.

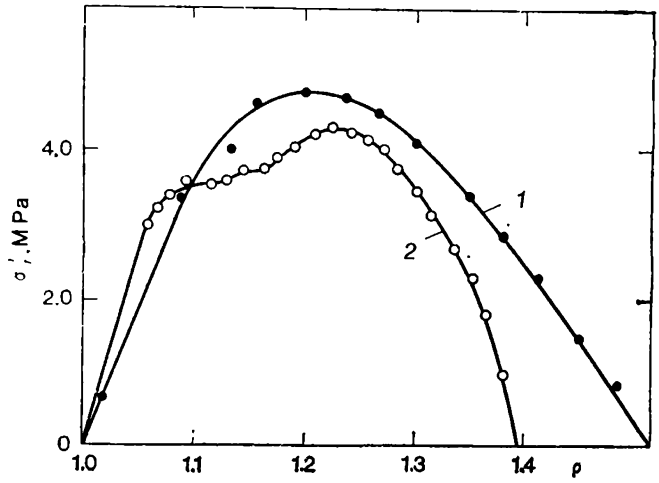

Fig. 8.13 Diagrams of initial stresses in (*1*) GFRP rings [43] and (*2*) CFRP rings [44]. The circles are experimental values

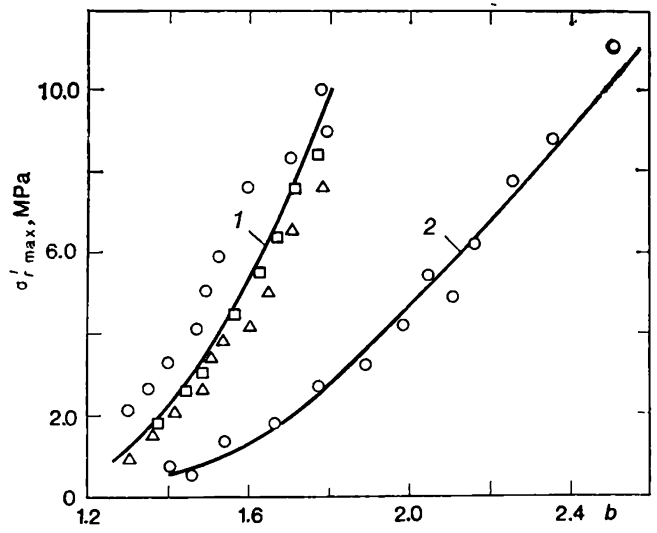

Fig. 8.14 The effect of relative ring dimensions on $\sigma^i_{r\,max}$:

1—under constant tension; *2*—under increasing tension. The circles, squares and triangles are experimental values [45]

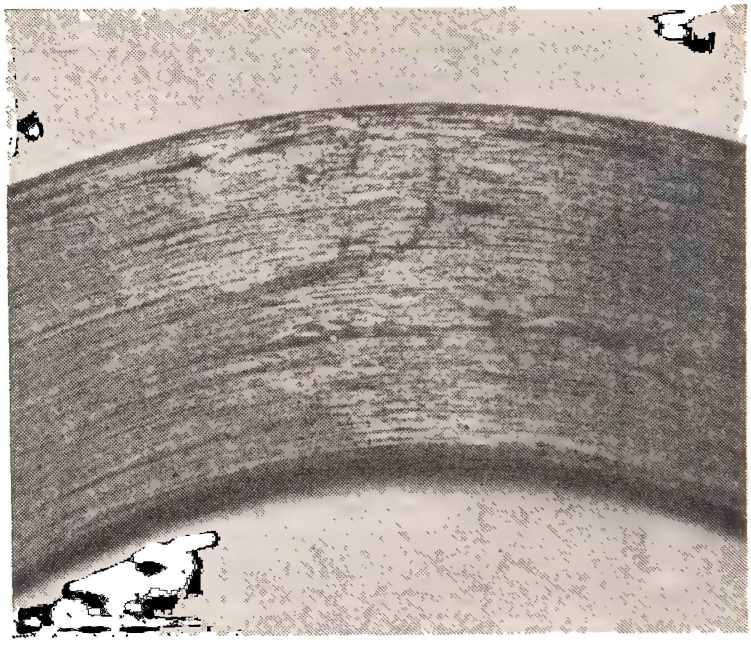

Fig. 8.15 Cracks in a CFRP ring formed upon cooling [44]

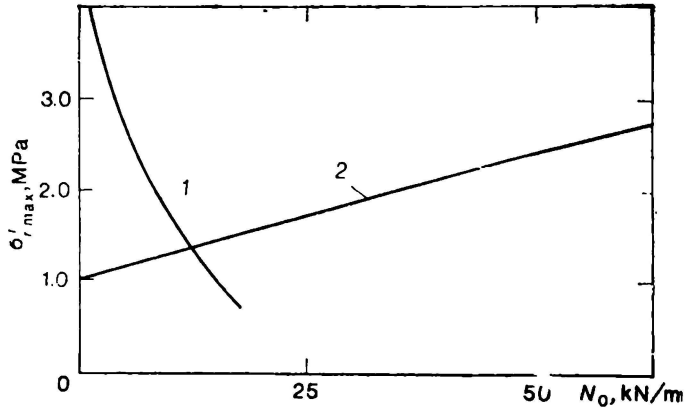

Fig. 8.16 The effect of tension during winding N_0 on $\sigma^i_{r\,max}$ for various GFRP rings:

curve *1*—winding of preheated tape onto preheated mandrel, $b = 1.6$ [46]; curve *2*—winding of cold tape onto cold mandrel, $b = 1.185$ [43]

Initial stresses sharply increase (Fig. 8.14) with an increase in the relative thickness of the products [45]. As a rule, this results in cracking of the products, whose wall thickness is comparable to the inner radius (Fig. 8.15).

Let us evaluate the experimental results of the effect of technological factors on initial stresses. The effect of tensioning is extremely marked. A rise in tension may lead to a substantial decrease or increase in initial stresses (Fig. 8.16), depending on the ring thickness, material properties and the adopted manufacturing method. The law of tension variation in the winding process is crucial. Experiments have shown (Fig. 8.17) that the winding under increasing tension allows a considerable decrease in the level of initial stresses. The curing temperature (Fig. 8.18) and the coefficient of linear thermal expansion of the mandrel material (Fig. 8.19) also affect the initial stresses. Decrease in curing temperature and the use of mandrels with low coefficients of linear thermal expansion result in lower initial stresses.

Thus the experimental results are in total qualitative accord with theoretical conclusions.

8.4 METHODS TO GOVERN INITIAL STRESSES

8.4.1 Programmed Winding

The solution of the direct problem of linear winding mechanics under varying tension has shown that tension variation during winding is an effective means of governing stress diagrams in wound products and, consequently, in the finished product. An inverse problem—formulation of the law of tension variation during winding to govern stresses—is the subject of programmed winding [48].

From (12) one can directly obtain the formula to relate the sought (postwinding) diagrams of circumferential σ_θ and radial σ_r stresses, corresponding to one another through satisfying the equilibrium equation, with the programmed winding σ_θ^0:

$$\sigma_\theta^0(\rho) = \sigma_\theta(\rho, b) - \beta\left[(\eta\rho^{2\beta} - 1)/(\eta\rho^{2\beta} + 1)\right] - \sigma_r(\rho, b) \qquad (38)$$

The following restrictions must be met: the stresses σ_θ in any circuit should not be compressive (to prevent fiber distortion) and the tension σ_θ^0 should not exceed the strength of the material being wound. These are the restrictions which put the upper bound of the range of relative and absolute dimensions of wound products within which tensioning can be effectively employed for governing initial stresses [49].

The interrelation between postwinding stresses and the resulting diagrams of initial stresses for a product is established by the rela-

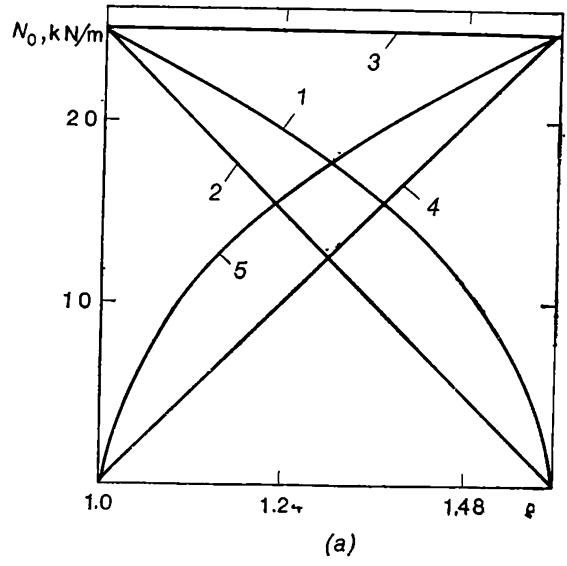

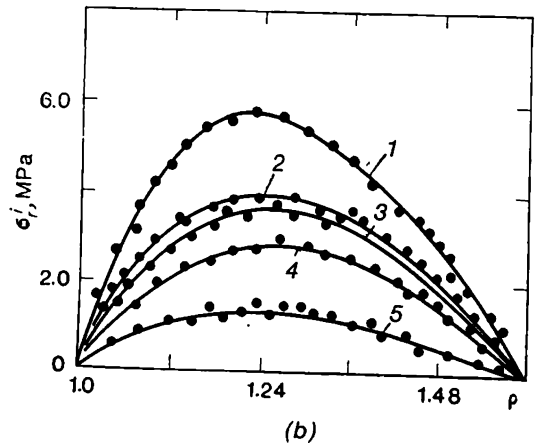

Fig. 8.17 The effect of variation in tension (*a*) on σ_r^i diagram (*b*). The circles are experimental values [45]

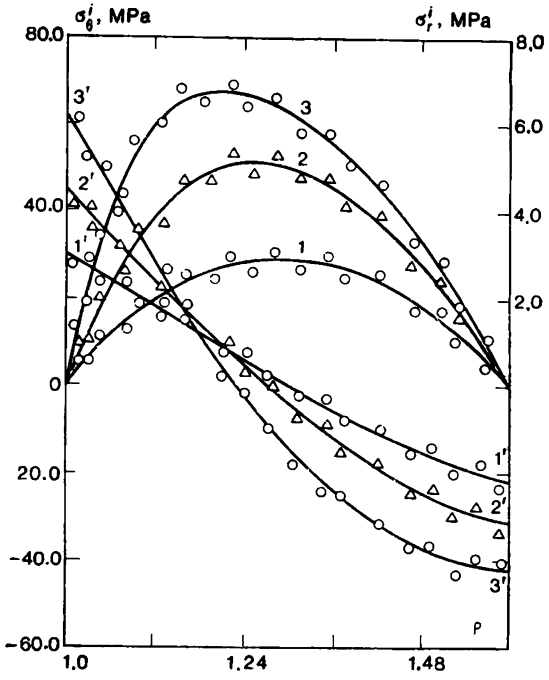

Fig. 8.18 Diagrams of initial stresses σ_r^i (curves *1-3*) and σ_θ^i (curves 1'-3') for GFRP rings at various curing temperatures:
1 and *1'*—at 110°C; *2* and *2'*—at 130°C; *3* and *3'*—at 150°C. The circles and triangles are experimental values [47]

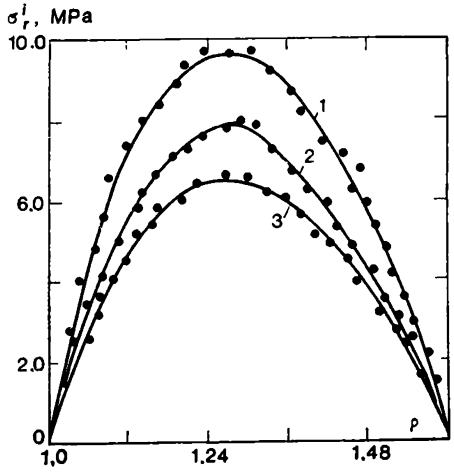

Fig. 8.19 The effect of mandrel material on σ_r^0 diagram:
1—aluminium; *2*—steel; *3*—combined mandrel (steel + GFRP). The circles are experimental values [45]

tions given in Section 8.3. Winding programs have been developed by means of a search procedure based on a piecewise linear model or the

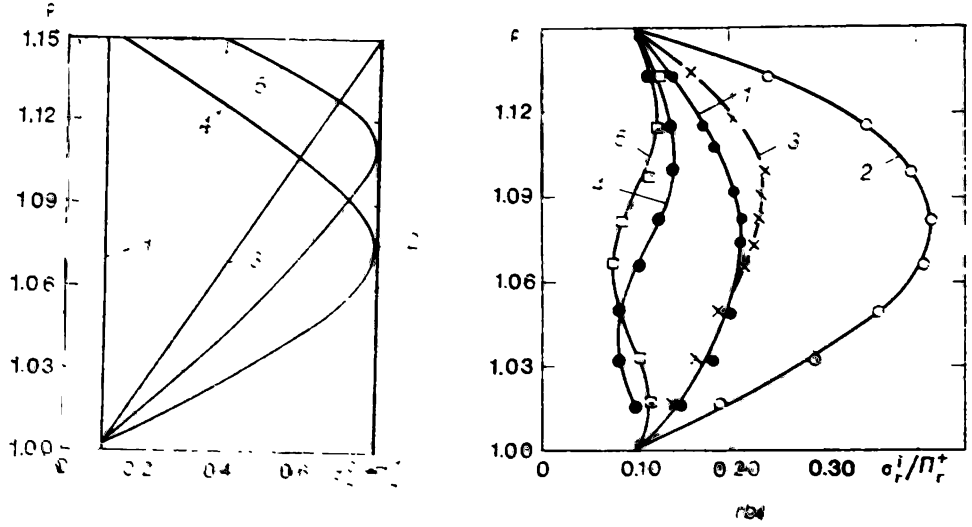

Fig. 8.20 Different winding programs for GFRP rings (a) and the corresponding initial stress diagrams σ_r^i (b). Π_φ^+ and Π_r^+ are ultimate tensile strengths in the circumferential and radial directions. The circles, squares and crosses are experimental values [51]

method of a small parameter at higher order derivative [50]. The efficiency of the programmed winding (Fig. 8.20) has been experimentally confirmed [51].

8.4.2 Pressing and Rolling

During the fabrication of products of large dimensions, the pressure built up in the tension winding process is insufficient for obtaining a monolithic material. Extra compaction may be produced by various means. Postwinding pressing is a combination of active loading and unloading (Fig. 8.21). The inducing of radial stresses in the product, substantially exceeding σ_r^*, is irrational, because it does not improve the level of compaction. Calculation of stresses induced during pressing is based on a piecewise linear winding model. Pressing may be accomplished under internal pressure, external one or a combination of both [52]. With pressing under internal pressure, it is necessary to reckon with the possible overloading of inner circuits because of high circumferential stresses defined by the applied pressure, relative wall thickness and anisotropy ratio. For the same reason, pressing under external pressure may lead to

fiber transition from the region of pretensioning into that of compression with subsequent buckling.

As shown by calculation, pressing under external pressure and under a combination of external and internal pressures is of practical significance only for products of small relative thickness wound onto a rigid mandrel. The products to be pressed must be wound under maximum possible tension (in particular, outer circuits), but pressed under low pressure. Therefore, in the fabrication of products of

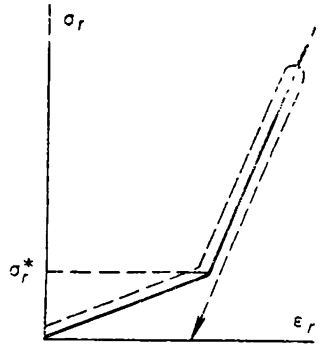

Fig. 8.21 Schematic diagram "loading-unloading" for prepreg layers under transverse compression

large thickness, it is reasonable to alternate the winding of a part of the circuits with their pressing.

Technologically, the use of rolling to achieve continuous extra compaction is more desirable [53-55]. Since pressure in the contact zone is high, the solution of an elastic contact problem may be employed in the calculations. Calculations and experiments show that it is reasonable to decrease the rolling force while increasing the actual thickness of the product. Rolling, in addition to compaction, results in a more uniform distribution of the coefficient of reinforcement over the volume which can be, evidently, ascribed to the opposite directions of local and macroscopic pressure gradients.

8.4.3 Winding with Layer-by-Layer Curing

The basic idea of the method is the same as for layer-by-layer pressing: by decreasing the compliance of wound layers to achieve less contraction of successive layers and also less loss of preliminary tension. With layer-by-layer winding the compliance is reduced as a result of partial or complete cure of a group of wound layers, followed by winding of the next group [56].

An experimental study of layer-by-layer winding has revealed the efficiency of the method in governing initial stresses [45, 56-58]. It

has been emphasized in all the works that it is possible to obtain products with compressive radial initial stresses by layer-by-layer winding. It is extremely important when cracking must be prevented (Fig. 8.22). As the number of layers (cure stages) increases, the process of layer-by-layer winding approaches some ideal final process,

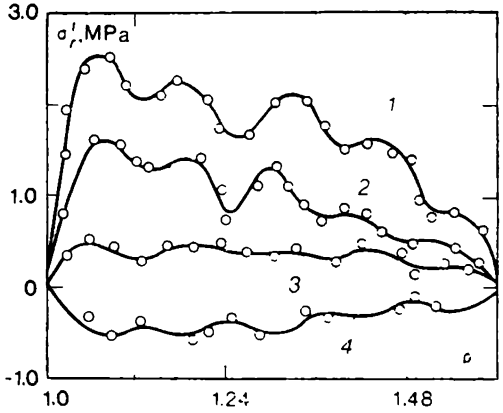

Fig. 8.22 Diagrams of initial stresses σ_r^i for programmed winding with layer-by-layer curing:
1 corresponds to winding program *1* in Fig. 8.17*a*; *2*—to program *2*; *3*—to program *4*; *4*—to program *5*. The circles are experimental values [45]

consisting in winding of a "cured" material. It is reasonable to combine the layer-by-layer winding with the programmed one. Complete or partial periodical curing causes a sharp reduction in output. The programmed winding involves: a search for a minimum number of cure stages ensuring the preset level of initial stresses, the best way of dividing the product thickness into a specified number of layers, and the selection of the tension program of winding.

8.4.4 Governing Initial Stresses at Polymerization and Cooling Stages

In some cases, by correlating the temperature kinetics of transverse strength with the growth kinetics of thermoelastic stresses it is possible to estimate the temperature range, within which either ultimate strength is lower than the stresses or strength-to-stress ratio is lower than the allowable safety factor [4-7, 41, 42, 59], while at final cooling temperature an excessive safety factor is possible. To maintain the integrity of the product at these temperatures technological procedures are used, which allow the tensile stresses to be reduced to a certain safe value.

In [59] it has been proposed to accomplish pressing at critical temperatures so that the overall stresses might reach the desired values.

The pressure is relieved at temperatures when the sum of extra tensile stresses (due to relieving) and thermoelastic radial stresses is lower than the ultimate strength taking into account the specified safety factor.

Based on a theoretical study of the relaxation process of thermoelastic stresses, a conclusion has been drawn in [60] that by either arresting the cooling process or by a stepwise cooling with prolonged exposure at each temperature level it is also possible to reduce thermoelastic stresses. By varying the cooling rate of the inner and outer surface of the product (the inner surface slower and the outer faster) it is possible to develop a temperature gradient, which can substantially improve the diagram of thermal stresses. The method has been treated in [13, 61-66].

The above technological procedures ensure compensation of temperature stresses within the temperature range from polymerization to final cooling yet they do not affect initial stresses. In addition to layer-by-layer winding it has been proposed in [67] to choose the polymerization temperature for each successive layer so that some tensioning would result which could partly compensate for the tensile radial stresses.

8.4.5 Governing Initial Stresses by Variation of Reinforcement Pattern

It follows from an analysis of formula (24) for radial thermal stresses that at high anisotropy of elastic properties ($E_\theta \gg E_r$) the stresses σ_r are proportional to the modulus of elasticity in the radial direction. The method of reducing temperature stresses by means of decreasing the modulus of elasticity in the radial direction can be based on this analysis. The positive effect of the method greatly depends on how, when reducing E_r, the change in transverse tensile strength is realized. One of the technological means of reducing E_r involves the introduction of thin compliant thermocompensating interlayers [68] between groups of layers. Thereby E_θ is also reduced so that the anisotropy ratio β does not change so abruptly and the effect of variation in β on the stresses σ_r is substantially weaker than that of E_r. The method is equivalent to dividing a ring into a number of thin rings having a weak kinematic coupling. Since a decrease in ring thickness causes an abrupt fall in initial stresses, a certain effect can be achieved. In Fig. 8.23 the diagrams of initial radial stresses for two rings of equal dimensions are presented, one of the rings containing interlayers of compensators. In such a way, the theoretical conclusion has been experimentally confirmed.

The relationship between thermal stresses and radial strength is weakened also in the case when, by varying the reinforcement pattern, the growth in strength in the radial direction Π_r^+ turns out to

be greater than the rise in the modulus of elasticity E_r. A similar effect may be achieved by additional radial reinforcing with short needles oriented along the radius by means of the electrostatic or magnetic field [69]. Since the action of these fields by itself causes an increase in the strength characteristics, the incorporation of small volume fractions of needles results in a substantial rise in the strength. Besides, the anisotropy of the wound prepreg is reduced leading to a more favourable postwinding distribution of radial stresses.

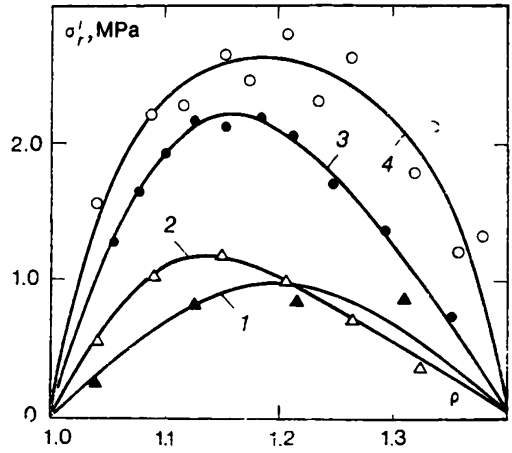

Fig. 8.23 Diagrams of initial radial stresses σ_r^i for GFRP rings with compensators (curves *1* and *2*) and without them (curves *3* and *4*). Cross-ply reinforcement pattern:

curves *1* and *3*—1:1 (0°—1 ply, 90°—1 ply); curves *2* and *4*—5:5 (0°—5 plies, 90°—5 plies). The circles and triangles are experimental values

For the outer part of the product after cooling to be mounted on the inner part, one can employ not only their polymerization at different temperatures, but also fabricate the parts from different composites having various coefficients of linear thermal expansion [70-72].

Radial thermoelastic stresses can equal zero not only in some ideal nonhomogeneous temperature field, when the thermal strains satisfy the equation of strain compatibility (7), but also at a uniform change in temperature, provided that in a cylindrically orthotropic ring the coefficients of linear thermal expansion α_r and α_θ change so as to satisfy that equation [61].

In [73] it is suggested that the required change in coefficients of linear thermal expansion be obtained through technologically easily realizable change in the winding angle φ (ρ) (an angle between the circumferential coordinate and one of the directions of a symmetric layup) with the radius of the wound product. By assuming α_r and α_θ as functions of φ the equation of compatibility of strains (7) fo

$\Delta T = \text{const}$ may be rewritten as

$$\alpha_r(\varphi) - \alpha_\theta(\varphi) = \rho \frac{d\alpha_\theta}{d\varphi} \frac{d\varphi}{d\rho} \tag{39}$$

Using the initial condition at $\varphi = \varphi_i$, $\rho = 1$, it is possible to obtain

$$\rho = \exp\left\{ \int_{\varphi_i}^{\varphi} (d\alpha_\theta/dy) \left[\alpha_r(y) - \alpha_\theta(y)\right]^{-1} dy \right\} \tag{40}$$

The formula defines the function $\rho(\varphi)$ which is inverse to the sought function $\varphi(\rho)$. A numerical analysis has shown that the winding should be performed at an angle φ increasing with the product thickness.

Governing the initial stresses by altering the reinforcement pattern influences simultaneously the load-carrying capacity of the product. This fact should be taken into account in each particular case.

8.5 CONCLUSION

Accordingly, the subdivision of the fabrication process into separate stages, consideration of the prepreg compliance, introduction of a ring model and the hypothesis about the heredity of stress-strain state enabled us to relate parameters of the process—and above all tension—to properties of the finished product, contact pressure on the part to be wound, and a system of initial stresses. Novel technological procedures have been proposed. Among them are: programmed winding, winding with layer-by-layer curing and winding under extra contact pressure, radial reinforcement with short needles, chordwise winding, the use of thermocompensating interlayers, the method of temperature gradients, winding at varying angles, etc. The procedures served as a point of departure for the research in the field of engineering winding mechanics. The fields of application of thick-walled wound products are constantly extending. It is necessary to continue the research within the framework of the ring model towards more detailed studies, taking into account the factors which have so far been ignored in formulation of the existing theory. In particular, it is necessary to determine the role of creep, filtration, finiteness of strains, physicochemical shrinkage, the change in deformability at all stages of the fabrication process. The research must be aimed at an evaluation of the scope of applicability of the theory presented here thus allowing a transition from the ring model to the design of products with a more complex configuration. Technological methods of governing the integrity and load-carrying capacity of wound products should be further evolved.

References

1. Rosato, D.V., Grove, C.S., *Filament Winding*, Interscience Publishers, New York, 1964.
2. Rosato, D.V., in: *Handbook of Fiberglass and Advanced Plastic Composites*, Van Nostrand Reinhold, New York, 1969, pp. 1-19.
3. Biderman, V.L., Dimitrienko, I.P., Polyakov, V.I., and Sukhova, N.A., *Mekh. polimerov*, **5**, 892-898 (1965).
4. Bolotin, V.V., and Novichkov, Yu.N., *Mechanics of Multilayered Structures*, Mashinostroyenie, Moscow, 1980 (in Russian).
5. Bolotin, V.V., Vorontsov, A.N., and Murzakhanov, R.Kh., *Mekh. komposit. materialov*, **3**, 500-508 (1980).
6. Bolotin, V.V., *Mekh. polimerov*, **3**, 529-540 (1972).
7. Bolotin, V.V., *Mekh. polimerov*, **1**, 126-133 (1975).
8. Bolotin, V.V., Gol'denblat, I.I., and Smirnov, A.F., *Mechanics of Structures. Present State and Prospects*, Stroiizdat, Moscow, 1972 (in Russian).
9. Elpat'evskii, A.N., and Vasil'ev, V.V., *Strength of Cylindrical Shells of Reinforced Materials*, Mashinostroyenie, Moscow, 1972 (in Russian).
10. Obraztsov, I.F., Vasil'ev, V.V., and Bunakov, V.A. *Optimum Design of Composite Shells of Revolution*, Mashinostroyenie, Moscow, 1977 (in Russian).
11. Mitkevich, A.B., and Protasov, V.D., *Mekh. polimerov*, **6**, 983-987 (1975).
12. Protasov, V.D., Ermolenko, A.F., Filipenko, A.A., and Dimitrienko, I.P., *Mekh. polimerov*, **3**, 443-451 (1978).
13. Isakov, Yu.A., Filipenko, A.A., and Protasov, V.D., *Mekh. polimerov*, **2**, 220-224 (1977).
14. Kharchenko, E.F., Protasov, V.D., Filipenko, A.A., and Polyakov, V.L., *Mekh. polimerov*, **3**, 439-444 (1977).
15. Blagonadezhin, V.L., Varushkin, Ye.M., and Protasov, V.D., *Mekh. komposit. materialov*, **4**, 634-640 (1979).
16. Rosenberg, B.A., and Enikolopyan, N.S., *Zhurn. Vsesoyuz. khim. obshch. im. D.I. Mendeleyeva*, **3** (23), 298-304 (1978).
17. Tarnopol'skii, Yu.M., and Roze, A.V., *Characteristic Features of Calculation of Reinforced Plastic Parts*, Zinatne, Riga (in Russian).
18. Tarnopol'skii, Yu.M., Beil', A.I., and Portnov, G.G., *Izv. Akad. Nauk Latv. SSR*, **12** (401), 80-97 (1980).
19. Tarnopol'skii, Yu.M., in: *Proc. First USA-USSR Symposium on Fracture of Composite Materials*, Sijthoff & Nordhoff, Alphen aan der Rijn (Netherlands), 1979, pp. 159-169.
20. Tarnopol'skii, Yu.M., in: *ICCM*-75, AIME, New York, 1976, vol. I, pp. 221-247.
21. Tarnopol'skii, Yu.M., and Kintsis, T.J., *Static Methods of Testing Reinforced Plastics*, 2nd revised edition, Khimia, Moscow, 1975 (in Russian).
22. Brivmanis, R.E., *Mekh. polimerov*, **I**, 123-129 (1966).
23. Tarnopol'skii, Yu.M., and Portnov, G.G., *Mekh. polimerov*, **2**, 278-284 (1966).
24. Brivmanis, R.E., and Tilyuk, A.G., *Mekh. polimerov*, **5**, 953-956 (1970).
25. Portnov, G.G., and Beil', A.I., *Mekh. polimerov*, **2**, 231-240 (1977).
26. Abibov, A.L., Bunakov, V.A., Kopeikin, V.N., and Kondratenko, R.M., *Mekh. polimerov*, **1**, 162-164 (1973).
27. Lekhnitskii, S.G., *Anisotropic Plates*, Gordon and Breach, New York, 1966.
28. Koval'skii, B.S., *Doklady Akad. Nauk SSSR*, **3** (24), 429-432 (1950).
29. Vasil'ev, V.V., *Mekh. polimerov*, **6**, 1069-1074 (1969).
30. Brivmanis, R.E., and Portnov, G.G., *Electrotekhnika*, **3**, 46-48 (1968).
31. Brivmanis, R.E., and Gaganov, A.K., *Winding Structural Elements in Electrical Machines and Apparatus*, Energia, Moscow, 1971 (in Russian).

32. Bokin, M.I., Yegorov, L.A., Meshkova, R.I., Stal', S.M., and Sinitskii, V.A. *Mekh. polimerov*, 5, 938-940 (1972).
33. Blagonadezhin, V.L., Mishenkov, G.V., and Perevozchikov, V.G., in: *Trudy MEI*, Moscow, 74, 133-138 (1970).
34. Bolotin, V.V., and Bolotina, K.S., *Mekh. polimerov*, 1, 136-141 (1967).
35. Bolotin, V.V., and Bolotina, K.S., *Mekh. polimerov*, 1, 134-139 (1969).
36. Nowinski, J., and Olszak, W., *Arch. mechaniki stosowanej*, 2 (5), 221-236 (1953).
37. Uzdalyev, A.I., *Izv. VUZov, Stroitel'stvo i arkhitektura*, 1, 30-34 (1960).
38. Sobolevskii, V.M., *Trudy Akad. Nauk BSSR, ser. fiz-tekh. nauk*, 3, 17-22 (1962).
39. Liu, C.Y., and Chamis, C.C., in: *Proc. 20th Anniversary Techn. Conf. SPI, Reinforced Plastics Division*, Chicago, 1965, Section 5-D, pp. 1-10.
40. Bolotin, V.V., in: *Trudy MEI*, Moscow, 101, 7-14 (1972).
41. Bolotin, V.V., and Bolotina, K.S., in: *Strength of Materials and Structures*, Naukova dumka, Kiev, 1975, pp. 231-239 (in Russian).
42. Bolotin, V.V., and Vorontsov, A.N., *Mekh. polimerov*, 5, 790-795 (1976).
43. Portnov, G.G., Goryushkin, V.A., and Tilyuk, A.G., *Mekh. polimerov*, 3, 505-511 (1969).
44. Tarnopol'skii, Yu.M., Portnov, G.G., Spridzans, Yu.B., and Bulmanis, V.N., *Mekh. polimerov*, 4, 673-683 (1973).
45. Varushkin, Ye.M., Polyakov, V.I., and Lapin, Yu.L., *Mekh. polimerov*, 1, 75-80 (1972).
46. Varushkin, Ye.M., *Khim. i neft. mashinostroyenie*, 11, 8-10 (1972).
47. Varushkin, Ye.M., *Mekh. polimerov*, 6, 1040-1046 (1971).
48. Tarnopol'skii, Yu.M., and Portnov, G.G., *Mekh. polimerov*, 1, 48-53 (1970).
49. Ochan, M.Yu., *Mekh. polimerov*, 6, 1011-1020 (1975).
50. Ochan, M.Yu., *Mekh. polimerov*, 6, 987-993 (1977).
51. Portnov, G.G., and Spridzans, Yu.B., *Mekh. polimerov*, 2, 361-364 (1971).
52. Polyakov, V.I., and Spridzans, Yu.B., *Mekh. polimerov*, 5, 793-796 (1972).
53. Blagonadezhin, V.L., and Mezentsev, N.S., *Trudy MEI*, Moscow, 185, 54-60 (1974).
54. Blagonadezhin, V.L., and Mezentsev, N.S., *Mekh. polimerov*, 6, 1043-1047 (1976).
55. Stal', S.M., Egorov, L.A., and Ivanov, V.K., in: *Trudy TsNIITS*, Leningrad, 138, 18-30, 1974.
56. Tarnopol'skii, Yu.M., Portnov, G.G., and Spridzans, Yu.B., *Mekh. polimerov*, 4, 640-645 (1972).
57. Blagonadezhin, V.L., and Perevozchikov, V.G., *Mekh. polimerov*, 1, 174-176 (1972).
58. Indenbaum, V.M., and Perevozchikov, V.G., *Mekh. polimerov*, 2, 284-289 (1972).
59. Rabotnov, Yu.N., and Ekel'chik, V.S., *Mekh. polimerov*, 6, 1095-1098 (1975).
60. Ogil'ko, T.F., *Mekh. polimerov*, 5, 949-951 (1974).
61. Birger, B.I., *Izv. Akad. Nauk SSSR, Mekh. tverd. tela*, 1, 92-94 (1971).
62. Birger, B.I., and Baranov, V.L., *Mekh. polimerov*, 2, 310-314 (1972).
63. Afanas'ev, Yu.A., Ekel'chik, V.S., and Kostritskii, S.N., *Mekh. komposit. materialov*, 4, 651-660 (1980).
64. Sborovskii, A.K., Bugakov, I.I., Ekel'chik, V.S., and Kostritskii, S.N., in: *GFRP Properties and Control Methods in Ship Building*, Issue 3, Sudostroyenie, Leningrad, 1974, pp. 17-21 (in Russian).
65. Bakharev, S.P., and Mirkin, M.A., *Mekh. polimerov*, 6, 1118-1121 (1978).
66. Tomashevskii, V.T., Naumov, V.N., and Shalygin, V.N., in: *Polymers in Machine Building*, Perm', 1977, pp. 10-17 (in Russian).
67. Shalygin, V.N., and Naumov, V.N., *Sb. Trudov Perm. Politekh. Inst.*, Perm', 127, 127-135 (1973).

68. Indenbaum, V.M., *Trudy MEI*, Moscow, **164**, 81-86 (1973).
69. Zhmud', N.P., Petrov, V.Yu., and Shalygin, V.N., *Mekh. polimerov*, **2**, 226-230 (1978).
70. Blagonadezhin, V.L., Mezentsev, N.S., Merkulov, V.D., and Polyakov, V.L., *Trudy MEI*, Moscow, **280**, 43-46 (1976).
71. Blagonadezhin, V.L., Perevozchikov, V.G., Merkulov, V.D., and Polyakov, V.L., *Mekh. polimerov*, **6**, 996-1004 (1975).
72. Dimitrienko, I.P., Filipenko, A.A., and Protasov, V.D., *Mekh. polimerov*, **4**, 681-686 (1976).
73. Beil', A.I., Portnov, G.G., Sanina, I.V., and Yakushin, V.A., *Mekh. komposit. materialov*, **6**, 1068-1075 (1980).

9 Theory of Composite Shells

V. V. Vasil'ev, *D. Sc. (Eng.)*

9.1 INTRODUCTION

Much attention is now being paid to the problem of the improvement of the classical theory of shells and it is by and large related to the necessity of designing structures of up-to-date composite materials. It is well-known that composite shells differ from metal ones in a number of ways, including: (1) anisotropy of the composite mechanical properties; (2) heterogeneity of the structure through its thickness; (3) low rigidity relative to shear and normal transverse stresses. For thick-walled shells the variation of curvature through the thickness is also of substantial importance.

Various modifications in the theory of laminated shells are generally performed by reducing the three-dimensional problem of elasticity theory to the two-dimensional one using mathematical means based either on an assumption of the existence of a small parameter—the relative shell thickness, or of ad hoc hypotheses defining the distribution of displacements or stresses through the thickness.

The simplest approach is based on the introduction of the classical Kirchhoff-Love hypotheses for a system of layers corresponding, essentially, to an assumption of the infinitely high transverse shear and normal rigidity of the composite. The shell thickness is assumed, as a rule, to be small. This approach allows the construction of a classical theory of anisotropic laminated shells [1, 2] used to solve a wide variety of applied problems. The theory of laminated shells based on the Kirchhoff-Love hypotheses and valid for shells of arbitrary thickness is presented in [3].

As noted earlier, the low transverse rigidity of laminated composites requires refinements to be made to the classical theory assuming infinitely high rigidity. Most refinements to the theory are constructed in application to thin orthotropic shells homogeneous through the thickness. These theories are based on the hypothesis of normal strain absence [4, 5], a combination of this hypothesis with the prescribed law of transverse shear stress distribution [1], or with the averaging of shear strain through the thickness [6, 7, 8] and also expansion of the solutions into finite series in respect to the normal coordinate. A salient feature of the approach under consideration as applied to laminated shells lies in the fact that the order of the solv-

ing set of equations does not depend on the number of layers. In this, the formulation of hypotheses unified for a system of layers requires the fulfilment of static and kinematic conditions of layer contact [9].

In case of laminated shells the hypotheses cited can be accepted for each layer with the order of equation set being dependent on the number of layers. The modifications of the shell theory based on a linear law of displacement distribution through the thickness of each layer are presented in [4, 10].

A fuller analysis of the questions under consideration is presented in [3, 11-15].

The present work contains a theory of laminated composite shells based on an interaction procedure to reduce the three-dimensional equations in elasticity to a sequence of two-dimensional equations allowing naturally and with increasing accuracy for variation in the shell curvature and the composite structure through the thickness, as well as shear and normal transverse strains to be taken into account.

9.2 DERIVATION OF GOVERNING EQUATIONS

Let us consider an element of the laminated shell shown in Fig. 9.1 and write the starting relations of elasticity theory in the orthogonal curvilinear coordinates $(\alpha_1, \alpha_2 \ \alpha_3)$.

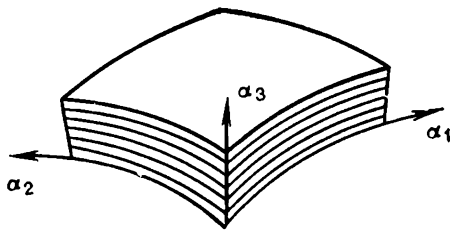

Fig. 9.1 Laminated shell element

The equations of equilibrium are as follows:

$$H_1 (H_2\sigma_1)_{,1} + (H_1^2\tau_{12})_{,2} - H_1H_{2,1}\sigma_2 + (H_1^2H_2\tau_{13})_{,3} + p_1H_1^2H_2 = 0 \ (1, 2) \tag{1}$$

$$(H_1H_2\sigma_3)_{,3} + (H_2\tau_{13})_{,1} + (H_1\tau_{23})_{,2} - H_2H_{1,3}\sigma_1 - H_1H_{2,3}\sigma_2 + p_3H_1H_2 = 0 \tag{2}$$

Here the indices 1, 2, 3 after commas denote differentiation with respect to α_1, α_2, α_3

$$H_1 = A_1 (1 + \alpha_3/R_1) \ (1, 2),$$

A_i and R_i are the coefficients of the first fundamental quadratic form and principal radii of curvature of an initial surface $\alpha_3 = 0$. The notation (1, 2) in equation (1) and further means that the analogous equation with 1 and 2 interchanged is also applicable.

The strain-displacement relations are:

$$\varepsilon_1 = \frac{u_{1,1}}{H_1} + \frac{H_{1,2}u_2}{H_1H_2} + \frac{H_{1,3}u_3}{H_1H_3}\,(1, 2) \tag{3}$$

$$\varepsilon_{12} = \frac{H_1}{H_2}\left(\frac{u_1}{H_1}\right)_{,2} + \frac{H_2}{H_1}\left(\frac{u_2}{H_2}\right)_{,1} \tag{4}$$

$$\varepsilon_3 = u_{3,3},\quad \varepsilon_{13} = H_1\left(\frac{u_1}{H_1}\right)_{,3} + \frac{u_{3,1}}{H_1}\,(1, 2) \tag{5}$$

Neglecting Poisson's ratio through the thickness we shall write the constitutive relations as

$$\sigma_1 = \overline{E}_1(\varepsilon_1 + \mu_{12}\varepsilon_2)\,(1, 2),\qquad \tau_{12} = G_{12}\varepsilon_{12} \tag{6}$$

$$\sigma_3 = E_3\varepsilon_3,\qquad \tau_{13} = G_{13}\varepsilon_{13}\,(1, 2) \tag{7}$$

where $\overline{E}_1 = E_1/(1 - \mu_{12}\mu_{21})$ (1, 2)

The elastic properties in relations (6) and (7) are arbitrary functions of the variable α_3, and for laminated shells they are discontinuous functions of that variable.

To derive the shell theory equations let us perform certain transformations. Integrating with respect to α_3 the first equation in (5) and taking into account the first equation in (7) one obtains

$$u_3 = w(\alpha_1, \alpha_2) + \theta_3 \tag{8}$$

where

$$\theta_3 = \int_0^{\alpha_3} (\sigma_3/E_3)\,d\alpha_3 \tag{9}$$

w is normal displacement of the surface $\alpha_3 = 0$. Integrating the second equation in (5) and taking into account the second equation in (7) and the equations (8), (9) one finds

$$u_1 = \frac{H_1}{A_1}u(\alpha_1, \alpha_2) - \frac{\alpha_3}{A_1}w_{,1} + H_1(\theta_1 - \theta_{31}) \tag{10}$$

$$u_2 = \frac{H_2}{A_2}v(\alpha_1, \alpha_2) - \frac{\alpha_3}{A_2}w_{,2} + H_2(\theta_2 - \theta_{32}) \tag{11}$$

where

$$\theta_1 = \int_0^{\alpha_3} \frac{\tau_{13}}{G_{13}}\frac{d\alpha_3}{H_1}\,(1, 2),\qquad \theta_{31} = \int_0^{\alpha_3} \frac{\theta_{3,1}}{H_1^2}\,d\alpha_3\,(1, 2) \tag{12}$$

u and v are displacements of the surface $\alpha_3 = 0$ in directions α_1 and α_2.

Substituting the displacements (8), (10), (11) into relations (3), (4) and later into (6), one obtains

$$\sigma_1 = F_1(u, v, w) + \Phi_1(\theta_1, \theta_2, \theta_3) \quad (1, 2)$$
$$\tau_{12} = F_{12}(u, v, w) + \Phi_{12}(\theta_1, \theta_2, \theta_3) \tag{13}$$

where

$$F_1 = \overline{E}_1(e_1 + \mu_{12}e_2) \quad (1, 2), \qquad F_{12} = G_{12}e_{12}$$
$$\Phi_1 = \overline{E}_1(t_1 + \mu_{12}t_2) \quad (1, 2), \qquad \Phi_{12} = G_{12}t_{12}$$
$$e_1 = \frac{1}{H_1}\left[\left(\frac{H_1 u}{A_1}\right)_{,1} + \frac{H_{1,2}v}{A_2} + \frac{A_1 w}{R_1}\right] - \frac{\alpha_3}{H_1}\left[\left(\frac{w_{,1}}{A_1}\right)_{,1} + \frac{H_{1,2}w_{,2}}{A_2 H_2}\right] \quad (1, 2)$$
$$e_{12} = \frac{H_1}{H_2}\left(\frac{u}{A_1}\right)_{,2} + \frac{H_2}{H_1}\left(\frac{v}{A_2}\right)_{,1} - \alpha_3\left[\frac{H_1}{H_2}\left(\frac{w_{,1}}{A_1 H_1}\right)_{,2} + \frac{H_2}{H_1}\left(\frac{w_{,2}}{A_2 H_2}\right)_{,1}\right]$$
$$t_1 = \frac{1}{H_1}\left[(H_1\theta_1)_{,1} + H_{1,2}\theta_2 + \frac{A_1}{R_1}\theta_3 - (H_1\theta_{31})_{,1} - H_{1,2}\theta_{32}\right] \quad (1, 2)$$
$$t_{12} = \frac{H_1}{H_2}(\theta_{1,2} - \theta_{31,2}) + \frac{H_2}{H_1}(\theta_{2,1} - \theta_{32,1})$$

In the foregoing equations the notation (1,2) means that a quantity indexed by 2 is obtained from that indexed by 1 via the substitution of 1, 2, u, v by 2, 1, v, u.

Hence the displacements u_1, u_2 and u_3 and also the stresses σ_1, σ_2, τ_{12} are expressed by means of equations (8), (10), (11) and (13) through the three functions of the two variables u (α_1, α_2), v (α_1, α_2), w (α_1, α_2) and the three functions of the three variables θ_i $(\alpha_1, \alpha_2, \alpha_3)$.

Consider the equilibrium equations. Integrating equation (1) with respect to α_3 and taking into account a static boundary condition on the inner surface of the shell $\tau_{13}(\alpha_3 = 0) = q_1^0$ (1, 2) we obtain (index 3 on α is omitted and further it is assumed that $\alpha_3 = \alpha$):

$$H_1^2 H_2 \tau_{13} = A_1^2 A_2 q_1^0 - \int_0^\alpha p_1 H_1^2 H_2\, d\alpha - \int_0^\alpha \mathcal{L}_1(F)\, d\alpha - \int_0^\alpha \mathcal{L}_1(\Phi)\, d\alpha \quad (1, 2) \tag{14}$$

where, for example,

$$\mathcal{L}_1(F) = H_1(H_2 F_1)_{,1} + (H_1^2 F_{12})_{,2} - H_1 H_{2,1} F_2 \quad (1, 2)$$

Integrating equation (2) with respect to α_3 and allowing for a boundary condition $\sigma_3(\alpha_3 = \alpha = 0) = q_3^0$ and relations (14) we have

$$H_1 H_2 \sigma_3 \quad A_1 A_2 q_3^0 - \int_0^\alpha q\, d\alpha + \int_0^\alpha p\, d\alpha - \int_0^\alpha p_3 H_1 H_2\, d\alpha$$
$$+ \int_0^\alpha \mathcal{L}(F)\, d\alpha + \int_0^\alpha \mathcal{L}(\Phi)\, d\alpha \tag{15}$$

where

$$q = \left(\frac{A_1^2 A_2}{H_1^2} q_1^0\right)_{,1} + \left(\frac{A_1 A_2^2}{H_2^2} q_2^0\right)_{,2}$$

$$p = \left(\frac{1}{H_1^2}\int_0^\alpha H_1^2 H_2 p_1 \, d\alpha\right)_{,1} + \left(\frac{1}{H_2^2}\int_0^\alpha H_1 H_2^2 p_2 \, d\alpha\right)_{,2}$$

$$\mathscr{L}(F) = \frac{A_1}{R_1} H_2 F_1 + \frac{A_2}{R_2} H_1 F_2 + \left[\frac{1}{H_1^2}\int_0^\alpha \mathscr{L}_1(F)\, d\alpha\right]_{,1}$$

$$+ \left[\frac{1}{H_2^2}\int_0^\alpha \mathscr{L}_2(F)\, d\alpha\right]_{,2}$$

Let us fulfil the static boundary conditions on the shell outer surface $\alpha = h$ (h is the shell thickness):

$$\tau_{13}(\alpha = h) = q_1^h(1,2), \quad \sigma_3(\alpha = h) = q_3^h \tag{16}$$

Assuming $\alpha = h$ in equations (14) and (15) and allowing for (16) one obtains

$$\int_0^h \mathscr{L}_1(F)\, d\alpha - A_1^2 A_2 q_1^0 + B_1^2 B_2 q_1^h + \int_0^h p_1 H_1^2 H_2 \, d\alpha$$

$$= -\int_0^h \mathscr{L}_1(\Phi)\, d\alpha \,(1,2) \tag{17}$$

$$\int_0^h \mathscr{L}(F)\, d\alpha + A_1 A_2 q_3^0 - B_1 B_2 q_3^h - \int_0^h q\, d\alpha + \int_0^h p\, d\alpha$$

$$- \int_0^h p_3 H_1 H_2 \, d\alpha = -\int_0^h \mathscr{L}(\Phi)\, d\alpha \tag{18}$$

where

$$B_1 = A_1(1 + h/R_1) \quad (1,2)$$

Three two-dimensional equations (17), (18) incorporate as unknowns the three displacements u, v, w of an initial surface and the three functions θ_i entering under the definite integrals through the shell thickness. The functions θ_i are defined by equations (9), (12),

(14), (15) and are of the form

$$\theta_1 = \int_0^\alpha \Big[A_1^2 A_2 q_1^0 - \int_0^\alpha p_1 H_1^2 H_2 \, d\alpha - \int_0^\alpha \mathcal{L}_1(F) \, d\alpha - \int_0^\alpha \mathcal{L}_2(\Phi) \, d\alpha \Big] \frac{d\alpha}{H_1^3 H_2 G_{13}} (1, 2) \tag{19}$$

$$\theta_3 = \int_0^\alpha \Big[A_1 A_2 q_3^0 - \int_0^\alpha q \, d\alpha + \int_0^\alpha p \, d\alpha - \int_0^\alpha p_3 H_1 H_2 \, d\alpha + \int_0^\alpha \mathcal{L}(F) d\alpha + \int_0^\alpha \mathcal{L}(\Phi) \, d\alpha \Big] \frac{d\alpha}{H_1 H_2 E_3} \tag{20}$$

Hence the integro-differential equation system obtained comprises three two-dimensional equations (17), (18) and three three-dimensional equations (19), (20). As the unknown quantities the system contains the three functions u, v, w of two variables and the three functions θ_i of three variables.

To reduce the equations obtained to the two-dimensional equations of the shell theory one should construct the following iteration pattern. Let us take as a first approximation $\theta_i \equiv 0$, which according to (19), (20) corresponds to $G_{13} \to \infty$, $G_{23} \to \infty$, $E_3 \to \infty$. Then the right-hand sides vanish in (17), (18) thus forming an equation set of the shell theory based on Kirchhoff-Love's hypotheses yet allowing a curvature variation through the thickness. Such equations expressed through the forces and moments for a laminated shell are presented in [3]. Introducing an additional assumption of the smallness of the shell thickness, i.e. taking $H_1 \approx B_1 \approx A_1$ (1, 2), one obtains an equation system of the classical theory of orthotropic laminated shells [1] having the eighth order with respect to the variables α_1, α_2.

To construct the next approximations let us substitute θ_i from (19) and (20) into (17) and (18) and transfer into the left-hand side the terms containing the external load and the function $F(u, v, w)$. Letting $\theta_i \equiv 0$ on the right-hand sides of the equations obtained one derives a set of three two-dimensional equations of the second approximation having the 18th order with respect to the variables α_1, α_2. Replacing once more θ_i according to formulas (19), (20) and retaining the terms containing u, v, w one may write a third approximation set, etc.

To illustrate the pattern described we present the governing equations for a rectangular transversally isotropic plate loaded over

a surface $\alpha = h$ by the pressure q. Letting

$$E_1 = E_2 = E, \quad \mu_{12} = \mu_{21} = \mu, \quad G_{12} = E/[2(1+\mu)], \quad \bar{E} = E/(1-\mu^2)$$
$$G_{13} = G_{23} = G_0, \quad E_3 = E_0, \quad R_1^{-1} = R_2^{-1} = 0, \quad q_1^0 = q_1^h = q_2^0 = q_2^h$$
$$= q_3^0 = 0, \quad q_3^h = -q, \quad p_1 = p_2 = p_3 = 0, \quad D = \bar{E}h^3/12$$

one obtains, to the first approximation:

$$D\nabla^4 w = -q$$

to the second,

$$D\,(1 - 0.67\cdot 10^{-3}\lambda\nabla^2 + 0.74\cdot 10^{-4}\eta\nabla^4)\,\nabla^4 w = -q$$

and, to the third,

$$D\,[1 - 0.67\cdot 10^{-3}\lambda\,(1 + 0.028\lambda\nabla^2)\nabla^2$$
$$+ 0.74\cdot 10^{-4}\eta\,(1 + 0.135\lambda\nabla^2 + 0.0148\eta\nabla^4)\nabla^2]\,\nabla^4 w = -q$$

where

$$\lambda = \bar{E}h^2/G_0, \quad \eta = \bar{E}h^4/E_0$$

The general set of equations (17)-(20), even to the first approximation, has a high order and does not allow an analytic solution for shells of arbitrary shape. The most suitable field of application of the equations derived seems to be in the study of shells with Lamé's coefficients being independent of the coordinates α_1, α_2. Such shells include shallow and cylindrical shells. Bearing in mind that cylindrical shells made of composite materials have gained extensive practical application we shall present a detailed version of the governing relations in the cylindrical coordinates.

9.3 A CYLINDRICAL SHELL

Let us consider an element of the laminated orthotropic cylindrical shell (Fig. 9.2). Let us introduce a system of dimensionless coordinates—an axial α_1 and a radial r related to an inner surface radius r_0, as well as a circumferential angle α_2. In this way $0 \leqslant \alpha_1 \leqslant L/r_0$ (L is the shell length), $0 \leqslant \alpha_2 \leqslant 2\pi$, $1 \leqslant r \leqslant s$ ($s = r_h/r_0$, Fig. 9.2).

Thereby expressions for the displacements (8)-(12) take the form:

$$u_3 = w + \theta_3$$
$$u_1 = u - (r-1)\,w_{,1} + \theta_1 - \int_1^r \theta_{3,1}\,dr \tag{21}$$
$$u_2 = vr - (r-1)\,w_{,2} + r\theta_2 - r\int_1^r \theta_{3,2}\,\frac{dr}{r^2}$$

where

$$\theta_1 = \int_1^r (\tau_{13}/G_{13})\, dr\ (1, 2), \qquad \theta_3 = \int_1^r (\sigma_3/E_3)\, dr$$

In (21) u, v, w are the dimensionless displacements related to a radius

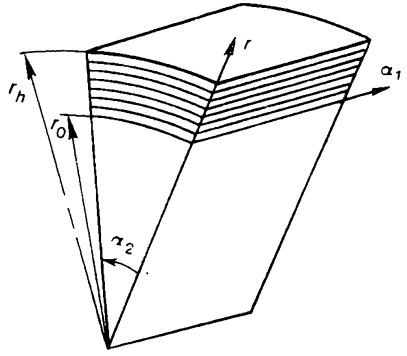

Fig. 9.2 Cylindrical laminated shell element

r_0. The expressions for stresses (13) are written in the form

$$\sigma_1 = \overline{E}_1\left[u_{,1} - (r-1)\, w_{,11} + \mu_{12}\left(\frac{w}{r} + v_{,2} - \frac{r-1}{r}\, w_{,22}\right)\right]$$

$$+ \overline{E}_1\left[\theta_{1,1} - \int_1^r \theta_{3,11}\, dr + \mu_{12}\left(\theta_{2,2} - \int_1^r \theta_{3,22}\frac{dr}{r} + \frac{\theta_3}{r}\right)\right]$$

$$\sigma_2 = \overline{E}_2\left\{v_{,2} + \frac{w}{r} - \frac{r-1}{r}\, w_{,22} + \mu_{21}\left[u_{,1} - (r-1)\, w_{,11}\right]\right\}$$

$$+ \overline{E}_2\left[\theta_{2,2} - \int_1^r \theta_{3,22}\frac{dr}{r} + \frac{\theta_3}{r} + \mu_{21}\left(\theta_{1,1} - \int_1^r \theta_{3,11}\, dr\right)\right]$$

$$\tau_{12} = G_{12}\left(\frac{1}{r}\, u_{,2} + r v_{,1} - \frac{r^2-1}{r}\, w_{,12}\right)$$

$$+ G_{12}\left[\frac{1}{r}\left(\theta_{1,2} - \int_1^r \theta_{3,12}\, dr\right) + r\left(\theta_{2,1} - \int_1^r \theta_{3,12}\frac{dr}{r^2}\right)\right]$$

Two-dimensional equations (17), (18) will be presented in the form

$$\mathcal{L}_{i1}(u) + \mathcal{L}_{i2}(v) + \mathcal{L}_{i3}(w) + \mathcal{L}_{ip}$$

$$= -\mathcal{L}_{i1}(\theta_1) - \mathcal{L}_{i2}(\theta_2) - \mathcal{L}_{i3}(\theta_3) \qquad (i = 1, 2, 3) \qquad (22)$$

where

$$\mathcal{L}_{11}(\ ) = \int_1^s \left[\overline{E}_1 r (\ )_{,11} + G_{12}\frac{1}{r}(\ )_{,22}\right] dr$$

$$\mathcal{L}_{12}(\ ) = \mathcal{L}_{21}(\ ) = \int_1^s (\overline{E}_1\mu_{12} + G_{12})(\ )_{,12}\, r\, dr$$

$$\mathcal{L}_{13}(\ ) = \int_1^s \overline{E}_1\mu_{12}(\ )_{,1}\, dr - \int_1^s \overline{E}_1 r\, dr \int_1^r (\ )_{,111}\, dr$$

$$- \int_1^s G_{12}\frac{dr}{r}\int_1^r (\ )_{,122}\, dr - \int_1^s (\overline{E}_1\mu_{12} + G_{12})\, r\, dr \int_1^r (\ )_{,122}\frac{dr}{r^2}$$

$$\mathcal{L}_{31}(\ ) = \int_1^s E_1\mu_{12}(\ )_{,1}\, dr - \int_1^s \overline{E}_1(r^2 - r)(\ )_{,111}\, dr$$

$$- \int_1^s \left(\overline{E}_1\mu_{12} + G_{12}\frac{r+1}{r}\right)(r-1)(\ )_{,122}\, dr$$

$$\mathcal{L}_{22}(\ ) = \int_1^s \overline{E}_2(\ )_{,22}\, r\, dr + \int_1^s G_{12}(\ )_{,11} r^3\, dr$$

$$\mathcal{L}_{23}(\ ) = \int_1^s \overline{E}_2(\ )_{,2}\, dr - \int_1^s (\overline{E}_1\mu_{12} + G_{12})\, r\, dr \int_1^r (\ )_{,122}\, dr$$

$$- \int_1^s G_{12} r^3\, dr \int_1^r (\ )_{,112}\frac{dr}{r^2} - \int_1^s \overline{E}_2 r\, dr \int_1^r (\ )_{,222}\frac{dr}{r^2}$$

$$\mathcal{L}_{32}(\ ) = \int_1^s \overline{E}_2(\ )_{,2}\, dr - \int_1^s [\overline{E}_1\mu_{12} + G_{12}(r+1)](r^2 - r)(\ )_{,112}\, dr$$

$$- \int_1^s \overline{E}_2(r-1)(\ )_{,222}\, dr$$

$$\mathcal{L}_{33}(\ ) = \int_1^s \overline{E}_2(\ )\frac{dr}{r} - \int_1^s \overline{E}_1\mu_{12}(r-1)(\ )_{,11}\, dr$$

$$- \int_1^s \overline{E}_2(r-1)(\ )_{,22}\frac{dr}{r} + \int_1^s \left(\overline{E}_1\mu_{12} + G_{12}\frac{r+1}{r}\right) \times$$

$$\times (r-1)\,dr \int_1^r (\,)_{,1122}\,dr - \int_1^s \overline{E}_1\mu_{12}dr \int_1^r (\,)_{,11}\,dr$$

$$+ \int_1^s \overline{E}_1 (r^2-r)\,dr \int_1^r (\,)_{,1111}\,dr - \int_1^s \overline{E}_2\,dr \int_1^r (\,)_{,22}\frac{dr}{r^2}$$

$$+ \int_1^s \overline{E}_2 (r-1)\,dr \int_1^r (\,)_{,2222}\frac{dr}{r^2}$$

$$- \int_1^s [\overline{E}_1\mu_{12} + G_{12}(r+1)]\,(r^2-r)\,dr \int_1^r (\,)_{,1122}\frac{dr}{r^2}$$

$$\mathcal{L}_{1p} = \mathcal{L}_{2p} = 0, \qquad \mathcal{L}_{3p} = q_1 - sq_s - \int_1^s pr\,dr$$

It is assumed that from the volume forces only the radial load $p\,(r)$ acts on the shell and the static boundary conditions on the inner and outer surfaces in the following form are satisfied

$$\tau_{13}(1) = \tau_{13}(s) = \tau_{23}(1) = \tau_{23}(s) = 0$$

$$\sigma_3(1) = q_1, \quad \sigma_3(s) = q_s$$

Since u, v, w are independent of r, the matrix on the left-hand side of equation system (22) is symmetric, i.e. $\mathcal{L}_{12} = \mathcal{L}_{21}$, $\mathcal{L}_{13} = \mathcal{L}_{31}$, $\mathcal{L}_{23} = \mathcal{L}_{32}$. The symmetry is not conserved on the right-hand side.

Expressions for θ_i in the case considered have the form:

$$\theta_1 = -\int_1^r \frac{dr}{rG_{13}} \int_1^r \Big\{\overline{E}_1 r u_{,11} - \overline{E}_1 (r^2-r)\,w_{,111}$$

$$+ \overline{E}_1\mu_{12}[w_{,1} + rv_{,12} - (r-1)\,w_{,122}]$$

$$+ G_{12}\Big[\frac{u_{,22}}{r} + rv_{,12} - \Big(r - \frac{1}{r}\Big)\,w_{,122}\Big]\Big\}\,dr$$

$$- \int_1^r \frac{dr}{rG_{13}} \int_1^r \Big\{\overline{E}_1 r\theta_{1,11} - \overline{E}_1\mu_{12}\Big[r\Big(\theta_{2,12} - \int_1^r \theta_{3,122}\frac{dr}{r}\Big) + \theta_{3,1}\Big]$$

$$+ G_{12}\Big[\frac{1}{r}\Big(\theta_{1,22} - \int_1^r \theta_{3,122}\,dr\Big)$$

$$+ r\Big(\theta_{2,12} - \int_1^r \theta_{3,122}\frac{dr}{r^2}\Big)\Big]\Big\}\,dr \qquad (23)$$

$$\theta_2 = \int_1^r \frac{dr}{r^2 G_{23}} \int_1^r \{\overline{E}_2 [w_{,2} + r v_{,22} - (r-1) w_{,222}]$$
$$+ \overline{E}_2 \mu_{21} [r u_{,12} - (r^2 - r) w_{,112}]$$
$$+ G_{12} [r u_{,12} + r^3 v_{,22} - (r^3 - r) w_{,112}]\} dr$$
$$- \int_1^r \frac{dr}{r^2 G_{23}} \int_1^r \left\{\overline{E}_2 \left[r \left(\theta_{2,22} - \int_1^r \theta_{3,222} \frac{dr}{r^2} \right) \right.\right.$$
$$\left. + \theta_{3,2} + \mu_{21} r \left(\theta_{1,12} - \int_1^r \theta_{3,112}\, dr \right) \right]$$
$$+ G_{12} \left[r \left(\theta_{1,12} - \int_1^r \theta_{3,112}\, dr \right) \right.$$
$$\left.\left. + r^3 \left(\theta_{2,11} - \int_1^r \theta_{3,112} \frac{dr}{r^2} \right) \right] \right\} dr \qquad (24)$$

$$\theta_3 = q_1 \int_1^r \frac{dr}{r E_3} - \int_1^r \frac{dr}{r E_3} \int_1^r p r\, dr + \int \frac{dr}{r E_3} \int \overline{E}_2 \left\{ \frac{w}{r} \right.$$
$$\left. + v_{,2} - \left(1 - \frac{1}{r}\right) w_{,22} + \mu_{21} [u_{,1} - (r-1) w_{,11}] \right\} dr$$
$$+ \int_1^r \frac{dr}{r E_3} \int_1^r dr \int_1^r \{\overline{E}_1 [r u_{,111} - (r^2 - r) w_{,1111}]$$
$$+ \overline{E}_1 \mu_{12} [w_{,11} + r v_{,112} - (r-1) w_{,1122}]$$
$$+ G_{12} \left[\frac{1}{r} u_{,122} + r v_{,112} - \left(r - \frac{1}{r} \right) w_{,1122} \right] \} dr$$
$$+ \int_1^r \frac{dr}{r E_3} \int_1^r \frac{dr}{r^2} \int_1^r \{\overline{E}_2 [w_{,22} + r v_{,222} - (r-1) w_{,2222}]$$
$$+ \overline{E}_2 \mu_{21} [r u_{,122} - (r^2 - r) w_{,1122}] + G_{12} [r u_{,122} + r^3 v_{,112}$$
$$- (r^3 - r) w_{,1122}]\} dr + \int_1^r \frac{dr}{r E_3} \int_1^r \overline{E}_2 \left[\theta_{2,2} - \int_1^r \theta_{3,22} \frac{dr}{r^2} \right.$$
$$\left. + \frac{1}{r} \theta_3 + \mu_{21} \left(\theta_{1,1} - \int_1^r \theta_{3,11}\, dr \right) \right] dr$$
$$+ \int_1^r \frac{dr}{r E_3} \int_1^r dr \int_1^r \left\{ \overline{E}_1 r \left(\theta_{1,111} - \int_1^r \theta_{3,1111}\, dr \right) \right.$$

$$-\overline{E}_1\mu_{12}\left[r\left(\theta_{2,\,112}-\int_1^r\theta_{3,\,1122}\frac{dr}{r^2}\right)-\theta_{3,\,11}\right]$$

$$-G_{12}\left[\frac{1}{r}\left(\theta_{1,\,122}-\int_1^r\theta_{3,\,1122}\,dr\right)\right.$$

$$\left.-r\left(\theta_{2,\,112}-\int_1^r\theta_{3,\,1122}\frac{dr}{r^2}\right)\right]\Bigg\}\,dr$$

$$-\int_1^r\frac{dr}{rE_3}\int_1^r\frac{dr}{r^2}\int_1^r\left\{\overline{E}_2\left[r\left(\theta_{2,\,222}-\int_1^r\theta_{3,\,2222}\frac{dr}{r^2}\right)\right.\right.$$

$$\left.+\theta_{3,\,22}+\mu_{21}r\left(\theta_{1,\,122}-\int_1^r\theta_{3,\,1122}\,dr\right)\right]$$

$$+G_{12}\left[r\left(\theta_{1,\,122}-\int_1^r\theta_{3,\,1122}\,dr\right)\right.$$

$$\left.+r^3\left(\theta_{2,\,112}-\int_1^r\theta_{3,\,1122}\frac{dr}{r^2}\right)\right]\Bigg\}\,dr \qquad (25)$$

To the first approximation, at $\theta_i = 0$ equations (22) describe a thick-walled cylindrical shell with strains satisfying Kirchhoff-Love's hypotheses and having, as noted earlier, the eighth order with respect to the variables α_1, α_2. The geometrical boundary conditions, e.g. at an end $\alpha_1 = \text{const}$, are written in a traditional manner in terms of the initial surface displacements u, v, w and a rotation angle $\varkappa_1$. The static boundary conditions are written in terms of the normal T_1 and in-surface shear T_{12} stress resultants, bending stress couple M_1 and Kirchhoff's thickness shear stress resultant $Q_1^* = Q_1 + (M_{12})_{,2}$, where

$$T_1 = r_0\int_1^s\sigma_1 r\,dr, \quad T_{12} = r_0\int_1^s\tau_{12}r\,dr, \quad M_1 = r_0^2\int_1^s r(r-1)\sigma_1\,dr$$

$$Q_1 = r_0\int_1^s\tau_{13}r\,dr, \quad M_{12} = r_0^2\int_1^s r(r-1)\tau_{12}\,dr$$

In the case of an axially symmetric problem for an isotropic cylindrical shell the homogeneous governing equation will be of the form:

$$D\left(1-\frac{\bar{h}^2}{12}\right)w_{,\,1111}+2\mu Dw_{,\,11}+\overline{E}\,\bar{h}\left(\frac{1}{\bar{h}}\ln\frac{1+\bar{h}/2}{1-\bar{h}/2}-\mu^2\right)w=0,$$

where $D = \overline{E}\overline{h}^3/12$, $\overline{h} = h/r_0$, h is the shell thickness, r_0 is the radius of the inner surface.

To the second approximation, on the right-hand sides of equations (23)-(25) one should take $\theta_i = 0$ and place the resulting expressions into the right-hand sides of equations (22). Putting expressions (23)-(25) for θ_i into the expressions for displacements (21) and using the variational principle one can obtain the boundary conditions written in terms of initial surface displacements u, v, w, though this is very unwieldy.

Putting θ_i from (23)-(25) in succession into the right-hand sides of equations (22) and retaining terms containing u, v, w one can arrive at set (22), which corresponds to third and higher order approximations.

As applications of the equations derived let us consider the problems of axially symmetric plane strain, static buckling, and local loading of orthotropic cylindrical shells.

9.4 AXIALLY SYMMETRIC GENERALIZED PLANE STRAIN OF AN ORTHOTROPIC LAMINATED CYLINDER

Consider a cylinder with the inner surface ($r = 1$) subjected to pressure p_1, the outer surface ($r = r_h/r_0 = s$, Fig. 9.2), to pressure $k_2 p$, and the domes, to inner pressure p_1 and outer pressure $k_1 p$ producing the resultant axial compressing force $\pi r_0^2 (k_1 s^2 p - p_1)$. At $p = 0$ one obtains the all-round internal pressure, at $p_1 = 0$, $k_1 = k_2 = 1$ the all-round external pressure, at $p_1 = 0$, $k_1 = 0$, $k_2 = 1$ the external lateral pressure and at $p_1 = 0$, $k_1 = 1$, $k_2 = 0$ the axial compression.

For the case of the generalized plane axially symmetric strain one has the following starting set of equations:

$$\frac{d}{dr}(r\sigma_3) - \sigma_2 = 0$$

$$\int_1^s \sigma_1 r\, dr = \frac{1}{2}(p_1 - k_1 s^2 p) \tag{26}$$

$$\sigma_1 = \overline{E}_1\left(\varepsilon + \mu_{12}\frac{u_3}{r}\right), \quad \sigma_2 = \overline{E}_2\left(\frac{u_3}{r} + \mu_{21}\varepsilon\right)$$

$$\sigma_3 = \overline{E}_3\frac{du_3}{dr} \tag{27}$$

where $\varepsilon = \text{const}$ is the axial strain, u_3 is the radial displacement related to r_0 and according to (21) has the form

$$u_3 = w + \theta_3, \quad \theta_3 = \int_1^r \frac{\sigma_3}{\overline{E}_3}\, dr \tag{28}$$

where $w = \text{const}$.

From (27) and (28) one has

$$\begin{aligned} \sigma_1 &= \overline{E}_1\left[\varepsilon + \frac{\mu_{12}}{r}(w+\theta_3)\right] \\ \sigma_2 &= \overline{E}_2\left[\frac{1}{r}(w+\theta_3) + \mu_{21}\varepsilon\right] \end{aligned} \tag{29}$$

Substituting σ_2 into the first equation of (26) and integrating the result with an allowance for a boundary condition $\sigma_3(1) = -p_1$ one obtains

$$\sigma_3 = -\frac{p_1}{r} + \frac{w}{r}\int_1^r \overline{E}_2 \frac{dr}{r} + \frac{\varepsilon}{r}\int_1^r \overline{E}_2\mu_{21}\, dr + \frac{1}{r}\int_1^r \overline{E}_2\theta_3 \frac{dr}{r} \tag{30}$$

From a boundary condition $\sigma_3(s) = -k_2 p$ by means of (30) one finds

$$w = \frac{1}{\int_1^s (\overline{E}_2/r)\, dr}\left(p_1 - k_2 s p - \varepsilon\int_1^s \overline{E}_2\mu_{21}\, dr - \int_1^s \overline{E}_2\theta_3 \frac{dr}{r}\right) \tag{31}$$

Taking into account equations (27), (28), (31) one obtains

$$\begin{aligned} \varepsilon = {} & \frac{p_1 - pk_2 s + \int_1^s (\overline{E}_2\theta_3/r)\, dr \int \overline{E}_1\mu dr}{\int_1^s \overline{E}_1 r\, dr \int_1^s (\overline{E}_2/r)\, dr - \left(\int_1^s \overline{E}_2\mu_{21}\, dr\right)^2} \\ & + \frac{\left[{}^1/_2(p_1 - pk_1 s^2) + \int_1^s \overline{E}_1\mu_{12}\theta_3\, pr\right]\int_1^s (\overline{E}_2/r)\, dr}{\int_1^s \overline{E}_1 r\, dr \int_1^s (\overline{E}_2/r)\, dr - \left(\int_1^s \overline{E}_2\mu_{21}\, dr\right)^2} \end{aligned} \tag{32}$$

In this way the stresses and strains in the cylinder are determined by equations (28)-(32). It might be noted that Poisson's ratios μ_{13}, μ_{31} are rather simply allowed for in the problem considered, yet the final expressions still become substantially complicated. The solution is accomplished by the successive approximation method presented above. To the first approximation, for example, $\theta_3 = 0$ is adopted,

to the second θ_3 is defined by substitution from (30) into the second equation of (28), etc.

Fig. 9.3 presents, as an example, a stress distribution through the thickness of a homogeneous cylinder with the radii ratio $s = 1.4$ and the elastic properties $E_2/E_3 = 9$, $\mu_{12} = \mu_{21} = 0$, loaded by the

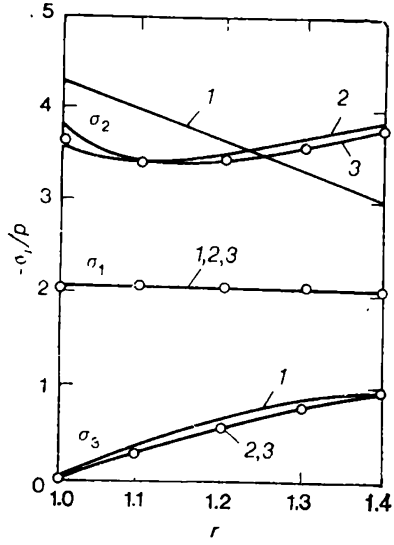

Fig. 9.3 Distribution of axial (σ_1), circumferential (σ_2) and radial (σ_3) stresses through the thickness of homogeneous orthotropic cylinder:
1—first approximation; *2*—second approximation; *3*—modified first approximation. The circles show exact solution

all-round external pressure p ($k_1 = k_2 = 1$, $p_1 = 0$). The circles correspond to an exact solution, curves *1* to the first approximation:

$$\sigma_2^{(1)} = -\frac{ps}{r \ln s}, \quad \sigma_3^{(1)} = -\frac{ps \ln r}{r \ln s}$$

and curves *2* to the second approximation:

$$\sigma_2^{(2)} = -\frac{ps}{r \ln s}\left[1 - \frac{c^2}{2}\left(\frac{1}{3}\ln^2 s - \ln^2 r\right)\right]$$

$$\sigma_3^{(2)} = -\frac{ps \ln r}{r \ln s}\left[1 - \frac{c^2}{6}(\ln^2 s - \ln^2 r)\right]$$

where $c^2 = E_2/E_3$. The axial stresses are the same in both cases: $\sigma_1^{(1)} = \sigma_1^{(2)} = -ps^2/(s^2 - 1)$.

It follows from Fig. 9.3 that the second approximation is in good agreement with the exact solution. As can be seen from the plot the distribution of the radial stresses σ_3 is close to the linear one Accordingly, one may at once prescribe the following distribution satisfying the boundary conditions on the outer and inner cylinder

surfaces:

$$\sigma_3 = \frac{1}{s-1}\left[pk_2 - p_1 s - r\,(pk_2 - p_1)\right]$$

Then from the second equation of (28) we obtain:

$$\theta_3 = \frac{1}{s-1}\left[(pk_2 - p_1 s)\int_1^r \frac{dr}{E_3} - (pk_2 - p_1)\int_1^r \frac{r\,dr}{E_3}\right] \tag{33}$$

The substitution of (33) into (29)-(32) enables a satisfying result to be obtained to the first approximation as yet. For the above example this approximate solution corresponds to curve *3* in Fig. 9.3.

9.5 STATIC BUCKLING OF ORTHOTROPIC LAMINATED CYLINDRICAL SHELLS

Consider the problem of buckling of a cylindrical shell under external pressure and axial compression. To eliminate the tedious process of successive approximations when determining the initial stresses σ_1^0 and σ_2^0 we shall presume that they are defined by equations (29), (31), (32), where θ_3 has the form (33). The linearized equations of shell stability are written in the form (22), where

$$\mathcal{L}_{sp} = w_{,11}\int_1^s \sigma_1^0 r\,dr + (w + w_{,22})\int_1^s \sigma_2^0 \frac{dr}{r}$$

$$+ \int_1^s \sigma_1^0 \theta_{3,11} r\,dr + \int_1^s \sigma_2^0 (\theta_3 + \theta_{3,22})\frac{dr}{r} \tag{34}$$

To evaluate the accuracy of the iteration pattern constructed above consider the problem of buckling of a homogeneous cylindrical shell of infinite length loaded by the uniform internal pressure p. An exact solution for the initial stresses is of the form:

$$\sigma_2^0 = -\frac{pcs^{c+1}(r^{2c}+1)}{(s^{2c}-1)\,r^{c+1}} \tag{35}$$

where $c^2 = E_2/E_3$. Simplifying set (22) in the appropriate manner and presenting the displacements in the form of the trigonometric series

$$v = \sum_{n=1}^{\infty} v_n \sin n\alpha_2, \quad w = \sum_{n=1}^{\infty} w_n \cos n\alpha_2 \tag{36}$$

one may obtain the solutions related to the different stages of iterations. For example, to the first approximation, at $\theta_2 = \theta_3 = 0$, one

has:

$$\mathcal{L}_{2v}(v) + \mathcal{L}_{2w}(w) = 0$$
$$\mathcal{L}_{3v}(v) + \mathcal{L}_{3w}(w) = 0 \tag{37}$$

where

$$\mathcal{L}_{2v}(\,) = 1/2E_2(s^2-1)(\,)_{,22}$$
$$\mathcal{L}_{2w}(\,) = \mathcal{L}_{3v}(\,) = E_2(s-1)[(\,)_{,2} - 1/2(s-1)(\,)_{,222}]$$
$$\mathcal{L}_{3w}(\,) = E_2\left[\left(\frac{s^2}{2} - 2s + \frac{3}{2} + \ln s\right)(\,)_{,2222}\right.$$
$$\left. - 2(s-1-\ln s)(\,)_{,22} + \ln s\right]$$
$$+ \frac{pcs^{c+1}}{s^{2c}-1}\left(\frac{s^{c-1}-1}{c-1} - \frac{s^{c-1}-1}{c+1}\right)[(\,) + (\,)_{,22}]$$

Substituting from (36) into (37) one obtains a set of homogeneous linear algebraic equations in respect to v_n and w_n. Zeroing the set determinant, deriving the eigenvalue p and minimizing it with respect to n, one obtains the following expression for the critical pressure:

$$p_{cr} = \frac{3E_2(s^{2c}-1)[\ln s - 2(s-1)/(s+1)]}{cs^{c+1}[(s^{c-1}-1)/(c-1) - (s^{-c-1}-1)/(c+1)]} \tag{38}$$

For a thin-walled shell with the thickness h at $s = 1 + h/r_0$ and $h \ll r_0$ equation (38) yields the classical result:

$$p_{cr} = E_2h^3/(4r_0^3) \tag{39}$$

The dependence of the critical pressure on the parameter s for a shell made of glass-fiber reinforced plastic with the parameters $E_1 = 18.6$ GPa, $E_2 = 58.8$ GPa, $E_3 = 15.7$ GPa, $G_{12} = 6.63$ GPa, $G_{13} = 3.42$ GPa, $G_{23} = 3.15$ GPa, $\mu_{12} = 0.29$, $\mu_{13} = 0.33$, $\mu_{32} = 0.28$ is depicted in Fig. 9.4. Curve *1* corresponds to the classical result (39). Curve *2* is plotted via formula (38) allowing for the radius variation through the thickness. As is seen, for a relatively thick-walled shell the radius variation through the thickness substantially influences the result, at $s = 1.3$ the correction amounts to approximately 20%.

Let us investigate the effect of nonuniformity of the distribution of the initial stresses σ_2^0 on the critical pressure. Averaging (35) one will obtain

$$\bar{\sigma}_2^0 = \frac{1}{s-1}\int_1^s \sigma_2^0\,dr = \frac{ps}{s-1} \tag{40}$$

In that case (38) takes the form:

$$p_{cr} = \frac{3E_2}{s \ln s}(s-1)\left(\ln s - 2\frac{s-1}{s+1}\right) \tag{41}$$

Formula (41) gives results only slightly differing from those of (38), i.e. for a homogeneous shell the nonuniform shape of the initial stress distribution through the thickness can be neglected.

The second approximation solution is indicated in Fig. 9.4 by curve *3*. It allows for the radial and shear compliances of the material,

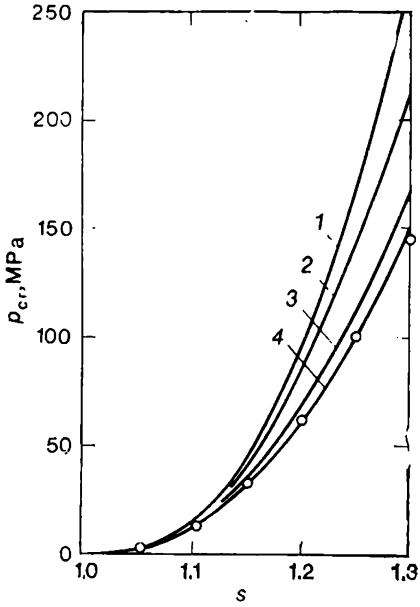

Fig. 9.4 Dependence of critical pressure on thickness parameter s for an infinitely long homogeneous cylindrical shell:
1—solution for thin-walled shell; *2*—first approximation; *3*—second approximation; *4*—third approximation at $E_3 \to \infty$. The circles show exact solution

but has an extremely unwieldy form and is not presented in full. Let us note that owing to the structure of the operator L_{3p} [see (34). for the critical pressure one obtains in that case the quadratic equation:

$$a_1(n)\, p^2 + a_2(n)\, p + a_3(n) = 0 \tag{42}$$

which has two real roots differing significantly in value. The smaller root corresponds to the general instability at $n = 2$ (curve *3* in Fig. 9.4), and the larger root, being two orders of magnitude greater than the smaller one, corresponds under prescribed parameters to local instability owing to radial compliance. Neglecting the latter and taking $\theta_3 = 0$, then $a_1 = 0$ and an equation similar to (42) will be, to an arbitrary approximation, linear. In particular, to the

econd approximation, at $\theta_3 = 0$ ($E_3 \to \infty$) one obtains

$$= \frac{E_2}{C_1}\left(\frac{C_2C_3}{C_4} - C_5\right) \tag{43}$$

here

$$_1 = -c(n^2-1)\frac{s^{c+1}}{s^{2c}-1}\left(\frac{s^{c-1}-1}{c-1} - \frac{s^{-c-1}-1}{c+1}\right)$$

$$_{2,3} = \mp n\left\{(s-1)\left(\frac{s-1}{2}n^2+1\right) - \frac{E_2}{G_{23}}n^2\left[e_{2,3}(n^2-1) - e_1n^2\right]\right.$$

$$_4 = -n^2\left(\frac{s^2-1}{2} + \frac{E_2}{G_{23}}n^2e_1\right)$$

$$_5 = \frac{(s-1)^2}{2}n^4 - n^2(n^2-2)(s-1-\ln s) + \ln s$$

$$-\frac{E_2}{G_{23}}n^2\{n^2[e_2(n^2-1) - e_1n^2] - (n^2-1)[e_4(n^2-1) - e_3n^2]\}$$

$$_1 = 0.25[(s^2+1)\ln s - s^2 + 1]$$

$$_2 = 0.5(0.5s^2 + \ln s) - s + 0.75$$

$$_3 = 0.5s(\ln s - 1.5) + 1 - \frac{1}{4s}$$

$$_4 = 0.5\left(s - \frac{1}{s}\right) - \ln s$$

For the example considered p_{cr} is realized at $n = 2$. At $G_{23} \to \infty$ 43) coincides with (38). Calculation via formula (43) shows that neglecting the radial material compliance does not practically change the result. In particular, at $s = 1.3$ the assumption of $\theta_3 = 0$ o the second approximation results in error of less than 2%. Hence he difference between curves *2* and *3* in Fig. 9.4 (in the order of 20% t $s = 1.3$) is related to the transverse shear strain.

Curve *4* in Fig. 9.4 illustrates the solution to the third approximation at $\theta_3 = 0$. A correction to the second approximation at $s = 1.3$ amounts to 9%.

As already noted, the nonuniformity of the initial stress distribution through the thickness is not significant.

Taking that distribution as a uniform one according to (40) one can obtain an exact solution of the problem in hand. Let us write out the starting equations:

$$\tau_{z,2} - \frac{1}{r}(r^2\tau_{23}),_3 = 0$$

$$(r\sigma_3),_3 - \sigma_2 + \tau_{23,2} - \bar{\sigma}_2^0\frac{1}{r}(u_{3,22} + u_3) = 0 \tag{44}$$

and

$$\varepsilon_2 = \bar{E}_2(\varepsilon_2 + \mu_{23}\varepsilon_3),\quad \sigma_3 = \bar{E}_3(\varepsilon_3 + \mu_{32}\varepsilon_2) \tag{45}$$

$$\tau_{23} = G_{23}\varepsilon_{23}$$

where

$$\varepsilon_2 = \frac{1}{r}(u_{2,2} + u_3), \quad \varepsilon_3 = u_{3,3}$$
$$\varepsilon_{23} = \frac{u_{3,2}}{r} + u_{2,3} + \frac{u_2}{r} \tag{46}$$

and

$$\overline{E}_2 = E_2/(1 - \mu_{23}\mu_{32}), \quad \overline{E}_3 = E_3/(1 - \mu_{23}\mu_{32})$$

as well as the boundary conditions at $r = 1$ and $r = s$:

$$\sigma_3 = \tau_{23} = 0 \tag{47}$$

Substituting the strains (46) into (45) and the resultant expressions for the strains into (44), one may write a set of two equations with respect to u_2 and u_3 where solution has the form:

$$u_2 = \sum_{i=1}^{4} \sum_{n=1}^{\infty} B_n^i r^{t_n^i} \sin n\alpha_2$$
$$u_3 = \sum_{i=1}^{4} \sum_{n=1}^{\infty} C_n^i r^{t_n^i} \cos n\alpha_2 \tag{48}$$

Here t_n^i are the roots of the characteristic equation

$$(t_n^i)^4 - (t_n^i)^2\Big[1 + \frac{E_2}{E_3} + n^2\frac{\overline{E}_2}{G_{23}} - n^2\mu_{32}\Big(\mu_{23}\frac{\overline{E}_2}{G_{23}} + 2\Big) - (n^2-1)\frac{\overline{\sigma}_2^0}{\overline{E}_3}\Big] + \frac{E_2}{E_3}(n^2-1)^2 - (n^2-1)\Big(n^2\frac{\overline{E}_2}{G_{23}} + 1\Big)\frac{\overline{\sigma}_2^0}{\overline{E}_3} = 0$$

and the coefficients B_n^i and C_n^i being related through the expression

$$B_n^i = \lambda_n^i C_n^i \quad (i = 1, 2, 3, 4)$$

where

$$\lambda_n^i = [(E_2/E_3)\, n\,(n - t_n^i - 1) - (\overline{E}_2/G_{23})\{(E_2/E_3)\,[n\,(1 + t_n^i\mu_{23}) - 1] + (\overline{\sigma}_2^0/\overline{E}_3\,(n^2-1) + (t_n^i)^2\}]$$
$$\times\{(E_2/E_3)\,[(\overline{E}_2/G_{23})\, n\,(n - 1 + t_n^i\mu_{23}) + (t_n^i - 1)\,(n - 1 - t_n^i)]\}^{-1}$$

Writing the stresses in terms of (45), (46), (48) and satisfying the boundary conditions (47) one obtains the following characteristic

equation with respect to $\bar{\sigma}_2^0$:

$$s^{t_n^1} N_1 (N_2 M_{34} - N_3 M_{24} + N_4 M_{23}) - s^{t_n^2} N_2 (N_1 M_{34} - N_3 M_{14} + N_4 M_{13}) + s^{t_n^3} N_3 (N_1 M_{24} - N_2 M_{14} + N_4 M_{12}) - s^{t_n^4} N_4 (N_1 M_{23} - N_2 M_{13} + N_3 M_{12}) = 0 \quad (49)$$

where

$$N_i = \lambda_n^i (t_n^i - 1) - n, \quad M_{ij} = (s^{t_n^i} - s^{t_n^j}) A_i A_j$$

$$A_i = t_n^i + \mu_{32} (n\lambda_n^i + 1)$$

σ_2^0 enters equation (49) via the indices t_n^i. This equation has an infinite set of real roots $\bar{\sigma}_2^0$, the first of which corresponds to general instability, and the others to the local forms related to the radial compliance. The dependence of the critical pressure, complying with the general instability, on s is indicated in Fig. 9.4 by the circles for the example cited above. The error of the above approximate solutions at $s = 1.3$ for curve *1* amounts to 69%, for curve *2*, 37%, for curve *3*, 16% and for curve *4*, 5.5%. Neglecting Poisson's ratio through the thickness ($\mu_{23} = \mu_{32} = 0$) changes the solution by less than 1%.

For a cylindrical shell of finite length the solution is sought in the form:

$$u = \sum_m \sum_n u_{mn} \cos \lambda_m \alpha_1 \cos n\alpha_2$$

$$v = \sum_m \sum_n v_{mn} \sin \lambda_m \alpha_1 \sin n\alpha_2 \quad (50)$$

$$w = \sum_m \sum_n w_{mn} \sin \lambda_m \alpha_1 \cos n\alpha_2$$

where $\lambda_m = \pi m/L$ (L is the shell length). Substituting expressions (50) into (22), where L_{3p} is defined by (34) and the initial stresses by (29)-(33), enables at each step of the iteration procedure a homogeneous set of linear algebraic equations to be obtained with respect to u_{mn}, v_{mn}, w_{mn}. The critical loads are determined from the condition of zeroing the set determinant as a result of the minimization of eigenvalues over the parameters λ_m and n.

Table 1.9 contains the theoretical critical values p_t of the lateral external pressure versus the experimental values p_e (v is the variation coefficient). The length of shells is 0.295 m, the radius of inner surface is 0.025 m (mechanical parameters were listed earlier). The theoretical results pertain to the second approximation solution at $\theta_3 = 0$.

The theoretical and experimental studies performed enable certain general conclusions to be drawn. In problems of stability of laminated composite cylindrical shells classical theory yields satisfactory

Table 9.1

s	p_t, MPa	p_e, MPa (v, %)
1.045	1.273	1.4 (10.7)
1.052	1.910	2.12 (7.05)
1.070	4.605	4.34 (4.7)
1.155	37.25	37.1 (2.75)
1.170	47.67	49 (4)
1.270	149	143.7 (3.22)

results at $s \leqslant 1.02$. Allowing for a variation in the radius through the thickness, i.e. the solution to the first approximation at $\theta_1 = \theta_2 = \theta_3 = 0$, provides satisfactory results at $s \leqslant 1.1$. For shells having $s \leqslant 1.30$ the radial compliance of the material, nonuniformity of the initial stress distribution through the thickness (for homogeneous and laminated shells), and Poisson's effect through the thickness are unimportant. Here the second approximation, allowing for the shear compliance of the material ($\theta_3 = 0$), yields satisfactory results. At $s > 1.3$ shells made of glass-fiber reinforced plastic fail owing to the initial stresses attaining the ultimate compressive strength of the material.

9.6 LOCAL LOADING OF ORTHOTROPIC CYLINDRICAL SHELLS

To evaluate the accuracy of the theory presented in Section 9.2 let us consider a classical problem of the local loading of a homogeneous ring (Fig. 9.5). Assuming in (22) $u = 0$, $q_1 = p = 0$

$$v = \sum_{n=1}^{\infty} v_n \sin n\alpha_2, \quad w = \sum_{n=0}^{\infty} w_n \cos n\alpha_2$$

$$q_n = \sum_{n=0}^{\infty} q_n \cos n\alpha_2 = \frac{2q}{\pi r_h}\left(\frac{1}{2} + \sum_{n=2,\,4} \cos n\alpha_2\right)$$

to the first approximation, one obtains

$$l_{2v}v_n + l_{2w}w_n = 0, \quad l_{3v}v_n + l_{3w}w_n = q_n/E_2 \tag{51}$$

where

$l_{2v} = -n^2 t,\ l_{2w} = -l_{3v} = -n\bar{h}\,(1 + 0.5n^2\bar{h})$

$l_{3w} = l + 2n^2\,(\bar{h} - l) + n^4\,(0.5s^2 - 2s + 1.5 + l)$

$s = s^2 - 1,\ \bar{h} = s - 1,\ l = \ln s$

From (51) one can find v_n and w_n, and then all of the displacements

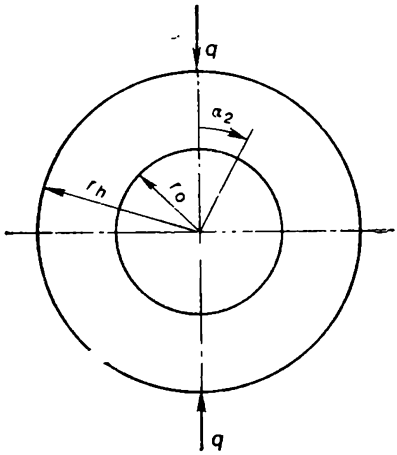

Fig. 9.5 Local loading of ring

and stresses. In particular, the circumferential stress σ_2 is of the form:

$$\sigma_2 = \frac{2q}{\pi r_0}\left\{\frac{1}{2} + \sum_{n=2,\,4}^{\infty} \frac{(l_{2v}/r)\,[1 + n^2\,(r-1)] - 2n\,l_{2w}}{l_{2v} l_{3w} - l_{2w}^2} \cos n\alpha_2\right\} \qquad (52)$$

To the second approximation, system (22) has the form:

$(l_{2v} - l'_{2v})\,v_n + (l_{2w} - l'_{2w})\,w_n = 0$

$(l_{3v} - l'_{3v})\,v_n + (l_{3w} - l'_{3w})\,w_n = q_n/E_2$

where

$$l'_{2v} = \frac{E_2}{E_3}\left\{\left(\frac{t}{2} - sl\right) n^2 + \left[\left(3s + \frac{\bar{h}^2}{2}\right) l - \frac{3t}{2}\right] n^4 - \left[\left(s + \frac{\bar{h}^2}{4}\right) l + \frac{t}{2}\right] n^6\right\} + \frac{E_2}{G_{23}}\left[\frac{l}{2}\left(s + \frac{\bar{h}^2}{2}\right) - \frac{t}{4}\right] n^4$$

$$l'_{2w} = \frac{E_2}{E_3}\left\{\left[\bar{h} - sl\left(1 - \frac{l}{2}\right)\right] n + \left[\bar{h}^2 - 3\bar{h} + l + sl\left(2 - \frac{3l}{2}\right)\right] n^3 - \left[\frac{3\bar{h}}{2}\left(\frac{3\bar{h}}{2} - 1\right) - \frac{\bar{h}^2 l}{2} + \frac{3l}{2}\,(1 + sl)\right] n^5\right.$$

$$+\left[\bar{h}^2-\frac{l}{2}\left(l-\frac{t}{2}\right)\right]n^7\Big\}$$

$$+\frac{E_2}{G_{23}}\left\{\frac{1}{2}\left(l-\bar{h}+\frac{\bar{h}^2}{2}\right)n^3-\frac{\bar{h}}{4}\left[2\bar{h}-(1+s)\,l\right]n^5\right\}$$

$$l'_{3v}=\frac{E_2}{E_3}\left\{\left[l\left(1+\frac{l}{2}\right)-\bar{h}\right]n\right.$$

$$-\left[3l\left(\frac{l}{2}+1\right)+\frac{\bar{h}}{2}\left(\frac{1}{s}-7+\bar{h}\right)\right]n^3$$

$$+\left[\bar{h}\left(3\bar{h}-1+\frac{1}{s}\right)-\frac{t}{2s}-\frac{3\bar{h}^2}{4s}+\frac{\bar{h}l}{2}(2+s)\right.$$

$$\left.+\frac{3l}{2}(1+l)\right]n^5-\left[\frac{\bar{h}}{4}\left(3\bar{h}-1+\frac{1}{s}\right)+\frac{l^2}{2}\right.$$

$$\left.-\frac{\bar{h}l}{4}(\bar{h}+4)\right]n^7\Big\}+\frac{E_2}{G_{23}}\left\{\left[\frac{\bar{h}}{2}\left(1+\frac{\bar{h}}{2s}\right)\right.\right.$$

$$\left.\left.-\frac{sl}{2}\right]n^3+\left[\bar{h}\,(1-l)-\frac{\bar{h}}{5}\right]n^5\right\}$$

$$l'_{3w}=\frac{E_2}{E_3}\left\{-\frac{l^3}{6}-\left[\bar{h}\left(3+\frac{1}{s}\right)\right.\right.$$

$$\left.+l\left(\frac{\bar{h}l}{2}-5+\frac{2l^2}{3}\right)\right]n^2+\left[l^2\left(\frac{3\bar{h}}{2}-l\right)\right.$$

$$\left.-3l\,(s+3)+\bar{h}\left(\frac{13}{2}-\bar{h}\right)+\frac{3\bar{h}}{2}+\frac{2t}{5}\right]n^4$$

$$-\left[\frac{3\bar{h}l}{2}(l-1)+l\left(\frac{\bar{h}^2}{2}-10\right)\right.$$

$$\left.-\frac{2l^3}{2}+\frac{5\bar{h}}{4s}+\frac{7\bar{h}}{4}+\bar{h}\left(7-\frac{9\bar{h}}{4}\right)\right]n^6$$

$$+\left[\frac{l^2}{2}\left(\bar{h}-\frac{2l}{3}\right)+l\left(\frac{\bar{h}^2}{4}-\frac{5}{2}\right)\right.$$

$$\left.+\frac{\bar{h}}{4}\left(\frac{1}{s}+9-4\bar{h}\right)\right]n^8\Big\}+\frac{E_2}{G_{23}}\left\{\left(l-\frac{\bar{h}^2}{2s}\right)n^2\right.$$

$$+\left[\frac{\bar{h}}{4}\left(9-\bar{h}+\frac{3}{s}\right)-\left(3+\frac{\bar{h}}{2}\right)l\right]n^4$$

$$\left.-\left[\frac{\bar{h}}{4}\left(5-2\bar{h}+\frac{1}{s}\right)+(\bar{h}-6)\,\frac{l}{4}\right]n^6\right\}$$

The circumferential stress, to the second approximation, is defined as:

$$\sigma_2 = \frac{q}{\pi r_0} + \frac{2q}{\pi r_0} \sum_{n=2,\,4}^{\infty} \Bigg[-(l_{2w} - l'_{2w}) \Bigg\{ n + \frac{E_2}{E_3} \Bigg[\frac{1}{r} (\gamma - \ln r)\, n - \left(\frac{6\gamma + 5\gamma^2}{2r^2} - \ln r - \frac{2}{r} \ln r \right) n^3 + \left(\frac{6\gamma + 5\gamma^2}{4r} - \frac{1}{2} \ln r - \frac{1}{r} \ln r \right) n^5 \Bigg] + \frac{E_{12}}{G_{23}} \left(\frac{1}{2} \ln r - \frac{\gamma^2 + 2\gamma}{4r^2} \right) n^3 \Bigg\} + (l_{2v} - l'_{2v}) \Bigg\{ \frac{1 + \gamma n^2}{r} + \frac{E_2}{E_3} \Bigg[\frac{1}{2} \ln^2 r - \left(\frac{3 \ln^2 r}{2r} + \frac{\ln r}{r} - \frac{2\gamma + 3\gamma^2}{2r^2} \right) n^2 + \left(\frac{3 \ln^2 r}{2r} + \frac{2}{r} \ln r + \ln r - \frac{4\gamma^2 + 3\gamma}{r^2} \right) n^4 - \left(\frac{\ln^2 r}{2r} + \frac{\ln r}{r} + \frac{\ln r}{2} - \frac{7\gamma^2 + 6\gamma}{4r^2} \right) n^6 \Bigg] + \frac{E_2}{G_{23}} \Bigg[\frac{\gamma^2}{2r^2} n^2 + \left(\frac{1}{2} \ln r - \frac{3\gamma^2 + 2\gamma}{4r^2} \right) n^4 \Bigg] \Bigg\} \Bigg] \times \frac{\cos n\alpha_2}{(l_{2v} - l'_{2v})(l_{3w} - l'_{3w}) - (l_{2w} - l'_{2w})(l_{3v} - l'_{3v})}$$

where $\gamma = r - 1$.

Fig. 9.6 presents the distribution of σ_2 along r at $\alpha_2 = 0$ in an isotropic ring with a parameter $s = r_h/r_0 = 2$. Curve *1* corresponds to the first approximation (52), curve *2* to the second one (53), the circles mark an exact solution by S.P. Timoshenko.

For a cylindrical shell the solution can be presented in the form of (50). Fig. 9.7 shows the variation in the deflection u_3 (dependent on α_1 at $\alpha_2 = 0$, $r = s$) of the outer surface of a homogeneous orthotropic shell under normal load. The latter was distributed uniformly over a small area of the inner surface. The shell edges $\alpha_1 = 0$ and $\alpha_1 = L/r_0$ were freely supported. The centres of the loading area are $\alpha_1 = L/(2r_0)$, $\alpha_2 = 0$, $r = 1$. The shell parameters are: $r_0 = 0.1$ m, $L = 0.32$ m, $E_1 = 18.1$ GPa, $E_2 = 27.7$ GPa, $E_3 = 3.5$ GPa, $G_{12} = 4.4$ GPa, $G_{13} = G_{23} = 2.2$ GPa, $\mu_{21} = 0.15$. Curves *1* and *2* in Fig. 9.7 refer to shells with the parameters $s = 1.043$ and $s = 1.143$. The dashed curves correspond to the first approximation, the solid ones to the second approximation, the circles fit the deflection measurements.

Fig. 9.8 shows the experimental dependences of the maximum deflection of an outer surface $u_3^{\max} = u_3$ ($\alpha_1 = L/2r_0$, $\alpha_2 = 0$, $r = s$) on the load value. Curves *1* and *2* correspond to shells with $s = 1.043$ and $s = 1.143$. Preliminary investigations of the local loading of rings (there the failure can be observed in situ) have shown that the onset of a nonlinear region is related to composite delamination.

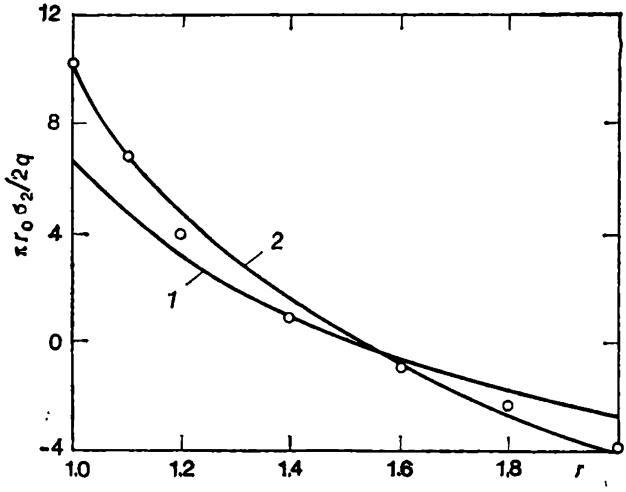

Fig. 9.6 Stress distribution σ_2 ($\alpha_2 = 0$) through the thickness of isotropic ring:
1—first approximation; *2*—second approximation. The circles show exact solution

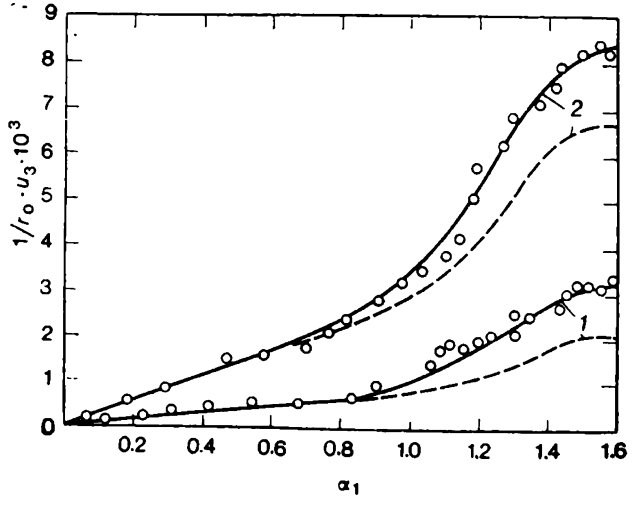

Fig. 9.7 Variation in deflection along the axis of cylindrical shell under local loading on the surface element with a centre at the point ($\alpha_1 = 1.6$; $\alpha_2 = 0$; $r = 1$): curves *1*, for $s = 1.043$; curves *2*, for $s = 1.143$. The dashed line shows first approximation, the solid line, second approximation

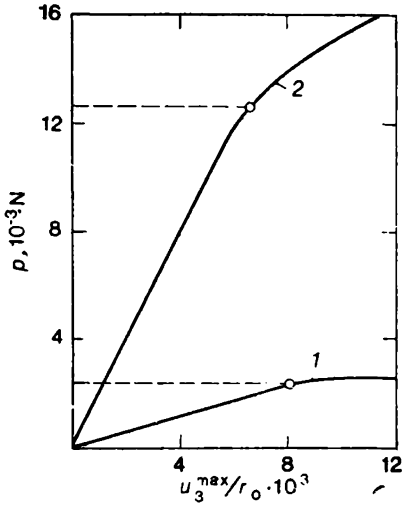

Fig. 9.8 Experimental curves for dependence of maximum shell deflection on concentrated load:
1—for $s = 1.043$; *2*—for $s = 1.143$. The circles are theoretical load values corresponding to initiation of material delamination

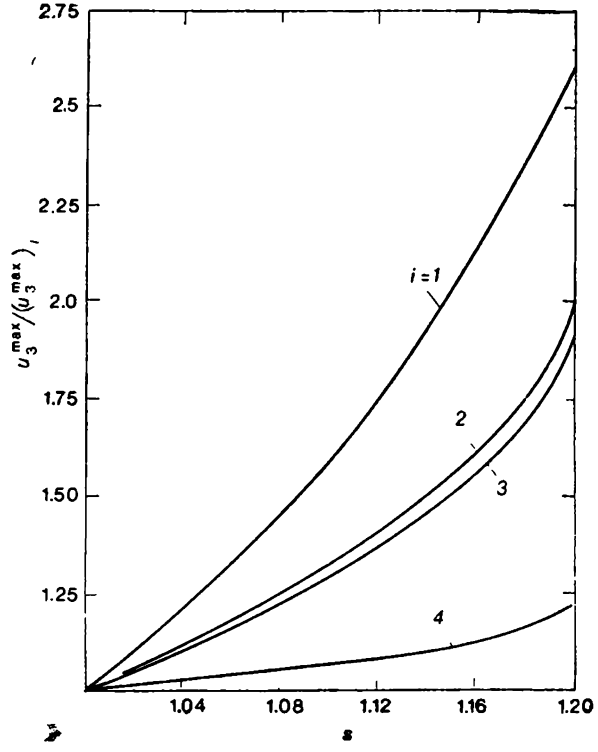

Fig. 9.9 Error in determination of maximum deflection

The circles in Fig. 9.8 denote the theoretical load values under which the maximum magnitude of shear stresses $\tau = \sqrt{\tau_{13}^2 + \tau_{23}^2}$ attains the suitable ultimate magnitude $\tau_s = 16.3$ MPa being found from experiments.

In conclusion we shall present the evaluations of errors, brought about by different simplifying assumptions. Fig. 9.9 depicts the dependence of the ratio $u_3^{\max}/(u_3^{\max})_i$ on s, where $u_3^{\max}$ is the maximum deflection corresponding to the second approximation, $(u_3^{\max})_i$ $(i = 1, 2, 3, 4)$ is the deflection corresponding to the different approximate solutions. Curve *1* shows the solution error to the first approximation $(G_{13} \to \infty, \ G_{23} \to \infty, \ E_3 \to \infty)$, which does not take into account radius variation through the thickness. Curve *2* corresponds to the first approximation being constructed allowing for radius variation through the thickness. Curve *3* yields the error owing to the neglect of the shear strain, whereas the deflection $u_3^{\max}$ is determined at $E_1/G_{13} = E_1/G_{23} = 10$, $E_3 \to \infty$, and $(u_3^{\max})_3$, at $G_{13} \to \infty$, $G_{23} \to \infty$, $E_3 \to \infty$. Curve *4* describes the error owing to the neglect of the radial strain, whereas the deflection $u_3^{\max}$ was calculated at $G_{13} \to \infty$, $G_{23} \to \infty$, $E_1/E_3 = 10$, and $(u_3^{\max})_4$, at $G_{13} \to \infty$, $G_{23} \to \infty$, $E_3 \to \infty$. It follows from the data obtained that in the same way as in the stability problem proper allowance for radius variation through the thickness and for shear strain appears to be the most significant issues.

References

1. Ambartsumyan, S.A., *General Theory of Anisotropic Shells*, Nauka, Moscow, 1974 (in Russian).
2. Grigorenko, Ya.M., *Isotropic and Anisotropic Laminated Shells of Revolution with Varying Rigidity*, Naukova dumka, Kiev, 1973 (in Russian).
3. *Composite Materials*, vol. 7, *Structural Design and Analysis* (C.C. Chamis, ed.), Part 1, Academic Press, New York and London, 1975.
4. Bolotin, V.V., and Novichkov, Yu.N., *Mechanics of Multilayer Structures*, Mashinostroyenie, Moscow, 1980 (in Russian).
5. Elpat'evskii, A.N., and Vasil'ev, V.V., *Strength of Cylindrical Shells from Reinforced Materials*, Mashinostroyenie, Moscow, 1972 (in Russian).
6. Korolyov, V.I., *Laminated Anisotropic Plates and Shells from Reinforced Plastics*, Mashinostroyenie, Moscow, 1965 (in Russian).
7. Pelekh, B.L., *Theory of Finite Shear Rigidity Shells*, Naukova dumka, Kiev, 1973 (in Russian).
8. Rikards, R.B., and Teters, G.A., *Stability of Composite Shells*, Zinatne, Riga, 1974 (in Russian).
9. Grigorenko, Ya.M., and Vasilenko, A.T., *Prikl. mekhanika*, **13** (10), 36-42 (1977).
10. Grigolyuk, E.I., and Chulkov, P.P., *Mekh. tverd. tela*, **1**, 163-169 (1967).
11. Aleksandrov, A.Ya., and Kurshin, L.M., in: *Proc. VII All-Union Conference on Theory of Shells and Plates* (Dnepropetrovsk, 1969), Nauka, Moscow, 1970 (pp. 714-721) (in Russian).
12. Ambartsumyan, S.A., *Izv. Akad. Nauk Arm. SSR*, ser. fiz.-mat. nauk, **17**, (3), 29-53 (1964).

13. Vorovich, I.I., in: *Proc. II All-Union Meeting on Theoretical and Applied Mathematics*, vol. 3, *Mechanics of Rigid Body*, Nauka, Moscow, 1965, pp. 116-136 (in Russian).
14. Grigolyuk, E.I., and Kogan F.A., *Prikl. mekhanika*, 8, (6), 3-17 (1972).
15. Galin'sh, A.K., in: *Studies into the Theory of Plates and Shells*, Izd. KGU, Kazan, vol. 5, 1967, pp. 66-92, vol. 6-7, 1970, pp. 23-63 (in Russian).

10 Optimum Design of Membrane Composite Shells of Revolution

V. A. Bunakov, *Cand. Sc. (Eng.)*,
V. D. Protasov, *D. Sc. (Eng.)*,
S. B. Cherevatskii, *D. Sc. (Eng.)*

10.1 INTRODUCTION

Composite materials, heterogeneous structures formed by the combination of reinforcing elements and an isotropic matrix, nowadays find application in different fields of engineering. Their efficiency is essentially dependent on the state-of-the-art of the methods of design and fabrication. It is not accidental that the availability of a highly productive fabrication method of shells of revolution, i.e. a process of continuous winding, has motivated their extended application in contemporary structures. On the other hand, a specific property of the composite to be produced concurrent with a structure enables a definite anisotropy pattern for shells of revolution to be created comparatively simply, realizing the merits of the reinforced material in the best possible way. Finally, advances in the theory of reinforced shells and in the methods of their optimum reinforcement enable design problems to be solved successfully.

The problem of the optimal reinforcement of shells of revolution made of composites requires three fundamental issues to be solved:

(1) selection of a composite model;

(2) foundation of a structure design model;

(3) formulation of an optimization criterion and restrictions imposed by the function and fabrication method of the structure.

At present two fundamental approaches have been developed in the choice of a composite model and the design of reinforced laminated shells based on this model. The first deals with the reinforced composites as an anisotropic monolithic structure, whose mechanical properties are either considered known [1, 2], or determined by design-experimental methods both based on micromechanical concepts [3] and the introduction of an orthotropic unidirectional element provided with stiffnesses in tension-compression in two directions and in shear. Further, the mechanical properties of the laminated structure composed of several arbitrarily oriented layers are determined through design assuming their compatible deformation [4, 5]. The second approach, netting analysis, assumes a model of the composite viewed as a system of flexible filaments. The model does not take into account the bearing capacity of the matrix and the stiffness of the unidirectional material across filament orientation. Its use is justified

for design calculations when the matrix bearing capacity is neglected [6]. Note also that in the design of minimum weight shells the condition of uniform strength using the filamentary model corresponds to the sufficient condition of an optimum since all the conditions of Levi's theorem on statically determinate truss structures of minimum weight are thereby met. The selection of an equilibrium shape of the shell meridian and the fiber orientation pattern on its surface for structures of the type of a filament wound pressure vessel have used such a formulation [7-10]. A number of results in the optimum design of the shells of revolution fabricated by the winding method and loaded by internal pressure and axial forces are presented in [11].

The purpose of the present work consists in a further generalization of the optimum reinforcement theory of the membrane shells of revolution. In so doing, a composite model is considered, being more universal as compared to the filamentary structure model and allowing for interlaminar shear stresses to be considered. The loading range is extended and optimum criteria are employed that are more universal than the uniform strength condition, and design methods of optimum structures.

10.2 GOVERNING EQUATIONS IN THE THEORY OF MEMBRANE COMPOSITE SHELLS OF REVOLUTION

Consider a shell of revolution consisting of k composite layers, each being formed by filaments inclined at the angles $+\varphi_i$ and $-\varphi_i$ in respect to a meridian (Fig. 10.1). The shell is subjected to an arbitrary axially symmetric distributed meridian load q and the normal pressure p which are, generally, functions of the coordinate r, and also by the axial forces Q_0 distributed uniformly along the edge of a polar hole of radius r_0. Each layer is regarded as a filamentary system, and an allowance is made for interlaminar interaction producing an additional tangential load for each layer.

The equilibrium equations of each layer under axially symmetric loading are of the form:

$$\begin{aligned}
&\frac{d}{dr}(BN_{\alpha i}^{\pm}) - N_{\beta i}^{\pm}\frac{dB}{dr} + ABp_{1i}^{\pm} = 0\\
&\frac{d}{dr}(BN_{\alpha\beta i}^{\pm}) + N_{\alpha\beta i}^{\pm}\frac{dB}{dr} + ABp_{2i}^{\pm} = 0\\
&\frac{N_{\alpha i}^{\pm}}{R_1} + \frac{N_{\beta i}^{\pm}}{R_2} = p_{3i}^{\pm}
\end{aligned} \tag{1}$$

Here the signs '+' and '—' correspond to the angles $+\varphi_i$ and $-\varphi_i$ (Fig. 10.1 depicts the forces relevant to a layer $+\varphi_i$); $A = \sqrt{1 + (z')^2}$

and $B = r$ are the coefficients of the first fundamental quadratic form of the surface of revolution prescribed by an equation $z = z(r)$; R_1, R_2 are the principal radii of curvature calculated using the relations

$$\frac{1}{R_1} = -\frac{z''}{[1+(z')^2]^{3/2}}$$

$$\frac{1}{R_2} = -\frac{z'}{r[1+(z')^2]^{1/2}}$$

Taking into account that the shell is subjected to the axially symmetric meridional q and normal p loads, and assuming that a pair

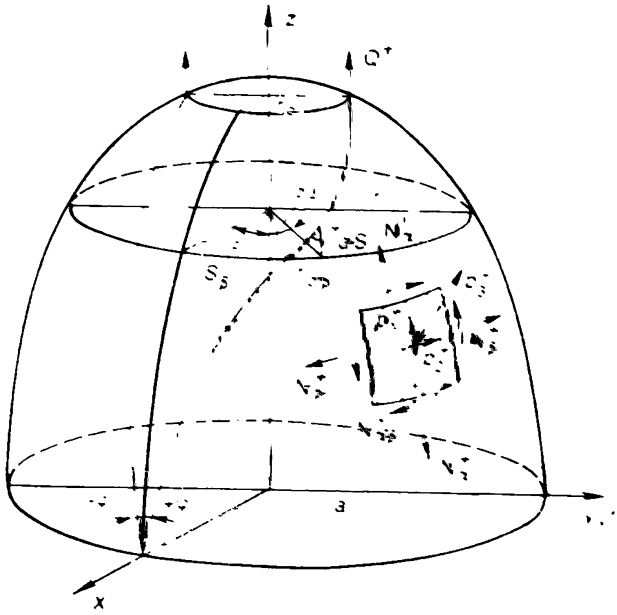

Fig. 10.1 Loading scheme and filament position on the surface of ith layer

of symmetric layers are under loads q_i and p_i, we obtain

$$p_{1i}^{\pm} = q_i/2, \qquad \sum_{i=1}^{k} q_i = q$$

$$p_{3i}^{\pm} = p_i/2, \qquad \sum_{i=1}^{k} p_i = p$$

There are interlaminar circumferential shear stresses $\pm\tau_i$, i.e. $p_{2i}^{\pm} = \pm\tau_i$, which are counterbalanced for each pair of layers. Hence, allowing for the loading conditions and prescribed notations, set (1)

after certain transformations can be reduced to the form:

$$\frac{d}{dr}(rN_{\alpha i}^{\pm}) - N_{\beta i}^{\pm} + r\sqrt{1+(z')^2}\,\frac{q_i}{2} = 0$$

$$\frac{1}{r}\frac{d}{dr}(r^2 N_{\alpha\beta i}^{\pm}) \pm r\sqrt{1+(z')^2}\,\tau_i = 0 \qquad (2)$$

$$\frac{rz''}{1+(z')^2}\,N_{\alpha i}^{\pm} + z'N_{\beta i}^{\pm} - r\sqrt{1+(z')^2}\,\frac{p_i}{2} = 0$$

Finding $N_{\beta i}^{\pm}$ from the third equation of set (2):

$$N_{\beta i}^{\pm} = -\frac{rz''}{z'\,[1+(z')^2]}\,N_{\alpha i}^{\pm} - \frac{r\sqrt{1+(z')^2}}{z'}\,\frac{p_i}{2} \qquad (3)$$

and substituting it into the first equation, after the transformations we obtain:

$$\frac{d}{dr}\left(\frac{rz'N_{\alpha i}^{\pm}}{\sqrt{1+(z')^2}}\right) + \frac{r}{2}(z'q_i + p_i) = 0$$

Integrating the last equation and allowing for the axial forces $Q_i/2$ distributed along the parallel of radius r_{0i}, we find

$$N_{\alpha i}^{\pm} = -\frac{\sqrt{1+(z')^2}}{2rz'}\left[Q_i r_{0i} + \int_{r_{0i}}^{r}(rz'q_i + rp_i)\,dr\right] \qquad (4)$$

Substituting (4) into (3) we finally obtain

$$N_{\beta i}^{\pm} = -\frac{\sqrt{1+(z')^2}}{2rz'}\left\{rp_i - \frac{z''}{z'\,[1+(z')^2]}\left[Q_i r_{0i} + \int_{r_{0i}}^{r}(rz'q_i + rp_i)\,dr\right]\right\} \qquad (5)$$

Consider the static relations of filamentary system mechanics. We assume each double spiral layer to be composed of n_i filaments. Then, the thickness $h_i/2$ of a layer oriented at an angle $+\varphi_i$ or $-\varphi_i$ can be expressed in terms of the number of filaments $n_i/2$ forming an individual layer and the reduced area of filament cross-section f (including the matrix):

$$\frac{h_i}{2} = \frac{n_i f}{4\pi r\cos\varphi_i} \qquad (6)$$

Equation (6) is essentially a technological restriction expressing the continuity condition for the reinforcement—the constancy in the number of filaments running through any shell cross-section.

Let us relate the membrane stress resultants $N_{\alpha i}^{\pm}$, $N_{\beta i}^{\pm}$, $N_{\alpha\beta i}^{\pm}$ to the stresses in the filament. Neglecting the bearing capacity of the

matrix and allowing for the loading symmetry we find:

$$N_{\alpha i}^{\pm} = \sigma_{1i} \frac{h_i}{2} \cos^2 \varphi_i = \frac{\sigma_{1i} n_i f}{4\pi r} \cos \varphi_i$$

$$N_{\beta i}^{\pm} = \sigma_{1i} \frac{h_i}{2} \sin^2 \varphi_i = \frac{\sigma_{1i} n_i f}{4\pi r} \sin \varphi_i \tan \varphi_i \qquad (7)$$

$$N_{\alpha\beta i}^{\pm} = \pm \sigma_{1i} \frac{h_i}{2} \sin \varphi_i \cos \varphi_i = \pm \frac{\sigma_{1i} n_i f}{4\pi r} \sin \varphi_i$$

Here σ_{1i} are the stresses in the filaments of the ith layer (equal for the layers $\pm\varphi_i$ owing to symmetry). Comparing (4) and (5) with the first two equations in (7) it is not difficult to see that the two membrane stress resultants $N_{\alpha i}$ and $N_{\beta i}$ will be taken up by a single system of filaments only in the case when the following relationship exists between the shape $z(r)$ of the shell, the layer orientation pattern $\varphi_i(r)$, and its loads Q_i, $p_i(r)$, $q_i(r)$:

$$\frac{z''}{z'[1+(z')^2]} = \frac{p_i r}{Q_i r_{0i} + \int_{r_{0i}}^{r} r(z' q_i + p_i)\, dr} - \frac{1}{r} \tan^2 \varphi_i \qquad (8)$$

Relation (8) may be called a condition of the existence of a shell of revolution formed by a system of flexible filaments. If this condition is not complied with the shell transforms into a mechanism, i.e. it does not take up the external loads within the filamentary system hypotheses. If the relationship between the shell shape, orientation pattern and loading conditions fits equation (8) the stresses in the filaments can be found by comparing equation (4) with the first of the static relations (7), or by comparing (5) with the second relation in (7) and adding (8), so that:

$$\sigma_{1i} = -\frac{2\pi \sqrt{1+(z')^2}}{n_i f z' \cos \varphi_i} \left[Q_i r_{0i} + \int_{r_{0i}}^{r} r(z' q_i + p_i)\, dr \right] \qquad (9)$$

The interlaminar interaction stresses can be deduced directly from the second equation in (2) taking into account (7) and (9), and is governed by the dependence:

$$\tau_i = \frac{n_i f}{4\pi r^2 \sqrt{1+(z')^2}} \frac{d}{dr} (\sigma_{1i} r \sin \varphi_i) \qquad (10)$$

The second condition of technological feasibility of the structure (the first one is imposed by (6)) reduces to a condition of filament equilibrium on the mandrel during winding defined by the inequality:

$$\max |\tan \theta_i| \leqslant \varkappa \qquad (11)$$

Here $\varkappa$ is the actual friction coefficient of the filament on the mandrel surface; θ_i is the angle of geodetic deviation of the filament in the ith layer (an angle between the normals to the orientation pattern and to the mandrel surface), whose tangent is expressed by

$$\tan \theta_i = R_{ni}/R_{gi}$$

where

$$\frac{1}{R_{ni}} = \frac{\cos^2 \varphi_i}{R_1} + \frac{\sin^2 \varphi_i}{R_2}$$

$$\frac{1}{R_{gi}} = \frac{\cos \varphi_i}{[1+(z')^2]^{1/2}} \frac{d\varphi_i}{dr} + \frac{\sin \varphi_i}{r[1+(z')^2]^{1/2}}$$

are the normal and geodetic curvatures of the curve on the surface of revolution.

Bearing in mind the expressions for the principal radii of curvature R_1 and R_2, we finally obtain:

$$\tan \theta_i = \frac{d(r \sin \varphi_i)/dr}{rz'' \cos^2 \varphi_i/[1+(z')^2] + z' \sin^2 \varphi_i} \tag{12}$$

Expressions (8)-(12) are the general relations providing for the design of an extended range of shell structures fabricated by the winding method and loaded by the axial forces, gasodynamic, hydrostatic or constant pressure, and inertial loads. The existence condition of a shell as a filamentary system (8) under a prescribed spectrum of acting loads is complemented, thereby, by the strength criteria for the filaments:

$$\left| \frac{2\pi \sqrt{1+(z')^2}}{n_i f z' \cos \varphi_i} \left[Q_i r_{0i} + \int_{r_{0i}}^{r} r(z' q_i + p_i)\, dr \right] \right| \leqslant \bar{\sigma}_{1i} \tag{13}$$

and for the matrix in interlaminar shear:

$$\left| \frac{n_i f}{4\pi r^2 \sqrt{1+(z')^2}} \frac{d}{dz} (\sigma_{1i} r \sin \varphi_i) \right| \leqslant \bar{\tau}_{12i} \tag{14}$$

where $\bar{\sigma}_{1i}$, $\bar{\tau}_{12i}$ is the strength of the ith layer under loading along orientation and in shear; it is also complemented by technological feasibility conditions:

reinforcement continuity

$$n_i f = \text{const} \tag{15}$$

equilibrium of the filaments during winding

$$\left| \frac{d(r \sin \varphi_i)/dr}{rz'' \cos^2 \varphi_i/[1+(z')^2] + z' \sin^2 \varphi_i} \right| \leqslant \varkappa \tag{16}$$

When designing a rational shape of the shell satisfying the existence condition (8) there are four variables: filament orientation pattern

on the surface, meridian shape, value and pattern of stress distribution in the filaments, variation of the interlaminar shear stresses. Prescribing the orientation pattern in a unique manner determines the meridian shape and, eventually, the stresses in the filament and the shear interlaminar stresses. The realization of a specific orientation pattern is here limited by inequality (16). The fabrication of uniformly stressed shells corresponding to the minimum weight designs requires a certain orientation pattern whose general equations will be treated below. Finally, a certain additional degree of freedom in design is yielded by the possibility of governing the interlaminar interactions within the material strength capacity. In formulating the general version of the problem of optimum design of the minimum weight shells of revolution, existence condition (8) and inequalities (13), (14), (16) play the role of restrictions.

10.3 DESIGN OF A MERIDIAN SHAPE WITH PRESCRIBED ORIENTATION PATTERN

Consider several filament orientations of a pressure vessel wound with a single system of filaments. The meridian load q is thereby absent and the internal pressure is constant. Note that such

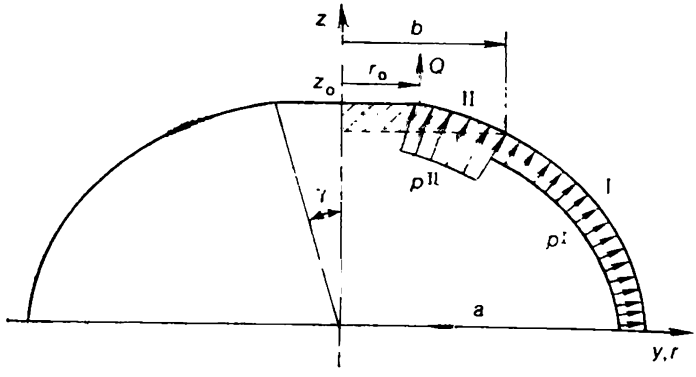

Fig. 10.2 Scheme of vessel loading and filament position in planar winding

structures always have a metal flange near the polar hole (Fig. 10.2), therefore, the meridian of the vessels has to be composed of two regions. In region I (assuming the polar hole to be closed) the load on the shell will be:

$$p^{\mathrm{I}} = p, \quad Q^{\mathrm{I}} = pr_0/2 \tag{17}$$

in region II the load of the vessel portion adjacent to the flange will be conditioned by the flange response. Assuming constant pressure

from the flange onto the shell, the load will be defined by

$$p^{II} = pb^2/(b^2 - r_0^2), \quad Q^{II} = 0 \tag{18}$$

where b is the flange radius chosen from a condition of nonnegativity of the meridian curvature $z''(b) \geqslant 0$.

One of the methods of pressure vessel fabrication is planar winding, whose chief merit is technological efficiency and construction simplicity. With such a technique the spiral circuit lies in a plane forming an angle γ with the axis of revolution z (Fig. 10.2). Pressure vessels fabricated by means of planar winding were first investigated in [12].

To determine the filament orientation pattern on the shell surface we consider the self-evident relations (Fig. 10.2):

$$x = r\cos\beta, \quad y = r\sin\beta, \quad z = y\cot\gamma$$

and, adding a differential condition (Fig. 10.1)

$$\frac{rd\beta}{dS} = \frac{r}{\sqrt{1+(z')^2}}, \quad \frac{d\beta}{dr} = \tan\varphi$$

after simple transformations we obtain

$$\tan\varphi = \frac{rz' - z}{\sqrt{1+(z')^2}\sqrt{r^2\cot^2\gamma - z^2}} \tag{19}$$

Equation (8), defining an equilibrium meridian shape, can be written in the form:

$$\frac{z''}{z'[1+(z')^2]} = \frac{2r}{r^2 - t_0^2} - \frac{1}{r}\tan^2\varphi \tag{20}$$

where the parameter t_0 is determined from the condition

$$t_0^2 = r_0^2 - (2Q/p)\, r_0 \tag{21}$$

and, according to (17) and (18), it takes the magnitudes $(t_0^I)^2 = 0$ in region I and $(t_0^{II})^2 = r_0^2$ in region II. Finally, the equilibrium meridian shape will be found via the integration of the equation:

$$\frac{z''}{z'[1+(z')^2]} = \frac{2r}{r^2 - t_0^2} - \frac{1}{r}\frac{(rz' - z)^2}{(r^2\cot^2\gamma - z^2)[1+(z')^2]} \tag{22}$$

The meridian is constructed by a numerical integration of equation (22) under the initial conditions:
in region I:

$$r = a, \quad 1/z_1' = 0, \quad z_1 = 0, \quad \tan\varphi = \tan\gamma$$

in region II:

$$r = b, \quad z_2' = z_1', \quad z_2 = z_1$$

Note that the integral to determine $z(r)$ becomes improper at $r = a$, but it is possible to prove its convergence. Besides, the determination of the tangent of winding angle with the prescribed

radius r_0 of the polar hole requires the employment of the successive approximation method to solve the equation

$$\tan \gamma = z_0/r_0$$

The condition of the technological feasibility of the design is governed by equilibrium condition (16), which can be written in the form:

$$\left| \tan \theta = \sqrt{\frac{[1+(z')^2]\,(r^2+z^2)-(rz'-z)^2}{[1+(z')^2]\,(r^2\cot^2\gamma - z^2)+(rz'-z)^2}} \right| \leqslant \varkappa$$

The stresses in the filament according to (9) are determined by the relation

$$\sigma_1 = -\frac{\pi p r^2}{nf}\,\frac{\sqrt{1+(z')^2}}{z'\cos\varphi}$$

The calculation results for the meridian of a pressure vessel are presented in Fig. 10.3 (curve *1*). Fig. 10.4 depicts the magnitudes of the tangent of the geodetic deviation angle (curve *1*), and Fig. 10.5 shows stress distribution in the filament (curve *1*).

Another possible version of the composite pressure vessel is winding along the lines of constant deviation from the geodetic line (CDL) [13]. Such a winding method enables an orientation pattern to be produced at the limits of technological feasibility, i.e. at the prescribed friction coefficient it allows the maximum deviation from a filament position suitable for the geodetic winding method. An equation of CDL according to (12) has the form:

$$\tan \theta = \pm \frac{r^2\xi'}{z'}\left\{\frac{rz''}{z'\,[1+(z')^2]}\,(r^2-\xi^2)+\xi^2\right\}^{-1} \tag{23}$$

Clairaut's function $\xi = r\sin\varphi$ is introduced here. At $\xi = \text{const}$ we obtain the well-known equation of the geodetic line on the surface of revolution. The equilibrium shape of the vessel must satisfy equation (20).

Transforming (23) with an allowance for (20) one finally obtains a set of equations which enable the determination of the meridian of the vessel and the fiber orientation pattern on its surface:

$$\begin{gathered}\tan\theta = \pm\frac{1}{z'}\,\frac{\xi'\,(r^2-t_0^2)}{2\,(r^2-\xi^2)} \\ \frac{z''}{z'\,[1+(z')^2]} = \frac{2r}{r^2-t_0^2} - \frac{1}{r}\,\frac{k\xi^2}{r^2-\xi^2}\end{gathered} \tag{24}$$

For convenience of calculation one can introduce the arc coordinate S_β at the equator and the meridian length S, which are represented

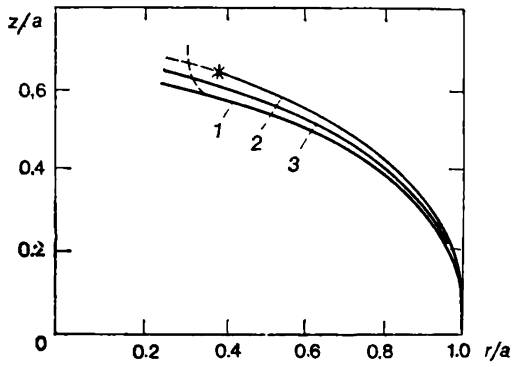

Fig. 10.3 Meridian of high-pressure vessel:
1—planar winding with $\tan\gamma = 0.4$, $r_0/a = 0.25$; *2*—winding along CDL (a line of constant deviation from a geodetic line) with $\tan\theta = 0.2$, $\sin\varphi_a = 0.4$, $r_0/a = 0.25$; *3*—geodetic winding with $r_0/a = 0.25$; *—a point of changing over to geodetic winding

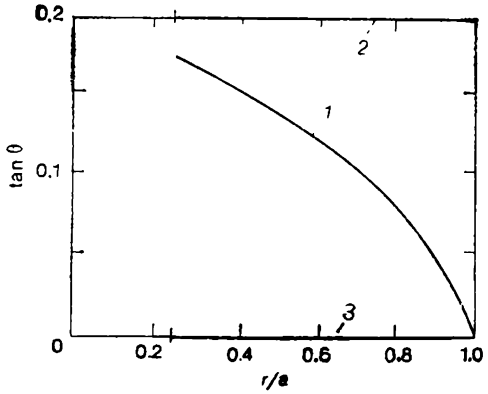

Fig. 10.4 Variation in tangent of geodetic deviation angle:
1—planar winding; *2*—winding along CDL with $\tan\theta = 0.2$; *3*—geodetic winding

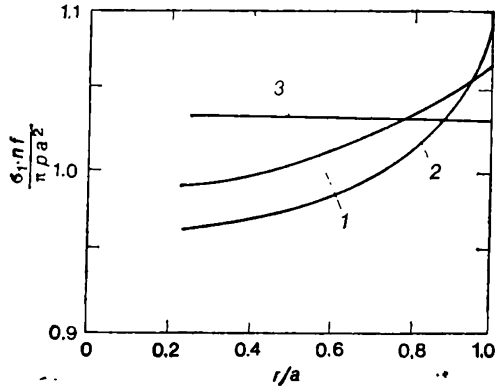

Fig. 10.5 Stress distribution in filaments:
1—planar winding with $\varphi_a = 22°$, $\tan\gamma = 0.4$, $r_0/a = 0.25$; *2*—winding along CDL with $\varphi_a = 23.5°$, $\tan\theta = 0.2$, $r_0/a = 0.25$; *3*—geodetic winding with $\varphi_a = 14.5°$, $r_0/a = 0.25$

in terms of the following relations (Fig. 10.1):

$$S_\beta = a\beta = a\int_a^r (\xi/r)\,\{[1+(z')^2]/(r^2-\xi^2)\}^{1/2}\,dr$$

$$S = \int_a^r \sqrt{1+(z')^2}\,dr$$

Combining the last expressions and adding relation (24) one finally obtains a set of equations to determine the meridian and the coordinates of the winding pattern [13]:

$$\begin{aligned}
\frac{d^2z}{dr^2} &= \frac{2rz'\,[1+(z')^2]}{r^2-t_0^2} - \frac{z'\xi^2\,[1+(z')^2]}{r\,(r^2-\xi^2)} \\
\frac{d\xi}{dr} &= \mp\frac{2z'\,(r^2-\xi^2)\tan\theta}{r^2-t_0^2} \\
\frac{dS_\beta}{dr} &= \frac{a\xi}{r}\sqrt{\frac{1+(z')^2}{r^2-\xi^2}} \\
\frac{dS}{dr} &= \sqrt{1+(z')^2}
\end{aligned} \tag{25}$$

The initial conditions in Cauchy's problem have the form

$$r = a, \quad z = 0, \quad 1/z' = 0, \quad \xi = \xi_a, \quad S_\beta = S = 0$$

As in the case of planar winding the integral to determine the meridian is improper and the meridian itself consists of two regions in the first of which $t_0 = 0$, and in the second $t_0 = r_0$.

Note an additional salient feature of the solution obtained. Depending on the value of the prescribed winding angle at the equator $\varphi = \varphi_a$ it is necessary to choose the sign of deviation from the geodetic line. Thus, at

$$\varphi_a > \arcsin(r_0/a),\ \tan\theta > 0;\ \text{at}\ \varphi_a < \arcsin(r_0\,a),\ \tan\theta < 0.$$

Besides, to form the polar hole with a prescribed radius $r = r_0$ it may be necessary to change over to geodetic winding. The change-over point is determined by the equality

$$\xi = \xi_0 = r_0$$

(see curve *2* in Fig. 10.3). Fig. 10.5 shows the distribution of stress in the filaments (curve *2*).

Finally, for purposes of comparison, let us consider a vessel reinforced over the geodetic lines. The orientation pattern of the filaments according to the requirement $\xi = r\sin\varphi = \text{const}$ is determined by the equation:

$$\sin\varphi = r_0/r \tag{26}$$

and it is borne in mind that the filament is tangential to the polar hole ($r = r_0$, $\varphi = \pi/2$). The meridian can be found numerically by integrating system (25) under a condition $\tan\theta = 0$. However, an analytical solution [5] exists in this case. Transforming the equation of equilibrium meridian existence (8) and allowing for the orientation pattern (26) we obtain

$$\frac{z''}{z'\,[1+(z')^2]} = \frac{2r}{r^2-t_0^2} - \frac{r_0^2}{r\,(r^2-r_0^2)} \tag{27}$$

Equation (27) admits the separation of variables and its first integral has the form:

$$z' = \frac{r\,(r^2-t_0^2)\,\sqrt{a^2-r_0^2}}{\sqrt{a^2\,(r^2-r_0^2)\,(a^2-t_0^2)^2 - r^2\,(a^2-r_0^2)\,(r^2-t_0^2)^2}} \tag{28}$$

The integration constant in (28) was inferred from a condition that the tangent to the meridian at $r = a$ is parallel to the axis Oz (see Fig. 10.2).

Equation (28) admits a solution in elliptic integrals, which can be presented for each of the shell regions in the following form:

For $b \leqslant r \leqslant a$ at $t_0 = 0$

$$z = \frac{z_2}{\sqrt{a^2-z_2}}\,F(k,\,\eta) + \sqrt{a^2-z_2}\,E(k,\,\eta)$$

where $F(k,\,\eta)$, $E(k,\,\eta)$ are the elliptic integrals of the first and second kind, $k = \sqrt{(a^2-z_1)/(a^2-z_2)}$ is the modulus of the elliptic integral, $\eta = \arcsin\sqrt{(a^2-r^2)/(a^2-z_1)}$ is its argument,

$$z_{1,2} = (a^2/2)\,[-1 \pm \sqrt{(a^2-3r_0^2)/(a^2-r_0^2)}]$$

For $r_0 \leqslant r \leqslant b$ at $t_0 = r_0$

$$z = -\frac{m_1}{\sqrt{m_1+m_2}}\,F(n,\,\lambda) + \sqrt{m_1+m_2}\,E(n,\,\lambda) + C$$

where

$$n = \sqrt{m_2/(m_1+m_2)}, \quad \lambda = \arccos\sqrt{(r^2-r_0^2)/m_2}$$

$$m_{1,2} = \sqrt{r_0^4/4 + a^4\,(b^2-r_0^2)^2/[b^4\,(a^2-r_0^2)]} \pm r_0^2/2$$

The integration constant C is found from a condition of the conjugation of the two shell portions.

Fig. 10.3 (curve *3*) shows the shape of the vessel meridian. Note that here $\tan\theta = 0$ (Fig. 10.4) and stresses in the filaments appear to be constant and equal to $\sigma_1 = \pi p a^2/(nf\cos\varphi_a)$ (Fig. 10.5). Thus, the condition of geodetic winding for the filament wound pressure vessel provides its uniform stress state and, hence, as already noted, its minimum weight.

10.4 GENERAL RELATIONS FOR UNIFORMLY STRESSED FILAMENT WOUND SHELLS OF REVOLUTION

The uniform stress conditions of filamentary systems working in uniaxial tension-compression are sufficient conditions for the shell minimum weight. Therefore, in designing composite structures, the design criterion of optimum—a condition of uniform stress—is commonly used.

Let us establish the general properties of uniformly stressed reinforced shells. Rewriting formulas for stresses (9) in the form:

$$Q_i r_{0i} + \int_{r_{0i}}^{r} r\,(z' q_i + p_i)\,dr = -\frac{\sigma_{1i} n_i f}{2\pi} \cos\varphi_i \frac{z'}{\sqrt{1+(z')^2}} \tag{29}$$

and differentiating the last equation in respect to r, assuming $\sigma_{1i} = \text{const}$, we obtain:

$$r\,(z' q_i + p_i) = -\frac{\sigma_{1i} n_i f}{2\pi} \frac{z'}{\sqrt{1+(z')^2}} \left\{ -\sin\varphi_i \frac{d\varphi_i}{dr} + \frac{z'' \cos\varphi_i}{z'\,[1+(z')^2]} \right\} \tag{30}$$

Having transformed the denominator on the right-hand side of equation (8) by means of (29) we arrive at

$$\frac{z''}{z'\,[1+(z')^2]} = -\frac{1}{r} \tan^2\varphi_i - \frac{2\pi}{\sigma_{1i} n_i f} \frac{1}{\cos\varphi_i} \frac{\sqrt{1+(z')^2}}{z'} r p_i \tag{31}$$

Substituting (31) into the right-hand side of relation (30) we finally find:

$$r \cos\varphi_i \frac{d\varphi_i}{dr} + \sin\varphi_i = \frac{2\pi r^2 \sqrt{1-(z')^2}}{\sigma_{1i} n_i f} q_i \cot\varphi_i \tag{32}$$

Equation (32), jointly with equation (8), defines the meridian shape and the orientation pattern providing the shell uniform stress state (more exactly, that of a pair of layers with the angles $\pm\varphi_i$) under the prescribed external load.

Note some specific features of the uniformly stressed shells. The uniform stress condition (32) can be written in the form:

$$\frac{d}{dr}(r \sin\varphi_i) = \frac{2\pi r^2 \sqrt{1+(z')^2}}{\sigma_{1i} n_i f} q_i \cot\varphi_i \tag{33}$$

Substituting the left-hand side of (33) into (10) to determine the interlaminar stresses we obtain under the condition $\sigma_{1i} = \text{const}$

$$\tau_i = (q_i/2) \cot\varphi_i \tag{34}$$

Finally, the condition of filament equilibrium on the mandrel surface (16) can be transformed in a more simple form. Substituting formulas (31) and (33) into expression (12) for the geodetic deviation angle

tangent, after certain transformations we find

$$\tan \theta_i = -q_i/(p_i \sin \varphi_i) \tag{35}$$

It could be shown that for uniformly stressed systems the existence condition (8) is identically satisfied with the simultaneous fulfilment of conditions (29) and (32) or (33). Hence a uniformly stressed shell of revolution fabricated by means of the winding of filaments oriented at the angles $\pm\varphi_i$ relative to the meridian is described by the following set of equations in which one has to take $\sigma_{1i} = \bar{\sigma}_{1i} = \text{const}$:

$$\frac{\bar{\sigma}_{1i} n_i f}{2\pi} \cos \varphi_i \frac{z'}{\sqrt{1+(z')^2}} + Q_i r_{0i} + \int_{r_{0i}}^{r} r (z' q_i + p_i)\, dr = 0$$

$$\frac{d}{dr}(r \sin \varphi_i) = \frac{2\pi r^2 \sqrt{1+(z')^2}}{\bar{\sigma}_{1i} n_i f} q_i \cot \varphi_i \tag{36}$$

$$|\tau_i = (1/2)\, q_i \cot \varphi_i| \leqslant \bar{\tau}_{12i}$$

$$|\tan \theta_i = -q_i/(p_i \sin \varphi_i)| \leqslant \varkappa$$

Relations (36) are the general conditions of existence of the uniformly stressed reinforced shells of revolution and in particular cases they allow both all the known and also a set of the new structural shapes of shells to be obtained.

Consider a shell under nonuniform, e.g. hydrostatic, pressure. According to conditions (36) the orientation pattern at $q_i = 0$ coincides with an equation of the geodetic surface $r \sin \varphi_i = \text{const}$. The first equation of the set comprising the equilibrium condition for a cut-off shell portion can be presented in the form:

$$z' = -\frac{2\pi}{\bar{\sigma}_{1i} n_i f \cos \varphi_i} \times \frac{Q_i r_{0i} + \int_{r_{0i}}^{r} p_i\, r dr}{\sqrt{[1/(4\pi^2)]\, \bar{\sigma}_{1i}^2 n_i^2 f^2 \cos^2 \varphi_i - \left[Q_i r_{0i} + \int_{r_{0i}}^{r} p_i r dr\right]^2}} \tag{37}$$

The shell thickness and hence the number n_i of the filaments can be found in an arbitrary cross-section, e.g. at $r = a$, $z'(a) = z'_o$,

$\varphi = \varphi_a$. Then we obtain

$$z' = -z'_a \cos\varphi_a \left(Q_i r_{0i} + \int_{r_{0i}}^{r} p_i\, r dr\right)$$
$$\times \left\{[1+(z'_a)^2]\cos^2\varphi \left(Q_i r_{0i} + \int_{r_{0i}}^{a} p_i\, r dr\right)^2 \right.$$
$$\left. -(z'_a)^2 \cos^2\varphi_a \left(Q_i r_{0i} - \int_{r_{0i}}^{r} p_i\, r dr\right)^2\right\}^{-1/2} \qquad (38)$$

Consider a shell filled with a liquid of density ρ. Let us choose the coordinate origin at a cross-section $r = r_{\max} = a$ and direct

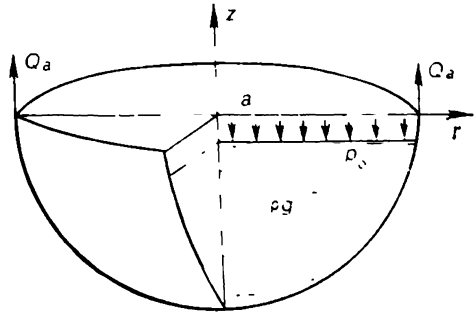

Fig. 10.6 Loading scheme of liquid-filled shell

the axis z upwards (Fig. 10.6). In that case pressure within the shell will obey the law $p = p_0 - \rho g z$, where $p_0 = \text{const}$ and is equal to the pressure at a cross-section $z = 0$. Taking into account that the first equation from (36) is an equilibrium condition of the cut-off portion one finds:

$$\frac{z'}{\sqrt{1-(z')^2}} = -\frac{\Psi}{\Psi_a}\frac{\cos\varphi_a}{\cos\varphi} \qquad (39)$$

where

$$\Psi = \pi p_0 (r^2 - a^2) + 2\pi\rho g \int_r^a z r\, dr + \Psi_a$$

$$\Psi_a = 2\pi a Q_a$$

Thus, to determine the meridian shape under hydrostatic pressure and geodetic winding one obtains the integral equation:

$$z(r) = \int_r^a \frac{\Psi \cos\varphi_a\, dr}{\sqrt{\Psi_a^2 \cos^2\varphi - \Psi^2 \cos^2\varphi_a}} \qquad (40)$$

which can be solved numerically by the successive approximation method.

One of the methods of constructing the meridian shape of a uniformly stressed shell filled with a liquid is described in [14]. Bearing in mind that meridian curvature is defined by the relation

$$\frac{1}{R_1} = \frac{d}{dr}\left(\frac{z'}{\sqrt{1+(z')^2}}\right)$$

and allowing for (39) one finds

$$\frac{1}{R_1} = \frac{(d\Psi/dr)\cos\varphi_a}{\Psi_a \cos\varphi} - \frac{\Psi\cos\varphi_a}{\Psi_a\cos^2\varphi}\frac{d\cos\varphi}{dr} \tag{41}$$

Otherwise, from the geodetic winding condition $r\sin\varphi = a\sin\varphi_a = r_0$ one obtains

$$\frac{1}{\cos\varphi}\frac{d\cos\varphi}{dr} = \frac{1}{r}\tan^2\varphi = \frac{1}{r}\frac{r_0^2}{r^2-r_0^2}$$

Finally, the meridian curvature radius will be defined by the relation:

$$\bar{R}_1 = \left[\frac{2\pi}{\Psi_a}\sqrt{1-\bar{r}_0^2}\,\frac{\bar{r}^2(p-\rho g\bar{z})}{\sqrt{\bar{r}^2-\bar{r}_0^2}} - \frac{1}{\bar{r}}\frac{\bar{r}_0^2}{\bar{r}^2-\bar{r}_0^2}\frac{z'}{\sqrt{1+(z')^2}}\right]^{-1} \tag{42}$$

where $\bar{R}_1 = R_1/a$, $\bar{r} = r/a$, $\bar{r}_0 = r_0/a$, $\bar{z} = z/a$.

Prescribing a boundary magnitude of the axial force Ψ_a and employing (42) one can find numerically or graphically the meridian shape. In the first region at $z_a' \to \infty$ and $z \to 0$, according to (42), one finds $\bar{R}_1^1$ and draws an arc of radius $\bar{R}_1^1$. Computing the magnitudes $z_1 = z_1'$ for $\bar{r}_1 = \Delta\bar{r}$ one finds $\bar{R}_1^2$, etc. The meridian possesses a spiral shape with the circuits contracting with the sinking of the spiral and its receding from the axis of revolution z (Fig. 10.7). Fig. 10.8 shows a shell meridian with the parameters $\bar{r}_0 = 0.1$, $p_0/\rho g a = 0.6$, $Q_a = p_0 a/2$.

One of the promising applications of reinforced composites is associated with the manufacture of inertial energy accumulators—flywheels. The high specific strength of composites allows an essential increase in the energy parameters to be anticipated as compared to flywheels made of conventional structural materials. We can imagine as one of the flywheel types a membrane shell of revolution for which the condition of stress uniformity provides the maximum rotation speed for the prescribed weight. The scheme of the shell loading is depicted in Fig. 10.9. The normal and tangential forces are thereby expressed in terms of the centrifugal force $t = \rho h\omega^2 r$ (ρ is the mate-

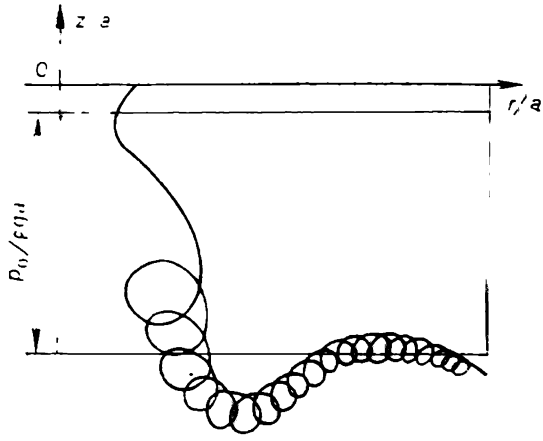

Fig. 10.7 General view of meridian of shell under hydrostatic pressure

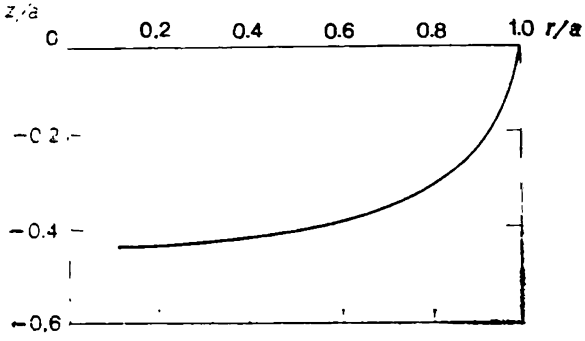

Fig. 10.8 Meridian of liquid-filled shell

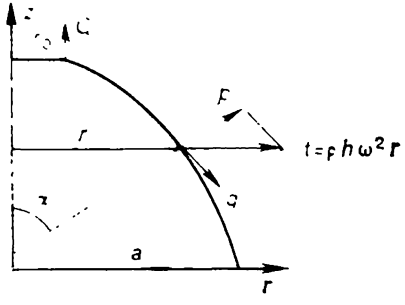

Fig. 10.9 Loading scheme for rotating shell

rial density, ω is the angular velocity):

$$p = t\sin\alpha = -\frac{\rho h\omega^2 rz'}{\sqrt{1+(z')^2}}$$
$$q = t\cos\alpha = \frac{\rho h\omega^2 r}{\sqrt{1+(z')^2}} \qquad (43)$$

Substituting loads p and q of (43) into the first equation of (36) and bearing in mind that $z'q + p = 0$ we find:

$$\frac{z'}{\sqrt{1+(z')^2}} = -\frac{2\pi Qr_0}{\bar{\sigma}_1 nf\cos\varphi} \qquad (44)$$

Then the second equation in (36), allowing for (43) and (44), will yield the equation defining the orientation pattern of the uniformly stressed shell:

$$\frac{d}{dr}(r\sin\varphi) = \frac{\lambda r^2}{a^2\sin\varphi}$$

where $\lambda = \rho\omega^2 a^2/\bar{\sigma}_1$. The solution of this equation, satisfying the condition $\varphi\,(r = a) = \varphi_a$, has the form

$$\sin\varphi = (a/r)\sqrt{\sin^2\varphi_a - (\lambda/2)(1 - r^4/a^4)} \qquad (45)$$

Let us investigate the pattern obtained. From condition $\sin^2\varphi \geqslant 0$ one obtains

$$r^2 \geqslant r_{01}^2 = a^2\sqrt{1-(2\sin^2\varphi_a/\lambda)}$$

At $\lambda > 2\sin^2\varphi_a$ this relation determines the radius of the polar hole $r = r_{01}$ on the contour of which the fibers are tangential to the meridian ($\varphi = 0$). At $\lambda < 2\sin^2\varphi_a$ the value of r_{01} appears to be imaginary. From condition $\sin^2\varphi \leqslant 1$ and equation (45) one has

$$r^2 \geqslant r_{02}^2 = (a^2/\lambda)\left[1 - \sqrt{(\lambda-1)^2 + 2\lambda\cos^2\varphi_a}\right]$$

At $\lambda < 2\sin^2\varphi_a$ the fibers are tangential to the contour of a polar hole of radius $r_0 = r_{02}$ ($\varphi = \pi/2$). At $\lambda = 2\sin^2\varphi_a$ it is evident that $r_0 = r_{01} = r_{02} = 0$, i.e. we have the pattern corresponding to a shell closed at the apex. According to (45) it is defined by

$$a\sin\varphi = r\sin\varphi_a$$

Let us find a meridian of the uniformly stressed shell. From (44) one directly obtains

$$z' = \pm\frac{2\pi Qr_0}{\sqrt{\bar{\sigma}_1^2 n^2 f^2\cos^2\varphi - 4\pi^2 Q^2 r_0^2}} \qquad (46)$$

Let us require that the tangent to the meridian at $r = a$ be parallel to the axis z. From (46) one thereby finds:

$$Q = \frac{\bar{\sigma}_1 nf\cos\varphi_a}{2\pi r_0}$$

allowing the axial forces Q corresponding to the ultimate stresses in the filaments to be determined. Substituting the orientation pattern (45) into (46) and integrating one can obtain two families of meridians:

at $0 \leqslant r \leqslant a$

$$z = a \frac{\cos \varphi_a}{\sqrt{2\lambda}} \left(\frac{\pi}{2} - \arcsin \frac{\lambda r^2 - a^2 \sin^2 \varphi_a}{\lambda a^2 - a^2 \sin^2 \varphi_a} \right) \tag{47}$$

at $r \geqslant a$

$$z = a \frac{\cos \varphi_a}{\sqrt{2\lambda}} \left(\frac{\pi}{2} - \arcsin \frac{a^2 \sin^2 \varphi_a - \lambda r^2}{a^2 \sin^2 \varphi_a - \lambda a^2} \right) \tag{48}$$

Equation (47) is valid at $\lambda > \sin^2 \varphi_a$ and equation (48) at $\lambda < \sin^2 \varphi_a$.

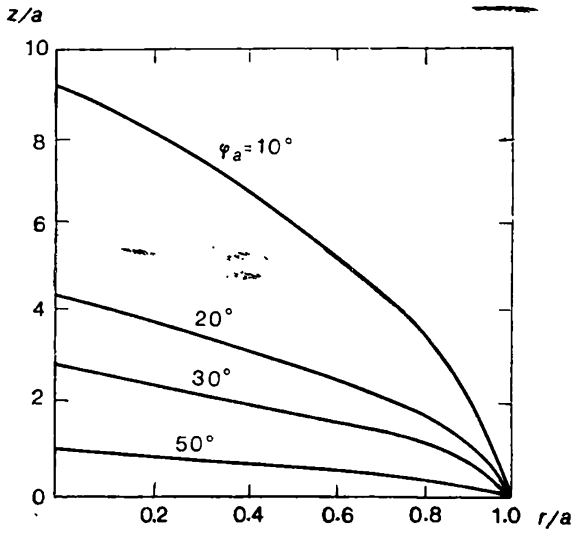

Fig. 10.10 Meridian of uniformly stressed rotating shell closed at the apex

At $\varphi_a = \pi/2$ one has $z = 0$, i.e. the solution obtained defines a uniformly stressed rotating disc. Orientation pattern (45) at $\varphi = \pi/2$ has been obtained and studied in [15].

For a shell closed at the apex at $\lambda = 2 \sin^2 \varphi_a$ it follows from (47) that

$$z = (a/2) \cot \varphi_a \left[\pi/2 - \arcsin (2r^2/a^2 - 1) \right] \tag{49}$$

The family of meridians drawn according to (49) is shown in Fig. 10.10. Here the angular velocity of the shell is determined by

$$\omega^2 = 2 \sin^2 \varphi_a \bar{\sigma}_1 / \rho a^2$$

Consider the design of a uniformly stressed shell of revolution consisting of k filament systems and loaded by internal pressure. For a shell composed of k layers the interlaminar forces should satisfy the following equations:

$$\sum_{i=1}^{k} p_i = p, \quad \sum_{i=1}^{k} Q_i = Q, \quad \sum_{i=1}^{k} q_i = 0 \tag{50}$$

Summing up the first equations from (36) for all layers, allowing for (50), and assuming the material of all the layers to be the same, one obtains

$$\frac{\bar{\sigma}_1}{2\pi} \frac{z'}{\sqrt{1+(z')^2}} \sum_{i=1}^{k} n_i f \cos\varphi_i + Qr_0 + \int_{r_0}^{r} pr\,dr = 0 \tag{51}$$

Consider the possible classes of optimum structures. The main class of optimum designs is determined by prescribing a distribution of the interlaminar forces, i.e. by the function $q_i(r)$, which must satisfy the two last equations in (36). So far only one case $q_i = 0$ from that class has been studied. Given $q_i(r)$ the integration of equation (36) provides the orientation patterns of all the layers and the shape of the meridian of a uniformly stressed shell. Note that, as a rule, the filament orientations of the ith layer are meaningful only over part of the whole shell surface. In connection with the latter let us divide a k-layer shell into k regions so that in a region labelled j the shell will be composed of j layers ($j = 1, 2, \ldots, k$). Since the equilibrium equation (51) should be satisfied in each region one has

$$\frac{\bar{\sigma}_1}{2\pi} \frac{z_j'}{\sqrt{1+(z_j')^2}} \sum_{i=1}^{j} n_i f \cos\varphi_i + Qr_{0j} + \int_{r_{0j}}^{r} pr\,dr = 0 \tag{52}$$

where $z_j(r)$ is the equation of the meridian in the region j.

Consider the problem of constructing a meridian of a uniformly stressed shell with an orientation pattern as in Fig. 10.11. To simplify the derivation we shall consider the polar hole as being closed and the internal pressure as constant. Assume that the shell in the region of the first layer consists of two portions in the first of which the pressure is conditioned by the flange response (18), and in the second by the internal pressure (17).

According to (52) for the first region at $Q = 0$, $p_1 = pb^2/(b^2 - r_{01}^2)$, $r_{0j} = r_{01}$ one has

$$z_0' = -\frac{r\sqrt{r^2 - r_{01}^2}}{\sqrt{C_0^2 - r^2(r^2 - r_{01}^2)}}$$

where

$$C_0 = \frac{\bar{\sigma}_1 n_1 f}{\pi p} \frac{b^2 - r_{01}^2}{b^2}, \quad \text{and} \quad r \sin \varphi_0 = r_{01}$$

Analogously, for the second region

$$z_1' = -\frac{r^3}{\sqrt{C_1^2 (r^2 - \bar{r}_{01}^2) - r^6}}$$

where $C_1 = \bar{\sigma}_1 n_1 f/(\pi p)$ and $r \sin \varphi_1 = r_{01}$.

For any part of the shell composed of the j layers and confined between the parallel lines $r = r_{0j}$ and $r = r_{0j+1}$ one obtains

$$z_j' = -r^3 \left[\left(\sum_{i=1}^{j} C_i \sqrt{r^2 - r_{0i}^2} \right) - r^6 \right]^{-1/2}$$

where $C_i = \bar{\sigma}_1 n_i f/\pi p$ and $r \sin \varphi_i = r_{0i}$

Direct checking can establish the identical fulfilment of the conjugation conditions for all the regions. Since the shells under consideration are, as a rule, bottom parts of pressure vessels (including

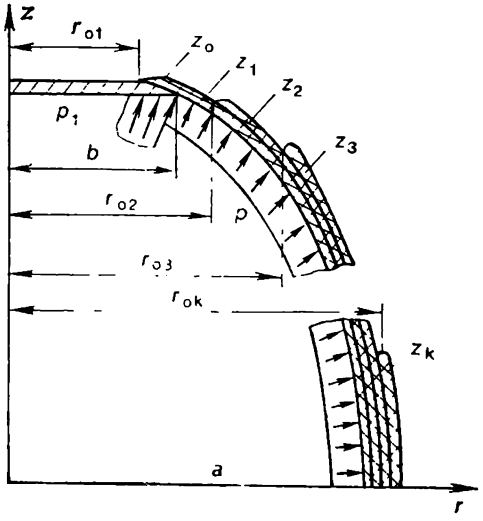

Fig. 10.11 Structure of multilayer shell **of revolution**

the case of a zero length cylindrical part), we require the tangent to the meridian at the equator be parallel to the shell axis, i.e. at $r = a$ it would be $(1/z_n') = 0$. Tending to zero the denominator of the meridian equation in the region of $j = k$ we obtain

$$[\bar{\sigma}_1'/(\pi p)] \sum_{i=1}^{k} n_i f \sqrt{a^2 - r_{0i}^2} = a^3$$

The last equation is the strength condition at the equator and can be written in the form:

$$\sum_{i=1}^{k} n_i f \cos \varphi_{ai} = \pi p a^2 / \bar{\sigma}_1 \tag{53}$$

The choice of the number of filaments composing each of the shell layers is fairly arbitrary [11]. Choosing the filament number for all

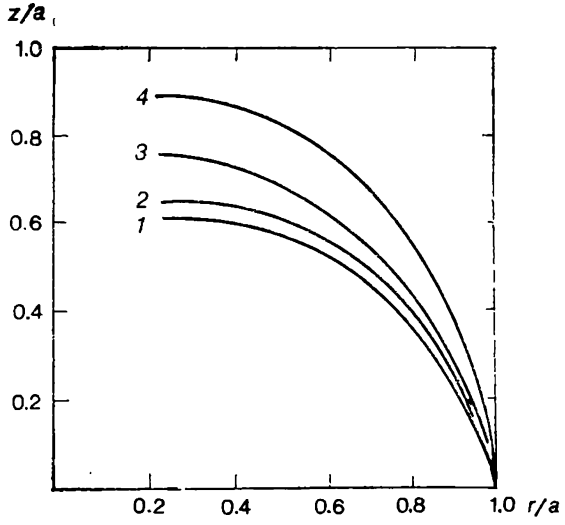

Fig. 10.12 Variation in meridian of multilayer shell of revolution with the number of layers k:
1—at $k = 2$, $\varphi_{a1} = 17°$; *2*—at $k = 2$, $\varphi_{a1} = 17°$, $\varphi_{a2} = 30°$; *3*—at $k = 3$, $\varphi_{a1} = 17°$, $\varphi_{a2} = 30°$, $\varphi_{3a} = 45°$; *4*—at $k = 5$, $\varphi_{a1} = 17°$, $\varphi_{a2} = 30°$, $\varphi_{a3} = 45°$, $\varphi_{a4} = 60°$, $\varphi_{a5} = 75°$

the $(j - 1)$ layers the limits of n_j are governed by the following conditions: on the one hand, the ultimate pressure is only borne by the jth layer filaments, i.e.,

$$(n_j f)_{\max} = \frac{a}{\sqrt{a^2 - r_{0j}^2}} \left(\frac{\pi p a^2}{\bar{\sigma}_1} - \sum_{i=1}^{j-1} n_i f \sqrt{1 - r_{0i}^2/a^2} \right)$$

and, on the other hand, in the region of the $(j - 1)$th layer, the shell degenerates into the cylinder

$$(n_j f)_{\min} = \frac{1}{\sqrt{r_{0,j+1}^2 - r_{0j}^2}} \left(\frac{\pi p r_{0,j+1}^3}{\bar{\sigma}_1} - \sum_{i=1}^{j-1} n_i f \sqrt{r_{0,j+1}^2 - r_{0j}^2} \right)$$

In this, firstly, the number of filaments in each layer should be an integer, and, secondly, for a single layer, e.g. the last one, the num-

ber of filaments cannot be chosen at will but is determined in a unique manner from condition (53).

Fig. 10.12 depicts the variation in the shell meridian with the number of constituent layers. It is not difficult to see that choosing in an appropriate way the number of filaments in the layers the meridian shape can be varied within rather wide limits.

10.5 GENERAL PROBLEM FORMULATION OF OPTIMUM REINFORCEMENT OF SHELLS OF REVOLUTION

It has been stated above that within the model of a composite seen as a filament system the absolute weight minimum of a membrane shell of revolution is attained within the class of uniformly stressed structures. Yet the existence of a uniformly stressed system is limited by the possible orientation pattern determined by equation (33). Generally, the problem of the optimum reinforcement of the membrane shell of revolution reduces to the identification of the filament orientation pattern and the meridian shape yielding a structure weight minimum defined by the equation

$$G = \sum_{i=1}^{k} \rho_i n_i f S_{1i}$$

where S_{1i} is the length of a filament from the ith system, ρ_i is the material density with restrictions expressed in terms of equations (8) and (13)-(16). In such a formulation the problem can be solved by means of a sufficiently well developed body of mathematics, namely the theory of optimum control. The substantial difficulties in this case are, firstly, the nonlinearity in both the functional being minimized and the restrictions imposed, and, secondly, representation of the restrictions in the form of inequalities. Therefore, to realize the solution in practice one can use the method of nonlinear transformations of variables [16].

Let us illustrate the application of the above method with an example of solving the problem of the search of an optimum orientation pattern and equilibrium form of the cylindrical vessel dome fabricated by the winding. In so doing, there exists no solution within the class of the uniformly stressed structures if $a \sin \varphi_a \neq r_0$. To decrease the number of restrictions imposed we shall assume that the stresses in the filaments of an optimum shell are maximum at the equator and monotonously decrease towards the pole [13]. From equation (9) with $q = 0$ one obtains

$$\sigma_1 = \frac{\pi \sqrt{1 + z'^2}}{nfz' \cos \varphi} p (r^2 - t_0^2) \qquad (54)$$

where a parameter t_0^2 is defined by (21). The existence equation of the equilibrium meridian (8) can be written in the form

$$\left[\ln \frac{\sqrt{1+(z')^2}}{z'}\right]' = \frac{2r}{r^2-t_0^2} - \frac{1}{r}\tan^2\varphi \tag{55}$$

and the condition of filament equilibrium on the mandrel surface during winding (16), taking into account (8), in the form:

$$\left|\tan\theta = \frac{1}{z'}\,\frac{(r\sin\varphi)'\,(r^2-t_0^2)}{2r^2\cos^2\varphi}\right| \leqslant \varkappa \tag{56}$$

A condition of the monotonous decrease in stresses is equivalent to the condition $(\ln \sigma_1)' \leqslant 0$. Then, combining (54) with (55), one obtains that the assumption accepted is realizable at

$$\sin\varphi\,(r\sin\varphi)'/(r\cos\varphi) \leqslant 0$$

The last inequality is satisfied for the problem stated if

$$(r\sin\varphi)' \leqslant 0 \tag{57}$$

then, according to (56)

$$0 \leqslant \tan\theta \leqslant \varkappa \tag{58}$$

The condition of filament strength (13) is thereby automatically satisfied.

Note also that the restriction on strength in interlaminar shear is, as a rule, immaterial under small pressures and an orientation deviating from the geodetic one within the friction cone. To formulate the problem in terms of optimum control we shall introduce the following notations: $x_1 = S_1 = \int_0^r \{[1+(z')^2]/\cos^2\varphi\}^{1/2}\,dr$ is the filament length; $x_2 = r\sin\varphi = \xi$ is Clairaut's function; $x_3 = \beta$ is the polar angle (Fig. 10.1); $x_4 = r$ is an additional coordinate introduced owing to the nonstationary nature of the restrictions; $x_5 = z'$; $u_1 = \beta'$, $u_2 = \xi'$. Here x_n are the coordinates of a system state and u_m those of control. We shall write restrictions (58) in the normal form:

$$|\,q\,(x_n,\,u_m)\,| \leqslant 1 \tag{59}$$

where

$$q = \frac{2\tan\theta}{\varkappa} - 1 = \frac{1}{\varkappa}\,\frac{u_2\,(x_4^2-t_0^2)}{x_4^2-x_3^2} - 1$$

Inequality (59) can be transformed into an equality by introducing an additional control v by means of the nonlinear transformation

ber of filaments cannot be chosen at will but is determined in a unique manner from condition (53).

Fig. 10.12 depicts the variation in the shell meridian with the number of constituent layers. It is not difficult to see that choosing in an appropriate way the number of filaments in the layers the meridian shape can be varied within rather wide limits.

10.5 GENERAL PROBLEM FORMULATION OF OPTIMUM REINFORCEMENT OF SHELLS OF REVOLUTION

It has been stated above that within the model of a composite seen as a filament system the absolute weight minimum of a membrane shell of revolution is attained within the class of uniformly stressed structures. Yet the existence of a uniformly stressed system is limited by the possible orientation pattern determined by equation (33). Generally, the problem of the optimum reinforcement of the membrane shell of revolution reduces to the identification of the filament orientation pattern and the meridian shape yielding a structure weight minimum defined by the equation

$$G = \sum_{i=1}^{k} \rho_i n_i f S_{1i}$$

where S_{1i} is the length of a filament from the ith system, ρ_i is the material density with restrictions expressed in terms of equations (8) and (13)-(16). In such a formulation the problem can be solved by means of a sufficiently well developed body of mathematics, namely the theory of optimum control. The substantial difficulties in this case are, firstly, the nonlinearity in both the functional being minimized and the restrictions imposed, and, secondly, representation of the restrictions in the form of inequalities. Therefore, to realize the solution in practice one can use the method of nonlinear transformations of variables [16].

Let us illustrate the application of the above method with an example of solving the problem of the search of an optimum orientation pattern and equilibrium form of the cylindrical vessel dome fabricated by the winding. In so doing, there exists no solution within the class of the uniformly stressed structures if $a \sin \varphi_a \neq r_0$. To decrease the number of restrictions imposed we shall assume that the stresses in the filaments of an optimum shell are maximum at the equator and monotonously decrease towards the pole [13]. From equation (9) with $q = 0$ one obtains

$$\sigma_1 = \frac{\pi \sqrt{1+z'^2}}{nfz' \cos \varphi} p (r^2 - t_0^2) \qquad (54)$$

where a parameter t_0^2 is defined by (21). The existence equation of the equilibrium meridian (8) can be written in the form

$$\left[\ln \frac{\sqrt{1+(z')^2}}{z'}\right]' = \frac{2r}{r^2-t_0^2} - \frac{1}{r}\tan^2\varphi \tag{55}$$

and the condition of filament equilibrium on the mandrel surface during winding (16), taking into account (8), in the form:

$$\left|\tan\theta = \frac{1}{z'}\,\frac{(r\sin\varphi)'\,(r^2-t_0^2)}{2r^2\cos^2\varphi}\right| \leqslant \varkappa \tag{56}$$

A condition of the monotonous decrease in stresses is equivalent to the condition $(\ln \sigma_1)' \leqslant 0$. Then, combining (54) with (55), one obtains that the assumption accepted is realizable at

$$\sin\varphi\,(r\sin\varphi)'/(r\cos\varphi) \leqslant 0$$

The last inequality is satisfied for the problem stated if

$$(r\sin\varphi)' \leqslant 0 \tag{57}$$

then, according to (56)

$$0 \leqslant \tan\theta \leqslant \varkappa \tag{58}$$

The condition of filament strength (13) is thereby automatically satisfied.

Note also that the restriction on strength in interlaminar shear is, as a rule, immaterial under small pressures and an orientation deviating from the geodetic one within the friction cone. To formulate the problem in terms of optimum control we shall introduce the following notations: $x_1 = S_1 = \int_0^r \{[1+(z')^2]/\cos^2\varphi\}^{1/2}\,dr$ is the filament length; $x_2 = r\sin\varphi = \xi$ is Clairaut's function; $x_3 = \beta$ is the polar angle (Fig. 10.1); $x_4 = r$ is an additional coordinate introduced owing to the nonstationary nature of the restrictions; $x_5 = z'$; $u_1 = \beta'$, $u_2 = \xi'$. Here x_n are the coordinates of a system state and u_m those of control. We shall write restrictions (58) in the normal form:

$$|\,q\,(x_n,\,u_m)\,| \leqslant 1 \tag{59}$$

where

$$q = \frac{2\tan\theta}{\varkappa} - 1 = \frac{1}{\varkappa}\,\frac{u_2\,(x_4^2-t_0^2)}{x_4^2-x_3^2} - 1$$

Inequality (59) can be transformed into an equality by introducing an additional control v by means of the nonlinear transformation

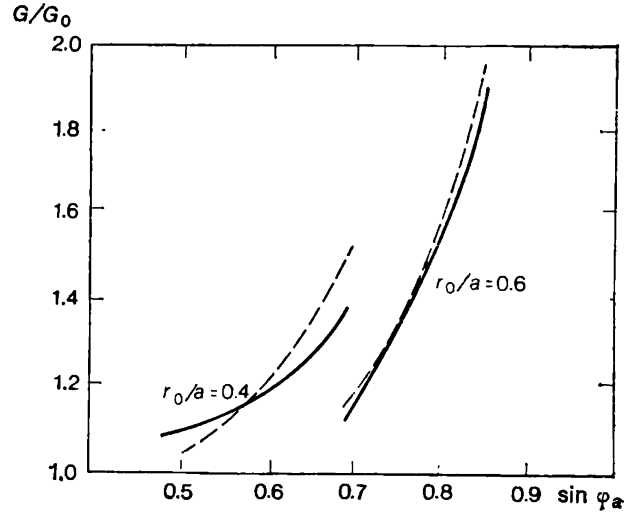

Fig. 10.14 Relative weight of vessel with different orientation patterns ($\varkappa = 0.2$). The dashed curves, $\tan\theta = \varkappa$, $\tan\theta = 0$; the solid curves, $\tan\theta = \varkappa$, $\tan\theta = -\varkappa$.

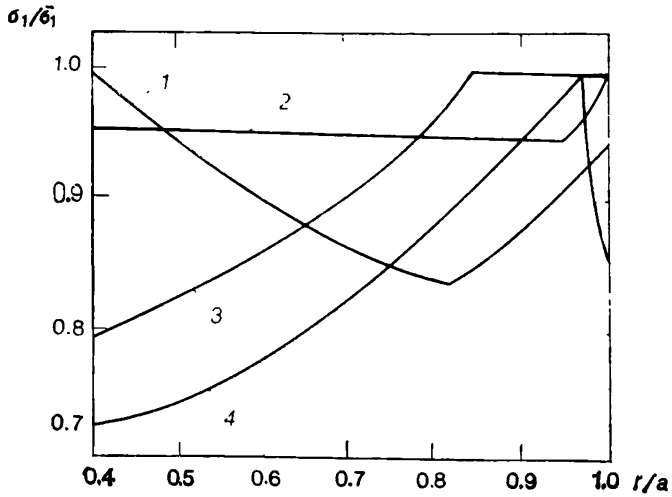

Fig. 10.15 Stress distribution in filaments for different orientation patterns ($r_a/a = 0.4$, $\varkappa = 0.3$):
1—at $\tan\theta = +\varkappa$, $\tan\theta = -\varkappa$; *2*—at $\tan\theta = +\varkappa$, $\tan\theta = 0$; *3*—at $\tan\theta = 0$, $\tan\theta = +\varkappa$; *4*—at $\tan\theta = -\varkappa$, $\tan\theta = +\varkappa$

the filaments. Not listing ponderous considerations, analogous to those mentioned above, let us note certain results of numerical analysis. In the general case the optimum orientation can be synthesized in terms of the three extremals $\tan\theta = +\varkappa$, $\tan\theta = -\varkappa$, $\tan\theta = 0$. The last condition corresponds to the uniform stress state of the shell. The weight of shells does not decrease with an increase in the number of switchover points. Thus, the weight of a shell, whose filament orientation pattern fits two switchover points and comprises a set of the extremals $\tan\theta = +\varkappa$, $\tan\theta = 0$, $\tan\theta = -\varkappa$, lies within an interval between the weight of shells fabricated by means of the winding with the orientation patterns $\tan\theta = +\varkappa$, $\tan\theta = -\varkappa$, and $\tan\theta = +\varkappa$, $\tan\theta = 0$, being in this sense limiting for an initial condition $\varphi_a > \arcsin(r_0/a)$. Besides, the optimum version of the filament orientation pattern with a single switchover point at the prescribed orientation angle at the vessel equator depends on the value of the polar hole radius and the available friction coefficient. Fig. 10.14 depicts the variation in the relative weight of a vessel with an open polar hole ($Q_0 = 0$, $t_0^2 = r_0^2$) with the relative value of the polar radius r_0 at different prescribed orientation angles at the equator. The vessel weight is related to the appropriate vessel weight which is formed by geodetic winding at $\varphi_a = \arcsin(r_0/a)$.

It is not difficult to see that for slight deviation from the geodetic orientation an orientation pattern of the type $\tan\theta = +\varkappa$, $\tan\theta = 0$ is the most effective. This very fact is illustrated in Fig. 10.15 where the stress distribution in the filaments is shown. Since the uniformly stressed filamentary system possesses an absolute weight minimum the efficiency of the orientation pattern can be evaluated over the degree of approximation of the condition $\sigma_1 = \text{const} = \overline{\sigma_1}$ by the stress distribution law.

Note that the presented method of generating the orientation pattern employing an optimum control technique is successfully applied to the construction of rational filament orientation in the shells of a given shape when the construction of a uniformly stressed system, i.e. the formation of a structure by means of several filament systems, presents some difficulties.

References

1. Biderman, V.L., in: *Strength Analysis*, vol. 11, Mashinostroyenie, Moscow, 1965, pp. 3-30 (in Russian).
2. Ambartsumyan, S.A., *General Theory of Anisotropic Shells*, Nauka, Moscow, 1974 (in Russian).
3. Bolotin, V.V., *Mekh. polimerov*, 2, 27-37 (1965).
4. Korolyov, V.I., *Laminated Anisotropic Plates and Shells from Reinforced Plastics*, Mashinostroyenie, Moscow, 1965 (in Russian).
5. Elpat'evskii, A.N., and Vasil'ev, V.V., *Strength of Cylindrical Shells from Reinforced Materials*, Mashinostroyenie, Moscow, 1972 (in Russian).

6. Bunakov, V.A., and Rodovinskii, A.L., *Mekh. polimerov*, 5, 822-828 (1975).
7. Zickel, J., *ARS, J.*, 6 (1962).
8. Schuerch, H., Burggraf, O., *AIAA J.*, 5 (1964).
9. Cherevatskii, S.B., in: *Studies into the Theory of Plates and Shells*, vol. 5, Izd. KGU, Kazan, 1967, pp. 554-573 (in Russian).
10. Vasil'ev, V.V., in: *Proc. VII All-Union Conference on Theory of Shells and Plates* (Dnepropetrovsk, 1969), Nauka, Moscow, 1970 pp. 721-735 (in Russian).
11. Obraztsov, I.F., Vasil'ev V.V., and Bunakov, V.A., *Optimum Design of Composite Shells of Revolution*, Mashinostroyenie, Moscow, 1977 (in Russian).
12. Hartung, R., *AIAA J.*, 12 (1963).
13. Mitkevich, A.B., and Protasov, V.D., *Mekh. polimerov*, 6, 983-987, 1975.
14. Cherevatskii, S.B., and Romashov, Yu.P., in: *Strength and Dynamics of Aircraft Engines*, vol. 4, Mashinostroyenie, Moscow, 1966 pp. 5-19 (in Russian).
15. Kyser, A., *AIAA J.*, 7 (1965).
16. Vorob'ev, L.M., and Vorob'eva, T.M., *Nonlinear Transformations in Applied Variational Problems*, Energia, Moscow, 1972 (in Russian).

TO THE READER

Mir Publishers would be grateful for your comments on the content, translation and design of this book. We would also be pleased to receive any other suggestions you may wish to make.

Our address is:
Mir Publishers
2 Pervy Rizhsky Pereulok
I-110, GSP, Moscow, 129820
USSR

Mechanics of Composites

Edited by I.F. Obraztsov and V.V. Vasil'ev

This book is concerned with topical problems of the mechanics of composite systems made up of high-strength continuous fibers and a polymeric or metal matrix. Ten papers, written by leading Soviet specialists working in this field, analyze the features of modern composites, discuss the central problems on whose successful solution the efficiency of application of these materials in structures of contemporary engineering depends, consider particular problems of micro- and macro-mechanics, and deal with the design and production of composite systems.

The book presents the statistical theory of composite fracture, microstructural methods of prediction of static, long-time, cyclic strength and creep of composites with metal and polymeric matrices under various loads, the micromechanics of fibrous composites with cracks, the macromechanics and nonlinear phenomenological models of the deformation and failure of laminated composites with a brittle polymeric matrix. The problems of composite production and the prediction of the properties of composites with whiskerized fibers, the mechanics of the formation of curing stresses, the methods of determination and control of the properties of thin-walled and thick-walled structural elements produced by winding are discussed. The theory of optimum design of membrane composite shells of revolution subjected to axially symmetrical loading, the general theory of orthotropic laminated shells and its applications to the design of composite cylindrical shells are described. The papers give results of both calculation and experiment.

The book is intended for specialists in the field of fracture mechanics, design and fabrication of structures made of composite materials.

Mir Publishers
2 Pervy Rizhsky Pereulok
I-110, GSP
USSR